Title
Uranium and vanadium binding studies for the selective extraction of uranium from seawater

Author
Parker, Bernard Frederick

Publication Date
2017

Peer reviewed|Thesis/dissertation

Uranium and vanadium binding studies for the selective extraction of uranium from seawater

By

Bernard Frederick Parker

A dissertation submitted in partial satisfaction of the

requirements for the degree of

Doctor of Philosophy

in

Chemistry

in the

Graduate Division

of the

University of California, Berkeley

Committee in charge:

Professor John Arnold, Chair
Professor T. Don Tilley
Professor Alexander Katz

Summer 2017

Abstract

Uranium and vanadium binding studies for the selective extraction of uranium from seawater
by
Bernard Frederick Parker
Doctor of Philosophy in Chemistry
University of California, Berkeley
Professor John Arnold, Chair

Chapter 1
An introduction to the uranium from seawater project.

Chapter 2
A non-oxo V(V) complex with glutaroimide-dioxime (H_3L), a ligand for recovering uranium from seawater, was synthesized from aqueous solution as $Na[V(L)_2]\cdot 2H_2O$, and the structure determined by x-ray diffraction. It is the first non-oxo V(V) complex that has been directly synthesized in and crystallized from aqueous solution. The distorted octahedral structure contains two fully deprotonated ligands (L^{3-}) coordinating to V^{5+}, each in a tridentate mode. Using ^{17}O-labelled vanadate, concurrent $^{17}O/^{51}V/^{1}H/^{13}C$ NMR, in conjunction with ESI-MS, unprecedentedly demonstrated the stepwise displacement of the oxo V=O bonds by glutaroimide-dioxime and verified the existence of the "bare" V^{5+}/glutaroimide-dioxime complex, $[V(L)_2]^-$, in aqueous solution. In addition, the crystal structure of an intermediate 1:1 V(V)/glutaroimide-dioxime complex, $[VO_2(HL)]^-$, in which the oxo bonds of vanadate are only partially displaced, corroborates the observations by NMR and ESI-MS. Results from this work provide important insights into the strong sorption of vanadium on poly(amidoxime) sorbents in the recovery of uranium from seawater. Because vanadium plays important roles in biological systems, the direct synthesis of the non-oxo V^{5+} complex and the unprecedented demonstration of the displacement of the oxo V=O bonds may also help with the ongoing efforts to develop vanadium compounds that could be of importance in biological applications.

Chapter 3
The kinetics of the binding of uranium, vanadium, and iron with glutaroimide-dioxime as a molecular analogue of polymer sorbents has been studied using stopped-flow and conventional UV-visible absorption spectroscopy to monitor the reactions over a range of time scales. Qualitatively, vanadium reacts the slowest of the three metals despite being able to form a very strong complex, with the 1:2 vanadium/ligand complex forming over weeks, likely due to the slow hydrolysis of the strong oxido ligands, while iron reacts fast and uranyl faster still, despite the presence of carbonate in the uranyl species. Conditional rate constants were determined for the formation of 1:1 glutaroimide-dioxime complexes with the three metal ions. In a narrow and near neutral pH region, a rate equation for the formation of the 1:1 vanadium/glutaroimide-dioxime complex was developed, showing the reaction is the first order with respect to [V], [ligand], and $[H^+]$. These observations, some qualitative and others quantitative, are consistent

with previous marine tests of polymer adsorbents, and give mechanistic insight into how glutaroimide-dioxime forms complexes with uranium, iron, and vanadium.

Chapter 4

Interactions of vanadium(IV) with amidoximes and similar ligands as molecular analogues of polymer sorbents used to extract uranium from seawater is explored. Vanadium is one of the main competing ions for uranium sorption as V(V) species, however, vanadium is also present as V(IV) in seawater so this reaction is of interest to U/V selectivity and polymer stability. The synthesis of V(IV) complexes of glutaroimide-dioxime was attempted under a wide variety of conditions, however, V(IV) was found to react irreversibly with glutaroimide-dioxime and other oxime groups which oxidize vanadium to the V(V) oxidation state by transferring an oxygen atom from the ligand or substrate. A mechanism has been proposed for this type of reactivity, and the redox behavior of the vanadium-glutaroimide-dioxime complex has been characterized.

Chapter 5

A triazine hydroxylamine ligand, H_2bihyat, has been investigated for its potential application to selective uranyl binding for extraction from seawater. The vanadium chemistry of this ligand is known; compared to glutaroimide-dioxime the binding is significantly weaker and it does not form a 2:1 non-oxido V(V) complex. This ligand has a very similar binding group configuration as glutaroimide-dioxime, and through potentoimetry it was found to be comparable in binding ability. NMR techniques were used to confirm the stoichiometry and species proposed by potentiometry over a wide pH range. Additionally, the 1:1 complex UO_2(bihyat) was isolated and the crystal structure obtained. Solid-state binding is also similar to glutaroimide-dioxime, further suggesting that this ligand may be a feasible alternative to glutaroimide-dioxime, but with much improved selectivity over vanadium.

Chapter 6

As a new strategy to discover new ligands for the selective binding of uranyl, a combinatorially synthesized peptoid library (*N*-substituted glycine oligomers) was screened for uranyl binding with the goal of identifying high-affinity ligands for use in polymer sorbents. Qualitative screening techniques using a dye, arsenazo III, identified three uranyl-binding sequences, all of which contained only carboxylic acids as the active binding groups. Fluorescence spectroscopy was used to determine a dissociation constant for one of the identified peptoids by monitoring the decrease in peptoid fluorescence upon uranyl binding. Density functional theory calculations were used to model the solution-state binding of these sequences to understand favored binding modes and geometries.

Table of Contents

Curriculum Vitae

Education

University of California, Berkeley, Berkeley CA
Doctor of Philosophy in Chemistry August 2017

Carnegie-Mellon University, Pittsburgh PA
Bachelor of Science in Chemistry May 2012

Publications

Parker, B. F., Hohloch, S., Pankhurst, J. R., Zhang, Z., Love, J. B., Arnold, J., Rao, L.
Vanadium redox reactivity with amidoxime ligands
Manuscript in preparation

Parker, B. F., Zhang, Z., Arnold, J., Rao, L.
Iron, vanadium, and copper complexation with amidoxime ligands
Manuscript in preparation

Garner, M. E., **Parker, B. F.**, Hohloch, S., Bergman, R. G., Arnold, J.
Catalytic hydrophosphination by a thorium-NHC metallacycle
Manuscript submitted

Hohloch, S., Pankhurst, J. R., Jaekel, E. E., **Parker, B. F.**, Lussier, D. J., Garner, M. E., Booth, C. H., Lukens, W. W., Love, J. B., Arnold, J.
Benzoquinonoid-bridged dinuclear actinide complexes
Manuscript submitted

Hohloch, S., Garner, M. E., **Parker, B. F.**, Arnold, J.
New supporting ligands in actinide chemistry: Tetramethyltetraazaannulene complexes with thorium and uranium
Manuscript submitted

Ivanov, I. S., Leggett, C. J., **Parker, B. F.**, Zhang, Z., Arnold, J., Dai, S., Abney, C. W., Bryantsev, V. S., Rao, L.
Origin of the unusually strong and selective binding of vanadium by polyamidoximes in seawater
Manuscript submitted

Parker, B. F., Leggett, C. J., Zhang, Z., Arnold, J., Rao, L.
Kinetics of complexation of V(V), U(VI), and Fe(III) with glutaroimide-dioxime: studies by stopped-flow and conventional absorption spectroscopy
Dalton Transactions, 2017, DOI: 10.1039/C7DT01597F

Boreen, M. A., **Parker, B. F.**, Lohrey, T. D., Arnold, J.
A Homoleptic Uranium(III) Tris(aryl) Complex
Journal of the American Chemical Society, 2016, **138** (49), 15865-15868

Parker, B. F., Knight, A. S., Vukovic, S., Arnold, J., Francis, M. B.
A Peptoid-Based Combinatorial and Computational Approach to Developing Ligands for Uranyl Sequestration from Seawater
Industrial & Engineering Chemistry Research, 2016, **55** (15), 4187-4194

Leggett, C. J., **Parker, B. F.**, Teat, S. J., Zhang, Z., Dau, P. D., Lukens, W. W., Peterson, S. M., Cardenas, A. J. P., Warner, M. G., Gibson, J. K., Arnold, J., Rao, L.
Structural and spectroscopic studies of a rare non-oxido V(V) complex crystallized from aqueous solution
Chemical Science, 2016, **7** (4), 2775-2786

Wang, Y., Zhang, Y., **Parker, B.**, Matyjaszewski, K.
ATRP of MMA with ppm Levels of Iron Catalyst
Macromolecules, 2011, **44** (11), 4022–4025

Presentations

"Binding modes and thermodynamics of iron and vanadium with amidoximes"
Parker, B. F., Zhang, Z., Arnold, J., Rao, L.
243rd ACS National Meeting and Exposition, San Francisco CA, April 2017

"Aqueous vanadium complexation with imide-dioxime ligands"
Parker, B. F., Zhang, Z., Arnold, J., Rao, L.
242nd ACS National Meeting and Exposition, Philadelphia PA, August 2016

"Combinatorial peptoid ligand screening for uranyl binding"
Parker, B. F., Knight, A. S., Vukovic, S., Arnold, J., Francis, M. B.
249th ACS National Meeting and Exposition, Denver CO, March 2015

Dedicated to
Frederick Arthur Gowen
my grandfather,
in loving memory

Chapter 1

Introduction to the uranium from seawater project

The recovery of uranium from seawater has received considerable attention in the last few years due to the size of this yet-untapped source, containing 4.5 billion tons of uranium, over a thousand times more than the entire known terrestrial supply.[1,2] Development of an efficient and economical technology for recovering uranium from seawater could therefore make the world's oceans a nearly limitless source of fuel for nuclear reactors. The concentration of uranium in the ocean is low, at approximately 3.3 parts per billion; additionally, seawater contains trace amounts of almost every naturally-occurring element, so high selectivity is necessary for efficient extraction. Table 1 lists the concentrations of selected metals in seawater for comparison.

Table 1. Abundance of selected ions in seawater[1]

Metal	Concentration		Notes
Na	1.08 % (w/w)	0.456 M	at 3.5% salinity
K	392 ppm	9.7 mM	
Ca	411 ppm	40 mM	
Li	0.17 ppm	24 μM	
Fe	3.4 ppb	59 nM	
Cu	0.9 ppb	14 nM	
U	3.3 ppb	13 nM	as $Ca(UO_2)(CO_3)_3$ [3]
V	1.9 ppb	36 nM	80-90% V(V), balance V(IV)[4]
Au	11 ppt	50 pM	

The chemistry of seawater plays a major role in extraction, both in chemical speciation of metals as well as necessitating working within relatively narrow constraints on extraction conditions, mainly regarding pH, salinity, and biological activity.[1] As a result of pH and other ions present, the chemical form of uranium in seawater is almost exclusively in the form of ternary uranium calcium carbonate complexes.[3,5] These complexes prove to be problematic for extraction, as the calcium and carbonate ions all need to be displaced, which is a challenge, especially considering the high concentrations of each of these ions in seawater. Vanadium is another element with complicated solution chemistry, both with polynuclear V(V) species as well as redox chemistry between V(V) and V(IV), which is a minor component of vanadium in seawater.[4,6,7] In general, elements that are taken up and used by marine organisms vary by season, oceanic depth, temperature, and location, which further complicate optimization of polymer selectivity.[4,8]

Of all the trace elements dissolved in seawater, only uranium and lithium are proposed to be economical to extract.[9–11] Base metals such as iron and vanadium are abundant and readily obtained from the earth's surface, while precious metals such as gold are present in such small amounts that extraction is not feasible. Indeed, extracting gold has been attempted historically, notably by Fritz Haber and has invariably lead to huge financial losses.[12,13] Lithium is of interest due to high demand for use in lithium batteries, although extraction technology has not been developed to the extent of uranium extraction.[11]

The extraction of uranium from seawater was first proposed in the 1960s in the UK, based on phosphates and other uranyl extractants that have been used in the PUREX process for processing spent nuclear fuel.[14,15] Using amidoxime sorbents for this purpose received much attention in Japan in the late 1980s, with some work continuing through the 2000s[16–21], although the use of amidoximes as a uranium chelator (not specifically for extraction from seawater) was proposed even earlier[22]. The United States Department of Energy started work in this area in 2011 to improve extraction efficiency, which continues to the present day.[21,23] Significant improvements in cost have been achieved, from estimates of $1300 – $3100 (unknown confidence, may be optimistic) for Japanese sorbent technology in 1984,[16] $1100 – $1540 in 2006 (95% confidence), to $510 – $735 in 2014 (95% confidence; all values in 2016 US$/kg U_3O_8).[10,21] However, the spot price of uranium from terrestrial sources has varied in the range of $45 – $160 over the past 8 years, peaking at $350/kg U_3O_8 in 2007, so further cost improvements will be needed, barring a drastic increase in uranium prices.[24]

Several technologies for selective uranyl extraction have been investigated, including hydrogels,[25] nanostructured ceramics,[26] porous aromatic frameworks,[27] chitin-based materials,[28] computationally-optimized proteins,[29] and combinatorial peptoid-based ligands.[30] however, functionalized polymer sorbents have been the most extensively studied system, the majority of which have binding moieties related to the amidoxime functional group (Figure 1). These have been investigated for over 50 years and have shown to be successful on pilot plant scales in Japan, although a comprehensive understanding of their chemistry has only been achieved recently.[17,21,31]

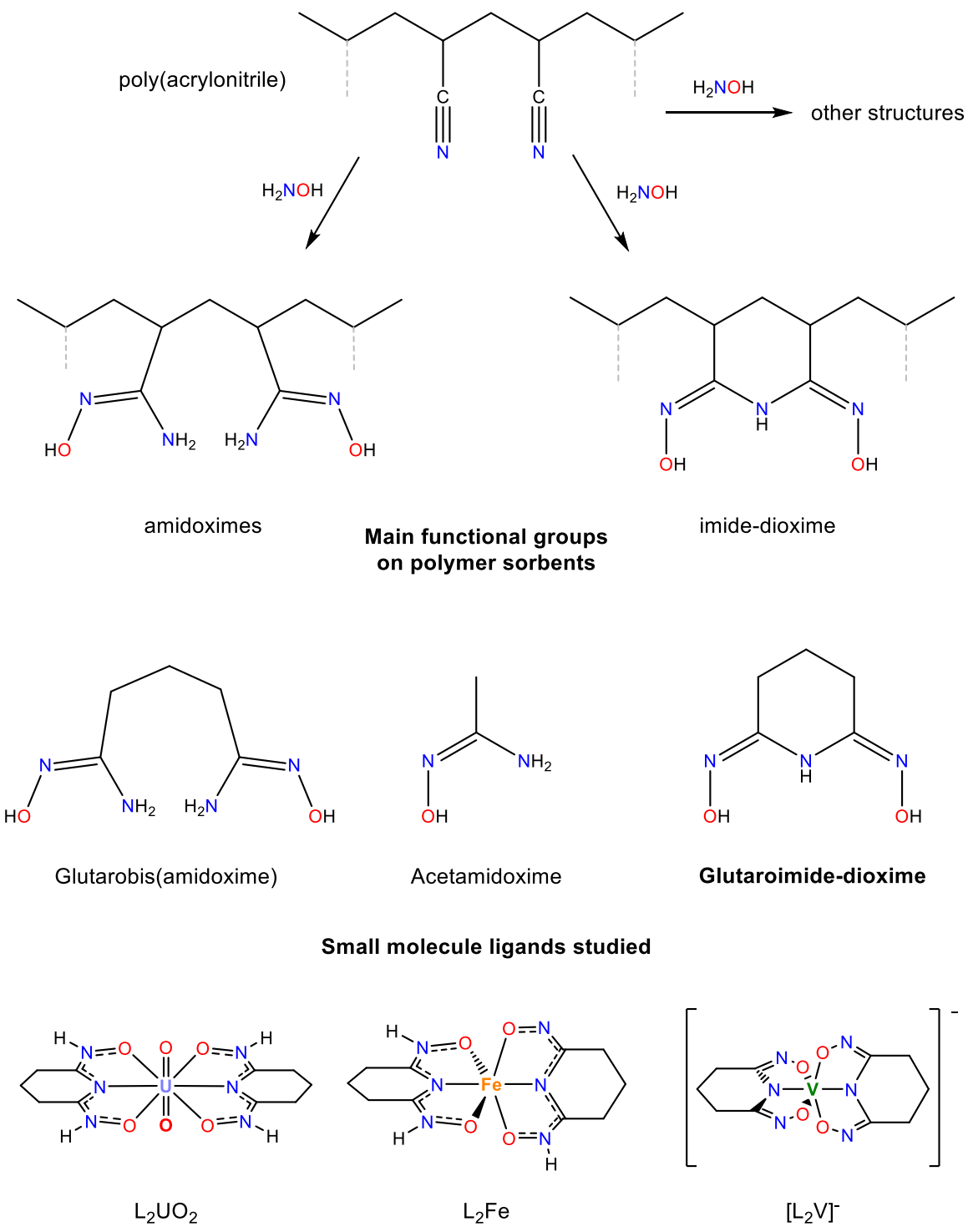

Figure 1. Top: synthesis and structure of polymer sorbents used for uranium extraction from seawater. Middle: small molecule analogues used as ligands for solution studies, notably glutaroimide-dioxime. Bottom: metal complexes of glutaroimide-dioxime[32–34].

In efforts to improve sorbent efficiency and ultimately reduce costs, many different aspects of this technology can be improved. Key areas of study for improvements include material preparation and characterization[2,35–38], polymerization and functionalization[39–41], thermodynamic, kinetic, and structural characterization[32,33,42–45], and ligand design[30,46,47], supported by economic assessments[10], computational work[48–50] and marine testing[31,51]. These recent efforts by the Unites States Department of Energy have led to significant increases in efficiency. Marine test results have been reported in Japan over a decade ago in which the uranium uptake was 1.5 g U/kg sorbent after 30 days[17,21] while more recently, marine tests conducted in the United States showed that up to 3.9 g U/kg sorbent was obtained after 8 weeks[2,38].

Most materials consist of polyacrylonitrile grafted from polyethylene or other support, followed by treatment with hydroxylamine to form amidoximes, followed by further conditioning.[23,52] Small molecule amidoximes are synthesized almost exclusively by the analogous reaction of hydroxylamine on organic nitriles (Figure 2).[53,54] The amidoxime functional group typically has one acidic site (OH) and one basic site (NH_2), with two pKa values of approximately 12 and 6, respectively.[50,55,56] As ligands, multiple coordination modes are possible, with metals either interacting with one or two donor atoms (Figure 3). The first three modes listed are all fairly common, with the last η^2 N,O binding mode being relatively rare, although uranyl is a notable exception.[48] Multiple donor atoms also means that suitably-designed amidoximes readily form clusters and multinuclear complexes. A comprehensive review of the coordination chemistry of amidoximes has been published recently.[54] Although much of the coordination chemistry of amidoximes, glutaroimide-dioxime and glutarobis(amidoxime) is relatively recent, these molecules and other similar amidoximes have been known since at least 1889,[57] and their metal binding properties have been applied as analytical reagents for many metals, including uranium(VI).[58–61] The reactivity of these molecules and other amidoximes has also been explored, which include multiple hydrolysis pathways, reduction, cyclization to oxazoles, *O*-alkylation, and numerous other substitution reactions.[53,62]

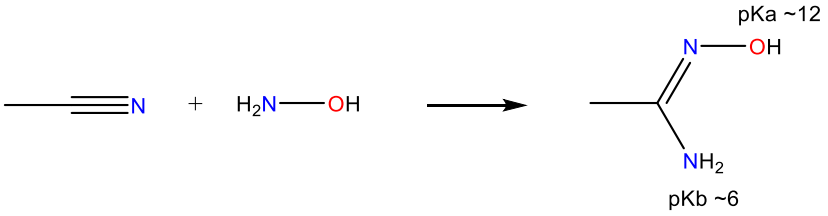

Figure 2. Typical synthesis of amidoximes and acidity of the amidoxime group

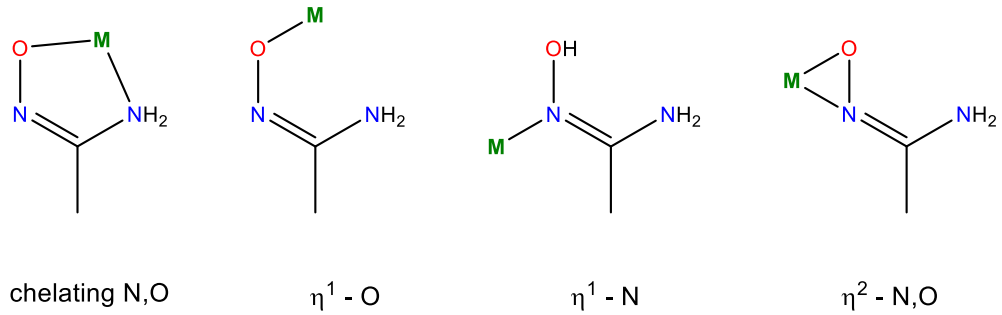

Figure 3. Common coordination modes of amidoximes

In addition to amidoximes, the glutaroimide-dioxime ligand – a condensation product of two adjacent amidoximes – is a proposed molecular analogue of one of the dominant functional groups on polymer adsorbents (Figure 1).[63,64] In addition to these functional groups, several other moieties are also present, either through adventitious hydrolysis or intentional inclusion. Minor functional groups on amidoxime polymers include partially hydrolyzed imide-oximes[43,65], 2,6-diiminopiperidin-1-ol[66], as well as amides and carboxylic acids[67] (Figure 4). These are generally poorer ligands for uranium binding than the functional groups discussed above, although the latter two are beneficial in another way by improving the hydrophilicity of the polymer for more effective and rapid sorption.[67–69]

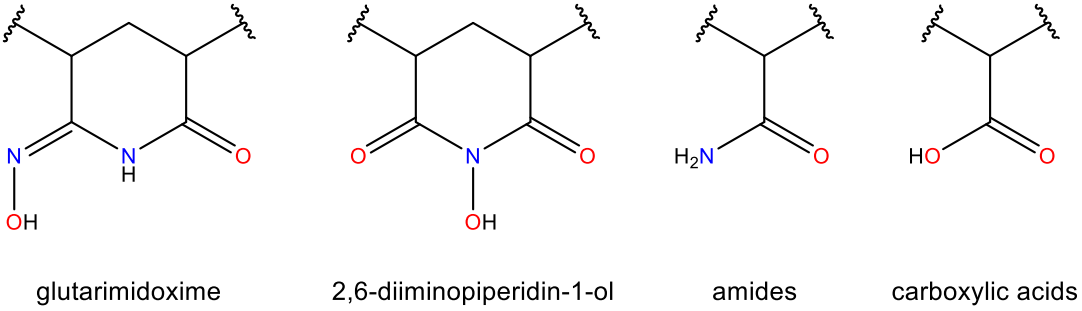

Figure 4. Minor functional groups present on amidoxime-based polymer sorbents

One of the major challenges with current amidoxime-functionalized polymer adsorbents is the relatively low selectivity of these functional groups for uranium over other metals, vanadium and iron in particular.[33,34] For example, 56-day marine tests have shown that the relative abundance of metal elements absorbed by amidoxime-functionalized polymer adsorbents (in molar percent) follows the order: vanadium (14.9%) >> iron (1.6%) > uranium (1.0%), with vanadium occupying nearly 20 times as many sites as uranyl, though the concentrations of the three elements in seawater are comparable.[31] In addition, the stripping conditions required to elute the sorbed V(V) from the sorbent for reuse are much harsher than those used to elute uranium and other cations and ultimately destroy the sorbent.[65,70] Understanding the coordination chemistry of competing metals, including iron, copper, lead[33], and especially vanadium[34,45,71] with glutaroimide-dioxime has been the focus of recent work in order to overcome selectivity problems of sorbents.

Within the uranium from seawater project, my work has been in fields of ligand design as well as characterization of metal coordination to small molecule ligands. Much of the work has focused on vanadium chemistry due to the previously mentioned problem of selectivity, understanding its coordination chemistry with amidoximes which had been previously unknown. Chapter 2 discusses the discovery of a rare non-oxido vanadium(V) complex with glutaroimide-dioxime, with extensive solution characterization and confirmation of this binding mode. Chapter 3 compares the kinetics of complexation of uranium as well as iron and vanadium, the two main competitors for uranium binding, and gaining mechanistic insights into these systems from kinetic results. Chapter 4 explores the redox activity of the vanadium-glutaroimide-dioxime complex, both attempting to prepare the analogous vanadium(IV) compound and investigating the reactions discovered between amidoximes and vanadium(IV). Chapter 5 characterizes the binding of a 1,3,5-triazine hydroxylamine ligand to uranyl, examining both solid-state and solution interactions and the ligand's affinity and selectivity for potential application in polymer sorbents. Finally, Chapter 6 uses an alternate approach to ligand discovery, using a combinatorial screening technique of peptoid-based ligands to find new binding moieties rather than direct ligand design.

References

(1) Turekian, K. K. *Oceans*; Prentice-Hall: Englewood Cliffs, N. J., 1968.
(2) Kim, J.; Tsouris, C.; Mayes, R. T.; Oyola, Y.; Saito, T.; Janke, C. J.; Dai, S.; Schneider, E.; Sachde, D. *Sep. Sci. Technol.* **2013**, *48*, 367–387.
(3) Endrizzi, F.; Rao, L. *Chem. - A Eur. J.* **2014**, *20*, 14499–14506.
(4) Wang, D.; Sañudo Wilhelmy, S. A. *Mar. Chem.* **2009**, *117*, 52–58.
(5) Endrizzi, F.; Leggett, C. J.; Rao, L. *Ind. Eng. Chem. Res.* **2016**, *55*, 4249–4256.
(6) Emerson, S. R.; Huested, S. S. *Mar. Chem.* **1991**, *34*, 177–196.
(7) Heath, E.; Howarth, O. W. *J. Chem. Soc. Dalt. Trans.* **1981**, 1105.
(8) Vraspir, J. M.; Butler, A. *Annu. Rev. Mar. Sci.* **2009**, *1*, 43–63.
(9) Sholl, D. S.; Lively, R. P. *Nature* **2016**, *532*, 435–437.
(10) Kim, J.; Tsouris, C.; Oyola, Y.; Janke, C. J.; Mayes, R. T.; Dai, S.; Gill, G.; Kuo, L. J.; Wood, J.; Choe, K. Y.; Schneider, E.; Lindner, H. *Ind. Eng. Chem. Res.* **2014**, *53*, 6076–6083.
(11) Hoshino, T. *Desalination* **2013**, *317*, 11–16.
(12) Haber, F. *Zeitschrift für Angew. Chemie* **1927**, *40*, 303–314.
(13) Kenison Falkner, K.; Edmond, J. M. *Earth Planet. Sci. Lett.* **1990**, *98*, 208–221.
(14) Davies, R. V.; Kennedy, J.; McIlroy, R. W.; Spence, R.; Hill, K. M. *Nature* **1964**, *203*, 1110–1115.
(15) Anderson, H. H.; Asprey, L. B. Solvent extraction process for plutonium. US Patent 2924506 A, 1960.
(16) Kanno, M. *J. Nucl. Sci. Technol.* **1984**, *21*, 1–9.
(17) Saito, K.; Uezu, K.; Hori, T.; Furusaki, S.; Sugo, T.; Okamoto, J. *AIChE J.* **1988**, *34*, 411–416.
(18) Egawa, H.; Harada, H. *Nippon Kagaku Kaishi* **1979**, 958–959.
(19) Schenk, H. J.; Astheimer, L.; Witte, E. G.; Schwochau, K. *Sep. Sci. Technol.* **1982**, *17*, 1293–1308.
(20) Egawa, H.; Nonaka, T.; Nakayama, M. **1990**, 2273–2277.
(21) Rao, L. *Recent International R & D Activities in the Extraction of Uranium from Seawater, LBNL Paper LBNL-4034E*; 2011.
(22) Soloway, S. Use of amidoximes in solvent extraction of metal ions from solution. US Patent 2909542 A, 1959.
(23) Kim, J.; Tsouris, C.; Mayes, R. T.; Oyola, Y.; Saito, T.; Janke, C. J.; Dai, S.; Schneider, E.; Sachde, D. *Sep. Sci. Technol.* **2013**, *48*, 367–387.
(24) Ux Consulting Company http://www.uxc.com (accessed Jul 20, 2017).
(25) Li, W. P.; Han, X. Y.; Wang, X. Y.; Wang, Y. Q.; Wang, W. X.; Xu, H.; Tan, T. S.; Wu, W. S.; Zhang, H. X. *Chem. Eng. J.* **2015**, *279*, 735–746.
(26) Chouyyok, W.; Pittman, J. W.; Warner, M. G.; Nell, K. M.; Clubb, D. C.; Gill, G. A.; Addleman, R. S. *Dalton Trans.* **2016**, *45*, 11312–11325.
(27) Yue, Y.; Zhang, C.; Tang, Q.; Mayes, R. T.; Liao, W.-P.; Liao, C.; Tsouris, C.; Stankovich, J. J.; Chen, J.; Hensley, D. K.; Abney, C. W.; Jiang, D.; Brown, S.; Dai, S. *Ind. Eng. Chem. Res.* **2016**, *55*, 4125–4129.
(28) Barber, P. S.; Kelley, S. P.; Griggs, C. S.; Wallace, S.; Rogers, R. D. *Green Chem.*

2014, 1828–1836.
(29) Zhou, L.; Bosscher, M.; Zhang, C.; Özçubukçu, S.; Zhang, L.; Zhang, W.; Li, C. J.; Liu, J.; Jensen, M. P.; Lai, L.; He, C. *Nat. Chem.* **2014**, *6*, 236–241.
(30) Parker, B. F.; Knight, A. S.; Vukovic, S.; Arnold, J.; Francis, M. B. *Ind. Eng. Chem. Res.* **2016**, *55*, 4187–4194.
(31) Gill, G. A.; Kuo, L.-J.; Janke, C. J.; Park, J.; Jeters, R. T.; Bonheyo, G. T.; Pan, H.-B.; Wai, C.; Khangaonkar, T.; Bianucci, L.; Wood, J. R.; Warner, M. G.; Peterson, S.; Abrecht, D. G.; Mayes, R. T.; Tsouris, C.; Oyola, Y.; Strivens, J. E.; Schlafer, N. J.; Addleman, R. S.; Chouyyok, W.; Das, S.; Kim, J.; Buesseler, K.; Breier, C.; D'Alessandro, E. *Ind. Eng. Chem. Res.* **2016**, *55*, 4264–4277.
(32) Tian, G.; Teat, S. J.; Zhang, Z.; Rao, L. *Dalton Trans.* **2012**, *41*, 11579.
(33) Sun, X.; Xu, C.; Tian, G.; Rao, L. *Dalton Trans.* **2013**, *42*, 14621–14627.
(34) Leggett, C. J.; Parker, B. F.; Teat, S. J.; Zhang, Z.; Dau, P. D.; Lukens, W. W.; Peterson, S. J. M.; Cardenas, A. J. P.; Warner, M. G.; Gibson, J. K.; Arnold, J.; Rao, L. *Chem. Sci.* **2016**, *7*, 2775–2786.
(35) Ladshaw, A. P.; Das, S.; Liao, W.-P. W.-P.; Yiacoumi, S.; Janke, C. J.; Mayes, R. T.; Dai, S.; Tsouris, C. *Ind. Eng. Chem. Res.* **2015**, acs.iecr.5b03456.
(36) Das, S.; Oyola, Y.; Mayes, R. T.; Janke, C. J.; Kuo, L. J.; Gill, G.; Wood, J. R.; Dai, S. *Ind. Eng. Chem. Res.* **2016**, *55*, 4103–4109.
(37) Kuo, L. J.; Janke, C. J.; Wood, J. R.; Strivens, J. E.; Das, S.; Oyola, Y.; Mayes, R. T.; Gill, G. A. *Ind. Eng. Chem. Res.* **2015**, *55*, 4285–4293.
(38) Das, S.; Oyola, Y.; Mayes, R. T.; Janke, C. J.; Kuo, L.-J.; Gill, G.; Wood, J. R.; Dai, S. *Ind. Eng. Chem. Res.* **2016**, *55*, 4110–4117.
(39) Lashley, M. A.; Mehio, N.; Nugent, J. W.; Holguin, E.; Do-Thanh, C.-L.; Bryantsev, V. S.; Dai, S.; Hancock, R. D. *Polyhedron* **2016**, *109*, 81–91.
(40) Alexandratos, S.; Kung, S.; Dai, S. Recovery of Uranium from Seawater : Preparation and Development of Polymer-Supported Extractants.
(41) Brown, S.; Yue, Y.; Kuo, L. J.; Mehio, N.; Li, M.; Gill, G.; Tsouris, C.; Mayes, R. T.; Saito, T.; Dai, S. *Ind. Eng. Chem. Res.* **2016**, *55*, 4139–4148.
(42) Sun, X.; Tian, G.; Xu, C.; Rao, L.; Vukovic, S.; Kang, S. O.; Hay, B. P. *Dalton Trans.* **2014**, *43*, 551–557.
(43) Endrizzi, F.; Melchior, A.; Tolazzi, M.; Rao, L. *Dalton Trans.* **2015**, *44*, 13835–13844.
(44) Abney, C. W.; Mayes, R. T.; Piechowicz, M.; Lin, Z.; Bryantsev, V. S.; Veith, G. M.; Dai, S.; Lin, W. *Energy Environ. Sci.* **2016**, *9*, 448–453.
(45) Parker, B. F.; Zhang, Z.; Leggett, C. J.; Arnold, J.; Rao, L. *Dalton Trans.* **2017**, DOI: 10.1039/C7DT01597F.
(46) Kelley, S. P.; Barber, P. S.; Mullins, P. H. K.; Rogers, R. D. *Chem. Commun.* **2014**, *50*, 12504–12507.
(47) Lashley, M. A.; Ivanov, A. S.; Bryantsev, V. S.; Dai, S.; Hancock, R. D. *Inorg. Chem.* **2016**.
(48) Vukovic, S.; Watson, L. a; Kang, S. O.; Custelcean, R.; Hay, B. P. *Inorg. Chem.* **2012**, *51*, 3855–3859.
(49) Vukovic, S.; Hay, B. P. *Inorg. Chem.* **2013**, *0*, 7805–7810.
(50) Mehio, N.; Lashely, M. A.; Nugent, J. W.; Tucker, L.; Correia, B.; Do-Thanh, C.-L.;

Dai, S.; Hancock, R. D.; Bryantsev, V. S. *J. Phys. Chem. B* **2015**, *119*, 3567–3576.
(51) Park, J.; Jeters, R. T.; Kuo, L.-J.; Strivens, J. E.; Gill, G. A.; Schlafer, N. J.; Bonheyo, G. T. *Ind. Eng. Chem. Res.* **2016**, *55*, 4278–4284.
(52) Kabay, N.; Katakai, A.; Sugo, T. In *Radiation Physics and Chemistry*; 1995; Vol. 46, pp. 833–836.
(53) Eloy, F.; Lenaers, R. *Chem. Rev.* **1962**, *62*, 155–183.
(54) Bolotin, D. S.; Bokach, N. A.; Kukushkin, V. Y. *Coord. Chem. Rev.* **2016**, *313*, 62–93.
(55) Mehio, N.; Williamson, B.; Oyola, Y.; Mayes, R. T.; Janke, C.; Brown, S.; Dai, S. *Ind. Eng. Chem. Res.* **2015**, *55*, 4217–4223.
(56) Endrizzi, F.; Leggett, C. J.; Rao, L. *Ind. Eng. Chem. Res.* **2016**, *55*, 4249–4256.
(57) Biedermann, J. *Berichte der Dtsch. Chem. Gesellschaft* **1889**, *22*, 2967–2973.
(58) Bernal, J. L.; Del Nozal, M. J.; Debán, L.; Nuñez, B.; Cerdá, V.; Estela, J. M. *Thermochim. Acta* **1986**, *103*, 259–266.
(59) Jara, R.; Cerdà, V. *Thermochim. Acta* **1989**, *142*, 135–141.
(60) Jara, R.; Estela, J. M.; Cerdá, V. *Thermochim. Acta* **1991**, *177*, 229–237.
(61) Grases, F.; Forteza, R.; March, J. G.; Cerda, V. *Anal. Chim. Acta* **1983**, *155*, 299–303.
(62) Elvidge, J. A.; Linstead, R. P.; Salaman, A. M. *J. Chem. Soc.* **1959**, 208–215.
(63) Endrizzi, F.; Melchior, A.; Tolazzi, M.; Rao, L. *Dalton Trans.* **2015**, *44*, 13835–13844.
(64) Yue, Y.; Mayes, R. T.; Kim, J.; Fulvio, P. F.; Sun, X. G.; Tsouris, C.; Chen, J.; Brown, S.; Dai, S. *Angew. Chemie - Int. Ed.* **2013**, *52*, 13458–13462.
(65) Kang, S. O.; Vukovic, S.; Custelcean, R.; Hay, B. P. *Ind. Eng. Chem. Res.* **2012**, *51*, 6619–6624.
(66) Kennedy, Z. C.; Cardenas, A. J. P.; Corbey, J. F.; Warner, M. G. *Chem. Commun.* **2016**, *52*, 8802–8805.
(67) Pan, H.-B.; Kuo, L.-J.; Wai, C. M.; Miyamoto, N.; Joshi, R.; Wood, J. R.; Strivens, J. E.; Janke, C. J.; Oyola, Y.; Das, S.; Mayes, R. T.; Gill, G. A. *Ind. Eng. Chem. Res.* **2016**, *55*, 4313–4320.
(68) Alexandratos, S. D.; Zhu, X.; Florent, M.; Sellin, R. *Ind. Eng. Chem. Res.* **2016**, *55*, 4208–4216.
(69) Oyola, Y.; Dai, S. *Dalton Trans.* **2016**, *45*, 8824–8834.
(70) Pan, H.-B.; Liao, W.; Wai, C. M.; Oyola, Y.; Janke, C. J.; Tian, G.; Rao, L. *Dalton Trans.* **2014**, *43*, 10713–10718.
(71) Ivanov, A. S.; Leggett, C. J.; Parker, B. F.; Zhang, Z.; Arnold, J.; Dai, S.; Abney, C. W.; Bryantsev, V. S.; Rao, L. *Manuscript Submitted* **2017**.

Chapter 2

Synthesis and characterization of a rare non-oxido V(V) complex from aqueous solution

Introduction

Selectivity for uranium over other ions is a key factor in its efficient extraction from seawater and all the other components within. Great improvements have been made in the capacity of amidoxime-based uranium sorbents, more than doubling uranium capacity over 10 years, however, selectivity remains a challenge.[1,2] Studies indicate that the sorption efficiency of vanadium(V), which is the stable valence state under the conditions of seawater E_h and pH[3], by poly(amidoxime) sorbents is much higher than those for Fe(III) and U(VI), following the order: vanadium(V) >> iron(III) > uranium(VI).[4] Though the concentrations of vanadium (1.9 μg/kg)[3,5] and uranium in seawater are comparable, vanadium in fact occupies nearly 20 times as many sorption sites as uranium on the poly(amidoxime) sorbents,[4,6] essentially limiting the sorption capacity for uranium. In addition, the stripping conditions required to elute the sorbed V(V) from the sorbent for reuse are much harsher than those used to elute uranium and other cations and ultimately destroy the sorbent.[6,7] Since vanadium is a particularly problematic element in the extraction of uranium from seawater using poly(amidoxime) sorbents, a fundamental understanding of vanadium coordination to amidoxime-type sorbents could help optimize this extraction technology.

Structural studies can be used to provide valuable insights into the coordination behavior of vanadium and other metal cations with amidoxime ligands and can also help explain their subsequent sorption behavior with poly(amidoxime) sorbents. For example, the crystal structures and thermodynamic stability constants have been reported for U(VI) and Fe(III) complexes with glutaroimide-dioxime (Figure 1), a cyclic imide-dioxime moiety that can form during the synthesis of the poly(amidoxime) sorbent and is reputedly responsible for the extraction of uranium from seawater.[8,9] For both cations, two glutaroimide-dioxime ligands bind in a tridentate mode to the metal center. However, the ligands were found to bind Fe(III) much more strongly than U(VI) as manifested by the shorter Fe-O and Fe-N bond lengths relative to the corresponding U-O and U-N bond lengths (even after taking into consideration the difference in ionic radii between Fe^{3+} and UO_2^{2+}). The shorter bond lengths in the Fe(III) complex were attributed to the higher charge density of Fe(III) as well as its larger orbital participation in bonding relative to uranium. The higher thermodynamic stability and shorter bond lengths of the Fe^{3+}/glutaroimide-dioxime complexes were postulated to be responsible for the higher sorption of Fe^{3+} compared to UO_2^{2+} in marine tests.

The contents of this chapter have been previously published in **"Structural and spectroscopic studies of a rare non-oxido V(v) complex crystallized from aqueous solution"**; Christina J. Leggett, Bernard F. Parker, Simon J. Teat, Zhicheng Zhang, Phuong D. Dau, Wayne W. Lukens, Sonja J. M. Peterson, Allan Jay P. Cardenas, Marvin G. Warner, John K. Gibson, John Arnold, Linfeng Rao; *Chemical Science*; **2016**, 7 (4), p. 2775-2786.

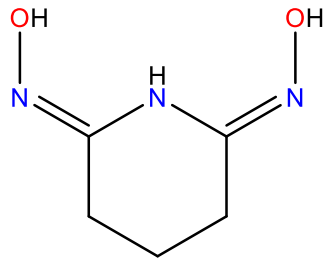

Figure 1 Glutaroimide-dioxime (LH_3)

Though the crystal structure of V(V) with glutaroimide-dioxime has not been previously reported, reasonable speculations about its structure can be made using information obtained from the known V(V) crystal structures. Based on the reported structures of V(V) complexes with organic ligands prepared from aqueous solutions (or ionic liquid equilibrated with water), it is known that the VO_2^+ moiety with two short oxo V=O bonds ($R_{V=O}$ = 1.60 – 1.63 Å) usually remains intact.[10–12] Therefore, unlike the UO_2^{2+} cation which possesses a linear *trans* dioxo configuration that allows two tridentate ligands to bind in the equatorial plane to form a strong 1:2 U(VI)/L complex,[8] the VO_2^+ cation with its bent *cis* dioxo configuration cannot accommodate two such ligands due to steric hindrance and insufficient coordination sites.

These observations raise questions about why V(V) is sorbed much more strongly than U(VI) by the amidoxime sorbents. One hypothesis that could explain the much stronger complexation of V(V) is that V(V) exists in the glutaroimide-dioxime complex as a non-oxo, "bare" V^{5+} ion coordinated with the ligand(s). A non-oxo V^{5+} cation could have a very high affinity for O and N donor ligands due to its high charge density and could easily accommodate two tridentate ligands in a mode similar to that in the Fe^{3+}/glutaroimide-dioxime complex.[9] However, crystal structure data in the Cambridge Structural Database (CSD)[13] indicate that, while limited numbers of structures are known that contain non-oxo V^{4+} (Figure 2), complexes with ligands such as *cis*-inositol[14], N-hydroxy-iminodiacetate[15], or catecholate[16] obtained from aqueous solutions, crystals of non-oxo V^{5+} complexes from aqueous solutions are extremely rare. One non-oxo V^{5+} complex, $[PPh_4][\Delta\text{-}V((S,S)\text{-HIDPA})_2]\cdot H_2O$ (HIDPA = 2,2'-(hydroxyimino)dipropionic acid), was crystallized as the oxidized analogue of the naturally-existing Amavadin[17,18] from aqueous solution through the oxidation of a V(IV) complex by Ce(IV). To the best of our knowledge, there have been no "bare" V^{5+} complexes directly synthesized from oxo V(V) species (pervanadyl or vanadates) and crystallized from aqueous solution. In addition, the formation of non-oxo V^{5+} complexes in aqueous solutions *via* the displacement of the oxo V=O bonds by chelating ligands (e.g., the hydroxamate derivative deferoxamine[19]) was only postulated but has not been demonstrated.

In an effort to provide structural insights into vanadium complexation with amidoxime ligands, the present work has been conducted to synthesize crystals of V(V)/glutaroimide-dioxime complexes and characterize their crystal- and solution structures by single-crystal X-ray diffraction (XRD), multinuclear (^{51}V, ^{17}O, ^{1}H, and ^{13}C) nuclear magnetic resonance (NMR), and electrospray ionization mass spectrometry (ESI-MS). This work represents the synthesis and identification of the first non-oxo V(V) complex that was directly synthesized from an oxo V(V) species and crystallized from aqueous solution. The displacement of oxo V=O bonds by chelating ligands that leads to the formation of a non-oxo V(V) complex in aqueous solution has been unprecedentedly demonstrated by concurrent $^{51}V/^{17}O$ NMR experiments. Results

from this work provide important insights into the strong sorption of vanadium on poly(amidoxime) sorbents in the recovery of uranium from seawater.

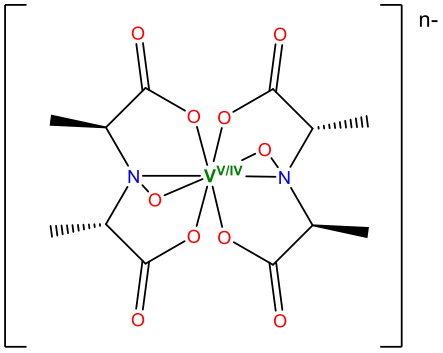

(a)

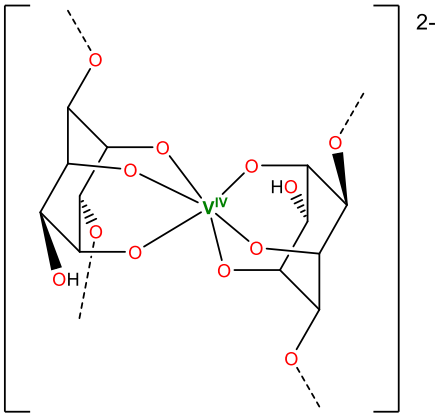

(b)

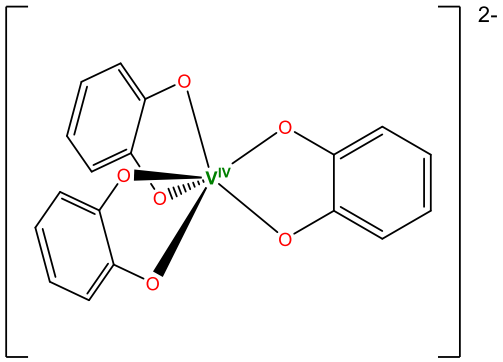

(c)

Figure 2. Selected previously reported non-oxo vanadium complexes that are stable in aqueous solution: (a) Amavadin[17], naturally occurring in the V(IV) oxidation state but it also can be oxidized and crystallized as the V(V) analogue. Substituted derivatives are also known; (b) cis-inositol V(IV) (with bridging cations)[14]; (c) tris(catecholato) V(IV)[16]

Experimental

Synthesis and single crystal XRD of $Na[V(L)_2]\cdot 2H_2O$

The glutaroimide-dioxime ligand was synthesized as described previously.[20] A 2 mL aliquot of an aqueous stock solution at pH 8 containing $NaVO_3$ (0.2 mmol), NaCl (12 mmol), and glutaroimide-dioxime (0.5 mmol) was slowly evaporated over the course of a week to generate shiny, dark brown/black acicular crystals. The crystals are very soluble in water, fairly soluble in ethanol and methanol, and insoluble in low-polarity solvents. Prolonged heating of the dissolved complex results in its decomposition as evidenced by the fading color.

A single crystal was selected, removed from Paratone oil with a MiTiGen microloop, and mounted on to a Bruker goniometer equipped with a PHOTON100 CMOS detector and Oxford Systems Cryostream 800 series on beamline 11.3.1 of the Advanced Light Source at LBNL. The data were collected at 100K using the Bruker APEX2 software[21] in shutterless mode using ω rotations at a wavelength of 0.7749 Å. The intensity data were integrated using SAINT v.8.34A and the absorption and other corrections were applied using SADABS 2014/5. The appropriate dispersion corrections for C, H, N, O, and V at $\lambda = 0.7749$ Å were calculated using the Brennan method in XDISP run through WinGX[22]. The structure was solved with intrinsic phasing using SHELXT 2014/4 and refined using SHELXL 2014/7[22]. All non-hydrogen atoms were refined anisotropically. Hydrogen atoms were found in the difference map and allowed to refine freely.

Synthesis and single-crystal XRD of $Na[VO_2(HL)]$

Glutaroimide-dioxime (30 mg, 0.21 mmol) was suspended in deionized water (1 mL). $NaVO_3$ (25 mg; 0.21 mmol) was added, resulting in a dark brown solution immediately. After stirring for 5 h, the solution was filtered and the solvent was removed. The residue was re-dissolved in ethanol and filtered. Orange crystals were obtained from vapor diffusion of hexane into the ethanol solution.

A Bruker-AXS Kappa Apex II CCD diffractometer with 0.71073 Å Mo Kα radiation was used for data collection. Crystals were mounted on a MiTeGen MicroMounts pin using Paratone-N oil. Data were collected at 100 K. The software used for data analysis includes Brüker APEX II[21] to retrieve cell parameters, SAINTPlus for raw data integration, and SADABS to apply the absorption correction. The structures were solved using either direct methods, charge flipping methods or the Patterson method and refined by a least-squares method on F2 using the SHELXTL program package. Space groups were chosen by analysis of systematic absences and intensity statistics.

^{17}O labelling of vanadate for ^{51}V, ^{17}O, ^{1}H, and ^{13}C NMR

^{17}O-enriched water (10% ^{17}O, ≥ 25% ^{18}O, balance ^{16}O) was purchased from Cambridge Isotope Laboratories, Inc. (Lot # I1-3969). 3.67 mg (0.296 mmol) NaVO3 was dissolved in 2.0 mL ^{17}O-enriched H_2O, followed by adding 50.7 mg 40% NaOD (in D_2O) solution. The colorless solution was agitated and set aside for 2 - 3 days at room temperature to allow $^{16}O/^{17}O$ exchange. The solution was checked by ^{17}O NMR after 2 and 3 days to confirm the oxo ligand exchange. Additionally, the free ligand was dissolved in the isotopically enriched water to check for $^{16}O/^{17}O$ exchange, and no exchange was observed over 4 days.

Preparation of vanadium/glutaroimide-dioxime solutions

The above-described vanadate solution was equally divided into four solutions (a, b, c, and d) for multinuclear NMR experiments. Different quantities of glutaroimide-dioxime were added into solutions b, c, and d to obtain an [L]/[V] ratio of 1, 2 and 3 for solutions b, c, and d, respectively. At this time, solution a (with vanadate only) remained colorless, but solutions b, c, and d (with vanadate and glutaroimide-dioxime) became pale yellow. A total of 0.12 mL 0.980 M HCl was added in two portions into each of solutions b, c, and d to adjust the pH of the solutions to around 8. Because the small volume (0.5 mL) of the $H_2{}^{17}O$ solutions precluded accurate pH measurements, the pH of the solutions were determined to be 7.5 (b), 8.5 (c) and 8.7 (d) by using H_2O solutions of a larger volume (4.0 mL) containing the same concentrations of vanadate and glutaroimide-dioxime as the $H_2{}^{17}O$ solutions. These solutions were allowed to equilibrate for one day after acid additions before acquisition of NMR spectra. The final colors of solutions b, c, and d were amber, brown, and dark brown, respectively. In addition to the four $H_2{}^{17}O$ solutions of V(V)/glutaroimide-dioxime described above (a, b, c, and d), one D_2O solution of pure glutaroimide-dioxime (a') and one D_2O solution of the $Na[V(L)_2]\cdot 2H_2O$ crystal (e) were also prepared for $^{1}H/^{13}C$ and ^{51}V NMR experiments.

NMR data collection

All NMR spectra were acquired at 20 - 22°C. The ^{51}V spectrum of the D_2O solution of $Na[V(L)_2]\cdot 2H_2O$ was acquired on a Bruker AV-300 spectrometer referenced to an external standard of $VOCl_3$ in C_6D_6. All other ^{17}O, ^{51}V, and ^{13}C NMR spectra were acquired on a Bruker DRX-500 spectrometer equipped with a Z-gradient broadband probe. The ^{1}H spectra were acquired on a Bruker AV-500 spectrometer equipped with a Z-gradient triple broadband inverse detection probe using WATERGATE solvent suppression. The ^{1}H, ^{13}C, and ^{51}V spectra were referenced to an external standard of $VOCl_3$ in C_6D_6 and the ^{17}O spectra were referenced to the $H_2{}^{17}O$ water resonance.

Electrospray Ionization – Mass Spectrometry

ESI-MS experiments were performed with a methanol spray on a Finnigan LTQ FT mass spectrometer (Thermo) at the QB3/Chemistry Mass Spectrometry Facility (UCB). Aliquots of the 1:1 and 2:1 [L]/[V] samples were taken and diluted in methanol. The samples were injected directly via a syringe at a flow rate of 5 $\mu L\cdot min^{-1}$ with a spray voltage of 3.5 kV.

Results and discussion

Crystal structure of $Na[V(L)_2]\cdot 2H_2O$.

The asymmetric unit of $Na[V(L)_2]\cdot 2H_2O$ consists of a "bare" V^{5+} center bound to two fully deprotonated glutaroimide-dioxime ligands (L^{3-}), through one nitrogen and two oxygen atoms of each ligand, along with a sodium ion and two water molecules (Figure 3a). The binding of the ligands around the vanadium center results in a highly distorted octahedral coordination environment in the triclinic space group P-1 (Figure 3b). The bond lengths for the V-N bonds are 1.9557(8) and 1.9551(8) Å while those for the V-O bonds are 1.8667(8), 1.8741(7), 1.9039(6), and 1.9024(8) Å. The extended crystal structure can be considered as successive VL_2^- complexes bridged by sodium atoms *via* N(2) and N(5) to form a one dimensional chain. The chains are then linked *via* bridging water molecules (O(1W)) between the sodium atoms to form a ribbon (Figure 3c). The ribbons are connected by hydrogen bonding interactions between the water molecules and the ligands for O(1W)-O(3)*, O(1W)-N(3)*, O(2W)-O(2)*, and O(2W)-N(6)*, where the superscript * denotes symmetry related positions.

The V-O bond distances in $Na[V(L)_2]\cdot 2H_2O$ are within the range of V-O bond distances reported for other non-oxo V^{5+} compounds obtained from non-aqueous solutions (1.8 - 2.0 Å),[13] and much longer than those of the V=O double bonds (~ 1.6 Å).[10,12,13]

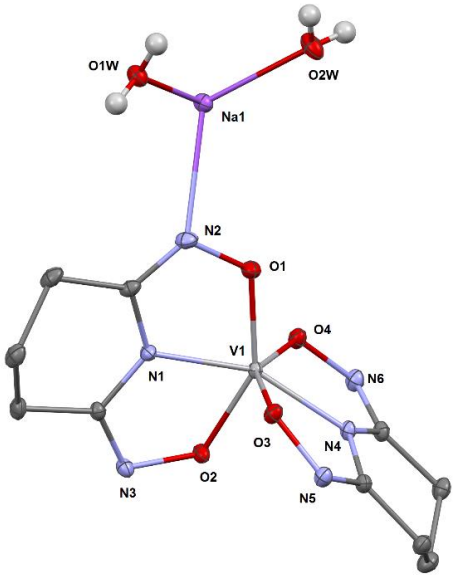

(a)

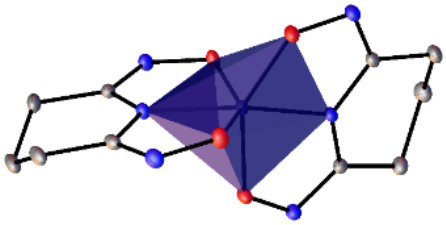

(b)

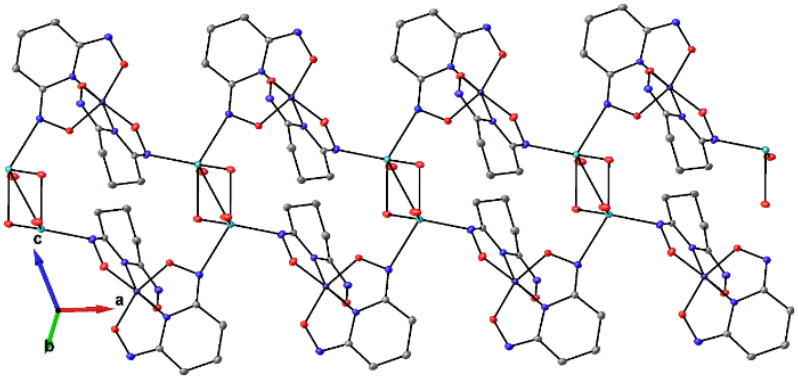

(c)

Figure 3. Crystal structure of the 1:2 vanadium/glutaroimide-dioxime complex, $Na[V(L)_2]\cdot 2H_2O$. (a) The asymmetric unit and numbering scheme, with the hydrogen atoms except those on water omitted for clarity; (b) the distorted octahedral environment around the vanadium atom; (c) the sodium ions bridge between the complexes to form a chain and the water molecules link the sodium ion to form a ribbon. Thermal ellipsoids are shown at the 50% probability level.

Table 1. Crystal structure data for $Na[L_2V]\cdot 2H_2O$ and $Na[(HL)VO_2]$

	$Na[L_2V]\cdot 2H_2O$	**$Na[(HL)VO_2]$**
Empirical formula	C10 H16 N6 Na O6 V	C5 H7 N3 Na O4 V
Formula weight	390.22	247.07
Temperature (K)	100(2)	100.15
Radiation	Synchrotron	MoKα
Wavelength (Å)	0.7749	0.71073
Crystal system	Triclinic	Monoclinic
Space group	P-1	P21/c
a (Å)	7.9375(3)	15.0543(8)
b (Å)	8.7365(4)	5.5070(3)
c (Å)	12.1972(5)	10.1794(5)
α (°)	102.684(2)	90.00
β (°)	107.187(2)	101.569(3)
γ (°)	103.796(2)	90.00
Volume ($Å^3$)	745.41(5)	826.77(7)
Z	2	4
ρ_{calc} (g/cm^3)	1.739	1.985
μ (mm^{-1})	0.931	1.242
F(000)	400	496.0
Crystal size	0.110 x 0.090 x 0.030 mm3	0.5 × 0.47 × 0.2
2θ range (°)	2.756 to 40.263	2.76 to 62.44
Index ranges	-13<=h<=13, -14<=k<=14, -20<=l<=20	$-21 \le h \le 17$, $-8 \le k \le 7$, $-11 \le l \le 14$
Reflections collected	13779	8438
Independent reflections	7062 [R(int) = 0.0192]	2662 [Rint = 0.0347]
Data / restraints / parameters	7062 / 0 / 281	2662/0/131
Goodness-of-fit on F2	1.034	0.963
Final R indices [I>2sigma(I)]	R1 = 0.0263, wR2 = 0.0707	R1 = 0.0330, wR2 = 0.0955
R indices (all data)	R1 = 0.0301, wR2 = 0.0729	R1 = 0.0485, wR2 = 0.1112
Largest diff. peak/hole ($e\cdot Å^{-3}$)	0.628 / -0.549	0.63/-0.56

Crystal structure of $Na[VO_2(HL)]$

The 1:1 V(V)/glutaroimide-dioxime complex (Figure 4) possesses a distorted square pyramidal structure with $\tau = 0.35$ in the monoclinic space group $P2_1/c$: a = 15.543(8) Å, b = 5.5070(3) Å, c = 10.1794(5) Å, $\alpha = 90.0°$, $\beta = 101.569(3)°$, and $\gamma = 90.0°$. The doubly deprotonated ligand (HL^{2-}) coordinates to the V center through a κ^3 binding motif via the imide N atom ($R_{V\text{-}N6}$ = 1.9885(17) Å) and the oxime O atoms ($R_{V\text{-}O2,\ V\text{-}O5}$ = 1.8931(14), 2.0054(13) Å). Notably, the 1:1 complex (Figure 3) is not a "bare" V^{5+} complex unlike the 1:2 complex (Figure 3). Instead, the 1:1 complex has the VO_2^+ moiety with two short oxo bonds (V-O3 and V-O14) with bond distances of 1.6781(15) and 1.6374(14) Å, respectively, which are typical of V=O double bonds. The ∠O3=V=O14 angle is 109.67°, close to that in a tetrahedral VO_4^{3-} species.

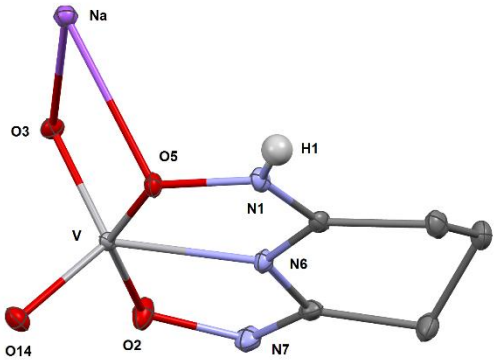

Figure 4. Crystal structure of the 1:1 vanadium/glutaroimide-dioxime complex, $Na[VO_2(HL)]$. Hydrogen atoms except H1 are omitted for clarity. Thermal ellipsoids are shown at the 50% probability level.

Multinuclear NMR

The successful synthesis of $Na[V(L)_2]\cdot 2H_2O$ shows that, using an oxo vanadate species as the starting material, a non-oxo V(V) complex with glutaroimide-dioxime can be synthesized and crystallized from aqueous solution. In other words, the glutaroimide-dioxime ligand can displace the oxo V=O bonds in vanadate and form a "bare" V^{5+} complex. In addition, the crystallization of $Na[VO_2(HL)]$ suggests that an intermediate 1:1 complex, in which the oxo V=O bonds in vanadate are only partially displaced by glutaroimide-dioxime, may also exist in aqueous solution. To verify the structure of the unusual non-oxo V^{5+} complex and demonstrate the stepwise displacement of the oxo V=O bonds in aqueous solutions, we hypothesized a reaction scheme (Scheme 1) and designed concurrent $^{51}V/^{17}O/^{1}H/^{13}C$ NMR experiments, coupled with ESI-MS, in ^{17}O-enriched H_2O to test the hypothesis. The 1:1 intermediate complex hypothesized in Scheme 1, $[V(O)(OH)L]^-$, has the same stoichiometry as $[VO_2(HL)]^-$ in the crystal structure (Figure 3), but differs in the location of one proton. In the crystal, the proton (H1) is located on the nitrogen (N1), probably due to the lattice interaction with Na^+. Nevertheless, whether the 1:1 complex is in the form of $[V(O)(OH)L]^-$ or $[VO_2(HL)]^-$ does not alter the validity of the discussions below.

^{51}V NMR (I = 7/2) is frequently used for structural characterization of V(V) complexes in solution due to its wide chemical shift range, high sensitivity, and high natural abundance.[23–25] On the other hand, oxygen-17, with I = 5/2, is an NMR-active isotope of oxygen with a very low natural abundance and low NMR sensitivity, so isotopic enrichment is usually necessary for its detection and study. Indirect scalar spin-spin coupling between ^{17}O and ^{51}V can also be observed by ^{17}O and ^{51}V NMR if both atoms are bound directly.[26,27]

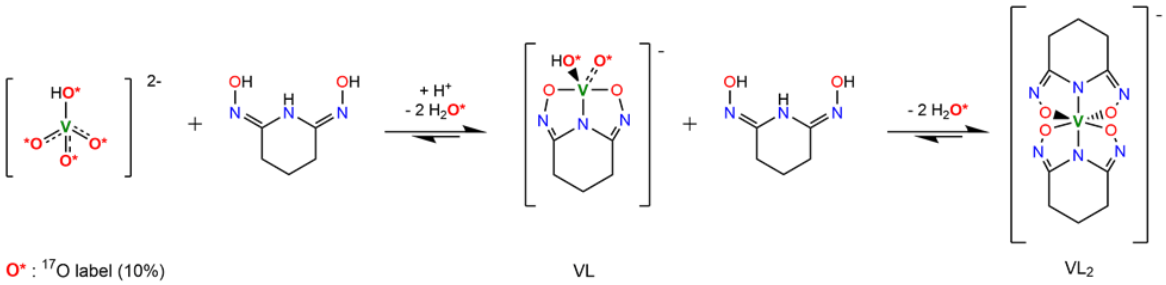

Scheme 1. Proposed reaction scheme of the formation of the non-oxido V^{5+} – glutaroimide-dioxime complex.

As shown in Scheme 1, starting with ^{17}O labelled vanadate in solution, the vanadate signal should show V-O coupling in both ^{17}O and ^{51}V NMR spectra. If the complexation reaction proceeds to the 1:2 complex as Scheme 1 suggests, no ^{17}O NMR signal(s) should be observed at the end when the $[V(L)_2]^-$ complex is the only vanadium species present. At this point, all of the V=^{17}O bonds of the starting vanadate would be displaced by the donor atoms of glutaroimide-dioxime and there would be no ^{17}O atoms in the $[V(L)_2]^-$ complex. Concurrently, the ^{51}V NMR signal for the vanadate (with V-O coupling) should disappear and a new ^{51}V NMR signal for the $[V(L)_2]^-$ complex with no V-O coupling would appear.

The ^{51}V/^{17}O NMR spectra of a series of solutions with [L]/[V] ratios ranging from 0 to 3 are shown in Figure 4. Additionally, the ^{51}V NMR spectrum of a D_2O solution of crystallized $Na[V(L)_2]\cdot 2H_2O$ was collected to help confirm the assignment of the vanadium signal and is also shown in Figure 4 (spectrum *e*). As Figure 4 shows, the ^{51}V NMR spectrum of the initial solution (*a*) in the absence of glutaroimide-dioxime shows the peaks for the vanadates (VO_4^{3-} and HVO_4^{2-}) at δ = -537, -561 ppm. The vanadate peak (♢) has broad shoulders indicating the spin-spin coupling with ^{17}O (see the inset for spectrum *a* in Figure 4). Concurrently, the ^{17}O NMR spectrum of the initial solution (*a*) shows a broad peak at ~ 560 ppm for the vanadate species (♢), with an apparent linewidth of 5250 Hz due to coupling with the spin-7/2 ^{51}V nucleus. These ^{17}O/^{51}V spin-spin coupling features agree with those reported for ^{17}O-labelled $NaVO_3$ in the literature.[27]

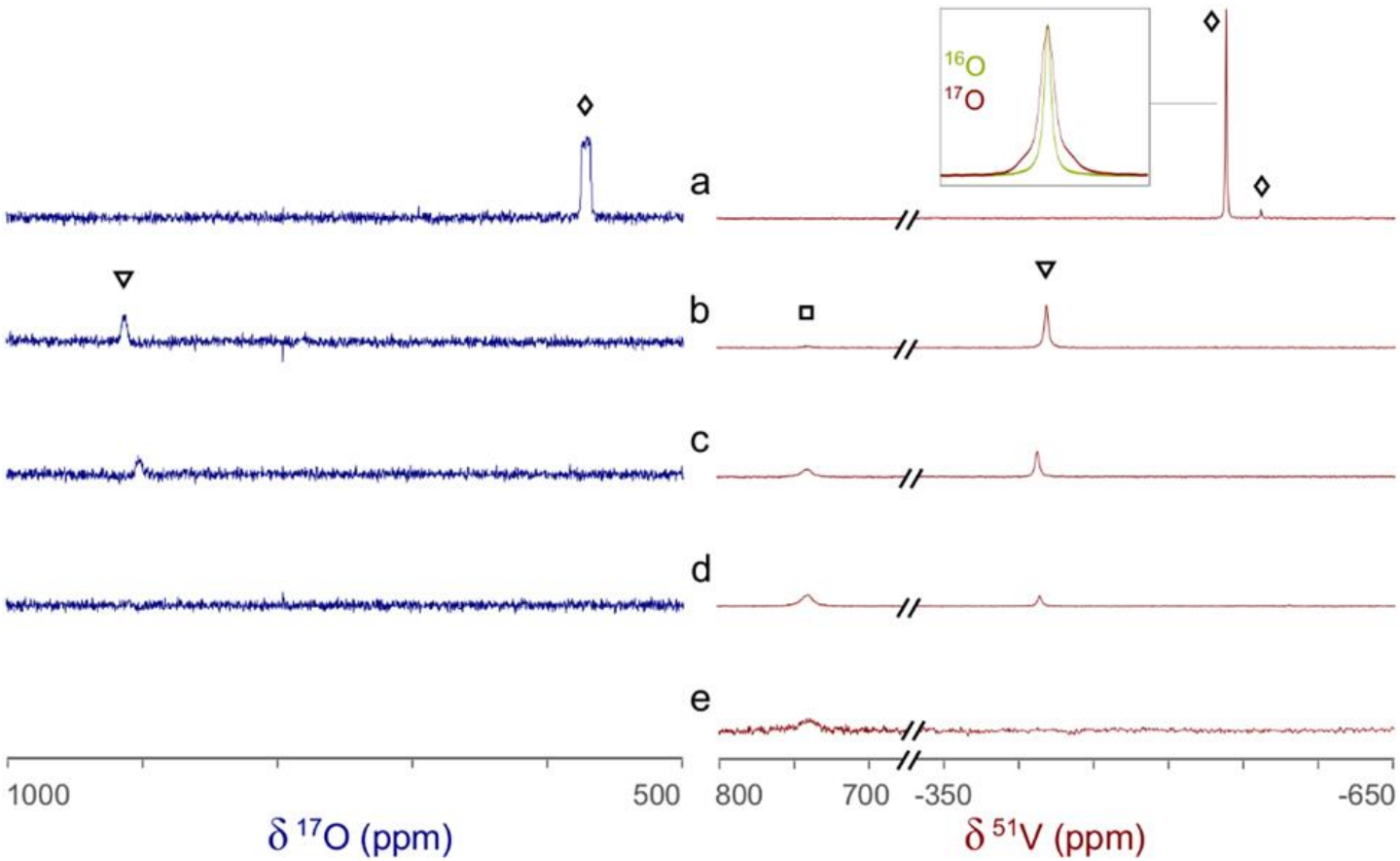

Figure 5. 51V and 17O NMR of L – vanadate mixtures demonstrating the formation of V(V)/glutaroimide-dioxime complexes in $H_2{}^{17}O$ via the displacement of oxo V=O bonds. Solutions: (*a*) vanadate only, no L; (*b*) 1:1 [L]/[V]; (*c*) 2:1 [L]/[V]; (*d*) 3:1 [L]/[V]; (*e*) $Na[V(L)_2]\cdot 2H_2O$. Peak assignments: (◊) VO_4^{3-}/HVO_4^{2-}; (▽) 1:1 V/L complex, $[V(O)(OH)L]^-$; (□) 1:2 V/L complex, $[VL_2]^-$. The inset on the ^{51}V spectrum *a* is an overlay of the ^{51}V peak in ^{17}O-enriched water and natural water showing the $^{17}O/^{51}V$ coupling. Detailed conditions of the solutions are provided in Table 2)

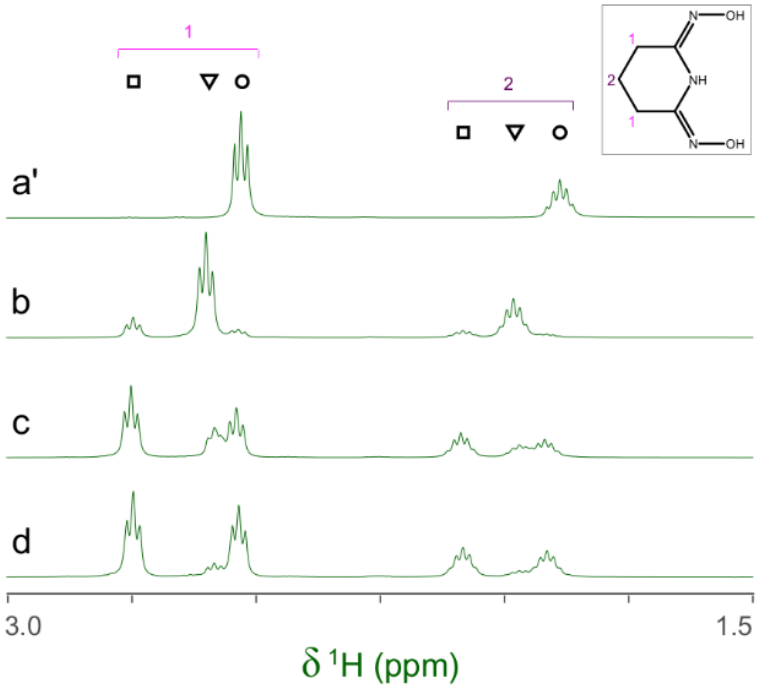

Figure 6. ^{1}H NMR spectra of the V(V)/glutaroimide-dioxime complexes. Solution labels: (*a*') glutaroimide-dioxime only; (*b*, *c*, *d*) identical to those in Figure 5.

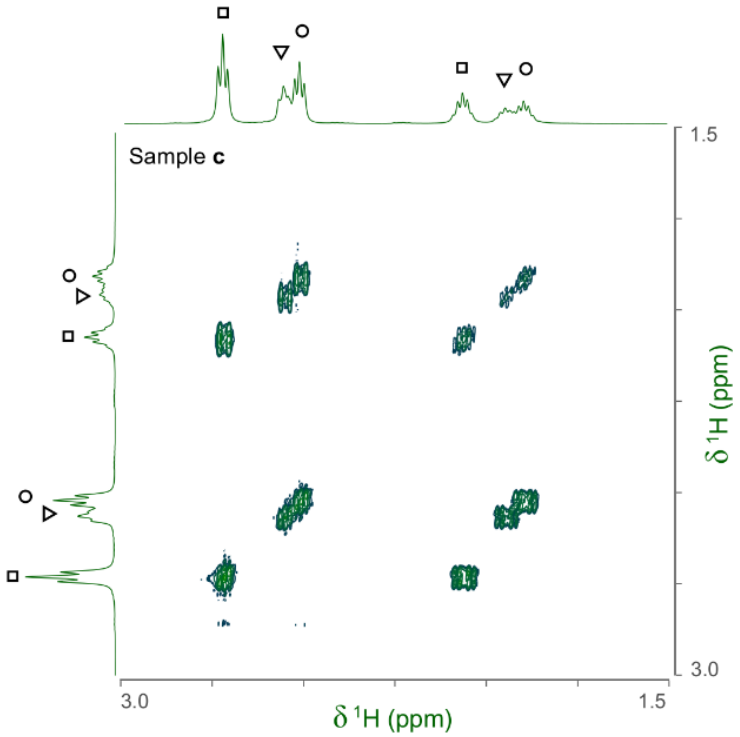

Figure 7. ^{1}H COSY NMR spectrum of solution *c* to confirm peak assignments and symmetry. ([L]/[V] = 2:1). Peak assignments: (○) free glutaroimide-dioxime ligand; (▽) 1:1 V/L complex, $[V(O)(OH)L]^{-}$; (□) 1:2 V/L complex, $[V(L)_2]^{-}$.

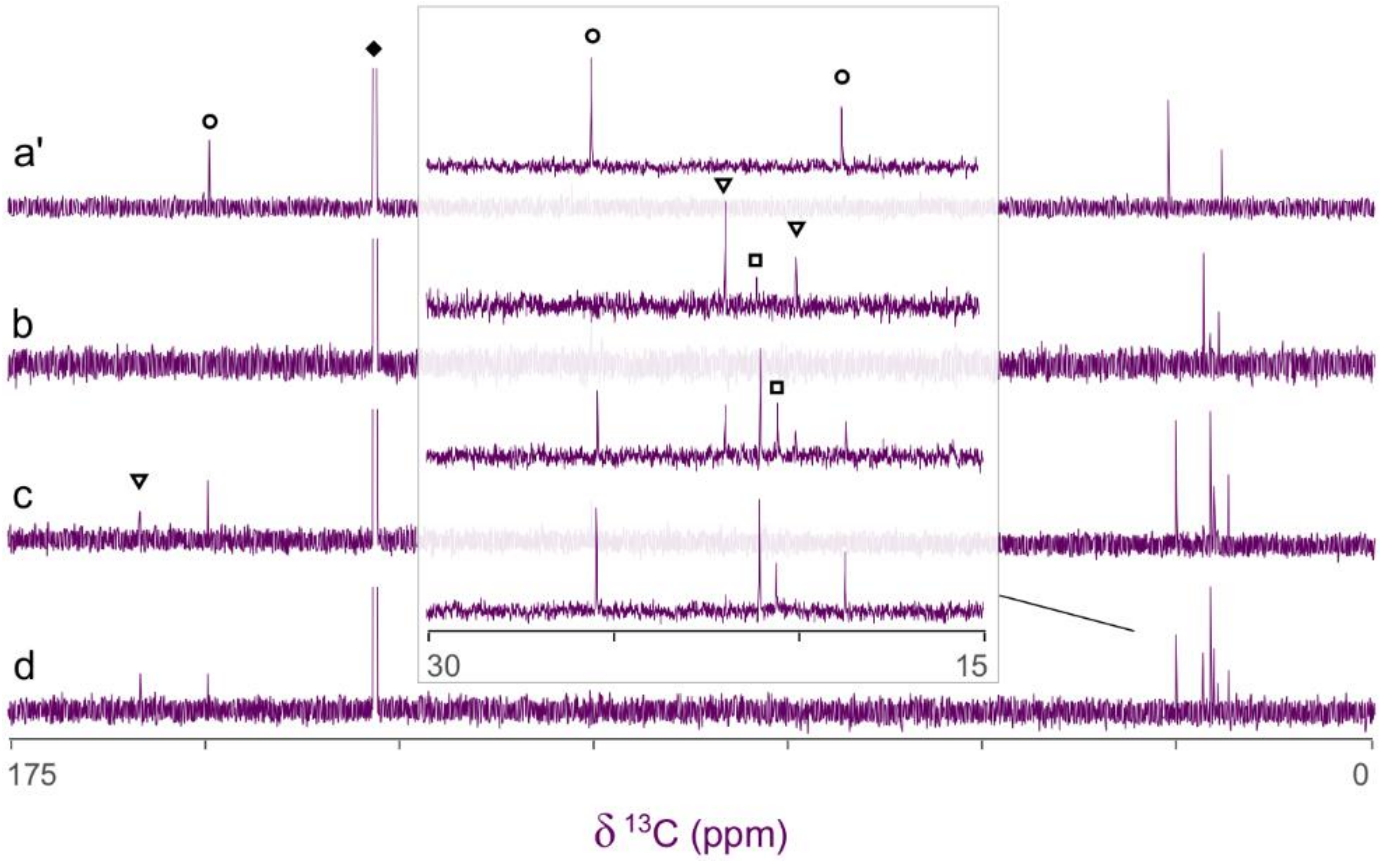

Figure 8. ^{13}C NMR spectra of L – vanadate mixtures in $H_2{}^{17}O$. Solution labels: (a') glutaroimide-dioxime ligand; (b) 1:1 [L]/[V]; (c) 2:1 [L]/[V]; (d) 3:1 [L]/[V]. Peak assignments: (○) free glutaroimide-dioxime ligand, (▽) 1:1 V/L complex, $[VL(O)(OH)]^-$, (□) 1:2 V/L complex, $[V(L)_2]^-$, (◆) external standard (C_6D_6).

Table 2. Concentrations of the solution samples for NMR experiments;
L stands for glutaroimide-dioxime.

Solution	NMR expts.	[V], mM	[L], mM	pH	Notes
a'	$^{1}H/^{13}C$	0	~15	12-13	in D_2O
a	$^{17}O/^{51}V$	14.8	0	12-13	in $H_2{}^{17}O$
b	$^{17}O/^{51}V/^{1}H/^{13}C$	14.8	14.8	7.5	in $H_2{}^{17}O$
c	$^{17}O/^{51}V/^{1}H/^{13}C$ /^{1}H COSY	14.8	29.6	8.5	in $H_2{}^{17}O$
d	$^{17}O/^{51}V/^{1}H/^{13}C$	14.8	44.4	8.7	in $H_2{}^{17}O$
e	^{51}V	~ 5	~ 10		D_2O solution of 1 mg $Na[V(L)_2]\cdot 2H_2O$

As different equivalents (1, 2, and 3) of glutaroimide-dioxime were added to the vanadate solution, both the ^{51}V and ^{17}O signals for vanadates (◊) disappeared. In addition, a new ^{51}V signal in the ^{51}V spectra began to appear at δ = -410 ppm (▽) and achieved maximum intensity at [L]/[V] = 1 (^{51}V spectrum b), diminished as [L]/[V] was increased to 2 (^{51}V spectrum c), and nearly disappeared as [L]/[V] was further increased to 3 (^{51}V spectrum d). Concurrently, a new peak appeared in the ^{17}O spectra around δ = 905 ppm (▽) and achieved maximum intensity at [L]/[V] = 1 (^{17}O spectrum b), diminished at [L]/[V] = 2 (^{17}O spectrum c), and completely disappeared at [L]/[V] = 3 (^{17}O spectrum d).

Based on the changes in the peak intensities with the increase of [L]/[V] and the occurrence of the maximum intensity at [L]/[V] = 1, it is reasonable to assign these peaks (▽) to a 1:1 intermediate complex, such as $[V(O)(OH)L]^-$, that is hypothesized in Scheme 1. The observation of the ^{17}O signal for the intermediate 1:1 V/L complex (▽) suggests that, in this complex, the glutaroimide-dioxime ligand only partially displaces the oxo V=O bond(s) from the initial ^{17}O-labelled vanadate, which is consistent with Scheme 1 and the crystal structure of the 1:1 complex, $Na[VO_2(HL)]$ (Figure 3). The ^{17}O chemical shifts for the 1:1 V/L complex at [L]/[V] = 1 (^{17}O spectrum b) and 2 (^{17}O spectrum c) were noted to be slightly different. The difference probably results from different degrees of protonation in the $[V(O)(OH)L]^-$ species due to slight differences in pH between the two solutions (pH 7.5 and 8.5 for [L]/[V] = 1 and 2, respectively).

Accompanying the appearance and disappearance of the peaks (▽) for the 1:1 V/L complex, a new and extremely shifted ^{51}V peak at δ = 740 ppm (□) appears at [L]/[V] = 1 (^{51}V spectrum b), intensifies at [L]/[V] =2 (^{51}V spectrum c), and achieves maximum intensity at [L]/[V] > 2 (^{51}V spectrum d). The chemical shift is identical to that of the ^{51}V peak in spectrum e for the solution of $Na[V(L)_2]\cdot 2H_2O$, implying that this peak (□) can be assigned to the 1:2 V/L complex, $[V(L)_2]^-$, hypothesized in Scheme 1. The ^{51}V peak for the 1:2 complex (spectra d and e, □) should not show $^{17}O/^{51}V$ spin-spin coupling features because the ligands in the 1:2 complex completely displace the oxo V=*O bonds of the initial ^{17}O- labelled vanadate. However, the large linewidth of the ^{51}V signal resulting from the low symmetry of the complex precludes the verification of the absence or presence of the coupling features for the ^{51}V NMR signal of the 1:2 (δ = 740 ppm) or 1:1 complex (δ = -410 ppm). However, the absence of NMR signals on the ^{17}O spectrum d clearly indicates that the 1:2 complex does not contain oxo $V=^{*}O$ bonds and is a "bare" V^{5+} complex.

The intensity of the ^{51}V NMR signal for the final complex at [L]/[V] > 2 remained unchanged beyond 12 days, which suggests that vanadium remained in the V(V) oxidation state in the solution at neutral to slightly alkaline pH. If reduction of V(V) to the paramagnetic V(IV) species were to occur, it would diminish and eventually "wash-out" the ^{51}V NMR signal. Further reduction to V(III) is very unlikely: V(III) is generally much less stable in aqueous solutions, and no signals were observed in the lower ^{51}V chemical shift range of below δ = -1000 ppm.[24,26]

$^{51}V/^{17}O$ NMR experiments in acidic solutions were not performed in this study because (1) $[V(L)_2]^-$ may not be the dominant and most stable complex in acidic regions and (2) preliminary experiments suggested that redox reactions could occur between V(V) and glutaroimide-dioxime in more acidic solutions. The stability of $[V(L)_2]^-$ in acidic solution is discussed in detail in Chapter 2 and the redox reactions between vanadium and the ligand are discussed in Chapter 3.

The ^1H and ^{13}C NMR spectra of the V(V)/glutaroimide-dioxime solutions used in the $^{17}O/^{51}V$ experiments (*b*, *c*, *d*, and *e*), as well as a solution of only glutaroimide-dioxime (*a*'), were also acquired. A ^1H COSY spectrum of solution *c* was also acquired to confirm the peak assignments. The ^1H NMR, ^1H COSY, and ^{13}C NMR spectra are shown in Figures 6-8.

The ^1H spectra of the V(V)/glutaroimide-dioxime solutions (*b*, *c*, and *d*) show two sets of signals at δ = 2.5 – 2.8 ppm and δ = 1.8 – 2.1 ppm, respectively. In each set, there are three signals (labelled as ○,▽, □) that were straight-forward to assign to the free glutaroimide-dioxime (○), the 1:1 V/L complex (▽), and the 1:2 V/L complex (□), respectively, based on the NMR spectrum of the pure ligand, the COSY spectrum, the spin-spin coupling patterns, and the intensity changes as a function of the [L]/[V] ratio. The signals for the 1:1 complex (▽) achieve maximum intensity at [L]/[V] = 1 (spectrum *b*) and diminish as [L]/[V] is increased to 2 and higher (spectra *c* and *d*), while the signals for the 1:2 complex (□) are weak at [L]/[V] = 1 (spectrum *b*), intensify as [L]/[V] is increased to 2 (spectrum *c*), and achieve a maximum at [L]/[V] > 2 (spectrum *d*). These observations support the proposed structures of the 1:1 and 1:2 V(V)/glutaroimide-dioxime complexes, corroborate the $^{17}O/^{51}V$ NMR data, and validate the hypothesized stepwise displacement of the oxo V=O bonds leading to the formation of the non-oxo $[VL_2]^-$ complex in aqueous solution.

Importantly, the ^1H spectra of the complexes showed that the equivalencies of the H atoms in the free ligand remain unchanged in the 1:1 and 1:2 complexes (Figure 5). In other words, the same number of ^1H resonances (two) with the same spin-spin coupling fine structures is observed for the complex and the free ligand, which agrees with the coordination modes of the ligand in the complexes hypothesized in Scheme 1 and confirms the structure of a non-oxido V^{5+}/glutaroimide-dioxime complex. The same analysis can be made with the ^{13}C NMR spectra (Figure 8).

To summarize, concurrent $^{51}V/^{17}O$ NMR experiments have unprecedentedly demonstrated that the displacement of oxo V=O bonds in vanadates by glutaroimide-dioxime leads to the formation of a non-oxo V^{5+} complex in aqueous solution. The ^{51}V chemical shift of the complex is identical to that of the solution of $Na[V(L)_2]\cdot 2H_2O$, suggesting that the complex in solution is probably $[V(L)_2]^-$. ^1H and ^{13}C NMR spectra are also consistent with these species and high symmetry in solution. Further verification of the stoichiometry was also achieved by ESI-MS, described below.

ESI-MS

The negative mode ESI-MS spectra for two aqueous solutions (^{17}O-enriched H_2O: 10% ^{17}O; ≥ 25% ^{18}O; balance ^{16}O) with [L]/[V] = 1 and 2 are shown in Figure 9. Both spectra were obtained by diluting the solutions with ethanol/natural water (90/10 volume ratio) and directly spraying in the instrument. The spectrum of the solution with [L]/[V] = 1 (upper spectrum) shows a main peaks at *m/z* = 238.00, which corresponds to the methoxide adduct of the 1:1 $[V(O)(OH)L]^-$ complex, $[V(O)(OCH_3)L]^-$ (calculated mass = 238.00) proposed in Scheme 1. Methoxide $(OCH_3)^-$ from the electrospray solvent substituted the hydroxide (OH^-) of the $[V(O)(OH)L]^-$ complex during the dilution and/or electrospray process. The solution with [L]/[V] = 3 (lower spectrum) shows a single peak with *m/z* = 331.04 corresponding to $[V(L)_2]^-$ (calculated mass of 331.04), confirming the formation of the 1:2 V/L complex.

According to the manufacturer's specifications, the 10% ^{17}O-enriched water also contains at least 25% ^{18}O (see Experimental section for more details). Consequently, the initial vanadate (Scheme 1) was actually labelled with ^{17}O as well as ^{18}O with the latter in significantly larger amounts. Therefore, unnatural isotopic patterns, particularly a large (*m* +2) peak corresponding to an isotopologue containing one ^{18}O, should be observed if the vanadium complex still contains an oxo V=*O bond from the vanadate and, more importantly, the (*m* +2) peak should be absent if all oxo V=*O bonds of the vanadate are displaced by the glutaroimide-dioxime ligand. This is indeed what is observed in both spectra. Notably, the base peak of the mixture with the higher [L]/[V] ratio (Figure 8, lower spectrum) at *m/z* = 331.04 does not show the unnatural (*m* + 2) isotopic pattern that could indicate the presence of one ^{18}O atom (or two ^{17}O atoms with a much lower probability) in the 1:2 complex. This is because all of the oxo V=*O bonds of the initial $^{17,18}O$-labelled vanadate are displaced by the ligands to form the non-oxo 1:2 V(V)/glutaroimide-dioxime complex in solution. The presence of a small (*m* +1) peak at *m/z* = 331.8 is in accord with the natural $^{13}C/^{15}N$ abundances.

In contrast, the base peaks for the 1:1 complex $[V(O)(OCH_3)L]^-$ shows an unnatural (*m* + 2) peak at 240.01, corresponding to the presence of one ^{18}O atom in the complex. The presence of the (*m* + 2) peak indicates incomplete displacement of the oxo V=*O bonds of the initial $^{17,18}O$-labelled vanadate in the intermediate 1:1 complex, in agreement with Scheme 1. It should be remarked that, for the 1:1 complex, the intensities of the (*m* + 1) peaks include the contributions from the natural $^{13}C/^{15}N$ abundances, and the additional contribution from the isotopologue containing one ^{17}O atom.

The methoxide adduct $[V(O)(OCH_3)L]^-$ results from facile substitution of OH^- by methoxide in methanol. This is consistent with the existence of the 1:1 V(V)/glutaroimide-dioxime complex as $[V(O)(OH)L]^-$ in aqueous solution as hypothesized in Scheme 1, not as $[VO_2(HL)]^-$ observed in solid. The exact mechanism of substitution is unclear, but it is reasonable to assume that, energetically and kinetically, substitution of a V=O bond in $[VO_2(HL)]^-$ is less favorable than that of a V-OH bond in $[V(O)(OH)L]^-$.

To summarize, all of the ESI-MS data have validated the hypothesized reaction scheme (Scheme 1) and confirmed the formation of the 1:2 non-oxo V^{5+}/glutaroimide-dioxime complex, $[V(L)_2]^-$, in aqueous solution *via* the displacement of the oxo V=*O bonds. The presence of an intermediate 1:1 complex that still contains oxo V=O bonds, $[V(O)(OH)L]^-$, in solution has also been confirmed.

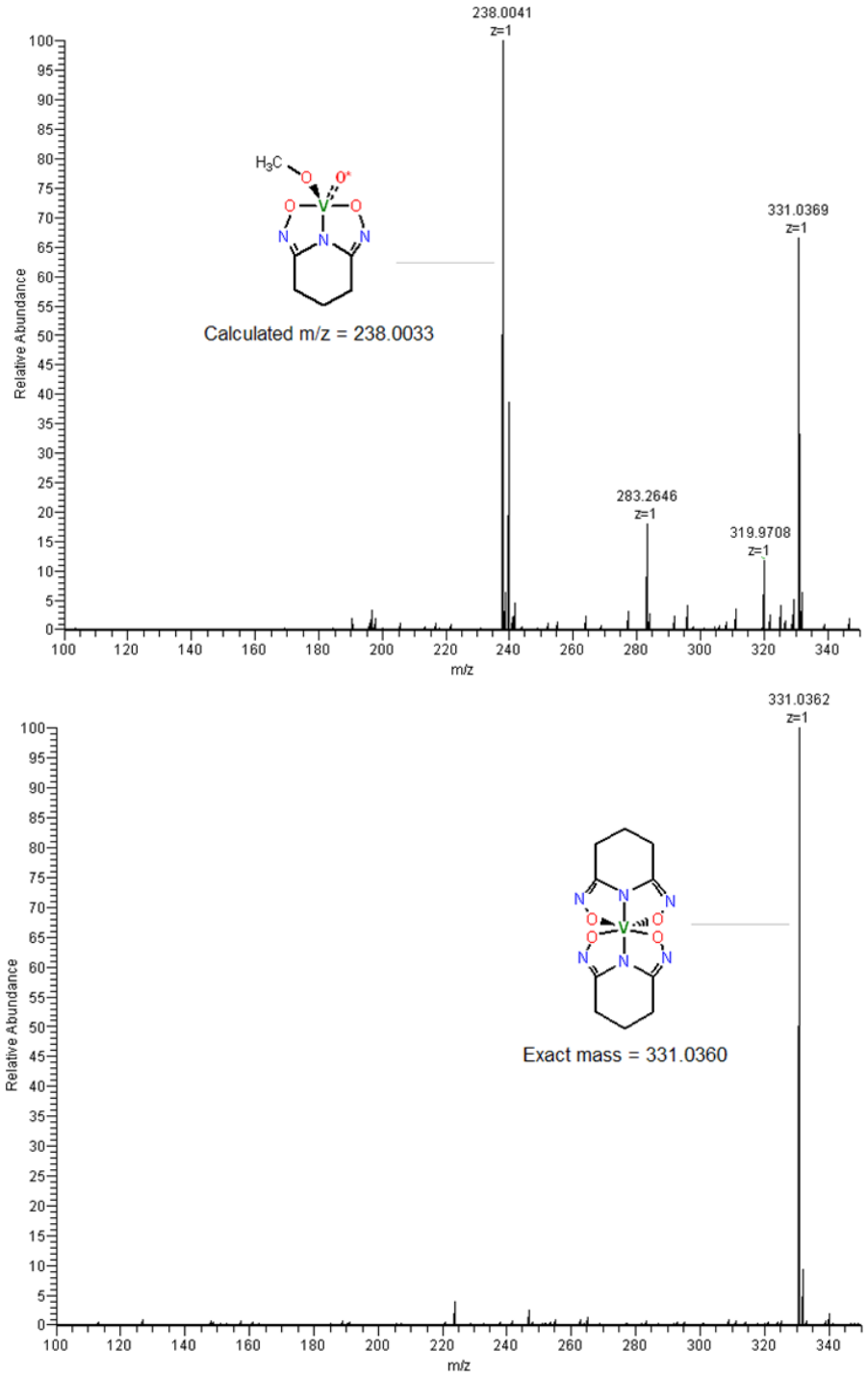

Figure 9. Negative mode ESI-MS spectra of V(V)/glutaroimide-dioxime complexes in ^{17,18}O-enriched H_2O (10% ^{17}O; ≥ 25% ^{18}O, balance ^{16}O), diluted and sprayed in methanol. (Upper) [L]/[V] = 1; (lower) [L]/[V] = 3. The (*m* + 2) peaks in the upper spectrum indicate one ^{18}O atom and retention of an oxo V=*O bond in the 1:1 complex; the lower spectrum confirms elimination of all V=*O bonds in the 1:2 complex.

Structural insights

As previously mentioned, the sorption of V(V) to poly(amidoxime) sorbents in marine tests was much higher than that of Fe(III) and U(VI). Useful structural insights into the higher sorption of V(V) can be gained by comparing the structural parameters and coordination modes of the glutaroimide-dioxime complexes with V(V), Fe(III), and U(VI), as shown in Table 3. Both $Na[V(L)_2]\cdot 2H_2O$ and $Fe(H_2L)(HL)\cdot 8H_2O$ are non-oxo metal (V^{5+} or Fe^{3+}) complexes in distorted octahedral environments with similar O-V-N and O-Fe-N bond angles of approximately 73-75°. The average bond distances of V-O and V-N in $Na[V(L)_2]\cdot 2H_2O$ are 1.8868 Å, and 1.9554 Å, respectively, and are shorter than those of Fe-O and Fe-N in $Fe(H_2L)(HL)\cdot 8H_2O$ by 0.16 Å and 0.06 Å, respectively. Taking into consideration that the ionic radii for V(V) (0.54 Å) and low spin Fe(III) (0.55 Å) are nearly identical,[28] these structure data indicate that V^{5+} forms a stronger complex with glutaroimide- dioxime than Fe^{3+}. The formation of stronger V^{5+} complexes is most probably responsible for the higher sorption of V(V) than Fe(III) by poly(amidoxime) sorbents.

The structure of the $UO_2(H_2L)(H_2L)\cdot H_2O$ complex is very different from those of $Na[V(L)_2]\cdot 2H_2O$ and $Fe(H_2L)(HL)\cdot 8H_2O$. In the U(VI) complex, the UO_2^{2+} moiety maintains its linear di- oxo configuration and the two ligands coordinate to U *via* its equatorial plane. Evidently, glutaroimide-dioxime is not sufficiently strong to displace the oxo U=O bonds to form a "bare" U^{6+} complex in aqueous solutions. However, it is interesting to note that the existence of a non-oxo U^{5+}/U^{4+} couple was reported in the aqueous solutions of redox systems containing the unsaturated polyoxometalate anions α-$[P_2W_{18}O_{62}]^{6-}$, $P_2W_{17}O_{61}^{10-}$, and $SiW_{11}O_{39}^{8-}$.[29,30] It is probably the strong binding ability of unsaturated heteropolyoxometalates as well as slow kinetics of formation of the U=O bonds (from U^{5+} to UO_2^{+}) that results in the existence of a non-oxo U^{5+} complex in aqueous solutions containing the U^{5+}/U^{4+} couple.

The degree of deprotonation of glutaroimide-dioxime (as H_3L) in the three complexes decreases in the order: V(V) > Fe(III) > U(VI). In $Na[V(L)_2]\cdot 2H_2O$, both ligands are triply deprotonated whereas in $Fe(H_2L)(HL)\cdot 8H_2O$, one ligand is doubly deprotonated and the other is singly deprotonated. Lastly, in $UO_2(H_2L)(H_2L)\cdot H_2O$, both ligands are singly deprotonated. The trend in the degree of deprotonation actually parallels that in the strength of complexation. Vanadium(V), in the form of the "bare" V^{5+} ion, undoubtedly forms the strongest complex with glutaroimide-dioxime in which complete deprotonation of the ligand is facilitated.

In summary, the extremely strong sorption of V(V) by the poly(amidoxime) sorbents is probably due to the formation of the very stable non-oxo V^{5+} complex with glutaroimide-dioxime. To improve the selectivity of the sorbent for U(VI) over V(V), an ideal ligand would be the one(s) with a binding ability that is sufficiently high for U(VI) but not high enough to displace the oxo V=O bond(s) in the V(V) species. Starting with the cyclic glutaroimide-dioxime platform, adding electron- withdrawing groups to the platform could reduce the basicity of the imide and oxime groups and "fine-tune" the binding ability of the ligand(s).

Table 3. Geometry and bond distances (Å) in $Na[V(L)_2]\cdot 2H_2O$ compared with $Fe(H_2L)(HL)\cdot 8H_2O$ and (III) $UO_2(H_2L)(H_2L)\cdot H_2O$.

	V(V)	Fe(III)[9]	U(VI)[8]
	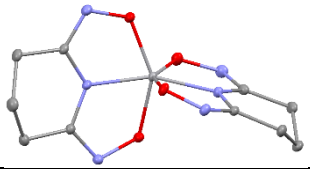		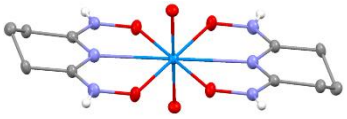
M-O	1.8667(8), 1.8741(7), 1.9039(6), 1.9024(8)	2.0465(11), 2.0569(12), 2.0268(11), 2.0692(11)	2.535(3), 2.535(3), 2.429(3), 2.429(3), 1.785(3), 1.785(3)
M-N	1.9557(8), 1.9551(8)	2.0298(13), 2.0035(13)	2.563(3), 2.563(3)

It should be noted that, in addition to helping improve the extraction of uranium from seawater, the structural information of the non-oxo V^{5+} complex in aqueous solution could help to understand and develop vanadium compounds that mimic the effects of insulin in the treatment of diabetes. It is known that vanadium plays very important roles in biological systems[18,31,32] and that some V(V) organic complexes, such as the oxo-V(V) complex with dipicolinic acid (2,6-pyridinedicarboxylic acid, *dpa*), $VO_2(dpa)^-$, have been developed as organic V(V) insulin mimetic compounds[10]. Continuing efforts are underway to identify more efficacious organic V(V) complexes, which tend to be less toxic than inorganic V(V) complexes such as vanadate. These complexes should be stable and fairly soluble in both aqueous and organic solutions and should remain intact at physiological pH (around 7.4). In fact, being extremely stable and highly soluble in aqueous solutions at neutral pH, the non-oxo V^{5+} complex with glutaroimide-dioxime from this study seems to meet the above criteria and deserves further studies on possible application in biological systems.

Summary and conclusions

A rare, non-oxo V(V) complex with glutaroimide-dioxime (H_3L), $Na[V(L)_2]\cdot 2H_2O$, was crystallized from aqueous solution and characterized via x-ray diffraction. The complex was found to contain two fully deprotonated L^{3-} ligands bound to the bare V^{5+} cation *via* two oxime oxygens and the imide nitrogen. An intermediate complex, $Na[VO_2(HL)]$, was also isolated and found to contain the typical VO_2^+ moiety present in many V(V) complexes. Further characterization using ^{51}V, ^{17}O, ^{1}H, and ^{13}C NMR spectroscopy unprecedentedly demonstrated the stepwise displacement of the oxo oxygens to form the bare V(V)-glutaroimide-dioxime complex. ESI-MS studies of V(V)-glutaroimide-dioxime solutions allowed the identification the intermediate 1:1 M:L complex as well as the bare $V(L)_2$ complex at m/z = 331.0.

Structural insights into the much higher sorption of V(V) to amidoxime-based sorbents relative to U(VI) and Fe(III) were gained by comparing the structural parameters of the V(V)-glutaroimide-dioxime complex with the analogous U(VI)- and Fe(III)-glutaroimide-dioxime complexes. For these complexes, the degree of protonation of the ligand was found to decrease from U(VI) to V(V). In conjunction with the substantially shorter bond lengths observed for the V(V) complex relative to the other complexes, this implies stronger bonding in the V(V) complex and higher thermodynamic stability. In fact, the trend in binding strengths parallels the observed trend in sorption of these cations to poly(amidoxime) sorbents in marine tests.

Lastly, as there are ongoing studies to synthesize vanadium(V) compounds suitable for the treatment of diabetes, the structural studies with glutaroimide-dioxime are useful for aiding the development of new, highly stable organic V(V) compounds. In fact, the high solubility of $Na[V(L)_2]\cdot 2H_2O$ in aqueous and ethanol solutions coupled with its stability at neutral pH could make it a potential candidate for study in bioinorganic vanadium studies such as for diabetic treatments.

References

(1) Tamada, M.; Seko, N.; Kasai, N.; Shimizu, T. Cost Estimation of Uranium Recovery from Seawater with System of Braid Type Adsorbent. *Transactions of the Atomic Energy Society of Japan*, 2006, *5*, 358–363.

(2) Kim, J.; Tsouris, C.; Oyola, Y.; Janke, C. J.; Mayes, R. T.; Dai, S.; Gill, G.; Kuo, L. J.; Wood, J.; Choe, K. Y.; Schneider, E.; Lindner, H. *Ind. Eng. Chem. Res.* **2014**, *53*, 6076–6083.

(3) Wang, D.; Sañudo Wilhelmy, S. a. *Mar. Chem.* **2009**, *117*, 52–58.

(4) Gill, G. A.; Kuo, L.-J.; Janke, C. J.; Park, J.; Jeters, R. T.; Bonheyo, G. T.; Pan, H.-B.; Wai, C.; Khangaonkar, T.; Bianucci, L.; Wood, J. R.; Warner, M. G.; Peterson, S.; Abrecht, D. G.; Mayes, R. T.; Tsouris, C.; Oyola, Y.; Strivens, J. E.; Schlafer, N. J.; Addleman, R. S.; Chouyyok, W.; Das, S.; Kim, J.; Buesseler, K.; Breier, C.; D'Alessandro, E. *Ind. Eng. Chem. Res.* **2016**, *55*, 4264–4277.

(5) Turekian, K. K. *Oceans*; Prentice-Hall: Englewood Cliffs, N. J., 1968.

(6) Kim, J.; Tsouris, C.; Mayes, R. T.; Oyola, Y.; Saito, T.; Janke, C. J.; Dai, S.; Schneider, E.; Sachde, D. *Sep. Sci. Technol.* **2013**, *48*, 367–387.

(7) Vukovic, S.; Watson, L. a; Kang, S. O.; Custelcean, R.; Hay, B. P. *Inorg. Chem.* **2012**, *51*, 3855–3859.

(8) Tian, G.; Teat, S. J.; Zhang, Z.; Rao, L. *Dalton Trans.* **2012**, *41*, 11579.

(9) Sun, X.; Xu, C.; Tian, G.; Rao, L. *Dalton Trans.* **2013**, *42*, 14621–14627.

(10) Crans, D. C.; Mahroof-Tahir, M.; Johnson, M. D.; Wilkins, P. C.; Yang, L.; Robbins, K.; Johnson, A.; Alfano, J. A.; Godzala, M. E.; Austin, L. T.; Willsky, G. R. *Inorganica Chim. Acta* **2003**, *356*, 365–378.

(11) Hoard, J. L.; Scheidt, W. R.; Countryman, R. *J. Am. Chem. Soc.* **1971**, *93*, 3878–3882.

(12) Kelley, S. P.; Barber, P. S.; Mullins, P. H. K.; Rogers, R. D. *Chem. Commun.* **2014**, *50*, 12504–12507.

(13) Allen, F. H. *Acta Crystallogr. Sect. B Struct. Sci.* **2002**, *58*, 380–388.

(14) Morgenstern, B.; Kutzky, B.; Neis, C.; Stucky, S.; Hegetschweiler, K.; Garribba, E.; Micera, G. *Inorg. Chem.* **2007**, *46*, 3903–3915.

(15) Carrondo, M. A. A. F. de C. T.; Duarte, M. T. L. S.; Fraústo da Silva, J. J. R.; da Silva, J. A. L. *Struct. Chem.* **1992**, *3*, 113–119.

(16) Cooper, S. R.; Koh, Y. B.; Raymond, K. N. *J. Am. Chem. Soc.* **1982**, *104*, 5092–5102.

(17) da Silva, J. A. L.; Fraústo da Silva, J. J. R.; Pombeiro, A. J. L. *Coord. Chem. Rev.* **2013**, *257*, 2388–2400.

(18) Smith, P. D.; Berry, R. E.; Harben, S. M.; Beddoes, R. L.; Helliwell, M.; Collison, D.; Garner, C. D. *J. Chem. Soc. Dalt. Trans.* **1997**, 4509–4516.

(19) Buglyó, P.; Culeddu, N.; Kiss, T.; Micera, G.; Sanna, D. *J. Inorg. Biochem.* **1995**, *60*, 45–59.

(20) Leggett, C. J.; Rao, L. *Polyhedron* **2015**, *95*, 54–59.

(21) Bruker Analytical X-ray Systems Inc. Bruker Apex 2, 2003.

(22) Sheldrick, G. M. *Acta Crystallogr. Sect. A Found. Crystallogr.* **2015**, *71*, 3–8.

(23) Heath, E.; Howarth, O. W. *J. Chem. Soc. Dalt. Trans.* **1981**, 1105.

(24) Howarth, O. W. *Prog. Nucl. Magn. Reson. Spectrosc.* **1990**, *22*, 453–485.

(25) Gresser, M. J.; Tracey, A. S. *J. Am. Chem. Soc.* **1985**, *107*, 4215–4220.

(26) Figgis, B. N.; Kidd, R. G.; Nyholm, R. S. *Proc. R. Soc. A Math. Phys. Eng. Sci.* **1962**, *269*, 469–480.
(27) Lutz, O.; Nepple, W.; Nolle, A. *Zeitschrift für Naturforsch. A* **1976**, *31*, 3–7.
(28) Shannon, R. D. *Acta Crystallogr. Sect. A* **1976**, *32*, 751–767.
(29) Chiang, M. H.; Soderholm, L.; Antonio, M. R. *Eur. J. Inorg. Chem.* **2003**, 2929–2936.
(30) Shilov, V. P.; Yusov, A. B.; Fedoseev, A. M.; Moisy, P. *Radiochemistry* **2008**, *50*, 455–459.
(31) Sigel, A.; Sigel, H. *Metal Ions in Biological Systems: Volume 31: Vanadium and its Role for Life*; CRC Press: Boca Raton, FL, 1995.
(32) *Metal Sites in Proteins and Models*; Hill, H.A.O., Sadler, P.J., Thomson, A. J., Ed.; Springer-Verlag Berlin Heidelberg, 1997.

Chapter 3

Kinetic studies of glutaroimide-dioxime binding to V(V), U(VI), and Fe(III)

Introduction

One of the major challenges with current amidoxime-functionalized polymer adsorbents is the relatively low selectivity of these functional groups for uranium over other metals, vanadium and iron in particular. For example, 56-day marine tests have shown that the relative abundance of metal elements absorbed by amidoxime-functionalized polymer adsorbents (in molar percent) follows the order: vanadium (14.9%) >> iron (1.6%) > uranium (1.0%), though the concentrations of the three elements in seawater are comparable.[1] To understand the sorption behavior of uranium and other elements and help to improve the efficiency and selectivity of amidoxime-functionalized adsorbents for the recovery of uranium from seawater, both thermodynamic and kinetic studies of the interactions between amidoxime and the key metals are necessary. Recently, a number of systematic thermodynamic and structural studies on the complexation of amidoxime-related ligands with U(VI), Fe(III), and V(V) have been reported, forming complexes with both 1:1 and 1:2 metal/ligand ratios as shown in Scheme 1.[2–8] The binding strength of the ligand toward the metal ions follows the trend V(V) > Fe(III) > U(VI), in agreement with the order of adsorption of these elements in marine tests.[1] The structures of the complexes have been identified both in aqueous solution as well as in isolated molecular complexes using a combination of characterization techniques including X-ray crystallography, X-ray absorption, and multi-nuclear NMR spectroscopy.[5–7,9] The data on the complexation of **L** with V(V) are especially enlightening; vanadium actually forms a rare non-oxido V(V) complex with glutaroimide-dioxime, **2**, in the solid state as well as in aqueous solution,[5] which provides convincing interpretation for the much stronger adsorption of vanadium than uranium and iron in marine tests (see Chapter 1).

In contrast to the number of thermodynamic studies, there have been no kinetic studies performed to determine the rates of complexation reactions between **L** and U(VI), Fe(III) and V(V). To fill in this gap and help optimize the performance of the sorption process, kinetic data on these complexation reactions were obtained and compared among the key elements in the present study. The kinetics of the formation of V(V) complex **2** is of particular interest because it requires the removal of the oxido V=O bonds in vanadate so that it is expected to be slower than the formation of V(V) complex **1**, U(VI) complexes **3** and **4**, and Fe(III) complexes **5** and **6** where no such oxido bonds need to break. As shown in Scheme 1, the formation of 1:2 complexes **2**, **4**, and **6** all occur stepwise, with the formation of the 1:1 complexes **1**, **3**, and **5** as intermediates, respectively. The relative rates of formation and speciation determine whether or not **1**, **3**, and **5** can be observed or isolated. Anticipating drastic differences in the rates of complexation reactions shown in Scheme 1, we have selected two spectroscopic techniques applicable to reactions with two drastically different time scales in the present study: stopped-flow absorption spectroscopy for fast reactions taking place over seconds and conventional absorption spectroscopy for slow reactions taking hours to days.

The contents of this chapter have been previously published in **"Kinetics of complexation of V(V), U(VI), and Fe(III) with glutaroimide-dioxime: studies by stopped-flow and conventional absorption spectroscopy"**; Bernard F. Parker, Zhicheng Zhang, Christina J. Leggett, John Arnold, Linfeng Rao; *Dalton Transactions***,** 2017**,** DOI: 10.1039/C7DT01597F.

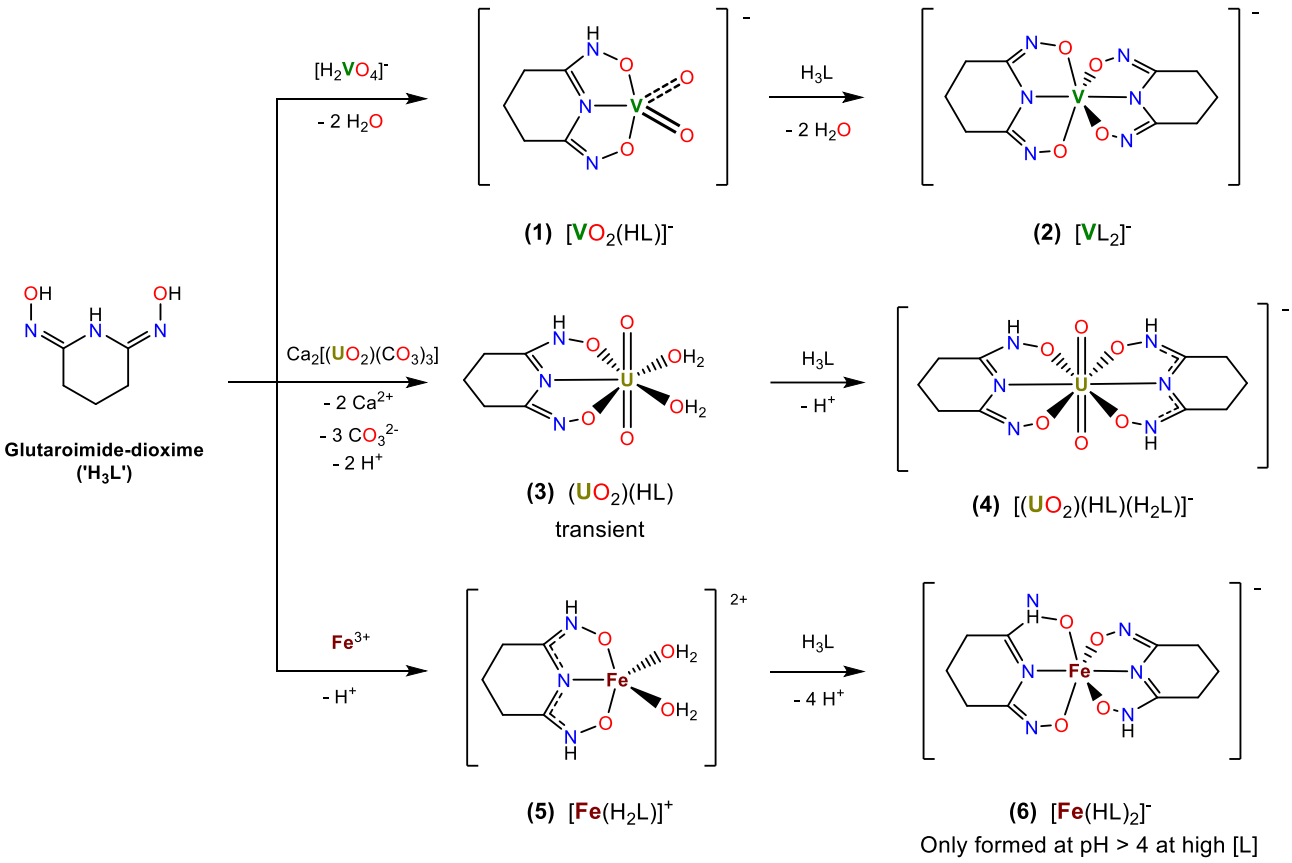

Scheme 1. Metal complexation reactions of glutaroimide-dioxime explored in this study.

Stopped-flow kinetic experiments coupled with a detection technique can be used to monitor reactions that occur on the millisecond to second timescale. Two reagent solutions are rapidly mixed, and fast spectroscopic techniques monitor the reaction mixture at regular intervals. This is a fairly common technique in analytical biochemistry since many processes occur on this scale, including but not limited to metal binding to proteins and other biomolecules, and enzyme-substrate interactions.[10] Species are generally quantified by fluorescence or optical absorbance, the latter of which we have used in our study. Redox reactions of metals are also commonly investigated, due to ease of monitoring their characteristic absorbances and timescales that are often suitable for stopped-flow techniques.[11,12]

The slow reaction of the formation of complex **2**, occurring in a time span from hours to days, was monitored by techniques including conventional UV-Visible spectroscopy and NMR experiments. ^{51}V NMR chemical shifts of all common vanadium species have been reported by Howarth and others, and the spectra are generally quantitative which allows detailed speciation studies.[13,14] Using these techniques in tandem, a much more complete picture of the vanadium-ligand interactions is obtained than by any one technique alone.

In the present study, the experimental conditions were optimized to attempt to obtain the rate of only one reaction for each metal ion, ideally with only one dominant protonation state to enable accurate and reproducible conversion of absorbance to concentrations. This allows us to propose the most reasonable mechanisms for the complexation reactions. Because

pseudo first-order reaction conditions are difficult to maintain in these systems, initial rates are always used in the analysis of the kinetic data.[15] It should be noted that, although all the above attempts have been made, explicit and complete rate equations were not determined in this study due to the complexity of the reaction systems, particularly with respect to $[H^+]$ and changing metal speciation. However, definitive reaction orders with respect to the metal ion and the ligand were derived and data of the rates of complexation were obtained that allowed a meaningful comparison of the kinetics among V(V), U(VI), and Fe (III) systems.

Experimental

Chemicals

Glutaroimide-dioxime was prepared according to literature procedure and recrystallized twice from methanol before use.[5] All other chemicals were obtained from commercial sources and used as received. Milli-Q water was used to prepare all solutions. Vanadium solutions were prepared by dissolving sodium orthovanadate (99.99%) in water. Iron solutions were prepared by dissolving $FeCl_3 \cdot xH_2O$ in dilute HCl, followed by titration with EDTA using salicyldehyde as a complexometric indicator. The Ca/Mg-U(VI)-triscarbonato solutions were prepared by appropriate dilutions of a standardized stock solution of U(VI) (C_U = 0.246 M) with added $CaCl_2$, $MgCl_2$, $NaHCO_3$, and NaCl as appropriate.

All experiments were performed at room temperature (21 - 23°C). No particular attempts were made to control the ionic strength. The ionic strength would vary with the acidity of the system due to different degree of ionization of reactants (e.g., vanadate and L). However, except for the NMR experiments where higher concentrations of reactants (up to 18 mM) were used, the concentrations of metal ions and the ligand are from 0.2 to 0.5 mM and the concentrations of other reactants (carbonate, Ca(II), Mg(II), etc.) are in a few mM range. By a rough estimation, the ionic strength of the reaction systems in the stopped-flow and conventional spectroscopic experiments was below 0.05 M.

Stopped-flow kinetic experiments

Stopped-flow experiments were performed on a computer-controlled OLIS RSM-1000 Stopped-Flow Spectrometer. Two reactant solutions (typically one containing the metal ion and the other the ligand) are loaded into two syringes, driven by pneumatic pistons, and rapidly mixed in the mixer that is specially designed to achieve > 99% mixing for liquids with normal viscosity within a millisecond. The OLIS RSM-1000 allows the collection of absorption spectra (or fluorescence spectra) of the reaction mixture at certain time intervals (as short as one millisecond) for a certain period of time, making it suitable for studying the kinetics of complexation reactions that usually have reaction times in seconds.

Because equal volumes of the reactant solutions (the metal solution and the ligand solution) were mixed to achieve the final reaction mixture, the ligand and metal solutions loaded into the syringes have concentrations 2-fold of the final concentrations. When acid or base was added, it was added to the ligand solution and allowed to reach equilibrium before the stopped-flow experiments in order to prevent problems arising from precipitation of iron or uranium, or formation of oligomers of vanadium. Iron solutions were prepared the same day they were used and were checked for hydrolysis products. The absorption of the 1:1 vanadium complex **1** was monitored at 290 nm; uranyl complexes **3** and **4** were monitored at 315 nm; the iron complex **5** was monitored at 375 nm (Scheme 1). No buffer was used to avoid interference that could result from the complexation between buffers and metal ions, and to prevent additional features in absorbance spectra, which has been noted to be problematic in previous kinetic studies performed by Larsson et. al.[16]. The pH of the iron and vanadium reaction systems were checked and were found to vary little over the course of the experiment (± 0.2 pH units after initial mixing). Blank-dilution experiments were performed and no changes in initial metal speciation or pH were observed from dilution on the stopped-flow time scale.

Between 3 and 10 replicate experiments were performed for each set of concentrations. Molar absorptivity was determined by standard dilutions of solutions of the same composition as used in stopped-flow experiments when needed. The initial rates of the reactions were calculated by fitting using least-squared methods in Microsoft Excel and errors in rates are those arising from fitting the initial reaction rate of the stopped-flow experiments. Attempts were made to fit the stopped-flow kinetic data using the Global Works software package from OLIS Company and the results were generally agreeable with those obtained by the analysis of initial rates. However, due to the reversibility and complex nature of the reaction, there are multiple possible solutions for the fit found in the OLIS software without a clear indication of which is most accurate and comparable across all data sets. Therefore, we elected to use the analysis of initial rates throughout the present work due to its simplicity and applicability also to the analysis of conventional spectrophotometric data for slower reactions.

Conventional UV-Visible spectrophotometry

Conventional UV-Visible spectroscopy experiments were performed on a Cary 50 Spectrophotometer to study the complexation reactions that are too slow for the stopped-flow technique, specifically, the formation of the non-oxido 1:2 vanadium complex **2**, $V(L)_2^-$ (Scheme 1). Complex **2** was monitored at 440 nm. Upon acquisition of the first data point (30 minutes), all of the vanadium was expected to have formed the 1:1 complex based on previous work and stopped-flow results, and decavanadate was never observed in any experiment.

^{1}H and ^{51}V NMR studies

^{1}H NMR spectra were acquired on a Bruker AV-500 instrument (500 MHz) using a WATERGATE solvent suppression pulse sequence. ^{51}V NMR spectra were acquired on a Bruker DRX-500 instrument (131 MHz). All spectra were referenced to an external standard of $VOCl_3$ in C_6D_6.

Results and Discussion

Interactions between vanadium(V) and glutaroimide-dioxime

Preliminary experiments and previous work indicated that the formation of the 1:1 V(V)/L complex, $VO_2(HL)^-$ (complex **1** in Scheme 1) is fast while the formation of the 1:2 V(V)/L complex, $V(L)_2^-$ (complex **2** in Scheme 1) is slow.[5] Therefore, stopped-flow spectroscopy and conventional spectroscopy were used to study the rate of formation of complexes **1** and **2**, respectively. In seawater, the concentration of vanadium is extremely low (10 - 30 nM, varying with salinity and seasons)[17], such that it exists mainly as monomeric V(V) vanadates of varying protonation states.

Rate of formation of $VO_2(HL)^-$

The stopped-flow experiments were conducted by rapidly mixing two solutions, one vanadium solution and the other glutaroimide-dioxime solution, and monitoring the change in the absorption spectra of the mixture over time in the wavelength region of 225 nm – 375 nm. To ensure that the absorbance was in the linear range throughout the experiment, vanadium concentrations of 0.050 – 0.200 mM and ligand concentrations of 0.375 – 1.00 mM were used. In the absence of additional acid or base added to the reactants, the final pH of the reaction mixture was 8.0 ± 0.2 for most experiments. Under these conditions the vanadium is in the monomeric form $[H_2VO_4]^-/[HVO_4]^{2-}$.[18,19]

Representative absorption spectra obtained on the stopped-flow spectrometer are shown in Figure 1, the increase in absorbance at 290 nm over time demonstrating the formation of **1** (Scheme 1) is shown in Figure 2, and kinetic data varying [L] and [V] are shown in Figures 3 and 4. The data indicate that complex **1** formed rapidly upon mixing of the two reactants, reaching a steady state within 20-60 seconds when [V] = 0.200 mM and [L] = 0.500 mM with no additional acid or base added into the reactant solutions. By analyzing the kinetic trace in Figure 2 (absorbance vs. time), the initial rate of the reaction, $(d[\mathbf{1}]/dt)_o$, is calculated.

For the complexation reaction between V(V) and L to form complex **1**, a simplified general rate equation can be written as:

$$(d[\mathbf{1}]/dt)_0 = k \times [V]^a[L]^b \times f([H^+]) \qquad (1)$$

Where [V] and [L] denote the initial concentrations of V and L, and *a* and *b* are reaction orders with respect to reactants V and L, respectively. Since the reaction mechanism involving H^+ is expected to be complex and may change over different pH ranges, and it is difficult to define the reaction order with respect to H^+, we use the term $f([H^+])$ as a function of $[H^+]$ in equation 1 rather than an exponential function.[15] By maintaining a constant acidity, the rate equation can be expressed as:

$$(d[\mathbf{1}]/dt)_0 = k' \times [V]^a[L]^b \qquad (2)$$

where k' denotes the conditional rate constant at a certain acidity.

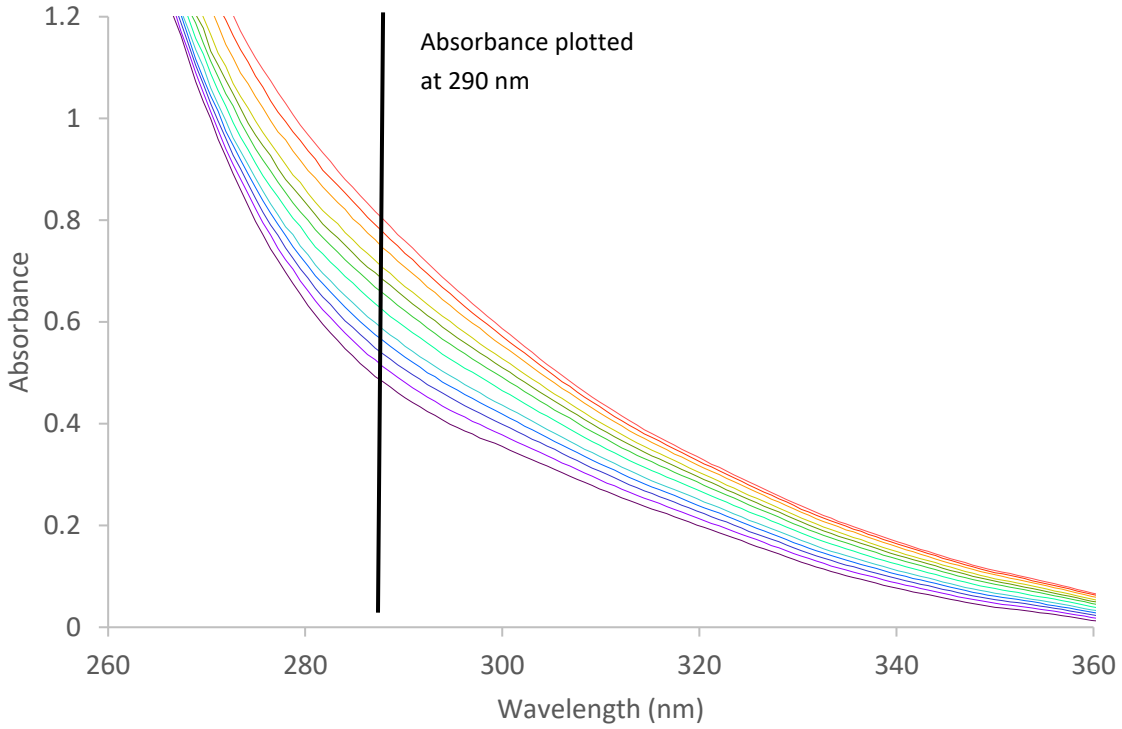

Figure 1. Representative spectra for the formation of complex **1** monitored by stopped-flow absorption spectroscopy, showing changes in the spectra over time (0.1 – 24.0 seconds; the number of spectra has been reduced for clarity). Conditions: [L] = 0.500 mM, [V] = 0.200 mM.

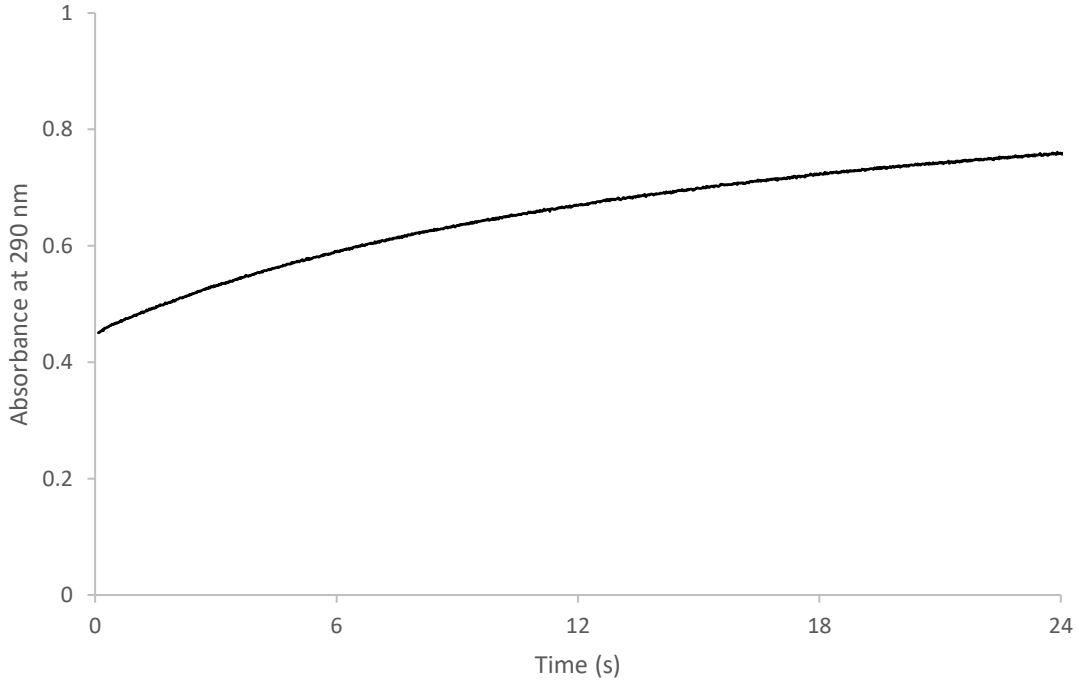

Figure 2. Absorbance changing over time at 290 nm (from Figure 1)

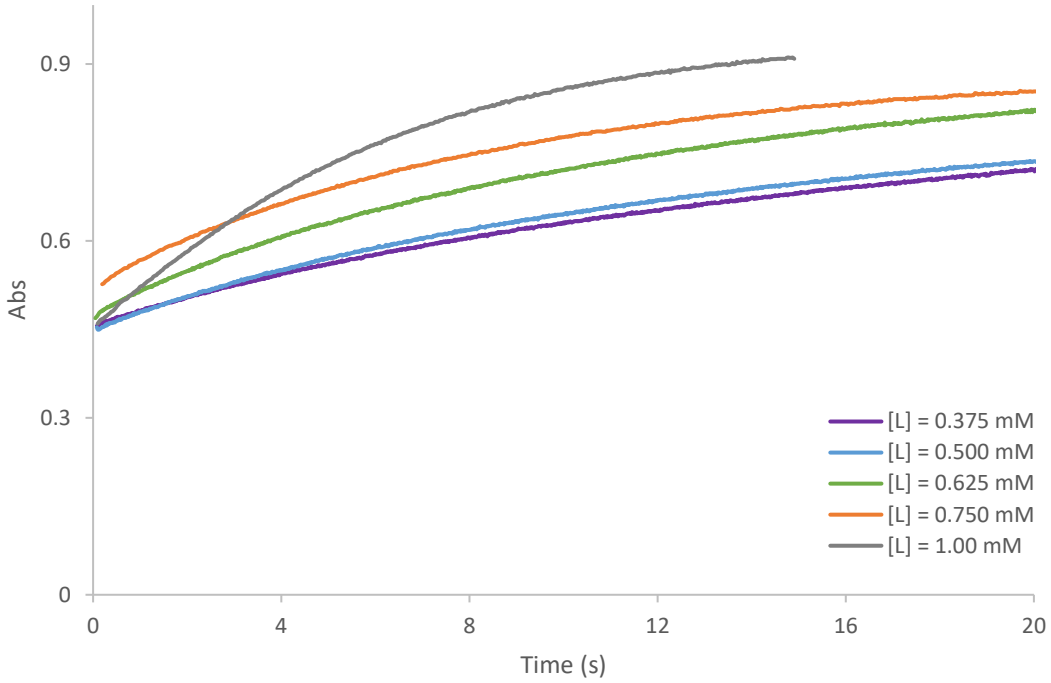

Figure 3. Sample curves for the formation of complex **1** from stopped-flow kinetic experiments showing the effect of ligand concentration. Conditions: [V] = 0.200 mM, pH = 8.

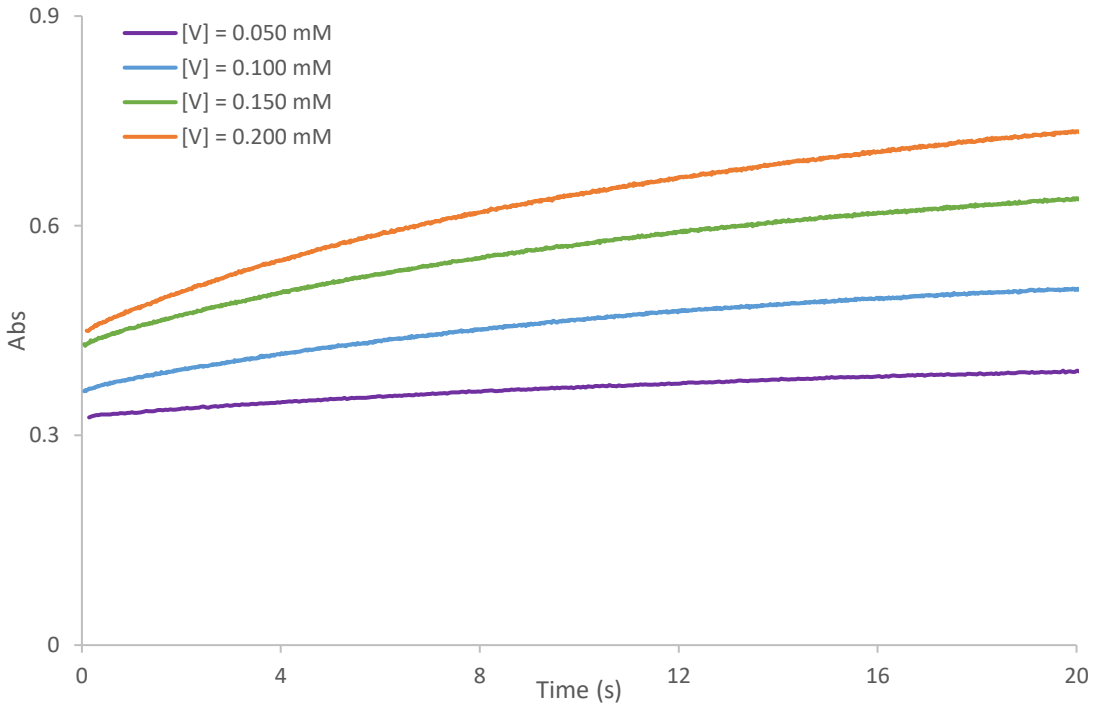

Figure 4. Sample curves for the formation of complex **1** from stopped-flow kinetic experiments showing the effect of vanadium concentration. Conditions: [L] = 0.500 mM, pH = 8.

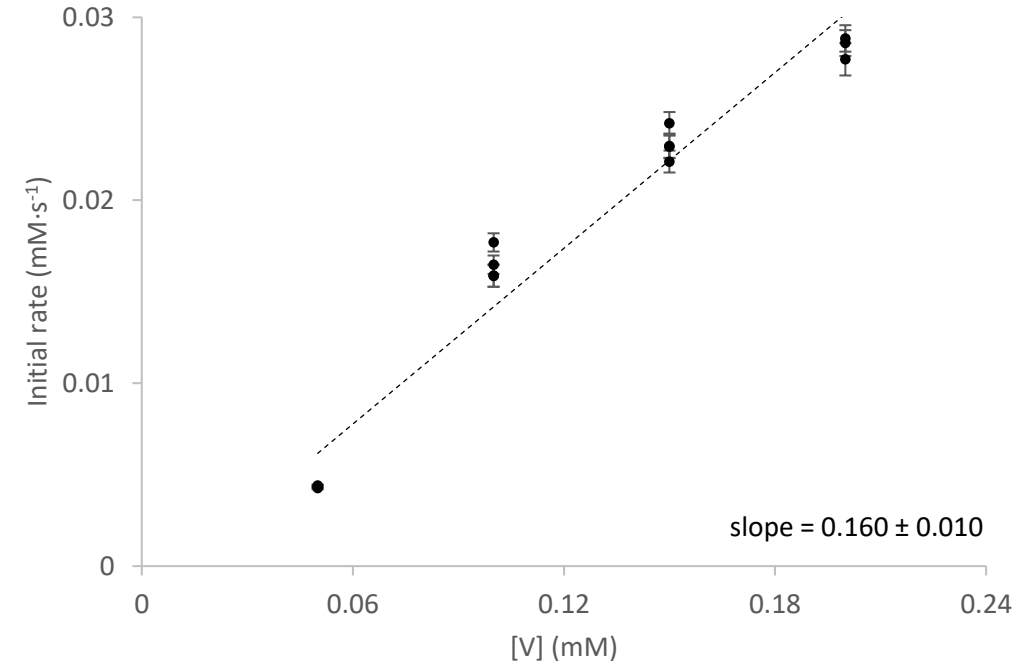

Figure 5. Initial rate of the formation of complex **1** as a function of [V], monitored by stopped-flow UV-Visible spectroscopy, from Figure 3. Conditions: constant [L] = 0.500 mM.

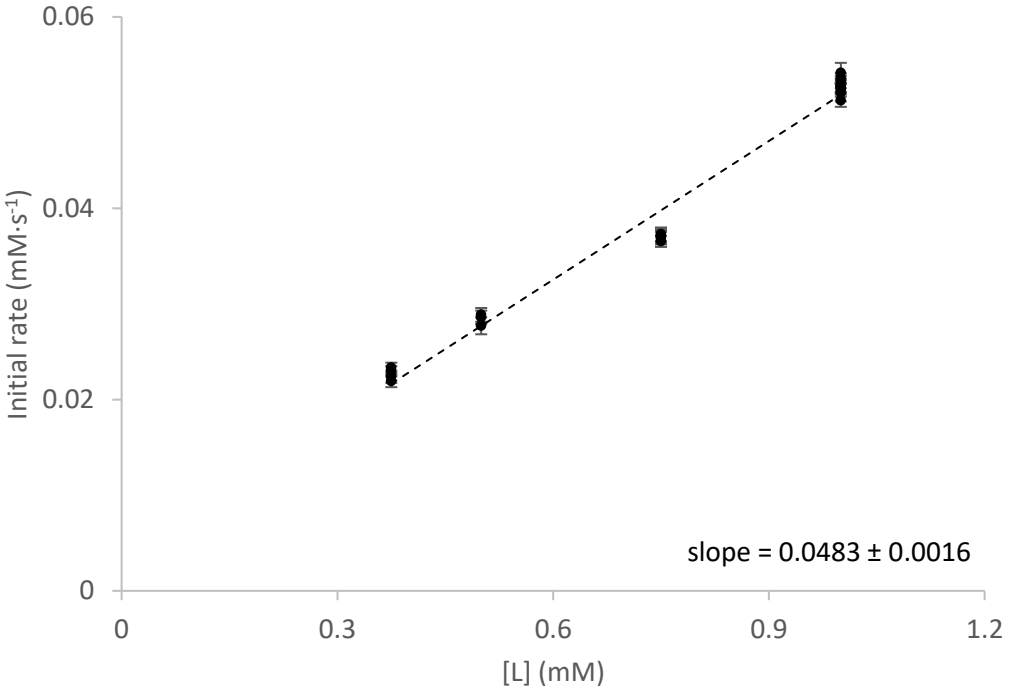

Figure 6. Initial rate of the formation of complex **1** as a function of [L], monitored by stopped-flow UV-Visible spectroscopy, from Figure 4. Conditions: [V] = 0.200 mM.

By keeping either [L] or [V] constant in the experiments, the rate equation becomes

$$(d[\mathbf{1}]/dt)_0 = k_{obs,V} \times [V]^a \quad (3)$$

or

$$(d[\mathbf{1}]/dt)_0 = k_{obs,L} \times [L]^b \quad (4)$$

By analyzing the initial reaction rate as a function of [V] or [L], the observed rate constants, $k_{obs,V}$ and $k_{obs,L}$, as well as the reaction orders a and b can be calculated.

Figures 5 and 6 show the plots of initial rate vs. [V] and [L], respectively. Both plots show linear relationships that pass through the origin, indicating that $a = 1$ and $b = 1$. In other words, the formation of complex **1** is first-order with respect to both [V] and [L]. From the slopes of these plots, the observed rate constants were calculated to be $k_{obs,V} = (0.16 \pm 0.01)$ s^{-1} (Figure 5) and $k_{obs,L} = (0.0483 \pm 0.0016)$ s^{-1} (Figure 6). From these values, the conditional rate constant in equation (2) (where $a = 1$ and $b = 1$) was calculated to be $k' = (0.28 \pm 0.02)$ $mM^{-1} \cdot s^{-1}$, corresponding to the rate of formation of complex **1** being 0.028 $mM \cdot s^{-1}$ when [V] = 0.200 mM and [L] = 0.500 mM and pH = 8.0 ± 0.2.

The reaction conditions shown in Figures 1-6 correspond to the systems where no additional acid or base was added to the solutions of V or L and the pH was 8.0 ± 0.2. Stopped-flow experiments were also conducted at different pH (from 5.9 to 9.4) from by adding different quantities of acid or base into the reaction mixture while maintaining constant concentrations of other reagents, with the objectives of investigating the reaction order with respect to H^+. However, as Figure 7 shows, the dependence on acid or base is complex. Higher acidity generally facilitates the formation of **1**, and an approximate 50-fold increase in rate is observed when adding two equivalents of acid, strongly suggesting that multiple reaction pathways could exist and the reaction mechanism varies in different pH regions. Therefore, it is difficult to calculate the reaction order with respect to H^+ for a broad pH region.

The equilibrium vanadium and vanadium-ligand systems also vary with pH, further complicating the reactions. However, the speciation can be calculated in the presence and absence of ligand (Figures 9 and 10), and in a simplified case for a narrow and near neutral pH region that is most relevant to seawater conditions, a plot of the initial rates (in the logarithm unit) as a function of pH (Figure 8) indicates a linear correlation with a slope of 0.90 ± 0.15, implying that the complexation reaction is approximately first order with respect to H^+, in the narrow region of acidity. The dependence of the reaction rate on acidity strongly suggests the deprotonation of the central N followed by protonation of the oxygen side arms in glutaroimide-dioxime is the rate-limiting step.

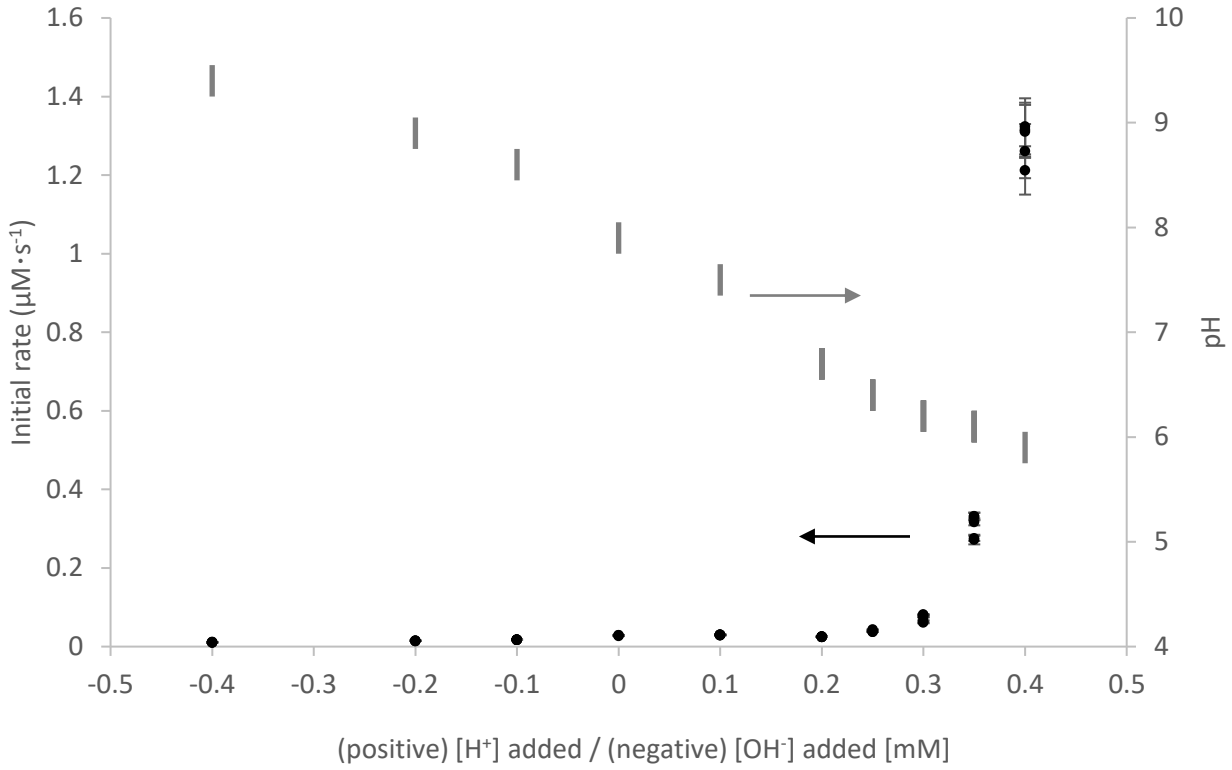

Figure 7. The effect of acidity on the initial rate of the formation of complex **1,** monitored by stopped-flow UV-Visible spectroscopy. Conditions: [L] = 0.500 mM, [V] = 0.200 mM.

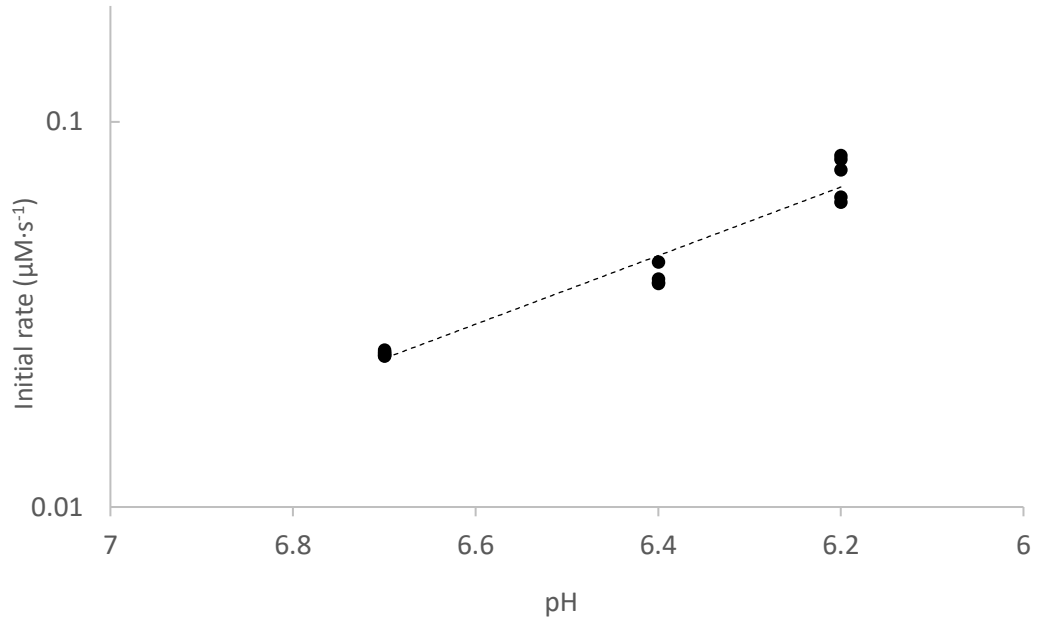

Figure 8. The effect of pH on the initial rate of the formation of complex **1,** showing the initial rate vs. pH in a narrow near-neutral region. Conditions: [L] = 0.500 mM, [V] = 0.200 mM.

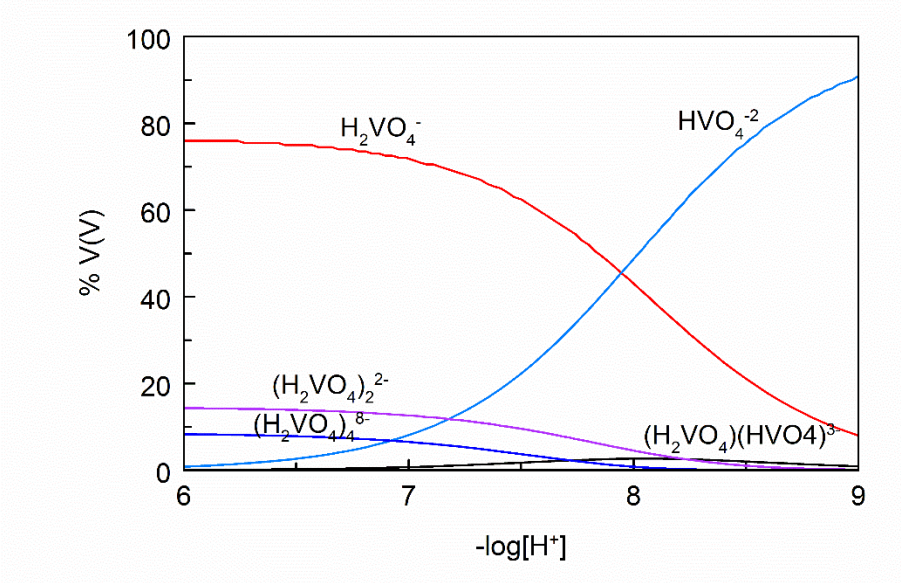

Figure 9. Speciation of 0.2 mM V(V) in the absence of L, using equilibrium constants of V(V) speciation from literature sources.[20] Conditions: [V] = 0.2 mM.

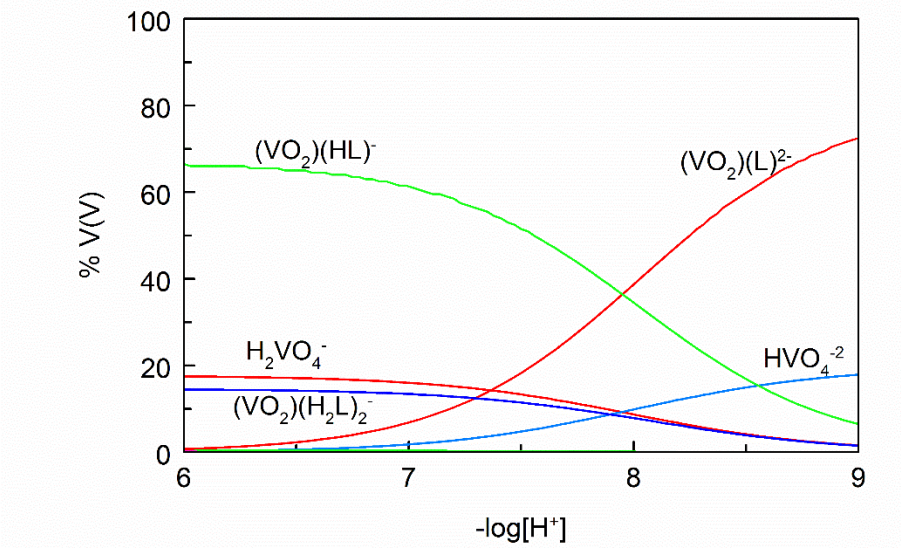

Figure 10: Speciation of 0.2 mM V(V) with 0.5 mM L, using equilibrium constants for V(V) speciation[20] and V(V) – L equilibrium constants.[21] Conditions: [V] = 0.2 mM, [L] = 0.5 mM.

Rate of formation of $V(L)_2^-$.

The formation of complex **2**, the 1:2 V/L complex (Scheme 1), is much slower, such that the reactions need to be monitored by conventional absorption spectroscopy over four weeks (acquiring spectra every 1-2 days). The absorbance at 440 nm was monitored for the formation of **2**. The same concentration ranges as those used in the stopped-flow experiments described in Section 3.1.1 were used to ensure that the absorbance was in the linear range. By analyzing the spectra, the rate of formation of **2** as a function of time under different conditions is calculated and shown in Figures 11-13.

The formation of the 1:2 complex **2** occurs much more slowly than that of the 1:1 complex **1**. In general, the rate of formation of complex **2** increases as the concentration of vanadium (Figure 11) is increased. In all of these experiments varying [L] and [V] (Figures 11 and 12), there seems to be an "induction" period of 1-2 days when the formation of complex **2** is extremely slow, though addition of acid eliminates this delay period along with increasing the reaction rate as shown in Figure 13.

Similar to the formation of complex **1**, the rate of formation of complex 2 is complicated and greatly affected by the acidity. As shown in Figure 13, the reaction rate of complex **2** is dramatically increased at higher acidity: at the two highest acid concentrations, the concentration of complex **2** reached a maximum within two days, followed by decomposition of complex **2** back to **1** and other products, which are discussed below. Again, like the formation of complex **1**, it is not possible to estimate the reaction order of the formation of complex **2** with respect to $[H^+]$ due to the complexity of the reaction mechanism involving the proton. However, it is possible to estimate the rate of formation of complex **2** to be 5×10^{-7} $mM \cdot s^{-1}$ under the concentrations of [V] = 0.2 mM, [L] = 0.5 mM without additional acid or base added (pH = 8.0 ± 0.5). In comparison with the rate of formation of **1** under the same concentrations (2.8×10^{-2} $mM \cdot s^{-1}$), the formation of complex **2** is approximately five orders of magnitude slower than that of complex **1**.

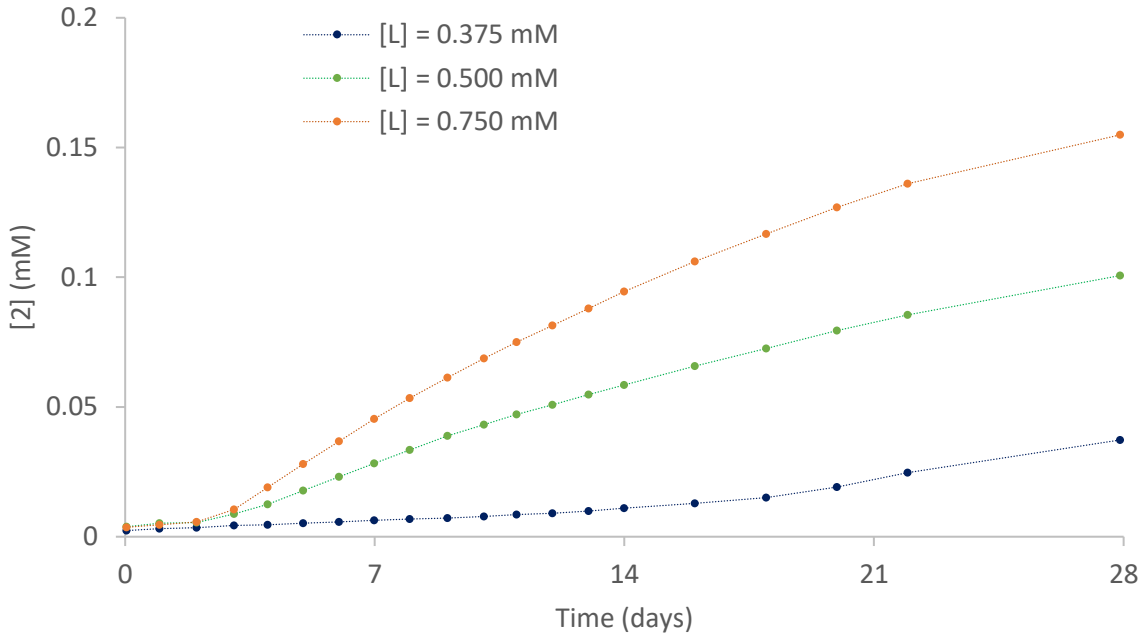

Figure 11. Formation of complex **2** over time, varying [L] at constant [V] = 0.200 mM.

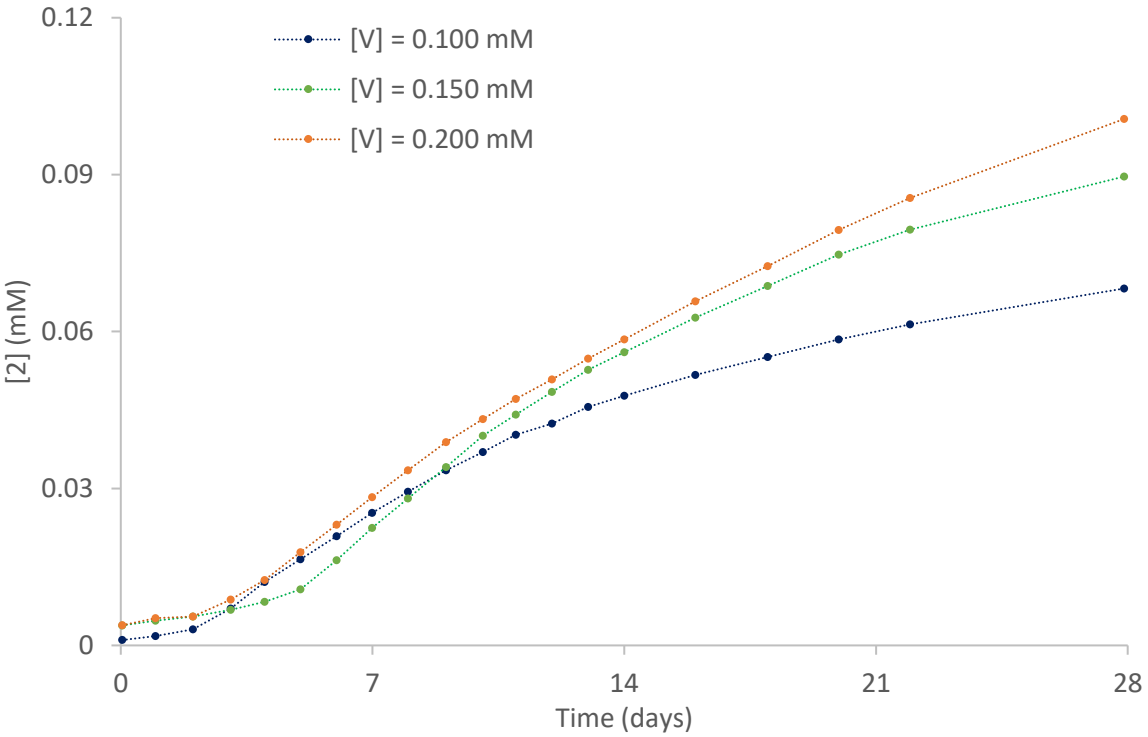

Figure 12. Formation of complex **2** over time, varying [V] at constant [L] = 0.500 mM.

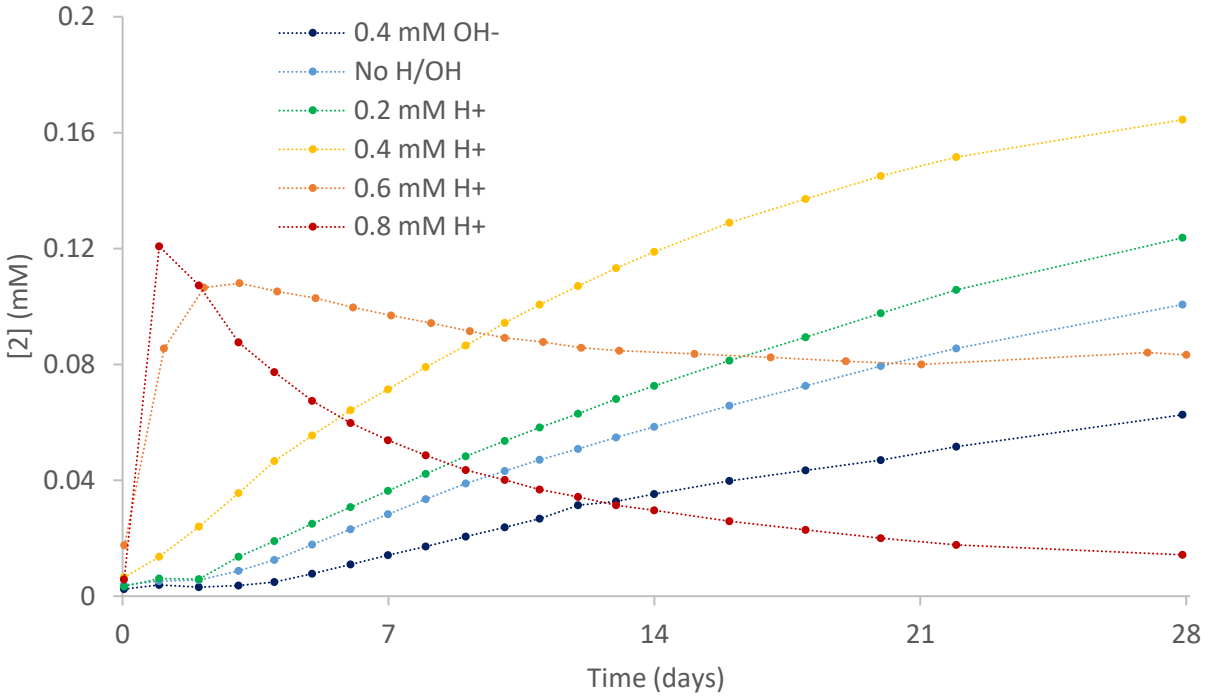

Figure 13. Formation of complex **2** over time, adding acid or base with constant [L] = 0.500 mM and [V] = 0.200 mM.

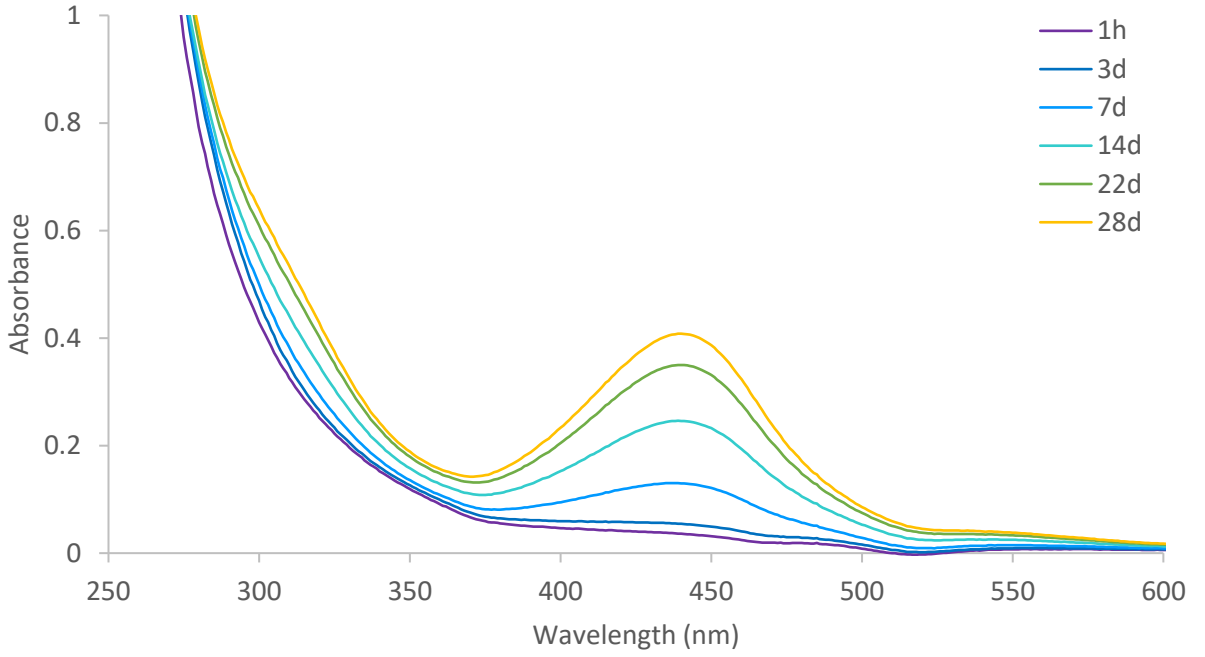

Figure 14. Spectra monitoring the formation of **2** over time by conventional UV-Vis absorption spectroscopy. The number of spectra shown has been reduced for clarity. Conditions: [V] = 0.200 mM; [L] = 0.500 mM.

Reaction mechanism of the formation of V(V) complexes 1 and 2

Due to the rarity of the non-oxido V(V) center, little is known about the kinetics of the reactions involving such species, although examples of non-oxido V(IV) are known, with limited kinetic studies of complex formation and decomposition.[22,23] As previously described, the dependence of the rate of formation of complexes **1** and **2** on the acid is complicated and difficult to define in the present study. Adding acid or base, especially acid, to the reaction mixture has significant impact on the speciation and the rate of formation of both **1** and **2**, but in fact the solution pH does not change much during the course of the reaction due to the presence of various weakly acidic species (ligand, vanadate, and most likely the complexes) and/or their conjugate bases that can buffer the solutions effectively. Based on the strong dependence of reaction rates on acid, a key step in the formation of both complexes **1** and **2** is likely the protonation and subsequent hydrolysis of one or more oxido ligands on vanadate. In the case of complex **2**, this step is many orders of magnitude slower (days) than the formation of complex **1** (seconds). Formation of a previously reported non-oxido V(IV) complex with the tridentate ligand derived from *cis*-inositol[22] has shown similar time periods for equilibration of a few days, although that reaction was found to be complex and no mechanism was elucidated.

A notable feature of the formation of complex **2** is that the rate of formation is apparently zero-order with respect to [L] in the initial period including the "induction" period (Figure 12), suggesting that the protonation of complex **1** and/or subsequent loss of water is rate-determining and are much slower than the complexation with the second ligand (Scheme 2). The induction period could be attributed to the slow onset of the reaction formally producing acid (i.e. the 1:1 complex is more basic than the 1:2 complex) resulting in acceleration of the reaction once it starts. The bonds of the two remaining oxido ligands in complex **1** should be stronger than the oxido bonds in orthovanadate based on bond lengths and the rate of ligand exchange. The V=O bonds in complex **1** are 1.6781(15) and 1.6734(14) Å, whereas in inorganic vanadates with four oxido groups, the bonds are longer, typically 1.72-1.75 Å, and oxido ligand exchange occurs readily in basic solution.[5,24,25] This is reflected in the slower reactivity of the last two oxido ligands to form complex **2** compared to the formation of complex **1** from vanadate. The above discussions are illustrated in Scheme 2.

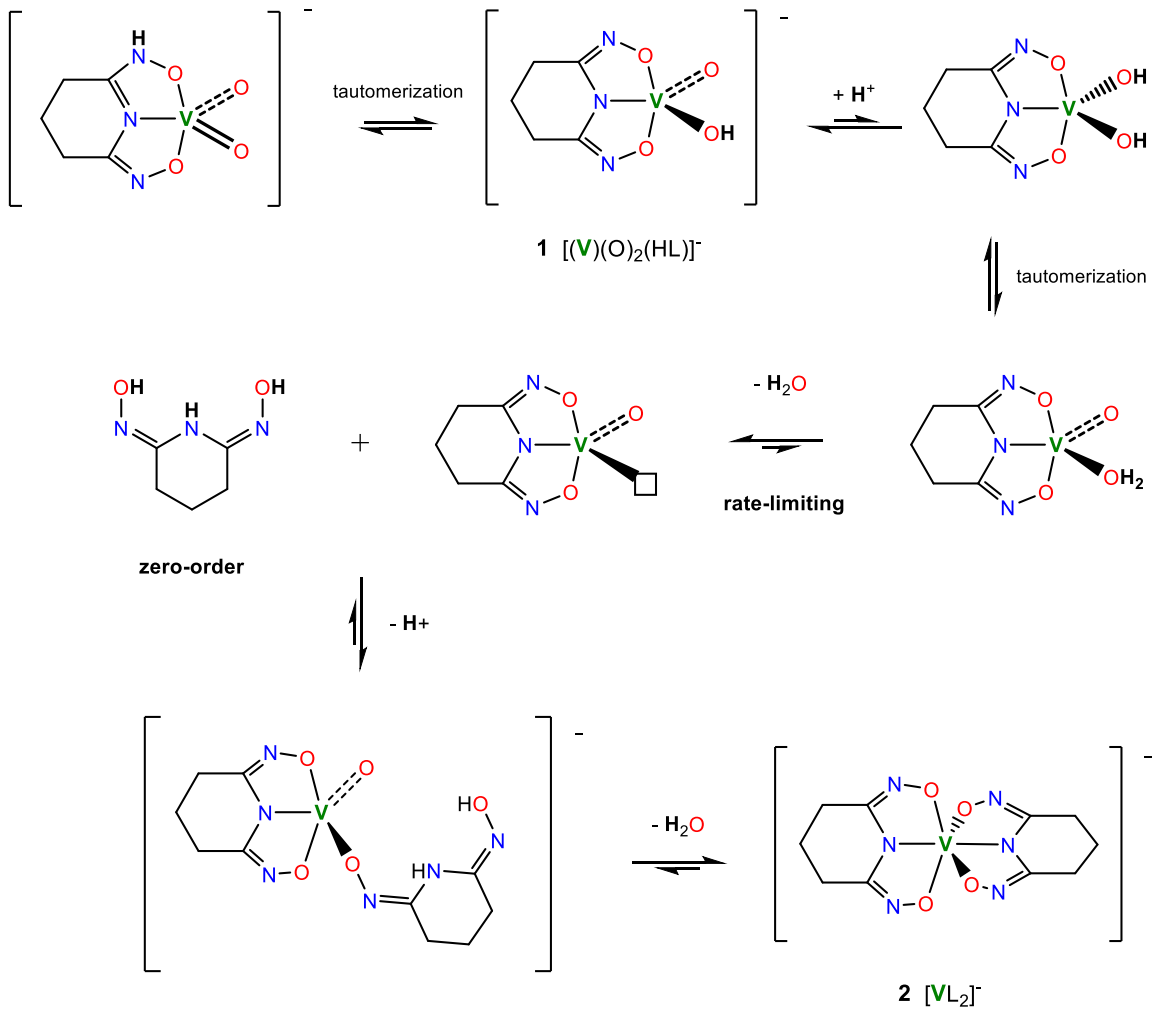

Scheme 2. Proposed stepwise mechanism of formation of **2** from **1** accounting for kinetic observations. Not all tautomers of complexes and intermediates are shown.

In the absence of vanadium, glutaroimide-dioxime is unstable towards acid hydrolysis in solutions at pH 3 or lower.[26] The decomposition of the ligand alone is probably a straightforward acid-catalyzed hydrolysis of a carboxylate derivative, ultimately to glutaric acid.[27] On the other hand, metal-catalyzed decomposition of ligand could also be a cause of the instability of **2**. The vanadium ion in **2** is a non-oxido "V^{5+}" which would be expected to be highly Lewis acidic, such that it could also promote ligand decomposition at much lower concentrations of [H^+] present at near-neutral pH. On the other hand, **1** appears to be stable indefinitely, presumably due to the metal's much lower Lewis acidity due to the presence of the two oxido ligands. When examining the reactivity at the metal center, we can view **1** as having the composition ([VO_2^+][HL^{2-}]), in contrast to **2** having the composition ([V^{5+}][$(L)_2^{3-}$]), with the lower charge density at the metal leading to lower Lewis acidity, which in turn does not promote ligand hydrolysis. This is also consistent with trends seen in the ^{51}V NMR chemical shifts, where the non-oxido compound **2** exhibits a very downfield chemical shift (+740 ppm)[5] , while most known oxovanadium(V) compounds have a much higher field signal (-410 ppm for **1**) due to significant shielding from the π-bonding oxido ligands.[13]

^{1}H and ^{51}V NMR of glutaroimide-dioxime – vanadium mixtures

^{51}V and ^{1}H NMR experiments were conducted to follow the speciation of vanadium(V) as a function of time (over 10 days), corroborate the data obtained by absorption spectroscopy, and help confirm our proposed mechanism. The chemical shifts on the ^{51}V and ^{1}H NMR spectra can be assigned to monomeric or oligomeric vanadates, or the 1:1 and 1:2 complexes **1** and **2**, respectively, based on previous studies.[5,13] Because NMR spectroscopy is relatively insensitive, higher vanadium concentrations are needed. In the present NMR experiments, the concentration of vanadium ranged from 3 to 18 mM, approximately 10-20 times higher than those in UV-Visible absorption experiments.

Results of ^{1}H and ^{51}V NMR experiments are shown in Figures 15-24, at three different [V]/[L] ratios. A wider variety of species are observed in this concentration regime than at low concentrations. The 1:1 complex **1** forms very fast, and the 1:2 complex, **2**, forms in days, reaching maximum concentration at around 3 days followed by decomposition back to complex **1** and other products. Because higher concentrations of V(V) were used in the NMR experiments, decavanadate ($[H_iV_{10}O_{28}]^{(6-i)-}$) was initially observed, but reverted to monomeric vanadate within 1-2 days, consistent with previously studied vanadate systems.[14,18] As shown in Figure 16, the concentration of decavanadate decreases in accordance with the formation of V(V) glutaroimide-dioxime complexes. The approximate rates of formation of V(V) complexes **1** and **2** observed by NMR corroborate very well those observed by absorption spectroscopy.

It appears that the time it took for the decavanate to revert to monomeric vanadate and react with glutaroimide-dioxime (1-2 days, Figures 17 and 21) coincides with the "induction" period of the formation of complex **2** (1-2 days, Figures 11-13). However, it is unlikely that the dissociation of decavanate is the direct cause of the delay since the same delay was also observed at lower vanadium concentrations where no decavanadate was present, and there is nothing inherent to the structure of decavanadate that would hinder the complexation of free vanadates.

The NMR data (Figures 18 and 22) indicate that the rate of formation as well as the stability of the 1:2 non-oxido V(V) complex **2** is highly dependent on added acid, in agreement with the optical absorption data (Figure 13). With more than 2 equivalents of acid (with respect to vanadium) added, complex **2** forms quickly and starts to decompose in 1-2 days. The decomposition results in partial or complete hydrolysis of the ligand, since some of the decomposition products observed are consistent with previously observed hydrolysis products and the ammonium ion was also formed in this process.[27]

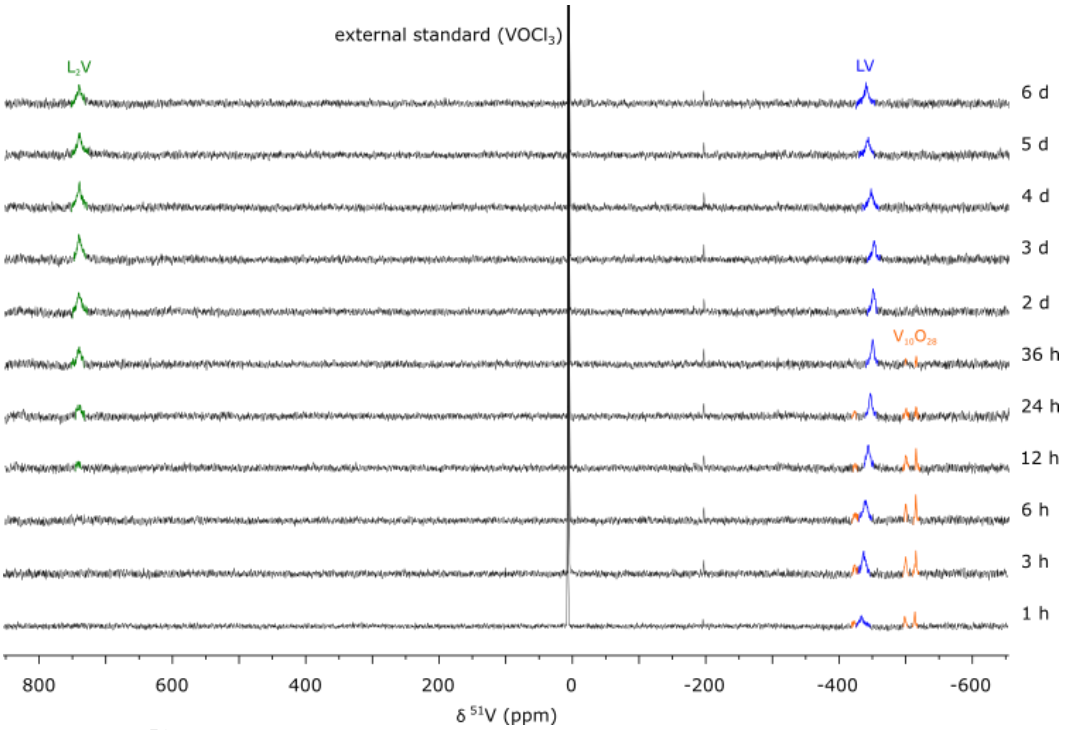

Figure 15. ^{51}V NMR spectra monitoring speciation of a V/L mixture over time. Conditions: [V] = 3 mM, [L] = 6 mM, pH = 7-8.

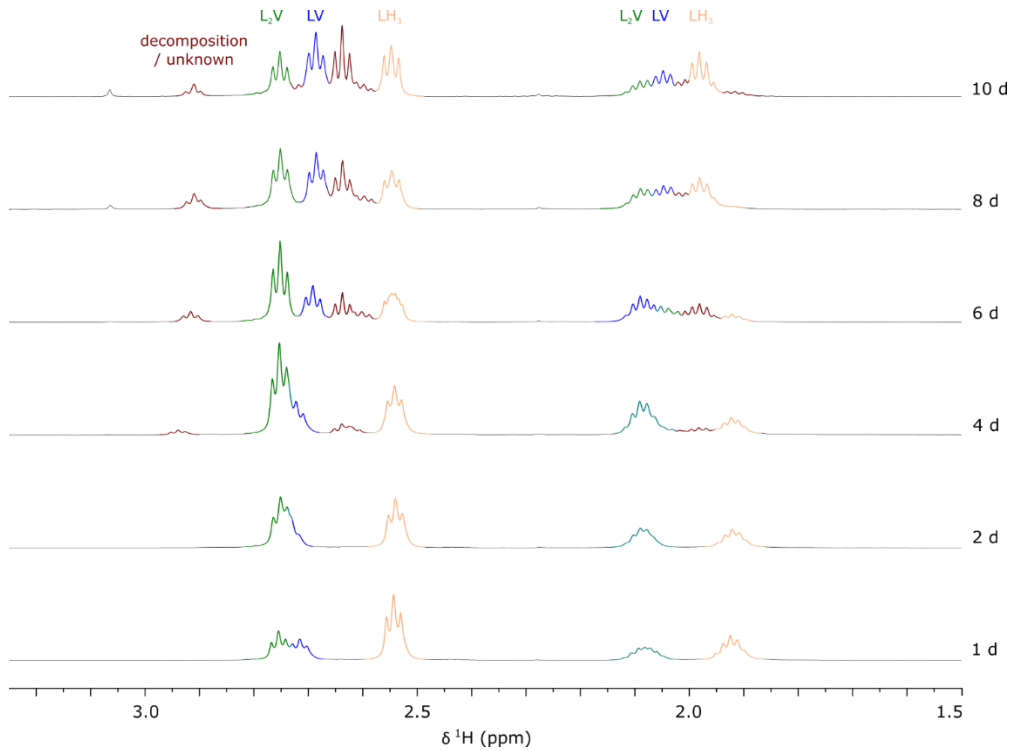

Figure 16: ^{1}H NMR spectra monitoring speciation of a V/L mixture over time Conditions: [V] = 3 mM, [L] = 6 mM, pH = 7-8.

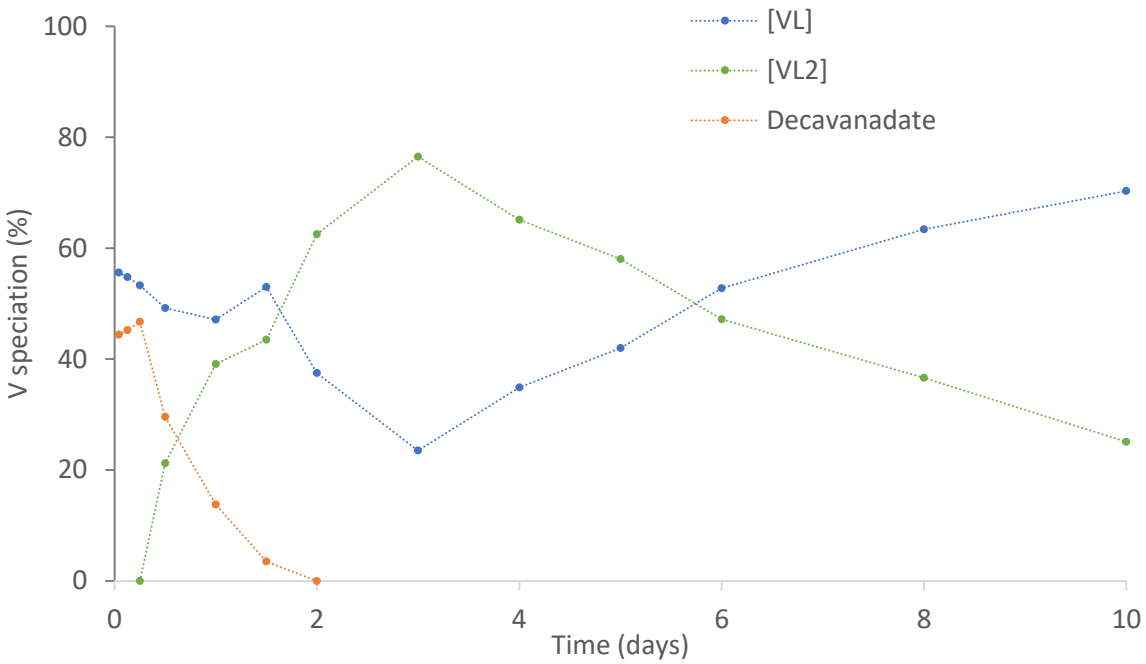

Figure 17. Speciation of a V/L mixture over time monitored by ^{51}V NMR (Figure 13). Conditions: [L] = 6 mM, [V] = 3 mM, pH = 8.0 ± 0.2.

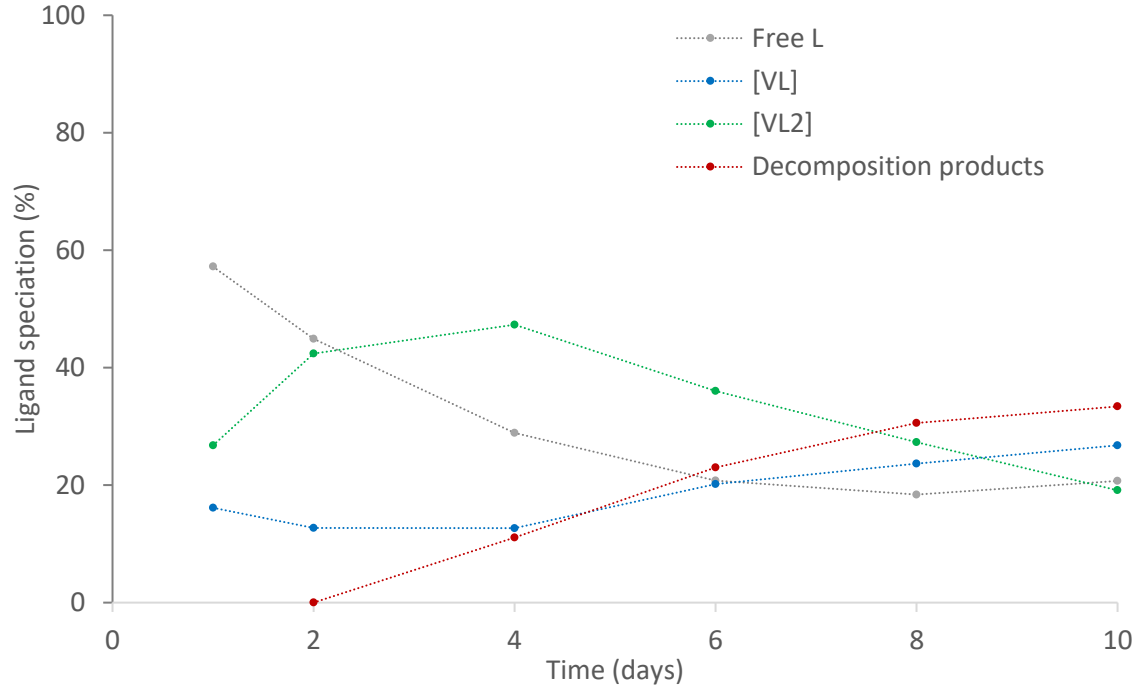

Figure 18. Speciation of a V/L mixture over time monitored by ^{1}H NMR (Figure 14). Conditions: [L] = 6 mM, [V] = 3 mM, pH = 8.0 ± 0.2.

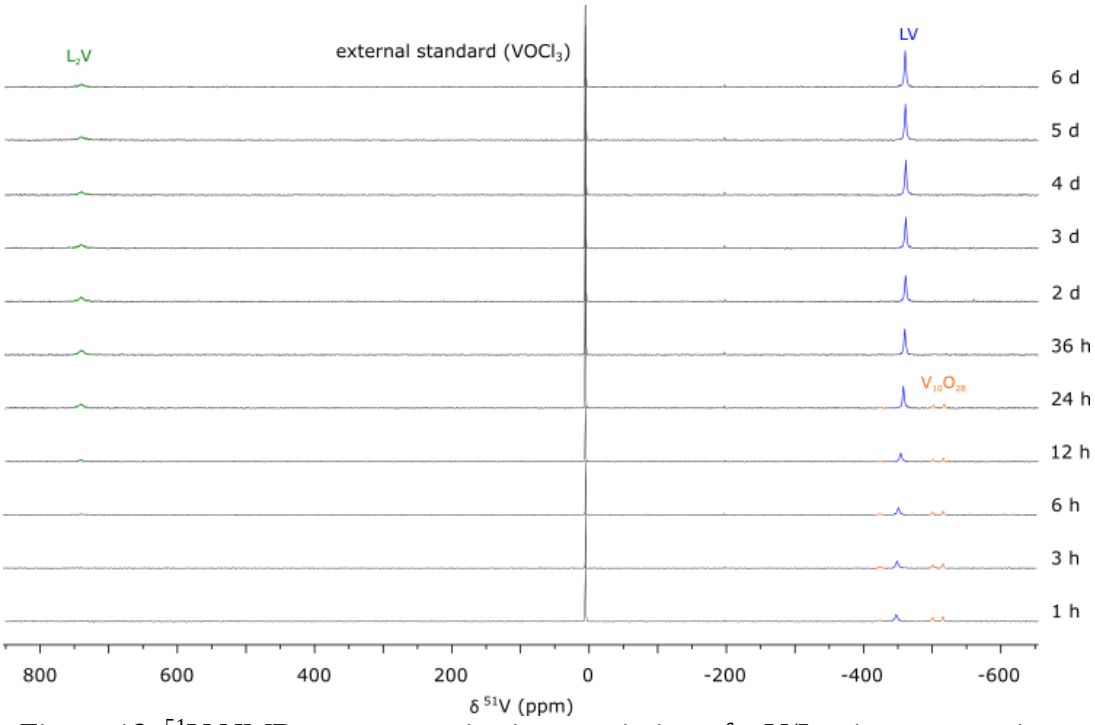

Figure 19. ^{51}V NMR spectra monitoring speciation of a V/L mixture over time. Conditions: [V] = 6 mM, [L] = 6 mM, pH = 7-8.

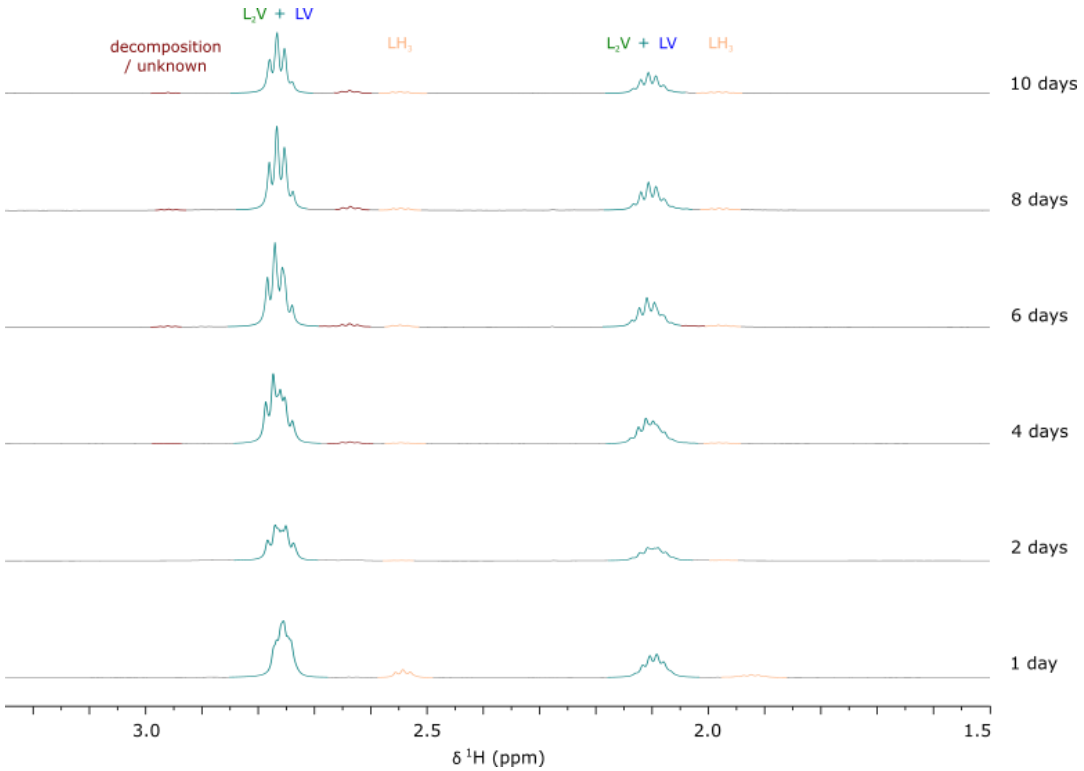

Figure 20. ^{1}H NMR spectra monitoring speciation of a V/L mixture over time. Conditions: [V] = 6 mM, [L] = 6 mM, pH = 7-8.

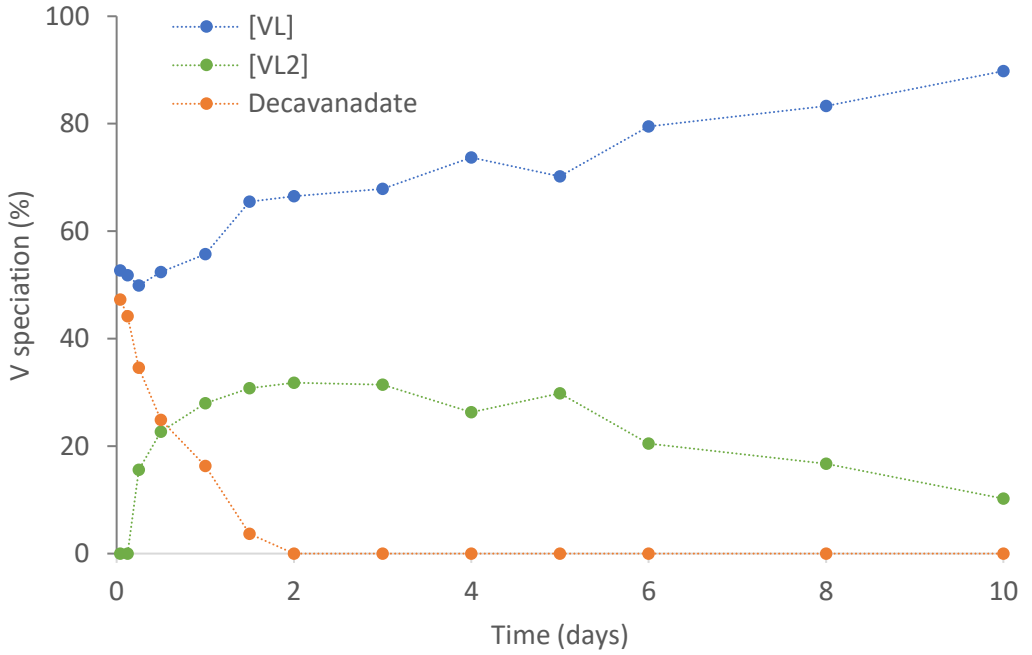

Figure 21. Speciation of a V/L mixture over time monitored by ^{51}V NMR (Figure 17). Conditions: [V] = 6 mM, [L] = 6 mM, pH = 7-8.

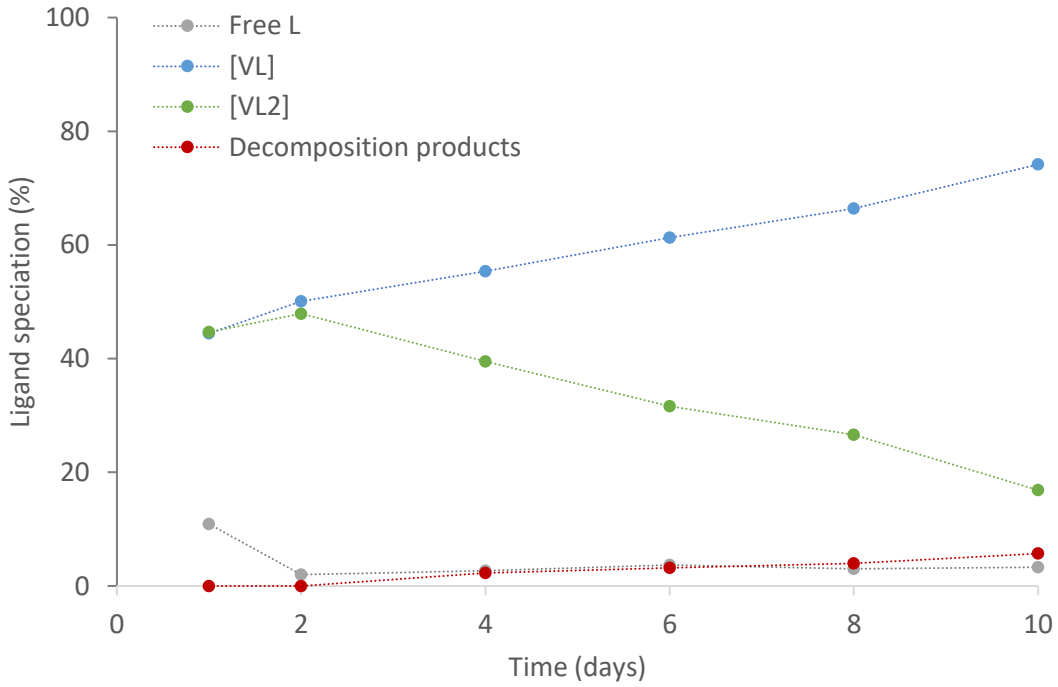

Figure 22. Speciation of a V/L mixture changing over time (note: [VL] and [VL_2] ratio determined from ^{51}V NMR due to overlap in the ^{1}H spectra; see Figures 18-19). Conditions: [V] = 6 mM, [L] = 6 mM, pH = 7-8.

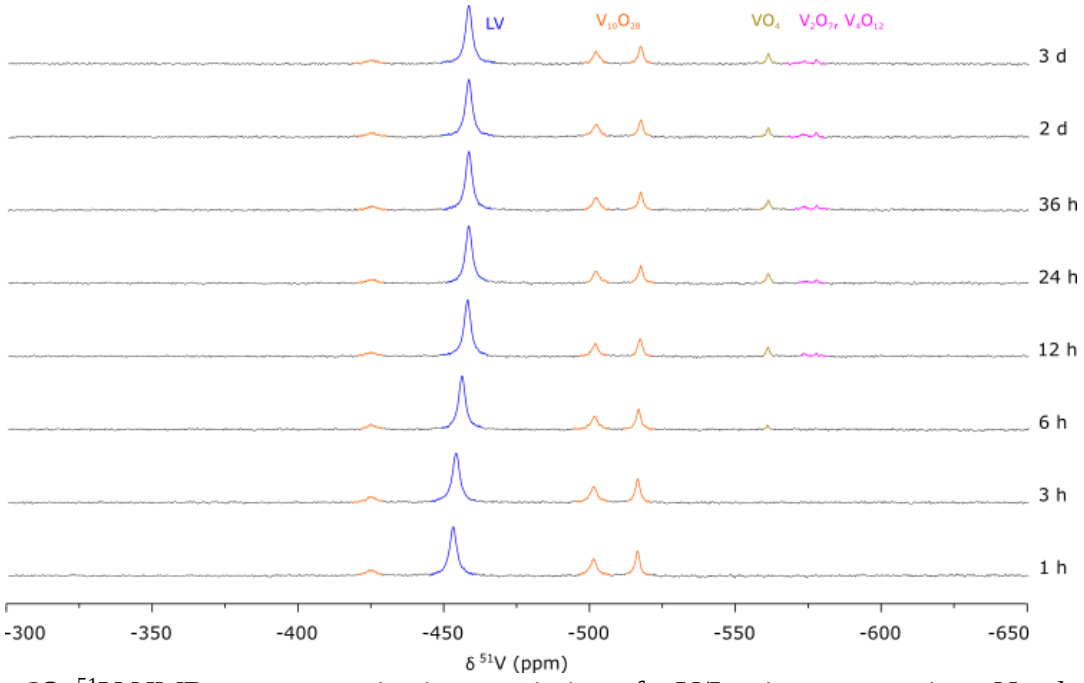

Figure 23. ^{51}V NMR spectra monitoring speciation of a V/L mixture over time. No changes were observed after 3 days, and no signals were observed at δ > -300 ppm. Conditions: [V] = 12 mM, [L] = 6 mM, pH = 7-8.

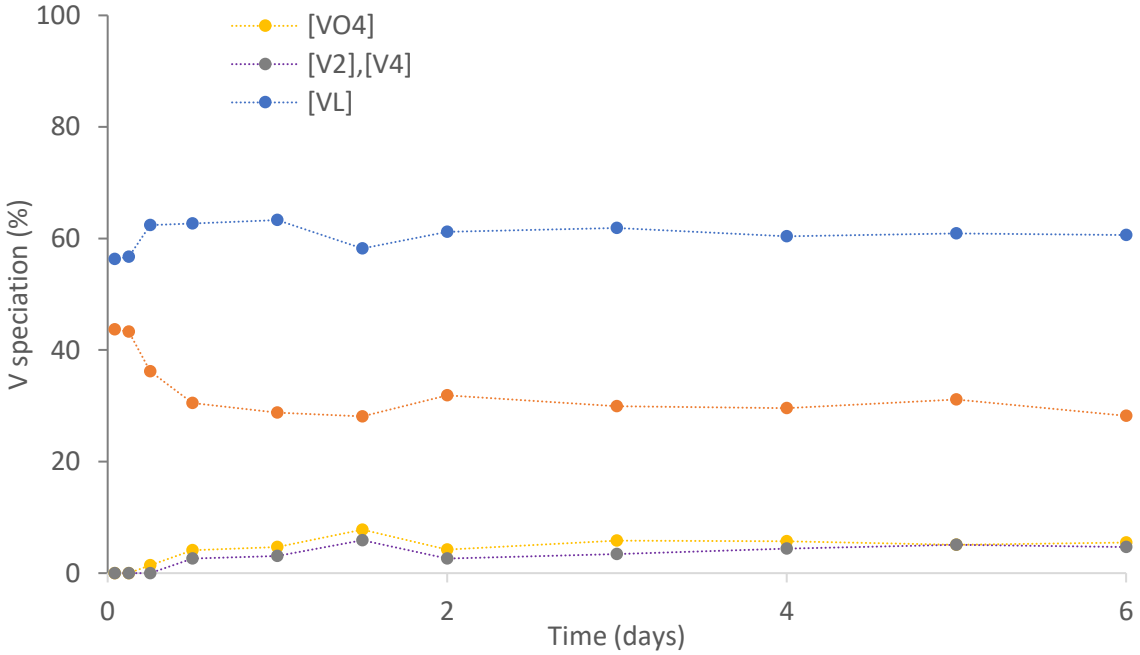

Figure 24. ^{51}V speciation of a V/L mixture changing over time (Figure 21). ^{1}H speciation (starting at 1 day) contains only VL. [V2] and [V4] are vanadium dimeric and tetrameric species, respectively. Conditions: [V] = 12 mM, [L] = 6 mM, pH = 7-8.

Interactions between U(VI) and glutaroimide-dioxime

Reaction orders of the complexation with respect to [U(VI)] and [L]

The reaction rates of uranyl with glutaroimide-dioxime to form complexes **3** and **4** (Scheme 1) were explored in the same way as vanadium. Figures 25-28 show representative spectra and kinetic traces at 315 nm from stopped-flow spectroscopy. Under the conditions of [U(VI)] = 0.200 mM, [L] = 0.500 mM, and [carbonate] = 1.6 mM, the kinetic trace shows two distinct steps with different rates of formation. We assume that the two steps correspond to the formation of **3** and **4**, respectively, under these conditions. In seawater, uranium exists as uranyl carbonate complexes, with the dominant one being calcium uranyl carbonate, $Ca_2[UO_2(CO_3)_3]$,[6,28] and we have attempted to replicate this species in the uranyl solutions used, as well as investigate the effect of changing the ratios of uranyl, calcium, and carbonate on the complexation kinetics. As with vanadium, the equilibrium speciation varies with pH, and speciation diagrams in the presence and absence of ligand are shown in Figures 31 and 32.

Figures 29 and 30 show that the correlations between the initial rates ($Abs \cdot s^{-1}$) and the concentrations of [U(VI)] or [L] are linear and pass the origin on x- and y- axis, strongly suggesting that, similar to the interaction between the ligand and vanadium, the initial rate of the reaction with U(VI) is first-order with respect to the initial concentrations of [U(VI)] and [L]. The slopes of these plots represent the observed first-order rate constants ($Abs \cdot mM^{-1} \cdot s^{-1}$) under the experimental conditions. The U:Ca:carbonate ratio was kept constant in these experiments to maintain constant initial uranyl speciation. Since complex **3** cannot be isolated, we are unable to determine its molar absorptivity so that the rate for the formation of **3** or **4** in the unit of $mM \cdot s^{-1}$ is not obtainable. However, it is qualitatively evident by comparing the observed rate constants in Figure 29 and 30 to those in Figures 5 and 6 that the formation of U(VI) complexes **3** and **4** is faster than that of V(V) complex **1**, and much faster than that of V(V) complex **2**. Further discussions on comparing the rates among V(V), U(VI) and Fe(III) using the half-time of the reaction are provided towards the end of this chapter.

The effect of other ions on the rate of formation of U(VI)/glutaroimide-dioxime complexes

Because uranium exists in seawater as ternary Ca/Mg-U(VI)-carbonate complexes,[6,28] the interaction between U(VI) with the ligand under seawater conditions will be affected by the presence of carbonate, calcium, and magnesium (sodium and potassium can also interact with uranyl carbonate species, but the interactions and complexes formed are very weak and are inconsequential for this discussion.) Therefore, in addition to varying [U] and [L] as discussed above, the rate of formation of **3** and **4** was also studied at different concentrations of carbonate, Ca^{2+}, and Mg^{2+} to obtain qualitative information on the effect of these reactants on the rate of formation of U(VI) complexes **3** and **4**. As shown in Figures 33-35, higher carbonate concentrations resulted in slower reactions due to competition of carbonate as a ligand and that increasing the concentration of calcium also decreased the reaction rate although this trend was not as clear as the effect of carbonate. The effect of carbonate and Ca/Mg on the rate of formation of U(VI)/glutaroimide-dioxime complexes is understandable because the ternary complexes, $Ca_2UO_2(CO_3)_3$ and $[(Ca/Mg)UO_2(CO_3)_3]^{2-}$, are stable in the absence of strong ligands such as glutaroimide-dioxime.

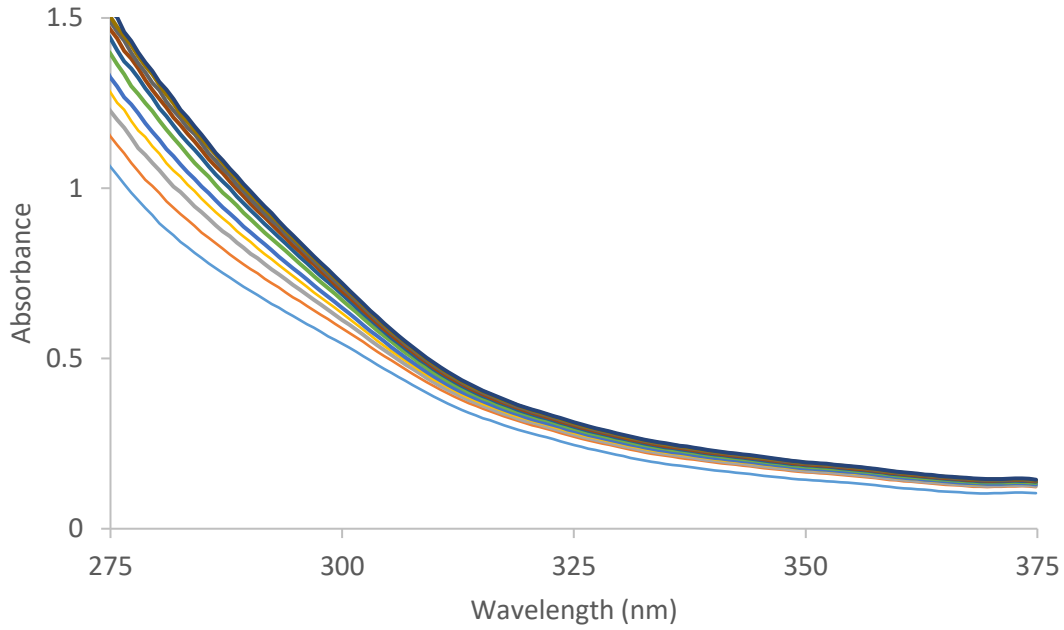

Figure 25. Spectra monitoring the formation of **4** over time. The number of spectra shown has been reduced for clarity (t = 0.1s to t = 8.0 s).
Conditions: [UO_2] = 0.200 mM, [L] = 0.500 mM, [CO_3] = 1.200 mM, [Ca] = 2.50 mM, pH = 7.

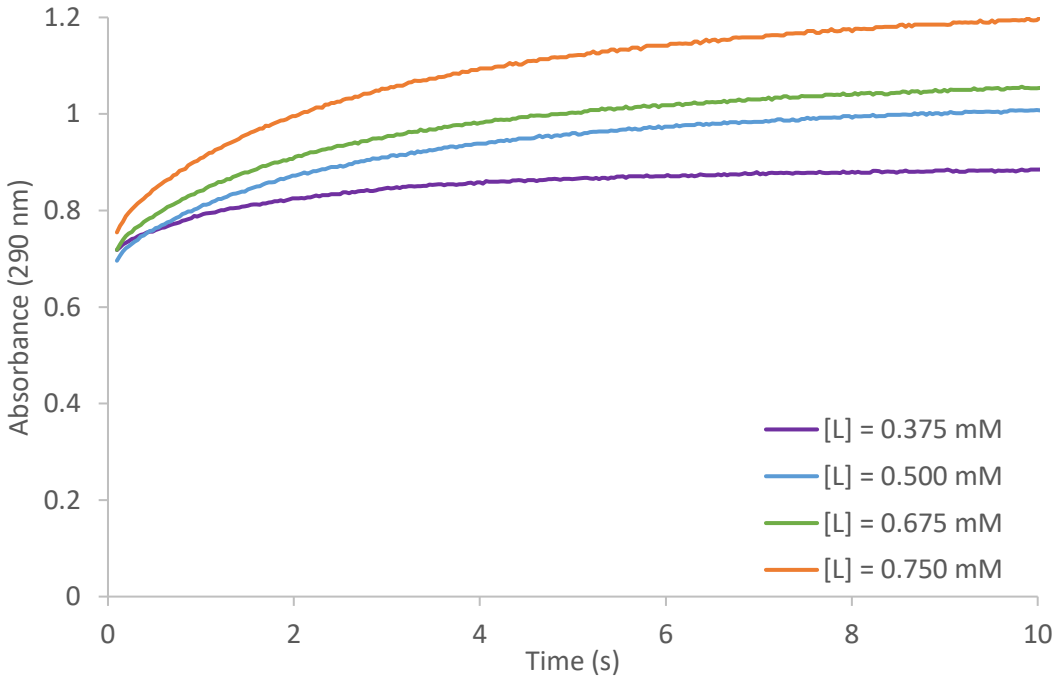

Figure 26. Sample curves from stopped-flow kinetic experiments showing the effect of ligand concentration. Conditions: [UO_2] = 0.200 mM, [carbonate] = 1.600 mM, [Ca] = 2.50 mM, pH = 7.

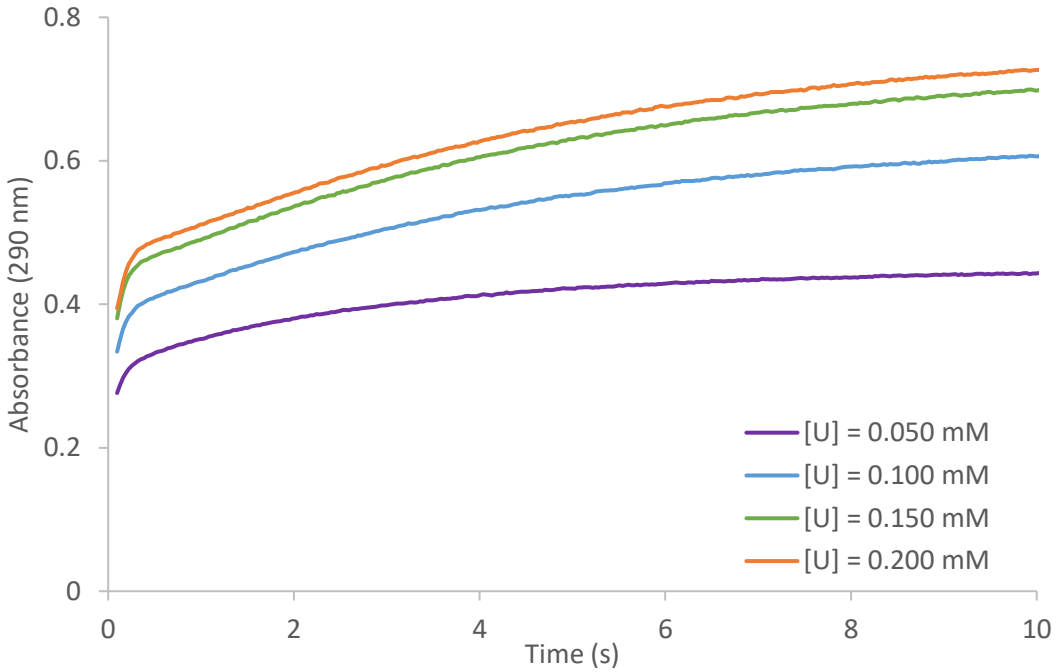

Figure 27. Sample curves from stopped-flow kinetic experiments showing the effect of uranyl concentration. Conditions: [L] = 0.500 mM, [carbonate] = 25×[UO_2], [Ca] = 25×[U], pH = 7.

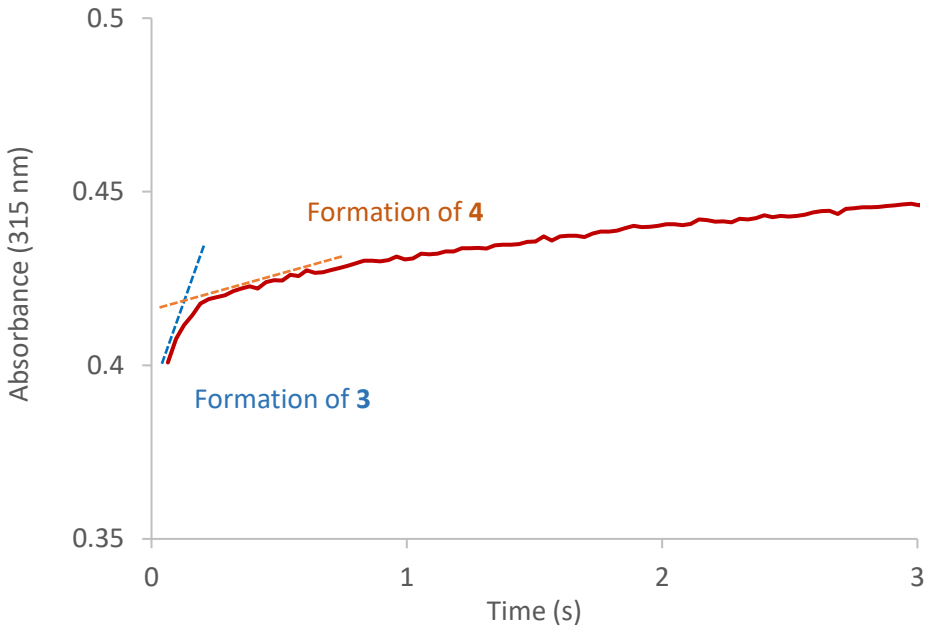

Figure 28. Formation of U(VI) complexes **3** and **4** monitored by stopped-flow UV-Visible spectroscopy showing two distinct slopes. Conditions: [U(VI)] = 0.200 mM, [L] = 0.500 mM, [Ca] = 2.50 mM, [carbonate] = 1.6 mM

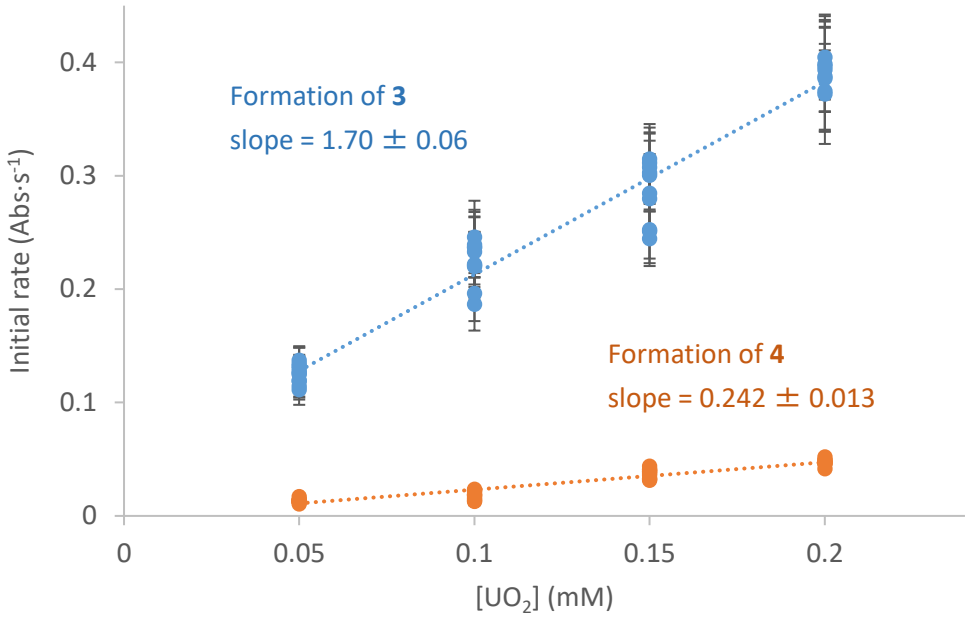

Figure 29. Formation of U(VI) complexes **3** and **4** monitored by stopped-flow UV-Visible spectroscopy. Conditions: constant [L] = 0.500 mM, [Ca] = 25×[U], [carbonate] = 8×[U].

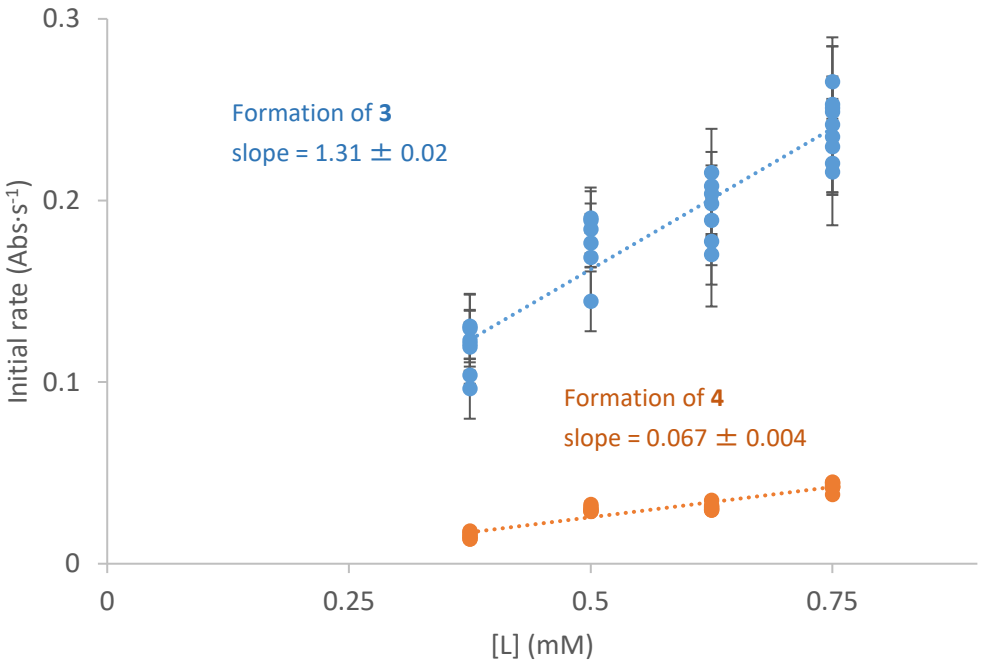

Figure 30. Formation of U(VI) complexes **3** and **4** monitored by stopped-flow UV-Visible spectroscopy. Conditions: [U] = 0.200 mM, [Ca] = 2.50 mM, [carbonate] = 1.60 mM.

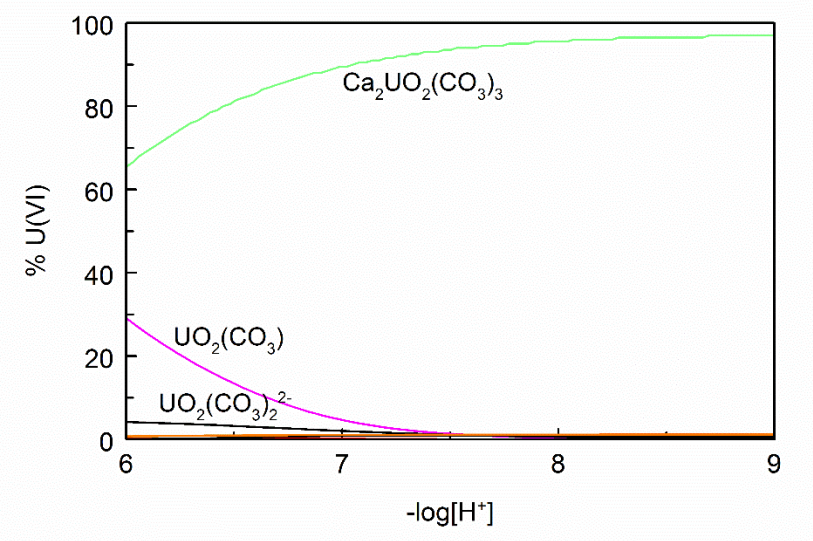

Figure 31. Speciation of 0.2 mM U(VI) in the absence of glutaroimide-dioxime, using literature hydrolysis constants for U(VI).[6] Conditions: [carbonate] = 0.6 mM, [Ca] = 2.5 mM.

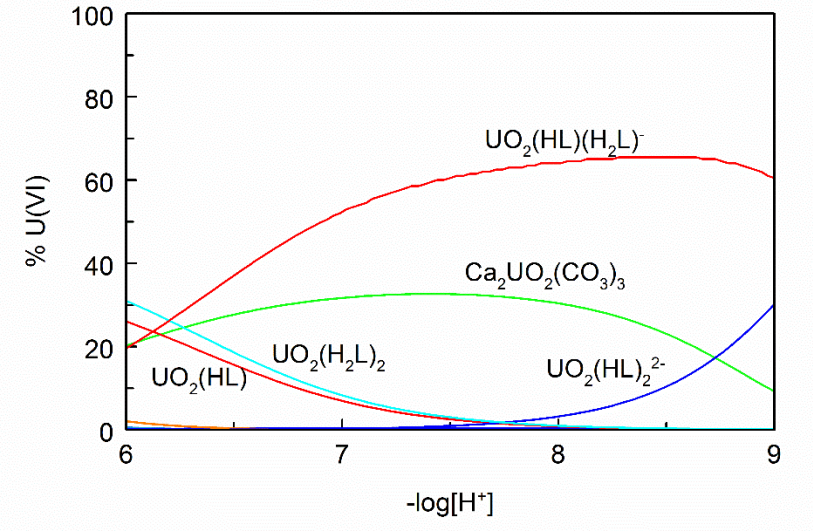

Figure 32. Speciation of 0.2 mM U(VI) with 0.5 mM glutaroimide-dioxime, using literature hydrolysis constants for U(VI)[6] and ligand – U(VI) complexation.[7]
Conditions: [carbonate] = 0.6 mM, [Ca] = 2.5 mM.

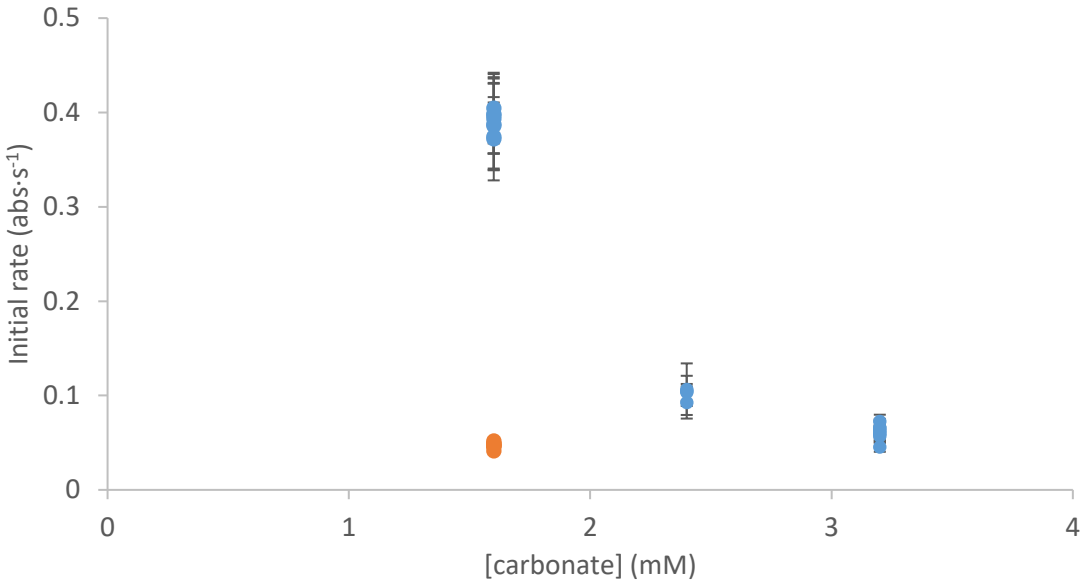

Figure 33. Effect of the concentrations of carbonate on the rate of formation of U(VI) complexes with glutaroimide-dioxime. Two distinct steps for the formation of **3** and **4** were observed at [carbonate] = 1.6 mM so that two initial rates (blue and orange symbols) were plotted, but at [carbonate] > 1.6 mM, only one step was observed corresponding to the formation of both **3** and **4**. Therefore, only one "composite" initial rate (blue symbol) was plotted for higher [carbonate]. Conditions: [U] = 0.200 mM, [L] = 0.500 mM.

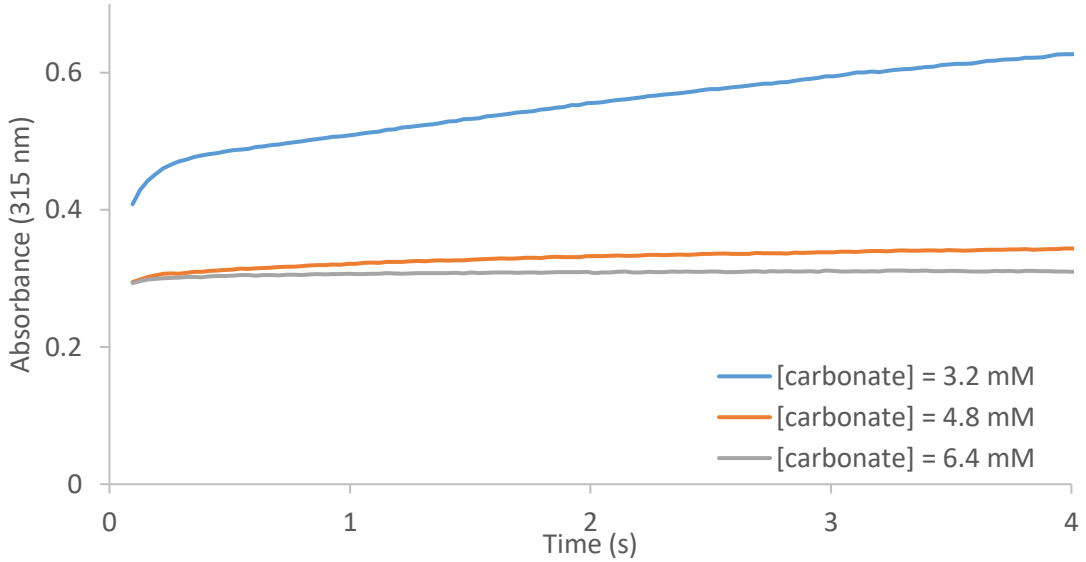

Figure 34. Sample curves showing the effect of the carbonate concentration on the rate of formation of U(VI) complexes with glutaroimide-dioxime. Note that two distinct slopes are only visible at the lowest [carbonate]. Conditions: [UO_2] = 0.200 mM, [Ca] = 2.50 mM, pH = 7.

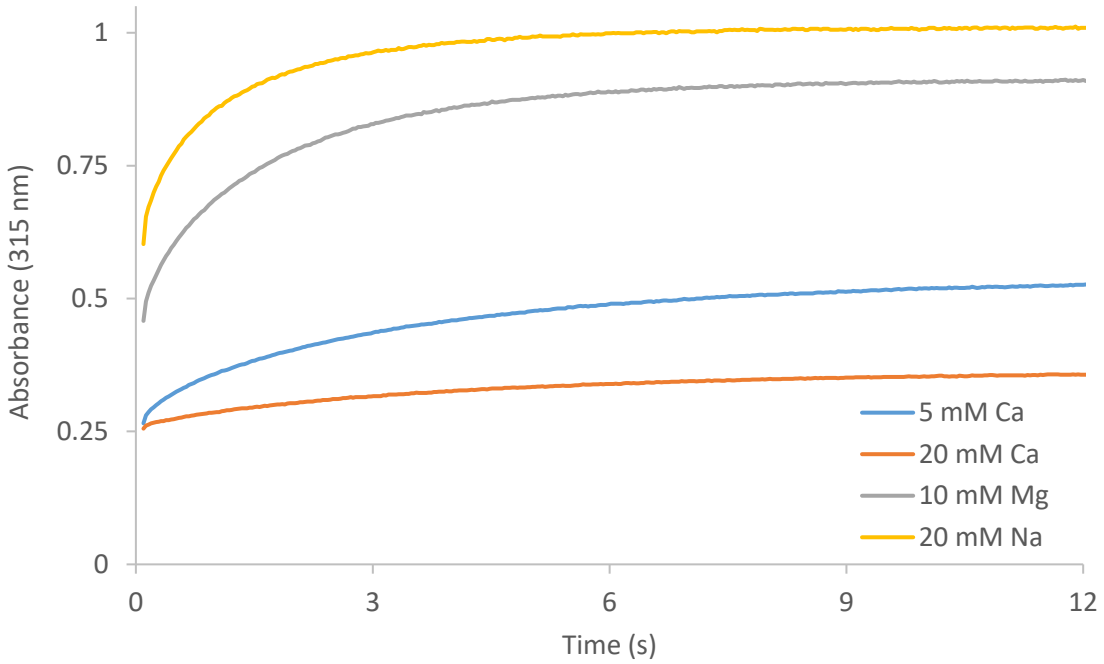

Figure 35. Sample curves showing the effect of the counterion (Ca, Mg, Na) on the rate of formation of U(VI) complexes with glutaroimide-dioxime.
Conditions: [U] = 0.200 mM, [L] = 0.200 mM, [carbonate] = 1.60 mM (as $NaHCO_3$).

As shown in Figure 35, the final absorbance (at 315 nm) of the reaction mixture with Ca(II) is substantially lower than those with Mg(II) or Na(I), which is unexpected if we assume the final product is the same U(VI)/L complex(es) in all the solutions and there are no interactions between the U(VI)/L complex and the cations. To explain this unexpected observation, separate experiments were conducted by adding Ca(II), Mg(II), or Na(I) into a solution of $UO_2(H_2L)(HL)^-$ and collecting the absorption spectra. It was noticed that the color of the solution with Ca(II) intensified and became pink-red while the color of the solutions with Na(I) or Mg(II) changed only slightly, remaining light-yellow or a bit darker yellow, suggesting stronger interactions between the U(VI)/L complex with Ca(II). Furthermore, the spectrum of the solution containing Ca(II) was significantly different with much lower absorbance at 315 nm than those containing Mg(II) or Na(I). Based on these results, we hypothesize that Ca(II) that was released from the $Ca_2UO_2(CO_3)_3$ species upon the formation of $UO_2(H_2L)(HL)^-$ could become associated with the latter, affecting the absorbance of $UO_2(H_2L)(HL)^-$ at 315 nm. The association of Mg(II) with $UO_2(H_2L)(HL)^-$ is probably much weaker and Na(I) weaker still, so that the absorbance of $UO_2(H_2L)(HL)^-$ at 315 nm was much less affected.

Reaction mechanism of the formation of U(VI) complexes 3 and 4

Illustrating the reaction mechanism of the formation of U(VI) complexes **3** and **4** is difficult due to a few reasons: (1) both complexes **3** and **4** absorb at 315 nm and it is not possible to obtain the molar absorptivity of either complex; (2) the acidity and the concentration of carbonate cannot be varied independently; and (3) two distinct steps with different rates of formation are observed only at low [carbonate] but are absent at higher [carbonate], where two

discrete steps are not observed as independent processes with individual slopes (Figures 33 and 34). The latter two reasons suggest that the effect of carbonate on the formation of U(VI)/L complexes is not as straightforward as simple first-order. As a result, only general, somewhat speculative discussions can be made on the mechanism.

A reaction mechanism is proposed in Scheme 3, in which complex **3** is a transient species that forms faster in the first step of the reaction while complex **4** is the final species that forms slower in the second step. The rate of formation as well as the thermodynamic equilibria of the U(VI)/L complexes depends not only on uranyl and ligand concentrations, but also on carbonate and other metal ions present. This also explains the observation that the rate of formation of complex **3** could be significantly slowed down at higher [carbonate] and become similar to that of complex **4**, (Figure 33), such that only one step corresponding to the now rate-limiting first step is observed instead of as two discrete steps.

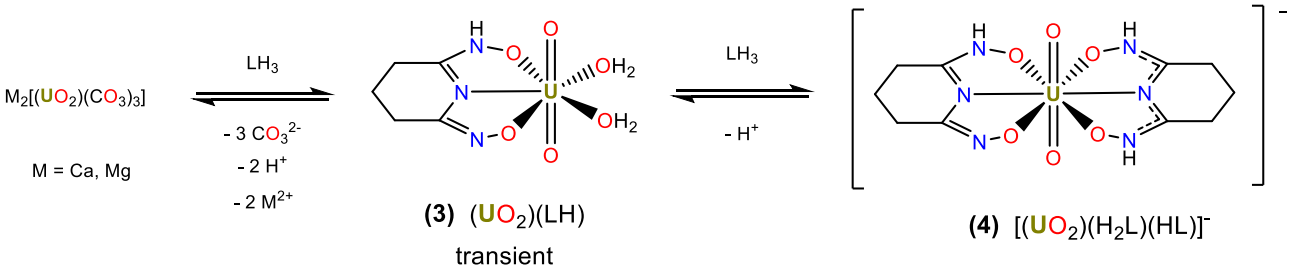

Scheme 3. Proposed reaction mechanism for the formation of U(VI) complexes **3** and **4**.

Interactions between iron(III) and glutaroimide-dioxime

The reaction between aqueous iron(III) and L to form the 1:1 complex **5** (Scheme 1) was performed in the same way as the vanadium reactions, with one set of experiments that vary in [Fe] and another set that vary in [L]. Rather than performing them at neutral pH, these reactions were performed at pH = 4.5 ± 0.5, by adding additional acid. These conditions were chosen because the dominant iron species in the reaction is only the 1:1 complex **5** $[Fe(HL)]^{+}$ rather than a mixture of **5**, **6**, and other species, and it is possible to assign the rate to the formation of this single species.[9] Additionally, precipitation of iron oxide was observed when additional base was added, rendering the solution-state kinetics impossible to determine accurately at neutral pH.[29]

The formation of iron complex **5** is fast and was monitored by stopped-flow spectroscopy. Sample spectra and kinetic traces from stopped-flow experiments are provided in Figures 36-38. From the kinetic traces (absorbance *vs*. time), the initial rates, $(d[\mathbf{5}]/dt)_o$, were calculated as a function of [Fe] (at constant [L] = 0.500 mM) and a function of [L] at constant [Fe = 0.200 mM], shown in Figures 39 and 40, respectively.

The linearity and the convergence of the lines to the origin of the x/y axis in Figures 39 and 40 indicate that, similar to the 1:1 vanadium complex **1**, the formation of the iron complex **5** is also first-order with respect to both iron and the ligand. Under the conditions tested at pH = 4.5, an approximate conditional rate constant of $k' = (1.3 \pm 0.2)\ mM^{-1}\cdot s^{-1}$ was calculated, where $(d[\mathbf{5}]/dt)_o = k'[Fe]\cdot[L]$, similar to equation 2 for V(V). At this acidity (pH = 4.5), the rate of formation, $(d[\mathbf{5}]/dt)_o$, was calculated to be $0.13\ mM\cdot s^{-1}$ when [Fe] = 0.200 mM and [L] = 0.500 mM, which is faster than that of $(d[\mathbf{1}]/dt)_o = 0.028\ mM\cdot s^{-1}$, noting that the latter rate is

at pH = 8.0. In dilute acid the iron exists as the hexaaquo cation, $[Fe(H_2O)_6]^{3+}$, effectively free iron.[29] Since the rate of water exchange in $[Fe(H_2O)_6]^{3+}$ is rapid, it is very likely that the rate-determining step in the formation of complex **5** is the complexation of the ligand to Fe(III), consistent with the mixed second-order kinetics.[15]

It should be pointed out that, similar to the vanadium system, the term *k*' is a function of the acidity, but was unfortunately not investigated in the present study because even slightly varying the acidity of the system resulted in a mixture of different iron species and complicated the analysis. In fact, significant changes in absorbance were observed when this was attempted and, as aforementioned, precipitation of iron species occurred when small quantities of base were added.

It is also worth noting that the concentration of dissolved iron in the ocean is very low due to the very low solubility of iron oxides, hydroxides, and carbonates, and the iron that is present in seawater is often bound to organic ligands and/or taken up and used by microorganisms.[30] This is also true of vanadium, although to a lesser extent.[17] Therefore, the conditions used in the study of Fe(III) in this work are less reflective of seawater conditions than the studies of V(V) and U(VI). Further studies will be needed with more knowledge of specific organic ligands present in the ocean and their speciation in order to accurately determine the rate of iron interactions with glutaroimide-dioxime in seawater.

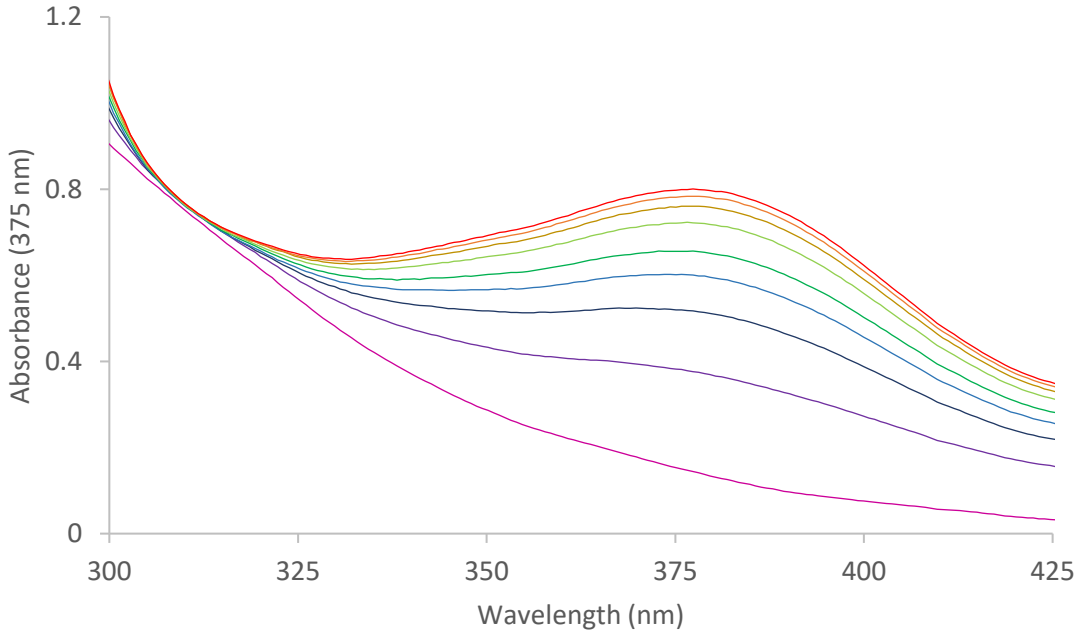

Figure 36. Sample spectra monitoring the formation of **3** over time. The number of spectra shown has been reduced for clarity (t = 0.2 s – 20.0 s).
Conditions: [Fe] = 0.200 mM, [L] = 0.500 mM.

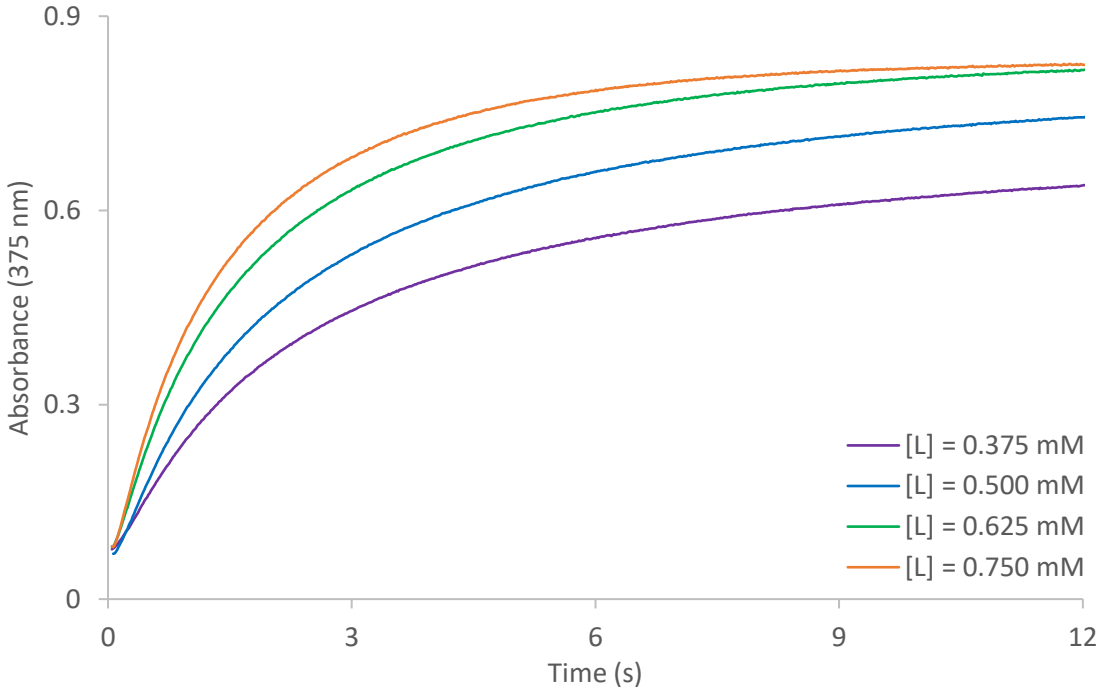

Figure 37. Sample curves from stopped-flow kinetic experiments showing the effect of varying [L]. Conditions: [Fe] = 0.200 mM, pH = 4.5.

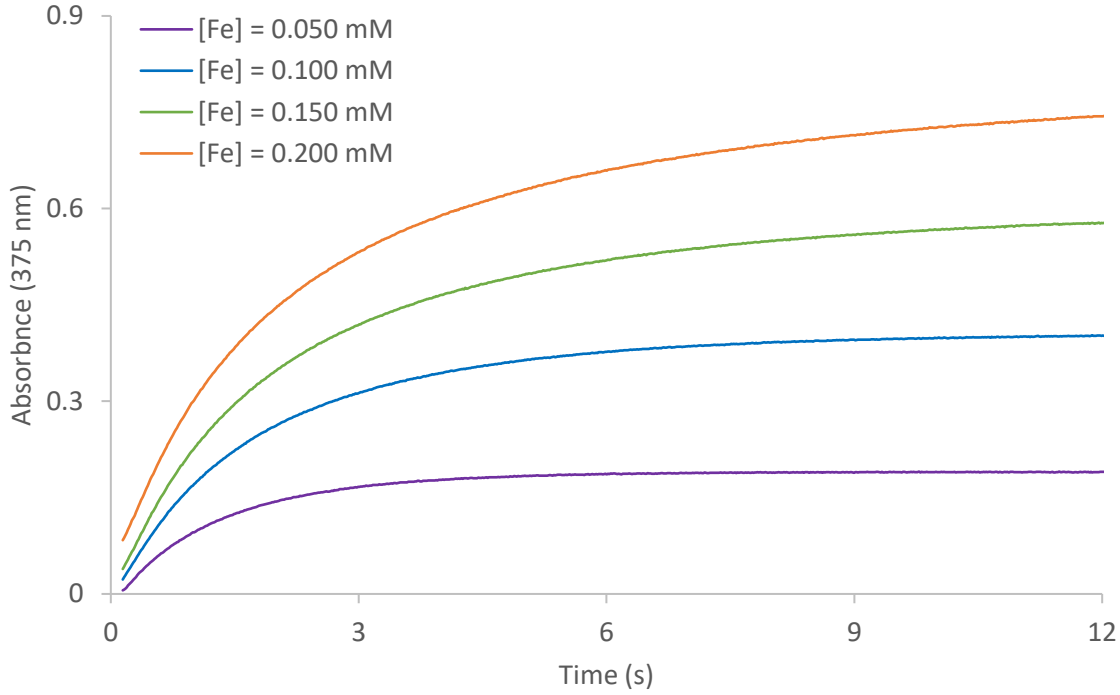

Figure 38. Sample curves from stopped-flow kinetic experiments showing the effect of varying [Fe]. Conditions: [L] = 0.500 mM, pH = 4.5.

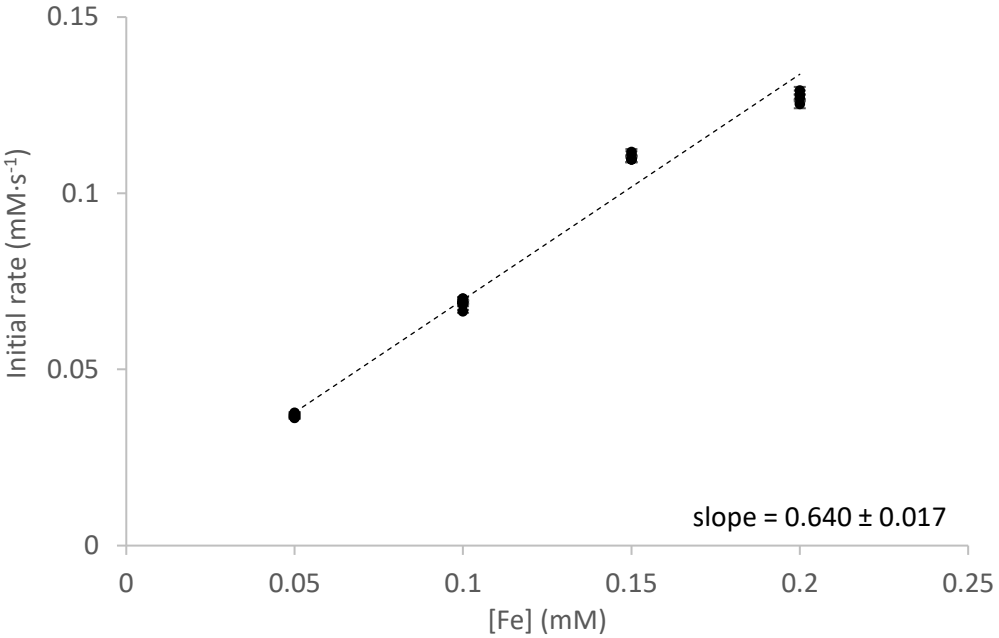

Figure 39. Initial rate of the formation of Fe(III) complex **5** at pH = 4.5 as a function of [Fe] monitored by stopped-flow UV-Visible spectroscopy. Conditions: [L] = 0.500 mM

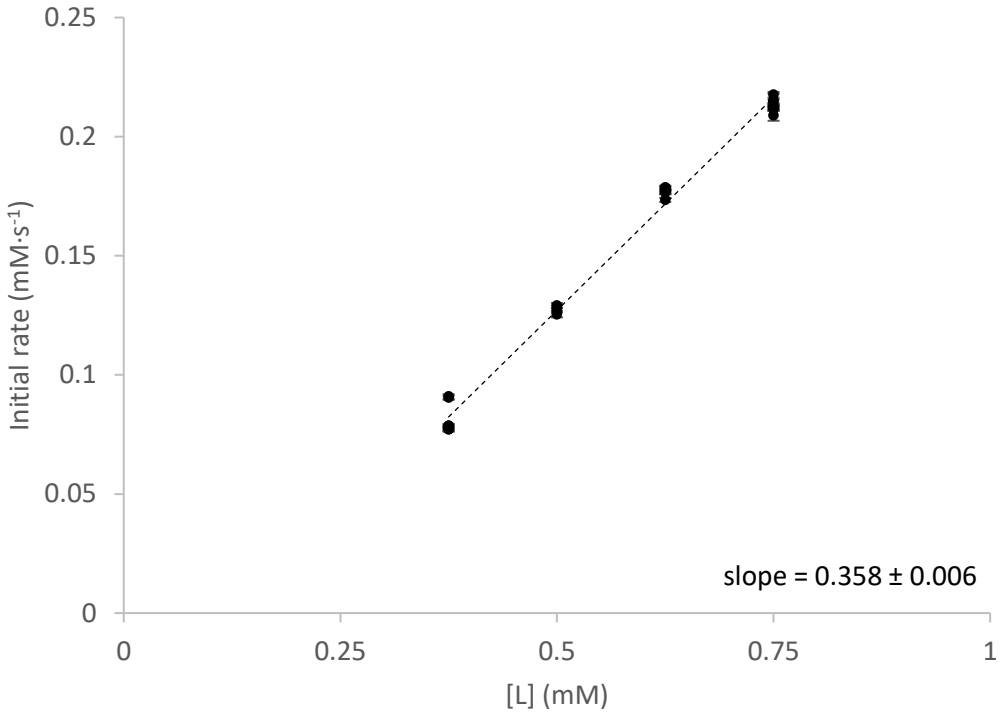

Figure 40. Initial rate of the formation of Fe(III) complex **5** at pH = 4.5 as a function of [L] monitored by stopped-flow UV-Visible spectroscopy. Conditions: [Fe] = 0.200 mM.

Comparison of rates of formation of glutaroimide-dioxime complexes with vanadium, uranium, and iron

Due to the difficulties in determining the reaction order with respect to the acidity in the case of all three ions and the reaction orders with respect to carbonate and Ca/Mg ions in the case of U(VI), the full rate equations for the interactions of glutaroimide-dioxime with the three metal ions were not derived in this study. Nevertheless, several generalizations can be discussed below, largely due to differences in the chemical form of the metal ions of interest.

For all three metal ions, formation of their respective 1:1 ligand-metal complexes, **1** for V(V), **3** for U(VI), and **5** for Fe(III), is first-order in ligand and metal. This indicates that complexation is a simple coordination reaction between one molecule of each, and the differences in the rate constant is due to the chemical form of the metals promoting or hindering reactivity. Based on the data from this study, the relative rates of complexation can be compared in terms of "half-life" of the reaction, $t_{1/2}$ (defined as the time at which the reaction has proceeded 50% to completion, and can be used to compare reactions when the full rate law is unobtainable.[15]), under the same concentrations of metal ions and the ligand. As shown in Figure 41, when [M] = 0.200 mM (M represents V(V), U(VI), and Fe(III)) and [L] = 0.500 mM, the formation of the U(VI) complex **3** is the fastest of the three ($t_{1/2}$ ~ 0.8 s), despite the need for carbonate to dissociate so the ligand can bind. The rate for the U(VI) system is a "composite" for both complexes **3** and **4**, because both complexes absorb at 315 nm and it was not possible to deduce individual absorptivities for each complex. Fe(III) reacts more slowly (k' = (1.3 ± 0.2) $mM^{-1}{\cdot}s^{-1}$; $t_{1/2}$ ~ 1.7 s) to form complex **5**. The formation of V(V) complex **1** is slower still (k' = (0.27 ± 0.02) $mM^{-1}{\cdot}s^{-1}$; $t_{1/2}$ ~ 8.7 s), approximately one order of magnitude slower than that of U(VI). The formation of the 1:2 V(V) complex **2** (Figures 11-13) is much slower than that of all three 1:1 complexes, with the reaction still proceeding after several weeks. The slow rate of formation of V(V) complex, the 1:2 complex **2** in particular, is understandable because the strong oxido bonds in vanadate need to be hydrolyzed and replaced by metal-ligand bonds through dehydration that is probably the rate-determining step in the reaction mechanism for the V(V) system.

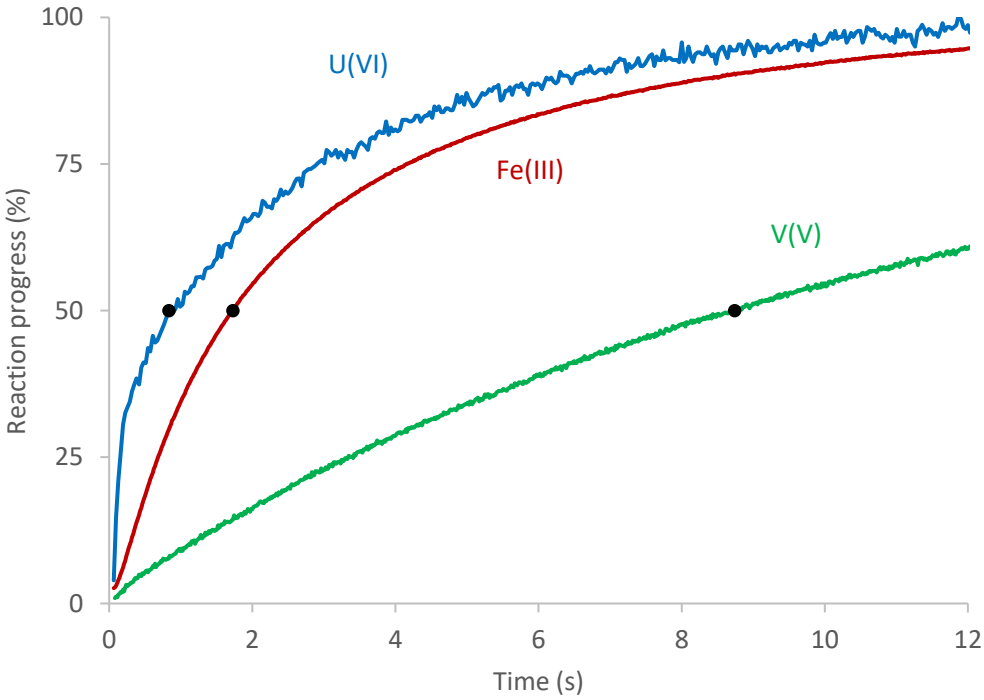

Figure 41. Comparison of the half-life of the formation of 1:1 glutaroimide-dioxime complexes with V(V), U(VI), and Fe(III). [L] = 0.500 mM; [M] = 0.200 mM (M represents V(V), U(VI), and Fe(III); pH = 8.0 for V(V) and U(VI), 4.0 for Fe(III).

Implications for polymer adsorbents

Though the present study has focused on the solution-state chemistry of small-molecule analogues of the amidoxime-type ligands, the results provide insight into the sorption of metal ions by amidoxime-based polymer fibers used in seawater tests and are highly relevant to the selective extraction of uranium from seawater. The findings in this study are in fact consistent with the observed sorption kinetics determined in marine tests with recently developed polymer adsorbent materials: uranium reaching sorption equilibrium the fastest, iron taking slightly longer time, and vanadium still increasing after 56 days in seawater flow columns.[31] Also, recent studies on the exact chemical form of metals on the sorbents using XAS spectroscopy have revealed that the imide-dioxme functional group is still one of the major components interacting with the metal ions. Therefore, the trends in kinetics due to the different metal ion chemistries should hold when comparing the same ligand independent of the exact binding mode.[32]

It is currently unknown whether the formation of a 1:2 V(V)/amidoxime complex occurs on polymer fibers, which would require the vanadium to be tethered between two polymer chains. The steric clash of the adjacent functional groups and the limited flexibility of the macromolecular polymer chains may not allow this, in which case the vanadium would remain in a 1:1 binding mode despite the thermodynamics favoring a 1:2 complex. This would also vary depending on the morphology and conditioning of the polymer adsorbent used, which would affect the thermodynamically and kinetically favored binding modes of all three different metals.[32,33]

The observed decomposition of the 1:2 V(V)/amidoxime complex has implications for the recycling and reusability of polymer adsorbents. If it does form, then even stoichiometric amounts of acid can accelerate and promote ligand decomposition. Hydrochloric acid has been used to strip metals for their recovery and reuse the adsorbent, which is especially problematic since harsh conditions (over 3M HCl, with heating) are needed to completely remove vanadium.[34] This treatment degrades the polymer, reducing capacity in future uses. Milder techniques to strip metals such as elution with peroxide, hydroxylamine, or carbonate solutions have been shown to help prevent decomposition through this method, although removal of vanadium may still be problematic.[35,36]

Summary and conclusions

Understanding metal binding of glutaroimide-dioxime as a small molecule analogue of functional groups on polymer adsorbents is critical to improve selectivity for uranium over other metals in the recovery of uranium from seawater. We have explored the kinetics of vanadium binding with glutaroimide-dioxime in comparison with U(VI) and Fe(III). The formation of the 1:1 complexes of all three metal ions were found to show a first-order relationship with metal and ligand concentrations. However, other factors such as acid concentration (for vanadium) and carbonate concentration (for uranyl) play very important roles in binding kinetics. In the narrow and near neutral pH region, the formation of the 1:1 vanadium(V)/L complex follows the first order with respect to $[H^+]$. Qualitatively, higher concentrations of carbonate and counter ions such as Ca(II) and Mg(II) lower the rate of formation of U(VI)/L complexes. Relative to each other, the 1:1 complexes, studied by stopped-flow spectroscopy, form rapidly with rates differing by only one order of magnitude, with U(VI) the fastest, followed by Fe(III), then V(V). Formation of the 1:2 V(V) complex takes place over a longer period of time of several days to weeks, and its concentration (rather than rate of formation) was monitored by conventional UV-visible spectrometry and NMR techniques, while formation of the 1:2 uranyl complex occurs on a similar timescale to the 1:1 uranyl complex.

Based on the data from this work, reaction mechanisms for the formation of metal complexes with glutaroimide-dioxime are proposed. In the case of vanadium, the rates of formation of the 1:1 and 1:2 complexes are both drastically increased by adding acid, strongly suggesting a slow protonation step followed by oxido ligand hydrolysis and loss of water to allow ligand binding. The faster kinetics and first-order reaction rate imply a simple associative binding mechanism for iron and uranyl as well despite the presence of strong carbonate complexes of the latter. The slow decomposition of the 1:2 non-oxido vanadium complex in acidic solutions was also investigated and the results can help explain the decomposition of the amidoxime-based sorbents observed during acid elution of polymer adsorbents in marine tests.

References

(1) Gill, G. A.; Kuo, L.-J.; Janke, C. J.; Park, J.; Jeters, R. T.; Bonheyo, G. T.; Pan, H.-B.; Wai, C.; Khangaonkar, T.; Bianucci, L.; Wood, J. R.; Warner, M. G.; Peterson, S.; Abrecht, D. G.; Mayes, R. T.; Tsouris, C.; Oyola, Y.; Strivens, J. E.; Schlafer, N. J.; Addleman, R. S.; Chouyyok, W.; Das, S.; Kim, J.; Buesseler, K.; Breier, C.; D'Alessandro, E. *Ind. Eng. Chem. Res.* **2016**, *55*, 4264–4277.

(2) Endrizzi, F.; Melchior, A.; Tolazzi, M.; Rao, L. *Dalton Trans.* **2015**, *44*, 13835–13844.

(3) Vukovic, S.; Hay, B. P.; Bryantsev, V. S. *Inorg. Chem.* **2015**, *54*, 3995–4001.

(4) Mehio, N.; Lashely, M. a.; Nugent, J. W.; Tucker, L.; Correia, B.; Do-Thanh, C.-L.; Dai, S.; Hancock, R. D.; Bryantsev, V. S. *J. Phys. Chem. B* **2015**, *119*, 3567–3576.

(5) Leggett, C. J.; Parker, B. F.; Teat, S. J.; Zhang, Z.; Dau, P. D.; Lukens, W. W.; Peterson, S. J. M.; Cardenas, A. J. P.; Warner, M. G.; Gibson, J. K.; Arnold, J.; Rao, L. *Chem. Sci.* **2016**, *7*, 2775–2786.

(6) Endrizzi, F.; Rao, L. *Chem. - A Eur. J.* **2014**, *20*, 14499–14506.

(7) Tian, G.; Teat, S. J.; Zhang, Z.; Rao, L. *Dalton Trans.* **2012**, *41*, 11579–11586.

(8) Sun, X.; Tian, G.; Xu, C.; Rao, L.; Vukovic, S.; Kang, S. O.; Hay, B. P. *Dalton Trans.* **2014**, *43*, 551–557.

(9) Sun, X.; Xu, C.; Tian, G.; Rao, L. *Dalton Trans.* **2013**, *42*, 14621.

(10) Zheng, X.; Bi, C.; Li, Z.; Podariu, M.; Hage, D. S. *J. Pharm. Biomed. Anal.* **2015**, *113*, 163–180.

(11) Rao, L.; Zhang, Z.; Friese, J. I.; Ritherdon, B.; Clark, S. B.; Hess, N. J.; Rai, D. *J. Chem. Soc. Dalt. Trans.* **2002**, 267.

(12) Xu, J.; Jordan, R. B. *Inorg. Chem.* **1988**, *27*, 4563–4566.

(13) Howarth, O. W. *Prog. Nucl. Magn. Reson. Spectrosc.* **1990**, *22*, 453–485.

(14) Aureliano, M.; Ohlin, C. A.; Vieira, M. O.; Marques, M. P. M.; Casey, W. H.; Batista de Carvalho, L. A. E. *Dalton Trans.* **2016**, *45*, 7391–7399.

(15) Espenson, J. H. *Chemical kinetics and reaction mechanisms*; 2nd ed.; McGraw-Hill, 1995.

(16) Larsson, K.; Cullen, T. D.; Mezyk, S. P.; McDowell, R. G.; Martin, L. R. *RSC Adv.* **2017**, *7*, 26507–26512.

(17) Wang, D.; Sañudo Wilhelmy, S. a. *Mar. Chem.* **2009**, *117*, 52–58.

(18) Heath, E.; Howarth, O. W. *J. Chem. Soc. Dalt. Trans.* **1981**, 1105.

(19) Gresser, M. J.; Tracey, A. S. *J. Am. Chem. Soc.* **1985**, *107*, 4215–4220.

(20) Pettersson, L.; Elvingson, K. 1998; pp. 30–50.

(21) Ivanov, A. S.; Leggett, C. J.; Parker, B. F.; Zhang, Z.; Arnold, J.; Dai, S.; Abney, C. W.; Bryantsev, V. S.; Rao, L. *Manuscr. Submitt.* **2017**.

(22) Morgenstern, B.; Kutzky, B.; Neis, C.; Stucky, S.; Hegetschweiler, K.; Garribba, E.; Micera, G. *Inorg. Chem.* **2007**, *46*, 3903–3915.

(23) Morgenstern, B.; Steinhauser, S.; Hegetschweiler, K.; Garribba, E.; Micera, G.; Sanna, D.; Nagy, L. *Inorg. Chem.* **2004**, *43*, 3116–3126.

(24) Wang, P.-L.; Werner, P.; Nord, A. G. *Zeitschrift für Krist.* **1992**, *198*, 271–276.

(25) Lutz, O.; Nepple, W.; Nolle, A. *Zeitschrift für Naturforsch. A* **1976**, *31*, 3–7.

(26) Bhattacharya, S.; Kumari, N. *Coord. Chem. Rev.* **2009**, *253*, 2133–2149.

(27) Kang, S. O.; Vukovic, S.; Custelcean, R.; Hay, B. P. *Ind. Eng. Chem. Res.* **2012**, *51*, 6619–6624.
(28) Bernhard, G.; Geipel, G.; Brendler, V.; Nitsche, H. *J. Alloys Compd.* **1998**, *271–273*, 201–205.
(29) Baes, C. F.; Mesmer, R. E. *The Hydrolysis of Cations*; John Wiley & Sons Inc: New York, London, Sydney, Toronto, 1976.
(30) Hirose, K. *Anal. Sci.* **2006**, *22*, 1055–1063.
(31) Das, S.; Oyola, Y.; Mayes, R. T.; Janke, C. J.; Kuo, L.-J.; Gill, G.; Wood, J. R.; Dai, S. *Ind. Eng. Chem. Res.* **2016**, *55*, 4110–4117.
(32) Abney, C. W.; Mayes, R. T.; Piechowicz, M.; Lin, Z.; Bryantsev, V. S.; Veith, G. M.; Dai, S.; Lin, W. *Energy Environ. Sci.* **2016**, *9*, 448–453.
(33) Kim, J.; Tsouris, C.; Oyola, Y.; Janke, C. J.; Mayes, R. T.; Dai, S.; Gill, G.; Kuo, L. J.; Wood, J.; Choe, K. Y.; Schneider, E.; Lindner, H. *Ind. Eng. Chem. Res.* **2014**, *53*, 6076–6083.
(34) Pan, H.-B.; Kuo, L.-J.; Wai, C. M.; Miyamoto, N.; Joshi, R.; Wood, J. R.; Strivens, J. E.; Janke, C. J.; Oyola, Y.; Das, S.; Mayes, R. T.; Gill, G. A. *Ind. Eng. Chem. Res.* **2016**, *55*, 4313–4320.
(35) Oyola, Y.; Vukovic, S.; Dai, S. *Dalton Trans.* **2016**, 8532–8540.
(36) Pan, H.-B.; Liao, W.; Wai, C. M.; Oyola, Y.; Janke, C. J.; Tian, G.; Rao, L. *Dalton Trans.* **2014**, *43*, 10713–10718.

Chapter 4

Redox activity of vanadium complexes of glutaroimide-dioxime

Introduction

Vanadium is present in seawater at approximately 0.5-2 ppb (10-40 nM)[1], which is similar to that of uranium at 3.3 ppb (13 nM)[2]. It is mainly present in the V(V) oxidation state due to slow oxidation of V(IV) by aerated water, however, approximately 10-15% of vanadium is present in the V(IV) state.[1] This naturally occurring mixture of oxidation states, which is subject to seasonal and geographical variation, is a consequence of biological uptake and use of vanadium in marine environments.[1,3] Vanadium is an essential element for many organisms, although typically in very small amounts. *In vivo*, vanadium is present in several chemical environments in oxidation states ranging from V(III) – V(V), most commonly V(IV), and when marine organisms die they release vanadium in multiple oxidation states.[4]

Although the complexation chemistry of V(V) has been studied recently with glutaroimide-dioxime,[5] as well as its interactions with polymer sorbents,[6] similar chemistry of V(IV) has not yet been investigated. Our initial work sought to study the interactions of V(IV) with seawater-relevant ligands (Figure 1) in the same manner as U, Fe, V(V) and other metals.[5,7,8] In this way, we would seek to understand the role that V(IV) plays in determining uranium sorption selectivity and see if non-oxido vanadium species could form in the V(IV) oxidation state as for V(V). However, we discovered that V(IV) readily oxidizes to V(V) in the presence of ligands and instead forms previously characterized V(V) complexes. Acetone oxime, a simple oxime substrate, also reacts readily with V(IV) and was used as a model substrate to study reaction conditions without interference due to complexation with vanadium.

The type of reactivity we investigate here has previously been observed with hydroxamic acids, a similar class of ligands with N-OH groups, where the O atom is abstracted upon complexation with V(III), V(IV), and Mo(V), forming the corresponding amide and higher oxidation state metal-oxo complexes.[9] One reported reaction between V(IV) and salicylaldoxime leads to the V(V) chelating oxime complex as well as smaller amounts of other complexes arising from coupled small organic molecules.[10] Other low oxidation state metal ions have also been observed to react similarly, including Mo(II)[11] and U(IV),[12] although in seawater uranyl is present exclusively as uranyl(VI) carbonate complexes.[13]

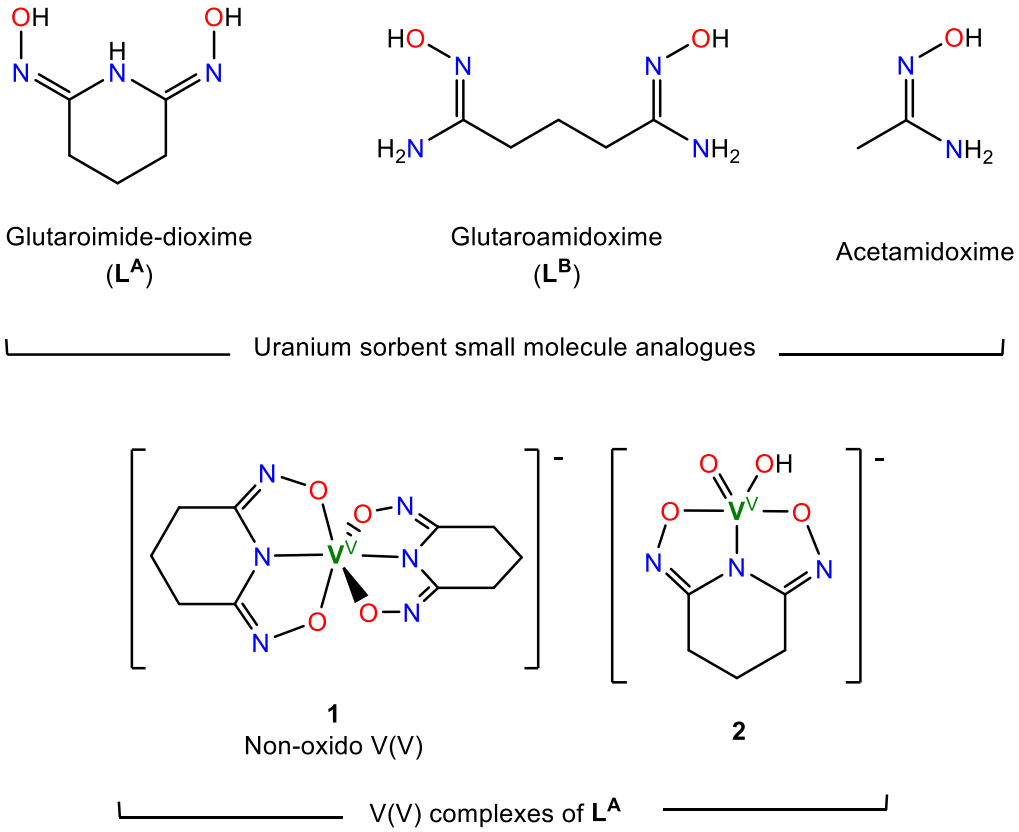

Figure 1. Ligands investigated for V(IV) reactivity and their known V(V) complexes.

In our attempts to prepare and characterize V(IV) complexes of the model oxime ligands and reagents shown in Figure 1, we found that they invariably reacted to form V(V) complexes. Cyclic voltammetry was performed on the 2:1 glutaroimide-dioxime V(V) complex **1** and, surprisingly, it was found to undergo reduction at strongly negative potential. We also attempted to synthesize a V(IV) complex in non-aqueous solvents both directly and through chemical reduction of the V(V) complex, however, no stable complexes could be isolated, suggesting that the V(IV) analogue is inherently unstable towards ligand reactivity or disproportionation.

Experimental

Chemicals

Acetamidoxime was synthesized by stirring equal volumes of a 50% aqueous hydroxylamine solution, acetonitrile, and ethanol (5 mL each) at room temperature for 24 hours, followed by heating to 40°C in a glass petri dish until all the volatiles evaporated and a white solid remained. It was then dissolved in water (5 mL) and evaporated again. The resulting solid was redissolved in approximately 10 mL of water and its concentration was determined by ^{1}H NMR spectroscopy and protonation titrations.

Glutaroamidoxime ($\mathbf{L^B}$)[14] and vanadyl toluenesulfonate[15] were synthesized according to literature procedures. Glutaroimide-dioxime ($\mathbf{L^A}$) was synthesized according to literature procedure and recrystallized twice from methanol before use.[16]

Vanadyl (V(IV)) solutions were prepared by reducing a solution of acidified V_2O_5 with excess hydroxylamine hydrochloride. V(IV) was precipitated as VO_2 by the addition of sodium hydroxide, then redissolved in hydrochloric acid. The concentration of V(IV) was determined by titration with a solution of $KMnO_4$ of known concentration.

Tetraethylammonium vanadium(V) bis(glutaroimide-dioxime) ([NEt_4][**1**]) was prepared by adding glutaroimide-dioxime (290 mg, 2.1 mmol), ammonium metavanadate (117 mg, 1.0 mmol), and tetraethylammonium bromide (168 mg, 0.80 mmol) to a mixture of water (10 mL) and methanol (5 mL). The mixture was stirred vigorously for 30 minutes at room temperature, during which the mixture turned dark brown and the solids completely dissolved. The mixture was transferred to a glass petri dish and warmed at 40°C overnight, during which all the solvent evaporated to leave a dark brown solid. The solid was extracted with dichloromethane (5×10 mL), dried over magnesium sulfate, filtered, and the solvent removed to give a brown oil. This was crystallized from dichloromethane (20 mL) layered with an equal volume of THF. Large dark brown-black blocks of [NEt_4][**1**] formed over several days. It is very soluble in chloroform, dichloromethane, alcohols, and most other polar solvents, has trace solubility in THF, and is insoluble in all low-polarity solvents. The same product can be obtained in similar yield by using sodium orthovanadate instead of ammonium metavanadate, adjusting the pH to 6-8. Yield: 230 mg (0.50 mmol, 63%). ^{1}H NMR ($CDCl_3$, 500 MHz): 1.23 ppm, t, 12H, $N(CH_2C\mathbf{H}_3)_4$, 1.95 ppm, quintet, 4H, $CH_2C\mathbf{H}_2CH_2$, 2.62 ppm, t, 8H, $C\mathbf{H}_2CH_2C\mathbf{H}_2$, 3.18 ppm, , t, 8H, $N(C\mathbf{H}_2CH_3)_4$; ^{13}C NMR($CDCl_3$, 126 MHz): 7.7 ppm, $N(CH_2\mathbf{C}H_3)_4$, 21.4 ppm, $CCH_2\mathbf{C}H_2CH_2C$, 21.6 ppm, $C\mathbf{C}H_2CH_2\mathbf{C}H_2C$, 52.5 ppm, $N(\mathbf{C}H_2CH_3)_4$, 154.0 ppm, **C**=N-O; ^{51}V NMR ($CDCl_3$, 132 MHz): 739 ppm.

All other chemicals were obtained from commercial sources and used as received.

Cyclic voltammetry

Cyclic voltammetry experiments were performed on a Gamry Instruments Reference 600 potentiostat and data acquired with Gamry Framework software. Experiments in acetonitrile and DCM were performed in an inert atmosphere glovebox using dry solvent with 0.1 M [NBu_4][PF_6] electrolyte, with a Pt disc working electrode, Pt gauze counter electrode and Pt wire quasi-reference electrode. Experiments in water and methanol were performed with a Pt disc working electrode, Pt wire counter electrode and Ag/AgCl reference electrode, with 0.2 M KCl as the electrolyte in water and 0.2 M [NEt_4][Cl] in methanol. Non-aqueous

potentials were referenced against ferrocene (Fc^+/Fc at 0 V) and aqueous potentials referenced against potassium ferricyanide ($[Fe(CN)_6]^{3-}/[Fe(CN)_6]^{4-}$ at +0.04 V; Fc^+/Fc nominally at 0 V).

NMR

An internal standard of approximately 1 mM *t*-butanol (the exact concentration calculated per experiment based on stock solution volumes) in D_2O/H_2O mixtures was used as the solvent for quantitative experiments. ^1H NMR spectra in water or H_2O/D_2O mixtures were acquired on a Bruker AV-500 instrument (500 MHz) with a WATERGATE solvent suppression pulse sequence. ^{51}V NMR spectra were acquired on a Bruker DRX-500 instrument (132 MHz).

Crystallography

X-ray structural determination was performed on a Bruker APEX diffractometer with a Bruker fixed-Chi 3-Circle goniometer, a Bruker SMART APEX II CCD detector, and a monochromatized fine-focus sealed Mo-kα X-ray source. A crystal was coated with paratone oil and mounted in a Kaptan loop, which was mounted on the goniometer with a nitrogen cryostream held at a temperature of 100 ± 0.5 K. Crystallography data was processed in the WinGX software package, solved using the SHELXTL software package and refined with the SHELXL software package, with semiempirical absorption correction with SADABS, included in SHELXTL.[17] All non-hydrogen and non-solvent atoms were refined anisotropically, and non-solvent hydrogens were placed using a riding model. Solvent oxygen atoms were refined isotropically and solvent hydrogens were not located.

Results and Discussion

Attempts to prepare reduced L^AA-vanadium(IV) complex

In order to study the complexation behavior of vanadium(IV) with $\mathbf{L^A}$, we initially attempted a direct synthesis from $\mathbf{L^A}$ and aqueous vanadyl under a variety of reaction conditions, varying pH, stoichiometry, and the rate and order of addition of reagents. However, in water, only known V(V) species were identified as products: **1**, **2**,[5] and free vanadates, the exact species of the latter was dependent on concentrations and pH.[18] Regardless of the conditions used, V(V) species were invariably produced, with the reaction changing to the amber-brown color of **1**. To preclude the role of oxygen in these reactions, water degassed by boiling or sparging with nitrogen was used with no change in outcome, indicating that V(IV) oxidation is caused by the ligand itself.

When the same reaction was performed in dry, degassed methanol, the reaction mixture turned a deep red color within seconds, followed by a slow change to amber, indicating the formation of **1**. If the reaction was carried out under argon and the solvent is removed rapidly just after the onset of the reaction, the only product that solidified from the reaction was toluenesulfonic acid. The remainder of the reaction was a viscous red oil which contains polyoxovanadates (V(V)).[18] When water is added to the red solution or oil, the vanadium clusters hydrolyze immediately and form the V(V) complex **1** with its characteristic dark amber color. If the reaction is performed in basic methanol (sodium methoxide) or methanol with a drop of added water, the red color was not observed, instead forming **1** directly.[19]

The reaction of V(IV) with glutaroimide-dioxime was also tested in aprotic solvents. Vanadyl acetylacetonate was dissolved in dry acetonitrile and excess $\mathbf{L^A}$. Due to the low solubility of $\mathbf{L^A}$, the reaction proceeded slowly, and the solution first turned green and then amber, also forming a brown-black precipitate. Small amounts of **1** were present in solution (determined by ^{51}V NMR spectroscopy), and the insoluble black product could not be extracted into any solvent, including water, implying some irreversible decomposition process. Disproportionation of a $\mathbf{L^A}$-V(IV) species formed initially could be occurring to form insoluble, reduced metal oxides. Based on these results, cyclic voltammetry was performed to determine the accessibility of the V(IV) oxidation state from **1** and establish possible reaction conditions.

Cyclic voltammetry of complex 1

In order to solubilize **1** in non-aqueous solvents to perform nonaqueous reductions, a cation exchange reaction was performed to synthesize the organic-soluble tetraethylammonium complex. The extraction of **1** in the presence of tetraethylammonium bromide from water into immiscible organic solvents failed and all compounds remained in the aqueous phase. However, the complex was successfully isolated by synthesizing **1** in the presence of tetraethylammonium bromide in a water/methanol mixture, evaporating the solution to dryness, then extracting into dichloromethane. [NEt_4][**1**] was obtained as very dark brown-black block crystals by layering a dichloromethane solution with THF. [NEt_4][**1**] was used in all cyclic voltammetry experiments due to its exact stoichiometry and higher purity, unlike the sodium salt isolated from water which may contain excess reagents and salts.

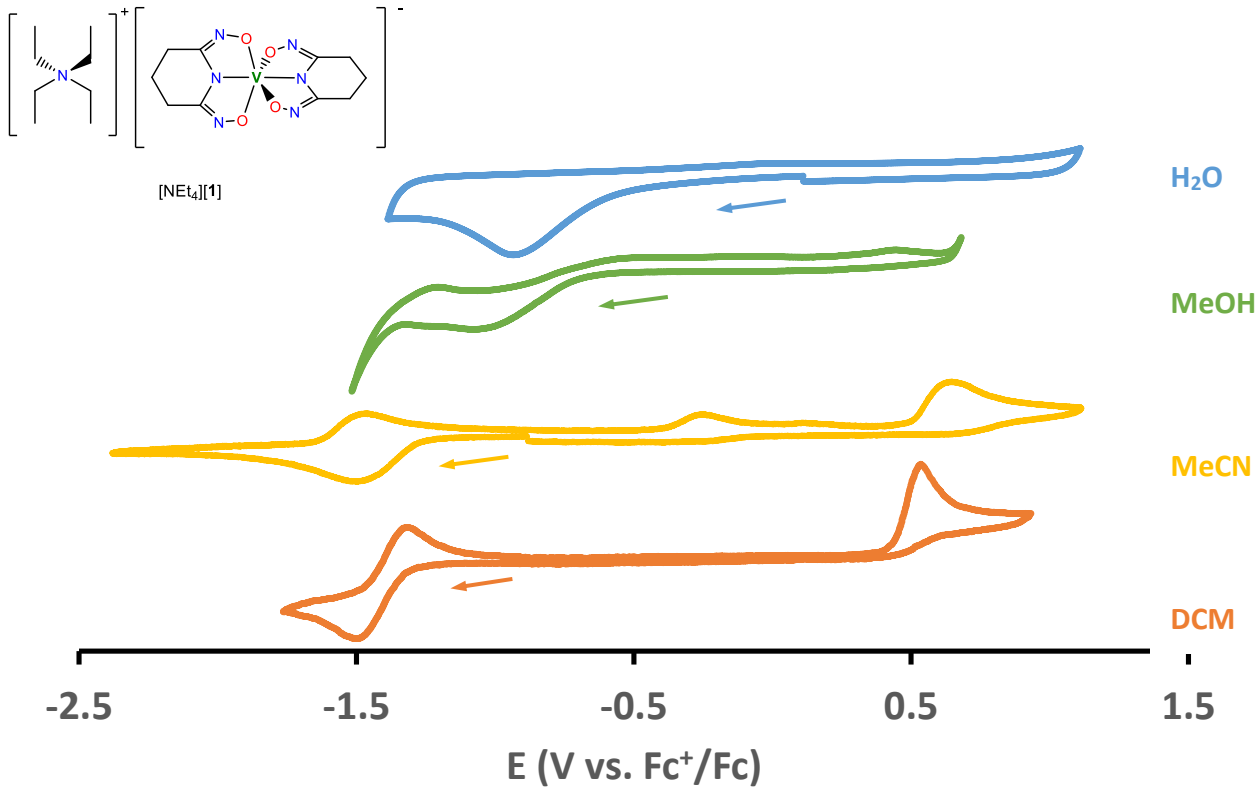

Figure 2. Cyclic voltammograms of **1** in several solvents, all measured at a scan rate of 100 mV/s against a Pt working electrode.

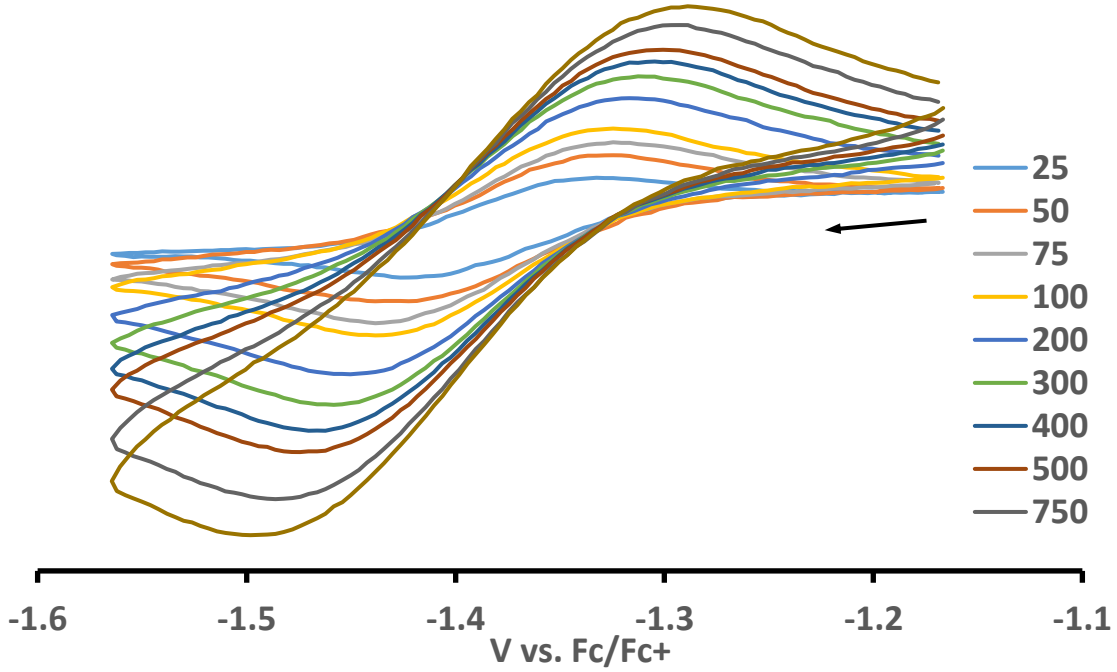

Figure 3. Reduction of [NEt_4][**1**] in DCM measured at different scan rates (in mV/s)

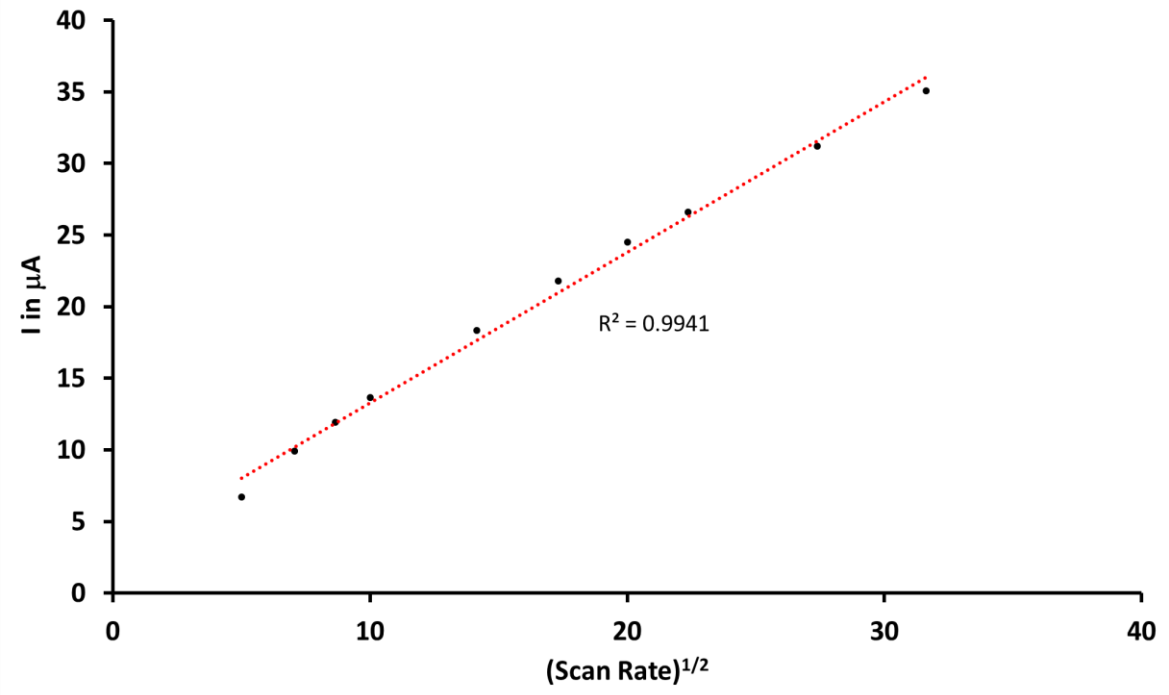

Figure 4. Linear plot of the flowing current vs the square root of the scan rate for the first reduction of [NEt_4][**1**] in DCM.

In water, one irreversible reduction was observed at E_p^c -920 mV vs. Fc^+/Fc, which we assign to the reduction of V(V) to V(IV), followed by subsequent decomposition. This is more negative than other V(V)/V(IV) redox potentials (-600 mV for $[V^VO_2]^+/[V^{IV}O]^{2+}$ in acid or -400 mV for $[V^VO_4]^{3-}/[H_2V^{IV}O_4]^{2-}$ in strong base, relative to ferrocene),[20] suggesting that the vanadium center is more electron rich due to binding of the strongly electron-donating ligand (Figure 2). No oxidation wave was observed on the return scan, and solids were observed to plate onto the electrode, so deposition of V(IV) as VO_2 is likely, since the V(IV) complex that is formed is not stable. Decomposition could conceivably proceed through ligand dissociation and hydrolysis to form free vanadium as VO_2.

Cyclic voltammetry was also performed in non-aqueous solvents to investigate if performing the experiments in water was precluding the isolation of a V(IV) complex. In methanol, the same irreversible behavior was observed, with an irreversible reduction at a similar potential of E_p^c -1000 mV. The similarity of the electrochemical behavior and chemical reactions (see above) suggest that a similar process may be taking place in both cases, with the V(IV) complex that is transiently formed reacting with the ligand and then dissociating and depositing as VO_2 or other vanadium oxide.

Different electrochemical behavior was observed in the aprotic solvents acetonitrile and dichloromethane. For the former, an irreversible reduction occurs at E_p^c -1.5 V, at more negative potential than in water or methanol. In this case, the initial reduction likely occurs in the same manner as in the protic solvents, but without a proton source for the ligand to dissociate completely and the V(IV) complex to hydrolyze, the acetonitrile coordinates or reacts, leading to a V(IV) complex that remains soluble. A reverse wave is observed on the return scan, but appears with almost no peak-to-peak separation, a different peak height, and

does not follow normal square-root law behavior. The oxidation occurring is likely this new V(IV) complex reoxidizing to V(V), with other oxidations of reacted ligands observed at more positive potentials.

Lastly, cyclic voltammetry was also performed in dichloromethane, as it is noncoordinating and may show different behavior as a result if solvent coordination is important. This appears to be the case, since the reduction shows reversible behavior unlike in the other solvents, with a reduction at E_p^c -1.41 V ($E_{1/2}$ -1.32 V) and a peak-to-peak separation of 190 mV. Although this value is relatively large, the square root law is linear (Figures 3 and 4) and the large separation is therefore attributed to uncompensated resistance from the solvent. This process is at a similar potential as in acetonitrile so we attribute it to the same initial reduction. However, the V(IV) complex is stable in DCM, since the solvent is noncoordinating and generally less reactive, making it reversible on the CV timescale.

We attempted the chemical reduction of **1** in both aqueous and nonaqueous solvents; to target a reduction at $E_{1/2}$ (-1.32 V) we used cobaltocene as a reducing agent (-1.33 V for $[Cp_2Co]^+/[Cp_2Co]$) which would be a mild reaction if it were irreversible.[21] This was attempted in both acetonitrile and DCM, and in both cases, no reaction was observed initially, but within an hour an intractable black solid started to form in the same manner as the direct reaction with vanadyl acetylacetonate (above), and no products could be isolated, implying that a possible V(IV) complex is inherently unstable, with this decomposition in aprotic solvents being caused by a lack of hydrolysis reaction pathways.

The reduction of **1** in protic solvents was also attempted with a variety of reducing agents in water or water-methanol mixtures before performing cyclic voltammetry experiments. Several common reducing agents including hydroxylamine, hydrazine, sodium thiosulfate, and zinc metal were all tested, spanning reduction potentials between -0.29 V and -1.16 V vs. ferrocene,[21,22] and in all cases, no reaction was observed. Although any V(IV) products would be paramagnetic and not necessarily observable by NMR spectroscopy, all ^1H and ^{51}V NMR spectra as well as absorption spectra remained unchanged. This lack of reactivity suggests that the presence of the two amidoxime ligands on vanadium greatly stabilizes the complex against reduction compared to other V(V) complexes, which have reduction potentials in the range of +0.6 V vs. ferrocene (for $[VO]^{2+}/[VO_2]^+$), +0.1 – + 0.75 V for non-oxido cis-inositol complexes[23] or -0.25 – +0.49 V for Amvadin derivatives, with the lower end of the range occurring in organic solvents (discussed below).[24] Since the ligands are strongly electron-donating, such that they displace all oxido groups on the metal upon coordination, they are poor ligands with respect to stabilizing the lower oxidation state on vanadium.

The unusual redox behavior of **1** and its reluctance to be reduced is not a direct consequence of the rare non-oxo environment, as several other air-stable non-oxo V(IV) complexes are known. One of them is Amvadin, a natural product that is found in the hyperaccumulating fungus *Amanita muscaria* (Figure 5, left).[25] In contrast to **1**, vanadium is present exclusively in the V(IV) oxidation state in naturally-occurring Amavadin as well as synthetic derivatives, and although the V(V) form is readily accessible by chemical oxidizing agents such as hydrogen peroxide, it will slowly revert to the stable V(IV) oxidation state over time with no apparent decomposition.[19] In some organic solvents, however, the V(V) form is favored, turning red, indicating an easily accessible redox couple. This is notable because the ligand in Amavadin, 2,2'-(hydroxyimino)dipropionate, contains a central N-OH

hydroxylamine group that is deprotonated in the complex, similar to the four N-O groups in **1**, yet it is inert when directly bonded to V(IV). A limited number of other non-oxido V(IV) complexes are known, including a complex with a *cis*-inositol derived ligand and other similar compounds (Figure 5, right) that are also unstable when oxidized to V(V).[23,26]

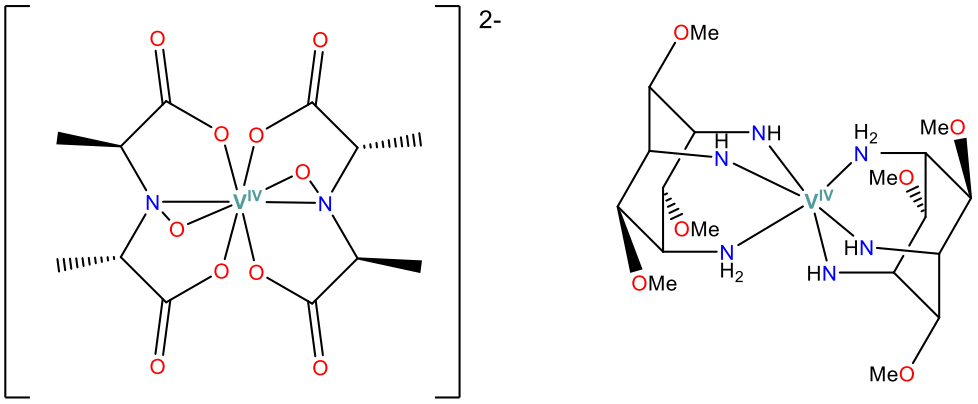

Figure 5. Stable non-oxido V(IV) complexes.

Vanadium(IV) reactivity with amidoximes and oximes

In addition to amidoxime A, the reactions of other amidoximes and oximes with V(IV) were also monitored by ^{1}H and ^{51}V NMR spectroscopy. We first tested glutarodi(amidoxime) (amidoxime B, $\mathbf{L^B}$)[14] and acetamidoxime[27] as models for other functional groups on uranium sorbents, and acetone oxime as a simple oxime which should react to form a single product, acetone (substrates shown in Figure 1). For these substrates, only free V(V) species were observed in the products instead of metal complexes, as the substrates and probable products are expected to be poor ligands (Figures 6-11). The presence of any ^{51}V NMR signals is indicative of oxidation from V(IV) to V(V) since V(IV) is NMR-silent.[18] Small amounts of VO_2 precipitation is observed, especially in the reactions of $\mathbf{L^B}$, although no attempts were made to quantify this. Table 1 shows the amount of products produced at different vanadium/oxime ratios.

Table 1. Product mixtures of V(IV) reactions with **L^{B}**, acetamidoxime, and acetone oxime.

Substrate (S)	[S]	V:S ratio	Unreacted [S]	[product]	[decomposition]
	1	6:1	0		0.85
L^{B}	6	1:1	2.4		3.2
	20	1:3	11.0		9.0
	2	3:1	0	1.2	0.2
acetamidoxime	12	1:2	6.1	2.4	0.01
	36	1:6	32	1.8	4.3
	2	3:1	1.1	0.97	
acetone oxime	12	1:2	9.3	5.6	
	36	1:6	32	2.9	

[VO^{2+}] = 6 mM for all reactions. All concentrations are in mM. Product is acetamide for acetamidoxime, acetone for acetone oxime. Decomposition is all other signals that are not product or unreacted substrate. Precipitate was present in the reactions of **L^{B}** and small amounts were present in reactions of acetamidoxime.

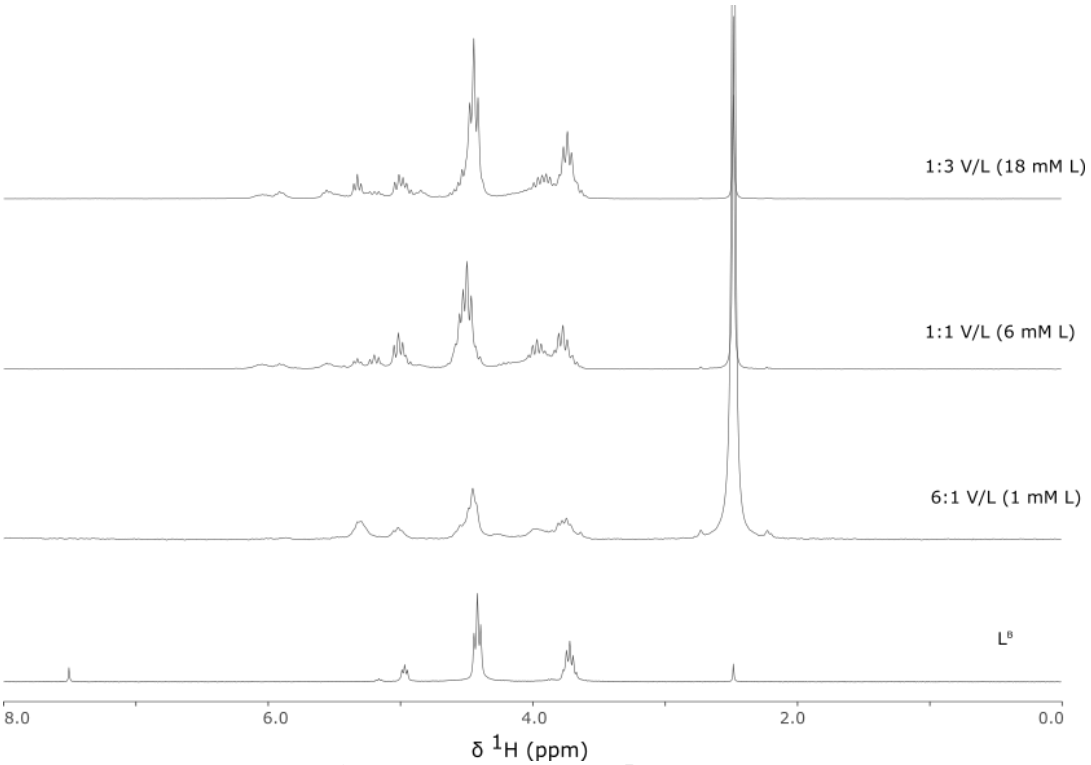

Figure 6. ^{1}H NMR spectra of **L^{B}** – V(IV) mixtures

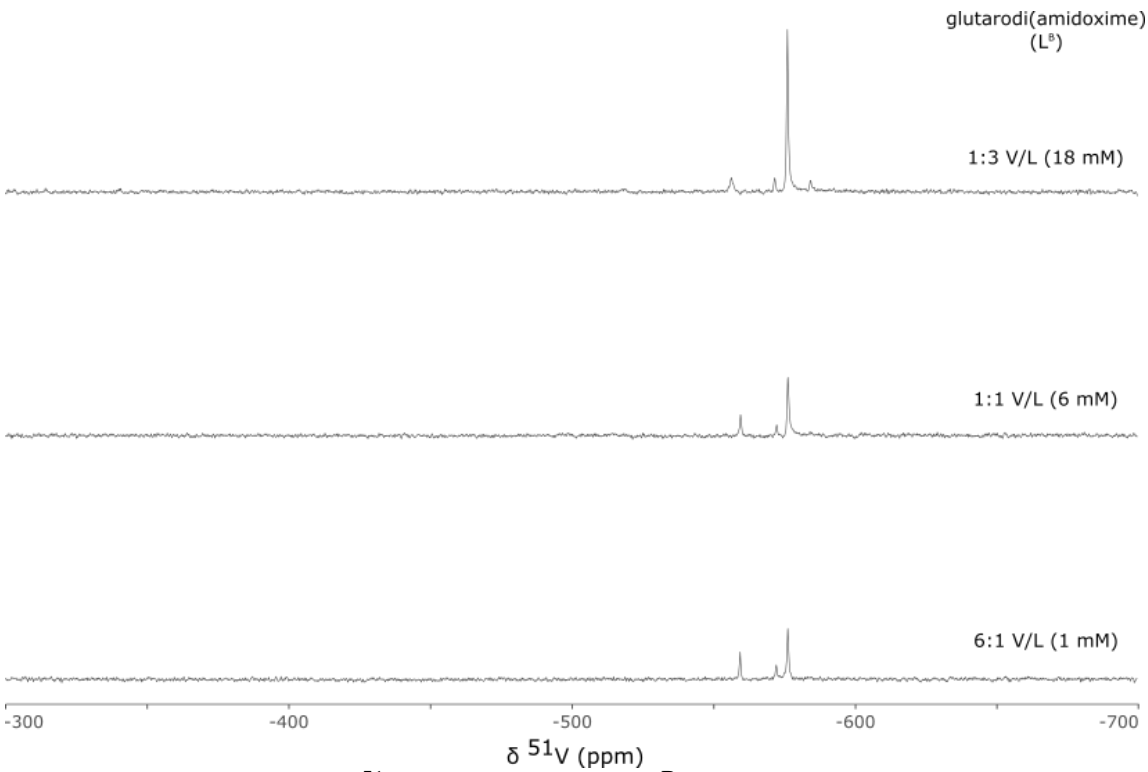

Figure 7. ^{51}V NMR spectra of $\mathbf{L^B}$ – V(IV) mixtures

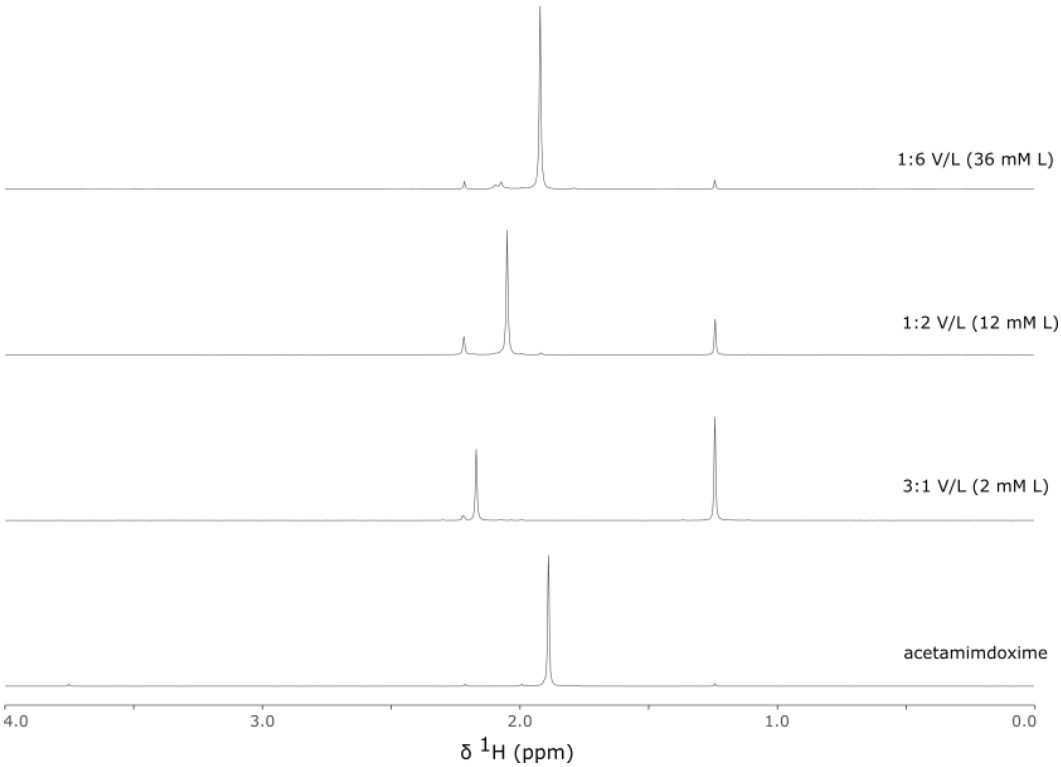

Figure 8. ^{1}H NMR spectra of acetamidoxime – V(IV) mixtures.

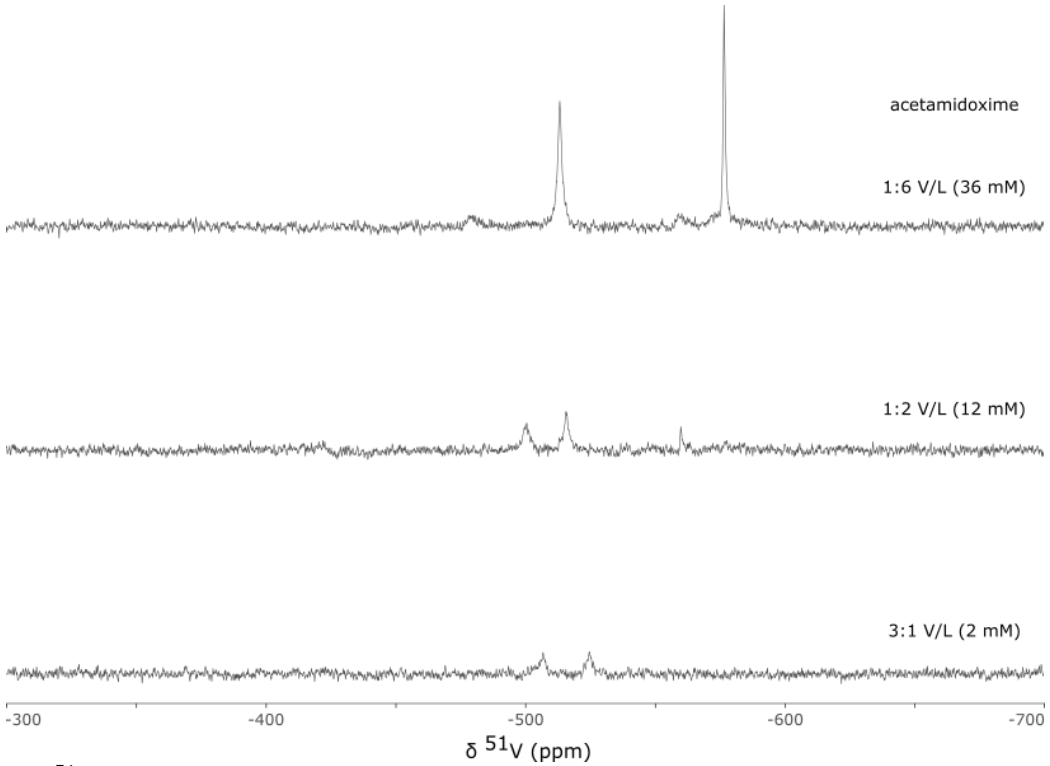

Figure 9. ^{51}V NMR spectra of acetamidoxime – V(IV) mixtures. All signals correspond to known V(V) vanadate species.

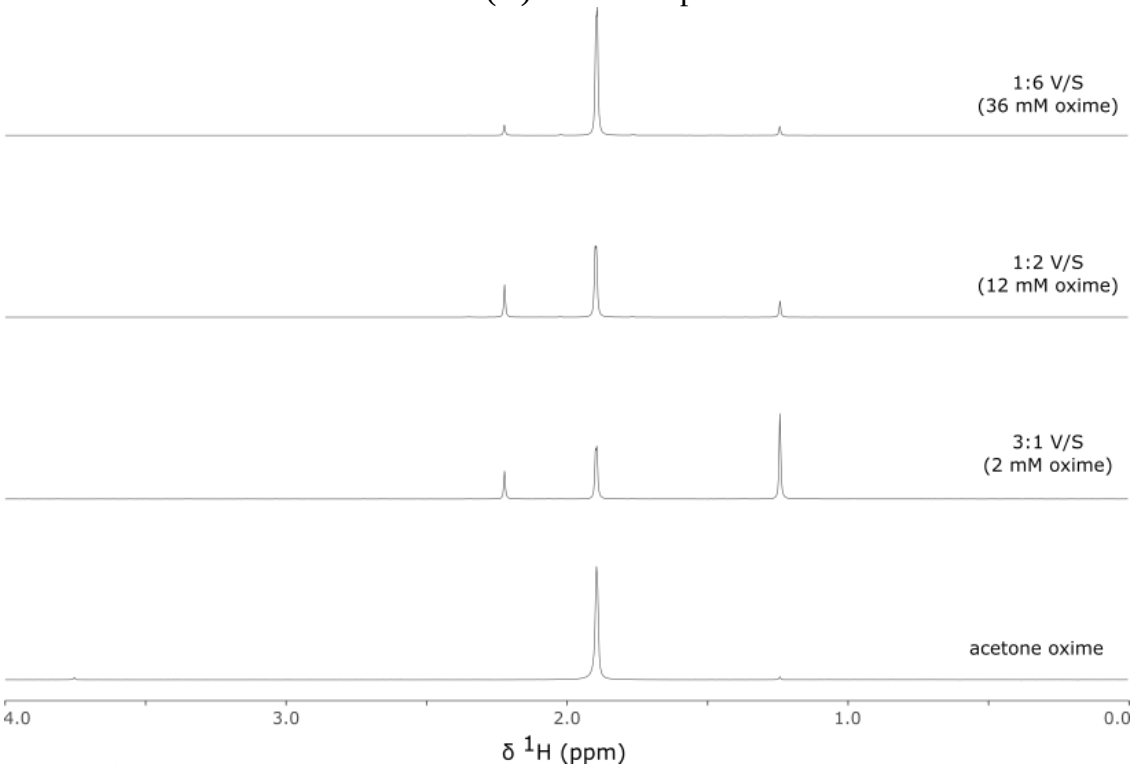

Figure 10. ^{1}H NMR spectra of acetone oxime – V(IV) mixtures. Only acetone and acetone oxime are observed.

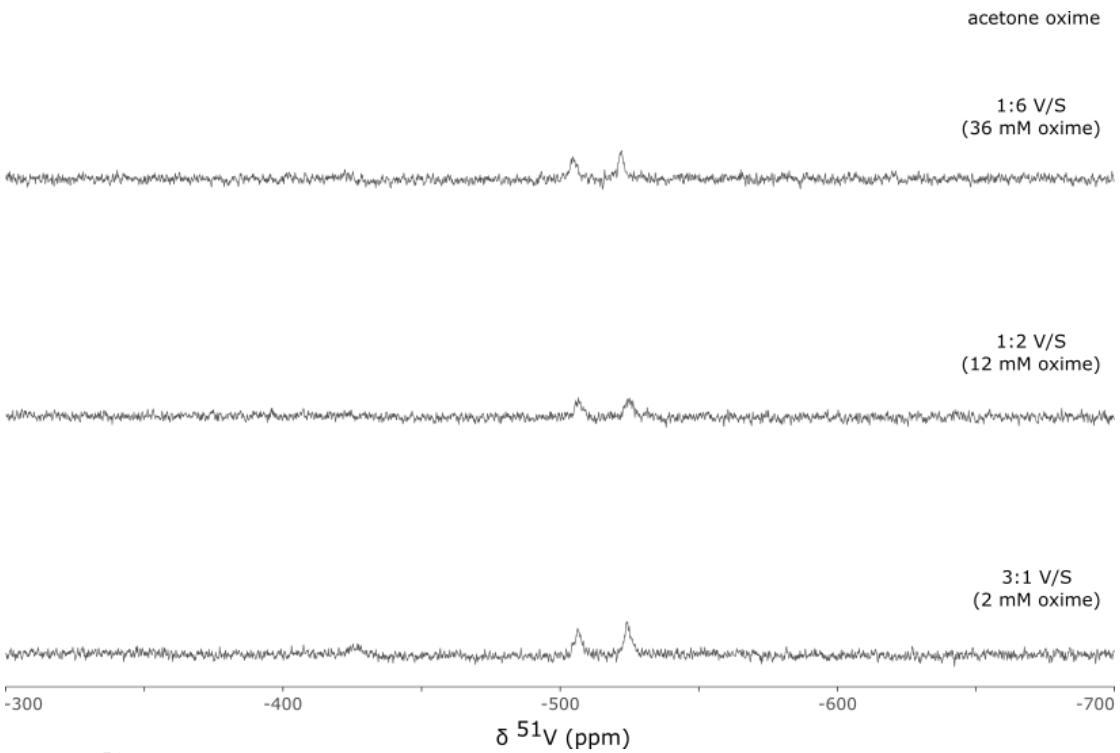

Figure 11. ^{51}V NMR spectra of acetone oxime – V(IV) mixtures. All signals correspond to known V(V) vanadate species.

For these substrates, the formation of a heterogeneous mixture by the addition of base was necessary for any reaction to occur. This could indicate that the formation of a hydrated vanadium oxide $VO(OH)_2$ or a similar species may be the reactive form of vanadium needed and the free vanadyl ion is inert.[3].These reactions transiently turn a blue-grey color with the formation of a colloid (as observed by the Tyndall effect, Images 1 and 2 below) which then reacts with the substrates (Scheme 1). The heterogeneous nature of this reaction also explains its slow and variable kinetics, taking hours to days to react fully. The reaction mixtures remain slightly acidic, around pH 4-6, so vanadium oxidation is not caused by strong base, and the substrates are not reactive towards hydrolysis due to low pH.[28]

The formation of the VO_2 colloid *in situ* appears to be necessary for reactivity of the substrates other than $\mathbf{L^A}$. With multiple vanadium centers in close proximity, this can allow for two-electron processes and oxygen atom abstraction. This type of reactivity is well known with vanadium oxides, notably in the contact process that is used on an industrial scale to produce sulfuric acid.[29] To confirm its reactivity, the colloidal material was isolated as a dark blue solid by centrifugation and decanting of the solution, after allowing a reaction involving acetone oxime to proceed for one hour. When a fresh solution of oxime was added to the solid the reaction proceeded, producing the expected amount of acetone, almost 0.5 equivalents. VO_2 prepared in the absence of acetone oxime was also tested for its reactivity, either as a wet solid after isolation by centrifugation and decanting of the solution, or after it had been heated to dryness. Both forms did react, although much smaller amounts of acetone were produced than when the VO2 was formed in the presence of acetone oxime and solid VO_2 was still present in the reactions, especially with dry VO_2 (Table 2).The large difference in amounts of acetone

produced can be attributed to the nature of the colloid and its surface. When the colloid is formed, acetone oxime or other substrate may act as a surfactant enhancing its reactivity, while hydrated VO_2 shows much lower reactivity and dried VO_2 lower still.

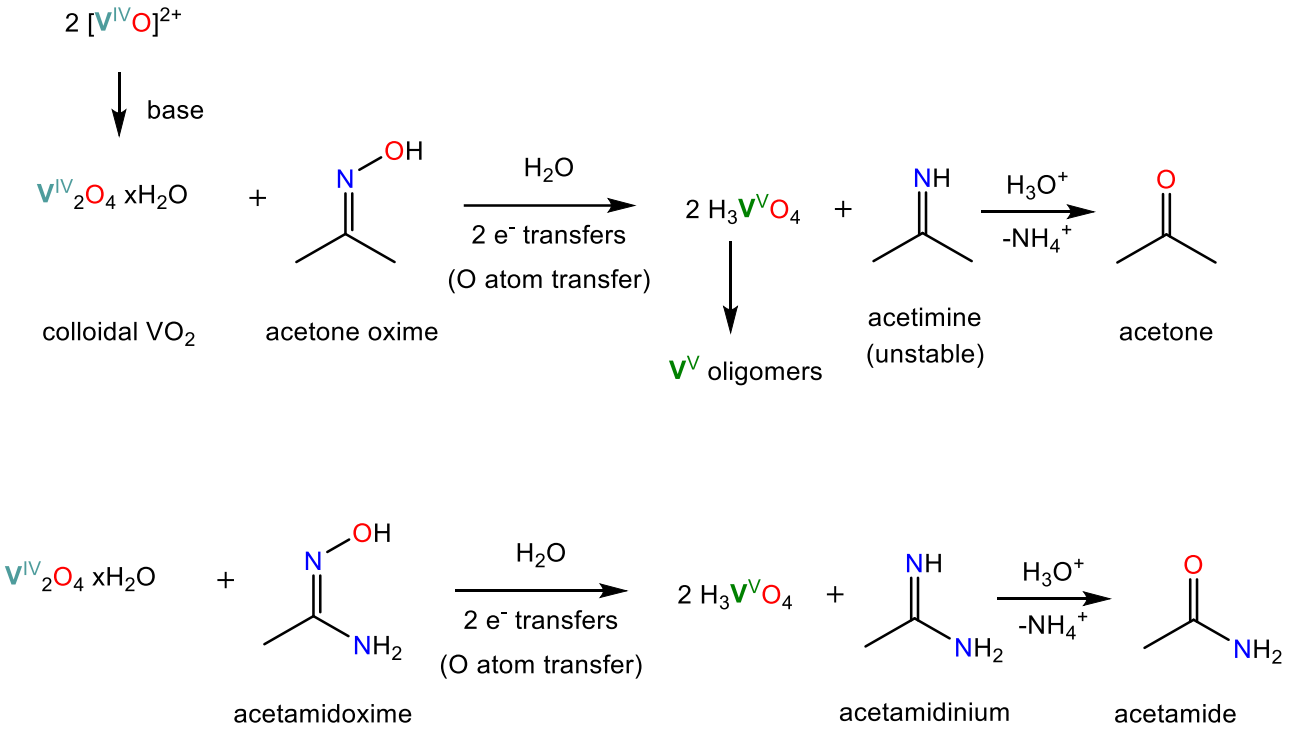

Scheme 1. reaction of acetone oxime (upper) or acetamidoxime (lower) with V(IV) and base. Similar reactions take place with $\mathbf{L}^{\mathbf{B}}$. The exact composition of the V(IV) colloid is unknown, and the product V(V) species depend on concentration and pH.

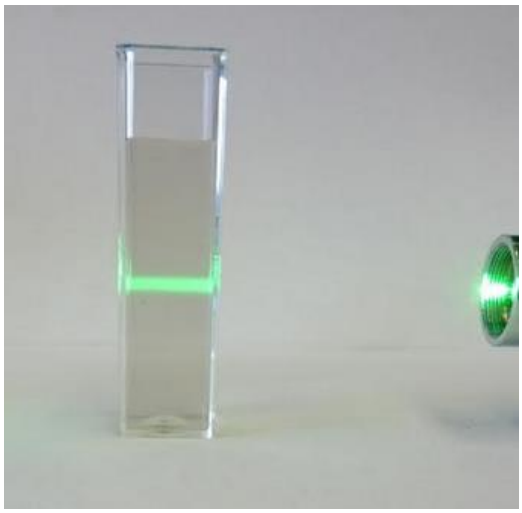

Image 1. Tyndall effect observed in V(IV) – acetone oxime reactions, forming colloidal VO_2

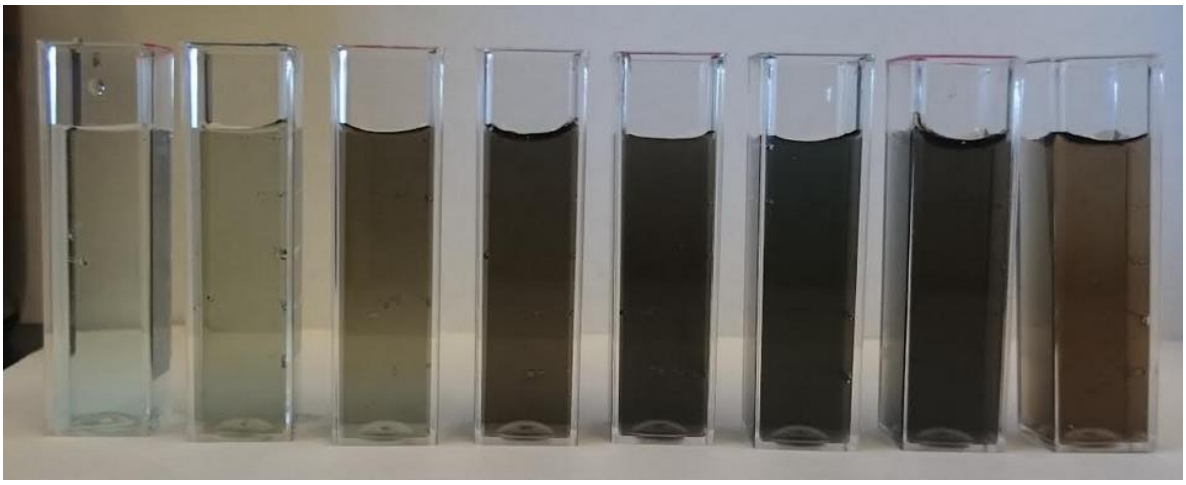

Image 2. Reaction appearance dependent on added base. 0.5 equivalents additional base added (with respect to V) from left to right; 0.5 eq. to 4.0 eq.
Excess acetone oxime is present as the substrate.

Table 2. Vanadium dioxide reactivity resulting from preparation method.

VO_2 preparation	Equivalents of acetone produced (relative to V)
Prepared in the presence of acetone oxime, decanted	0.49
Precipitated without acetone oxime	0.16
Precipitated without acetone oxime, dried at 120°C	0.12
[acetone oxime] = 20 mM	

When the reaction of $\mathbf{L^B}$ was performed at higher concentrations and on a larger scale in an attempt to isolate products, VO_2 precipitated which slowly settled over one week, during which the solution turned from blue to green to yellow-brown. The supernatant was then decanted and allowed to slowly evaporate, upon which brown crystals of glutardi(amidinium) decavanadate, $[(H_2N)_2C(CH_2)_3C(NH_2)_2]_6{\cdot}[V_{10}O_{28}]_2$, were obtained. The structure was confirmed by single crystal X-ray diffraction (Figure 12 and Table 3). Decavanadate formation is observed as a consequence of an acidic solution, high vanadium concentration, and a poor ligand that does not interact directly with vanadium at all.[18] Although the amidinium ion was isolated in the crystal structure, hydrolysis can occur to form the more stable amide, as seen previously in amidoxime reactivity.[30] Therefore, in many cases the ammonium ion was observed in the ^{1}H NMR spectra of these reactions as a distinctive 1:1:1 triplet at δ = 7.16 ppm due to ^{1}H-^{14}N coupling, along with the formation of amides or carboxylic acids. The integration of the ammonium signal is significantly lower than ideal stoichiometry, however this is due to incomplete hydrolysis of amidines, H-D exchange in solution, and possible loss of volatile NH_3.

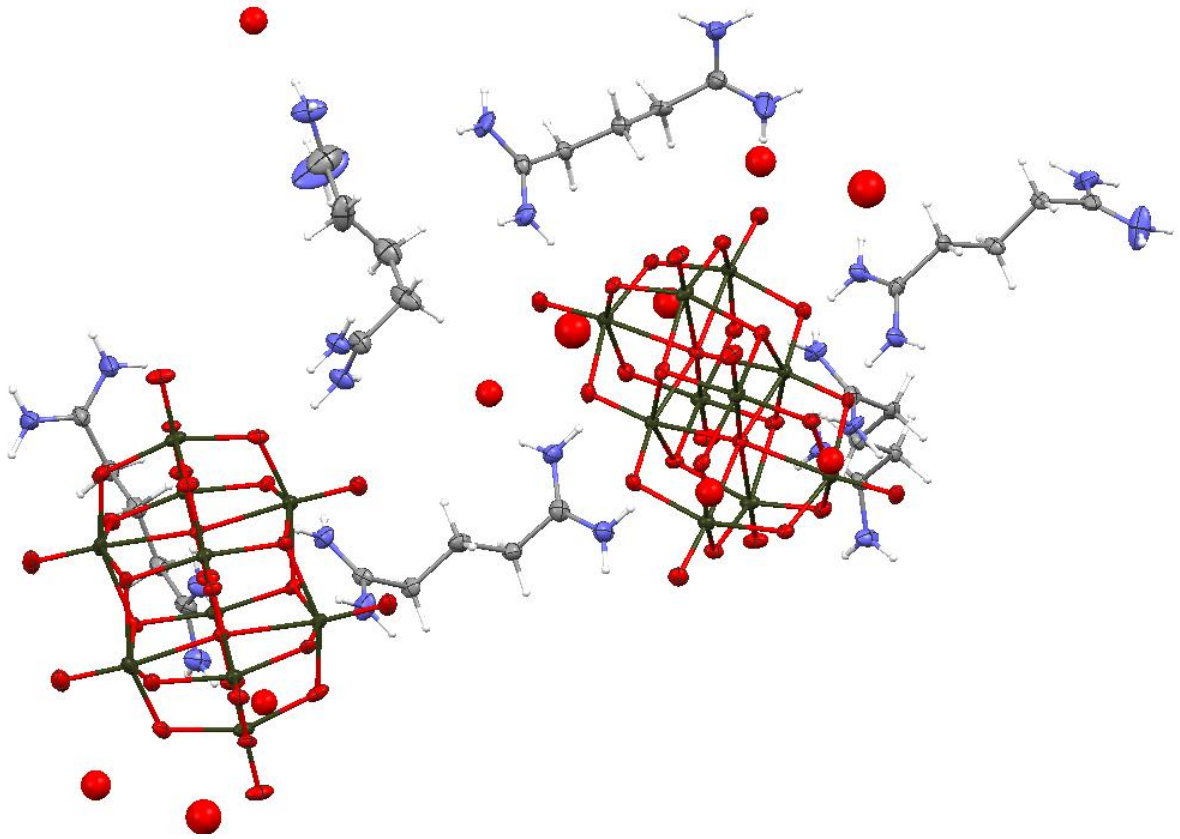

Figure 12. Crystal structure of glutaramidinium decavanadate ($[(H_2N)_2C(CH_2)_3C(NH_2)_2]_6[V_{10}O_{28}]_2 \cdot 11H_2O$).

This type of reductive deoxygenation of amidoximes has been reported previously with transfer hydrogenation reactions[31] and enzyme activity.[32] In the latter case, O-substituted amidoximes were used as prodrugs for relatively reactive and less bioavailable amidines *in vitro* and *in vivo* after deoxygenation by liver enzymes. A somewhat similar deoxygenation reaction of amidoximes and imide-dioximes has been reported with nitrous acid, although in that case the amine portion of the amidoxime also reacts, as the reaction produces nitrous oxide and the amide.[30,33,34] Similar reactivity has been observed with hydroxamic acids, although only when *N*-substituted, reacting with reduced V(III), V(IV), Mo(IV), and Mo(V).[9] In contrast, stable hydroxamate complexes are known with all of these oxidation states without *N*-substitution. Limited examples of V(IV) reacting with salicylaldoxime and salicylamidoxime have also been reported, where the V(V) complex was isolated in low yield.[10] The low yield reported is consistent with 2 equivalents of V(IV) reacting with each ligand, in a one-electron process on the metal and two-electron process abstracting an oxygen atom from the ligand, resulting in at least half of the ligand remaining intact.

Table 3. Crystallographic data for glutaramidinium decavanadate

	$[(H_2N)_2C(CH_2)_3C(NH_2)_2]_6[V_{10}O_{28}]_2 \cdot 11H_2O$
Formula	$C_{40}H_{106}N_{24}O_{67}V_{20}$
Formula weight ($g \cdot mol^{-1}$)	2894.11
Space group	$Pna2_1$
a (Å)	18.6232(16)
b (Å)	37.606(3)
c (Å)	13.3441(11)
α (°)	90
β (°)	90
γ (°)	90
V ($Å^3$)	9345.6(14)
Z	4
ρ_{calc} ($g \cdot cm^{-3}$)	2.057
μ (mm^{-1})	2.014
Crystal size (mm×mm×mm)	0.15×0.15×0.05
Crystal color and form	brown block
R1 ($I > 2\sigma(I)$)	0.0390
wR2 ($I > 2\sigma(I)$)	0.0952
R1 (all data)	0.0427
wR2 (all data)	0.0974
GoF	1.028
Largest difference peak/hole ($e \cdot Å^3$)	1.303 / -0.655

In seawater, the majority of vanadium is present in the V(V) oxidation state and so V(IV) is not expected to be a major competitor for binding. Moreover, V(IV) may be bound to proteins or small bioligands from which it occurs in organisms, which could attenuate its reactivity. Despite these mitigating factors, V(IV) is still a potential concern, since the irreversible reaction would permanently reduce polymer capacity for uranium, forming amides and similar functional groups that cannot easily be converted back to amidoximes. The very high affinity of glutaroimide-dioxime towards many metals is also a disadvantage here since it could extract V(IV) efficiently from other ligands and then the complex proceed to react with other possible reducing agents other than a second equivalent of V(IV). Because this reaction is irreversible, it contributes to sorbent degradation and loss of uranium capacity upon cycling and as such further study is warranted with sorbent samples.

Vanadium(IV) reactivity with glutaroimide-dioxime (L^A)

After exploring the reactivity of V(IV) with simple oximes and amidoximes, we then looked the reaction of $\mathbf{L^A}$ with V(IV) by NMR to explain our observations described earlier. Unlike the other substrates, the reactions remained homogeneous throughout the reaction and no added base was needed. We attribute this difference in reactivity between $\mathbf{L^A}$ and the other substrates to the effectiveness of $\mathbf{L^A}$ as a ligand, where a transient V(IV) complex forms in solution.

In order to determine if O-atom transfer or other reactivity was occurring between vanadyl and $\mathbf{L^A}$, quantitative NMR experiments were performed. When the two reagents were mixed, the reaction mixtures turned dark brown within seconds as observed previously. NMR spectra were acquired after approximately 6 hours to allow more complete reaction. In these reactions, the ^{51}V NMR spectra contained the known 1:1 and 2:1 complexes as well as free vanadium when excess vanadium is present.[5] Glutaroimidoxime was identified as one decomposition product by comparison with an NMR spectrum of the pure compound (Figures 13 and 14) although the major decomposition product, likely arising from further reaction of glutaroimidoxime, was not able to be identified, not matching previously reported intermediates of hydrolytic decomposition.[28]

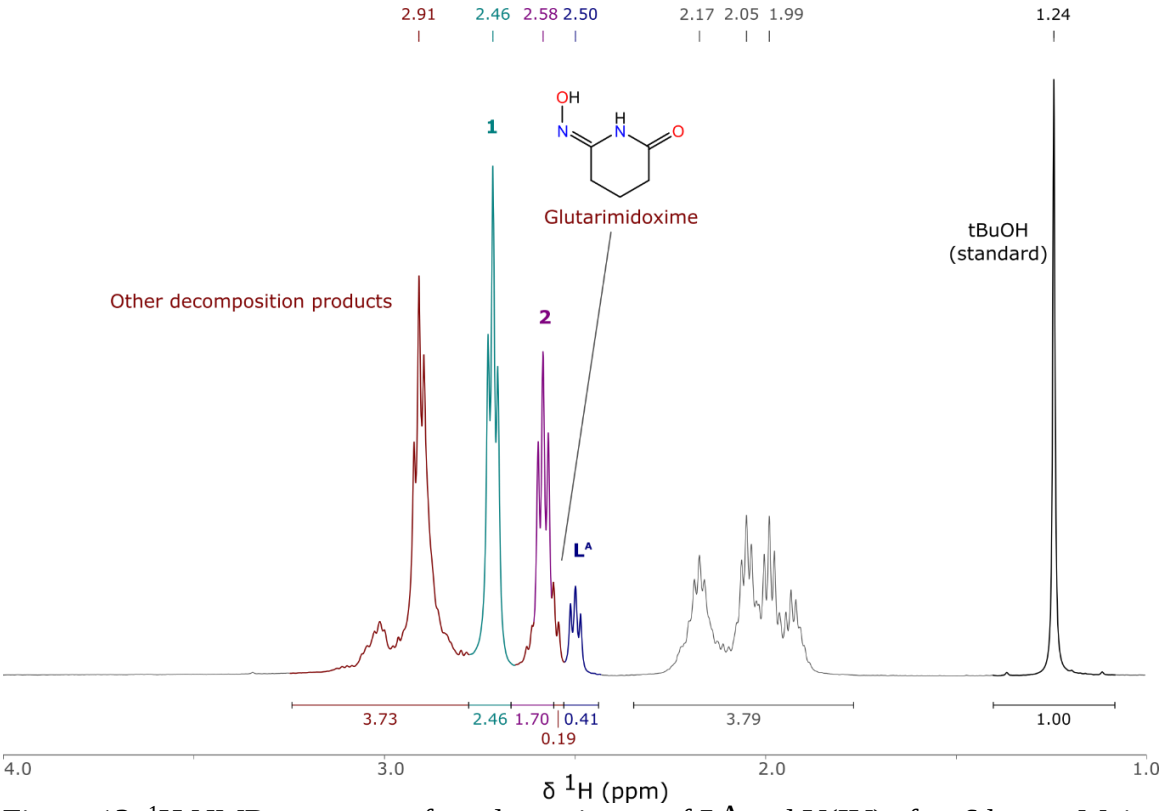

Figure 13. ^{1}H NMR spectrum of product mixture of $\mathbf{L^A}$ and V(IV) after 6 hours. Major decomposition product at δ = 2.91 ppm unidentified. Conditions. 18 mM $\mathbf{L^A}$, 6 mM VO^{2+}.

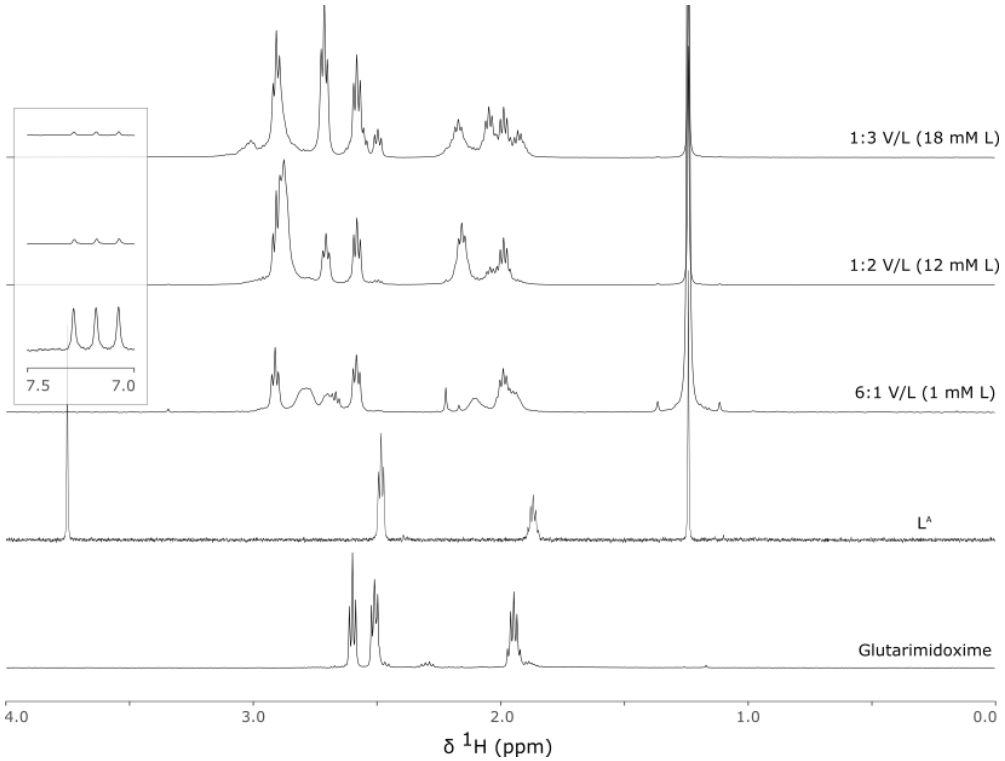

Figure 14. ^{1}H NMR spectra of $\mathbf{L^A}$ – V(IV) mixtures. The ligand spectrum contains dioxane as an additional internal standard, and the inset showing the presence of NH_4^+.

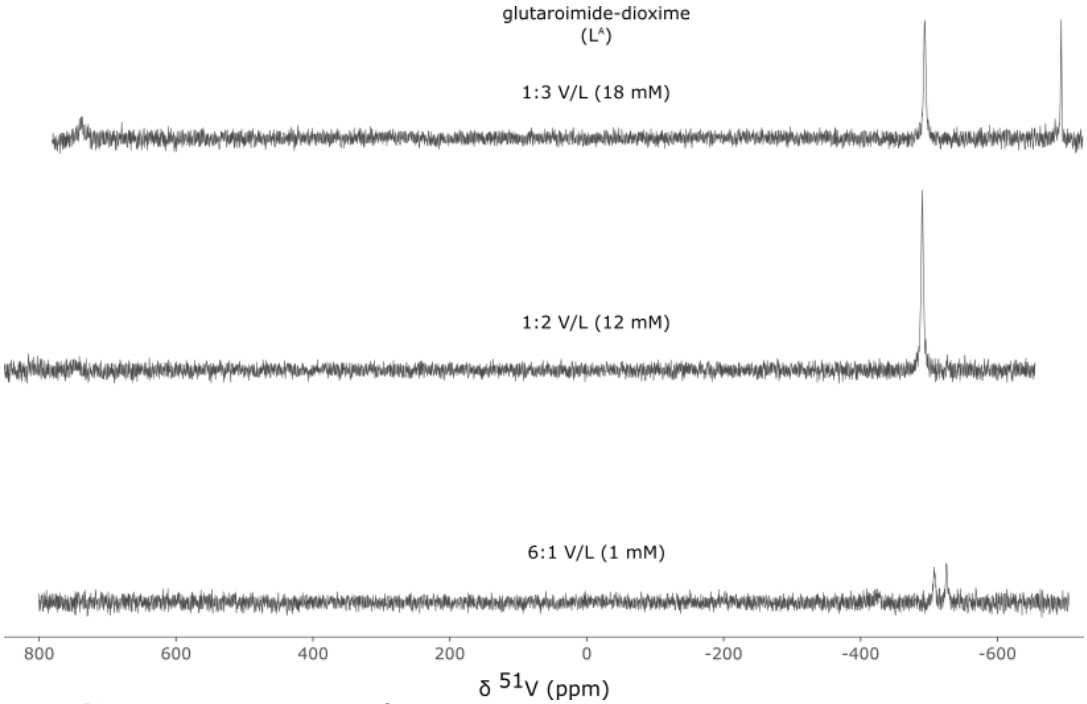

Figure 15. ^{51}V NMR spectra of $\mathbf{L^A}$ – V(IV) mixtures. Complex **1** is the signal at +740 ppm, complex **2** is at -460 ppm, and other signals are vanadates.

Table 4. Product mixtures of V(IV) and glutaroimide-dioxime (**L^{A}**).

[**L^{A}**]	V:**L^{A}** ratio	Unreacted [**L^{A}**]	[**L^{A}**] in **1**	[**L^{A}**] in **2**	[decomposition]
1	6:1	0	0	0.24	0.69
12	1:2	0.23	1.7	2.0	8.6
18	1:3.3	1.0	3.0	4.1	9.1

[VO^{2+}] = 6 mM for all reactions. All concentrations are in mM. Multiple decomposition products were observed that could generally not be identified or quantified separately. Spectra acquired 6 hours after mixing.

The concentrations of products vary depending on the ratio of reagents used, shown in Table 4. Here we can see that more than one equivalent of vanadyl reacts with one molecule of **L^{A}**, as the concentration of decomposition products exceeds the vanadium concentration when excess **L^{A}** is used. Additionally, if excess ligand remains after the V(IV) is oxidized to V(V), it forms the complexes **1** and **2**, which are the products observed previously.

We propose that the rapid homogeneous reaction of **L^{A}** with vanadyl occurs through the formation of a transient V(IV) complex followed by reaction with another equivalent of V(IV) (Scheme 2). This effectively amounts to disproportionation of the vanadium, but rather than being reduced to V(III), the ligand is reduced instead to form a second equivalent of V(V). This mechanism is also consistent with the lack of sensitivity to oxygen (see above), making a free radical mechanism very unlikely. Without complexation to form a transient **L^{A}**-V(IV) complex or the presence of organic radicals, a third-order reaction would be needed, which is not consistent with the rapid reaction and is relatively rare.

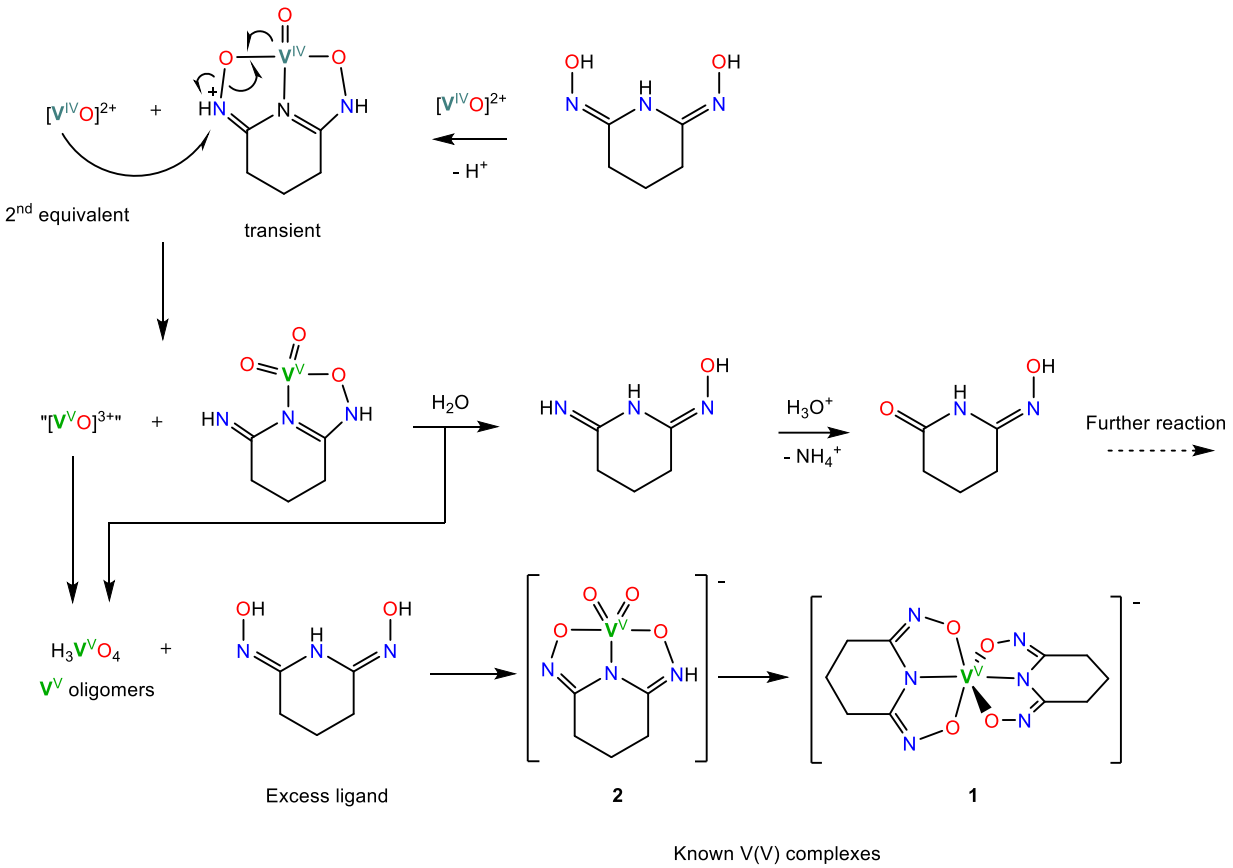

Scheme 2. Proposed reaction mechanism of glutaroimide-dioxime with V(IV). The V(IV) species shown are hydrated with variable amounts of water and the V(V) product species vary depending on concentration and pH.

Summary and conclusions

In this work we have investigated the reactivity taking place between vanadium(IV) and amidoxime ligands. Rather than form stable V(IV) complexes with glutaroimide-dioxime ($\mathbf{L^A}$), the ligand reacts to oxidize the vanadium to V(V), resulting in the formation of the known non-oxido V(V) complex of $\mathbf{L^A}$, **1**. Based on the observed stoichiometry of the reaction and products observed, we propose that a V(IV) complex is formed transiently due to the strong chelating ability of $\mathbf{L^A}$, but this then reacts with more reduced vanadium to form V(V) in solution. The reductive reaction of V(IV) was also explored with ligands and substrates that are similar to $\mathbf{L^A}$; glutarodi(amidoxime) ($\mathbf{L^B}$), acetamidoxime, and acetone oxime. These three substrates required the precipitation of VO_2 as a colloid, followed by the same oxygen transfer reaction to form V(V) with an observed vanadium/oxime stoichiometry.

Cyclic voltammetry was performed on the non-oxido V(V) complex of glutaroimide-dioxime, [NEt_4][**1**], to investigate whether reduction of this complex is possible, and we found that reduction is possible electrochemically but at a very reducing potential ($E \approx -1.0$ to -1.5 V vs. ferrocene), and is generally irreversible. Only in dichloromethane was it found to be reversible electrochemically, but upon attempted chemical reduction no products could be isolated. We attribute this to slow reaction of a transient V(IV) complex and lack of available hydrolysis pathways in an aprotic, relatively inert solvent. In protic solvents, no V(IV) complex could be formed either through reduction of **1** or direct reaction of $\mathbf{L^A}$ with V(IV) sources, and only V(V) complexes were obtained.

The ligands explored in this study ($\mathbf{L^A}$, $\mathbf{L^B}$, and acetamidoxime) are analogues of functional groups on polymer sorbents for the extraction of uranium from seawater. Vanadium is the most problematic competitor for binding sites, but past work has focused on V(V), which makes up the majority of vanadium in seawater. However, vanadium also naturally occurs as V(IV) due to biological redox activity, and V(IV) composes a small but non-negligible amount of total dissolved vanadium in the ocean. Due to the prompt and irreversible reaction of V(IV) with $\mathbf{L^A}$ and other analogues, V(IV) will react to permanently damage amidoxime-functionalized polymer sorbents, which is a potentially greater concern than the reversible, albeit strong, binding of V(V) which simply competes with U(VI) for binding and extraction.

References

(1) Wang, D.; Sañudo Wilhelmy, S. A. *Mar. Chem.* **2009**, *117*, 52–58.
(2) Turekian, K. K. *Oceans*; Prentice-Hall: Englewood Cliffs, N. J., 1968.
(3) Kustin, K.; McLeod, G. C.; Gilbert, T. R.; Le Briggs, B. R. In *Structure and Bonding. Copper, Molybdenum, and Vanadium in Biological Systems.*; 1983; Vol. 53, pp. 139–160.
(4) Dennis Chasteen, N. In *Copper, Molybdenum, and Vanadium in Biological Systems*; Springer Berlin Heidelberg: Berlin, Heidelberg, 1983; pp. 105–138.
(5) Leggett, C. J.; Parker, B. F.; Teat, S. J.; Zhang, Z.; Dau, P. D.; Lukens, W. W.; Peterson, S. J. M.; Cardenas, A. J. P.; Warner, M. G.; Gibson, J. K.; Arnold, J.; Rao, L. *Chem. Sci.* **2016**, *7*, 2775–2786.
(6) Pan, H.-B.; Kuo, L.-J.; Wai, C. M.; Miyamoto, N.; Joshi, R.; Wood, J. R.; Strivens, J. E.; Janke, C. J.; Oyola, Y.; Das, S.; Mayes, R. T.; Gill, G. A. *Ind. Eng. Chem. Res.* **2016**, *55*, 4313–4320.
(7) Tian, G.; Teat, S. J.; Zhang, Z.; Rao, L. *Dalton Trans.* **2012**, *41*, 11579.
(8) Sun, X.; Xu, C.; Tian, G.; Rao, L. *Dalton Trans.* **2013**, *42*, 14621.
(9) Brown, D. A.; Bögge, H.; Coogan, R.; Doocey, D.; Kemp, T. J.; Müller, A.; Neumann, B. *Inorg. Chem.* **1996**, *35*, 1674–1679.
(10) Zerbib, V.; Robert, F.; Gouzerh, P. *J. Chem. Soc. Chem. Commun.* **1994**, *98*, 2179.
(11) Chilou, V.; Gouzerh, P.; Jeannin, Y.; Knobler, C. B. *Inorganica Chim. Acta* **1990**, *178*, 23–25.
(12) Smith, W. L.; Raymond, K. N. *J. Inorg. Nucl. Chem.* **1979**, *41*, 1431–1436.
(13) Endrizzi, F.; Rao, L. *Chem. - A Eur. J.* **2014**, *20*, 14499–14506.
(14) Tian, G.; Teat, S. J.; Rao, L. *Dalton Trans.* **2013**, *42*, 5690–5696.
(15) In *Inorganic Syntheses*; Coucouvanis, D., Ed.; John Wiley & Sons, Inc.: New York, USA, 2002; Vol. 33, pp. 75–121.
(16) Leggett, C. J.; Rao, L. *Polyhedron* **2015**, *95*, 54–59.
(17) Sheldrick, G. M. *Acta Crystallogr. Sect. A Found. Crystallogr.* **2015**, *71*, 3–8.
(18) Howarth, O. W. *Prog. Nucl. Magn. Reson. Spectrosc.* **1990**, *22*, 453–485.
(19) *Vanadium: Biochemical and Molecular Biological Approaches*; Michibata, H., Ed.; 2014.
(20) Bratsch, S. G. *J. Phys. Chem. Ref. Data* **1989**, *18*, 1–21.
(21) Connelly, N. G.; Geiger, W. E. *Chem. Rev.* **1996**, *96*, 877–910.
(22) *CRC Handbook of Chemistry and Physics*; Rumble, J. R., Ed.; 98th Editi.; CRC Press/Taylor & Francis: Boca Raton, FL, 2017.
(23) Lodyga-Chruscinska, E.; Szebesczyk, A.; Sanna, D.; Hegetschweiler, K.; Micera, G.; Garribba, E. *Dalt. Trans. An Int. J. Inorg. Chem.* **2013**, *42*, 13404–13416.
(24) Smith, P. D.; Berry, R. E.; Harben, S. M.; Beddoes, R. L.; Helliwell, M.; Collison, D.; Garner, C. D. *J. Chem. Soc. Dalt. Trans.* **1997**, 4509–4516.
(25) da Silva, J. A. L.; Fraústo da Silva, J. J. R.; Pombeiro, A. J. L. *Coord. Chem. Rev.* **2013**, *257*, 2388–2400.
(26) Morgenstern, B.; Kutzky, B.; Neis, C.; Stucky, S.; Hegetschweiler, K.; Garribba, E.; Micera, G. *Inorg. Chem.* **2007**, *46*, 3903–3915.

(27) Vukovic, S.; Watson, L. a; Kang, S. O.; Custelcean, R.; Hay, B. P. *Inorg. Chem.* **2012**, *51*, 3855–3859.
(28) Kang, S. O.; Vukovic, S.; Custelcean, R.; Hay, B. P. *Ind. Eng. Chem. Res.* **2012**, *51*, 6619–6624.
(29) Holmes, H. N.; Elder, A. L. *Ind. Eng. Chem.* **1930**, *22*, 471–473.
(30) Elvidge, J. A.; Linstead, R. P.; Salaman, A. M. *J. Chem. Soc.* **1959**, 208–215.
(31) Mahajan, U. S.; Godinde, R. R.; Mandhare, P. N. Preparation of Amidines from Amidoximes via Transfer Hydrogenation. *Synthetic Communications*, 2011, *41*, 2195–2199.
(32) Clement, B. *Drug Metab. Rev.* **2002**, *34*, 565–579.
(33) Eloy, F.; Lenaers, R. *Chem. Rev.* **1962**, *62*, 155–183.
(34) Garny, F. *Berichte der Dtsch. Chem. Gesellschaft* **1891**, *24*, 3426–3437.

Chapter 5

Uranyl binding studies with a 1,3,5-triazine hydroxylamine ligand

Introduction

In addition to glutaroimide-dioxime, acetamidoxime and similar amidoxime-type ligands that are analogous to polymer sorbents for uranium, other ligands are being explored for both improved affinity and selectivity. In order to find optimal ligands for this purpose, several strategies can be employed, each with their own drawbacks. One is direct ligand design, exploiting differences in geometry and electronic structure that favour certain binding modes over others, which has been done with uranyl by using appropriately large binding pockets for its selective complexation,[1–4] however, such ligands are relatively complex and are unsuitable for large-scale synthesis and applications. Ligand screening is another approach which lends itself well to high-throughput techniques, and this technique has been applied to selective uranyl extraction[5,6] (Chapter 6). A third approach is to use ligands that are known to form complexes with other metals, and then study binding affinity and selectivity for uranyl, and make improvements through design modifications.[7–10] All of these techniques can benefit from computational analysis, especially when trends are established with known complexes, then applied to the study of new ligands.[11–13]

For the purpose of extracting uranium from seawater, several similar ligands with similar geometries are possible candidates (Figure 1). Dipicolinic acid is a simple, naturally occurring carboxylic acid that forms strong chelating complexes with many metal ions, including vanadium[14,15], actinides[10,16], and hundreds of other complexes with transition metals[17]. The rigid and favourable geometry of the ligand means that it forms strong complexes with uranyl, although selectivity is not optimal for this purpose as it chelates strongly with many different metals.

The bis(hydroxylamino)-1,3,5-triazine ligand (H_2bihyat) is the subject of investigation in this study. The morpholine-substituted ligand is used exclusively in this study due to its relative ease of synthesis and characterization of these complexes, as well as enabling direct comparison to the known iron[18] and vanadium[19,20] complexes. Nonetheless, many similar ligands in this class are known with varying functional groups at the third position (Figure 2), and the modular synthesis allows for the straightforward derivatization, albeit with varying yields and solubilities.[18] The 1,3,5-triazine core also has potential for the design of other ligands with binding groups other than hydroxylamine, including thiolates[21], phosphonates[22], pyrazoles[23], or as a building block for larger functional groups such as pyridyl derivatives[24].

The vanadium chemistry of this ligand has been studied extensively, and one key feature is that it is known to not form 2:1 non-oxido complexes with vanadium(V), instead only forming a dioxo complex with 1:1 stoichiometry, $[(VO_2)(\text{bihyat})]^-$,[19] in contrast to glutaroimide-dioxime[25] (see Chapter 2). Additionally, this complex is several orders of magnitude weaker ($\log \beta = 17.87$) than the 1:1 glutaroimide-dioxime complex ($\log \beta = 21.2$ for $[(VO_2)(\text{glutaroimide-dioxime})]^{2-}$)[26]. In highly basic solution with pH > 11, free vanadate is released from the H_2bihyat complex, while glutaroimide-dioxime remains tightly bound. This is a useful property, as this allows strong base to be used as an eluent to free vanadium rather than relying on strong acid as is currently done, because strong acid often results in sorbent degradation.[27,28] The triazine does form a stronger complex than dipicolinic acid at neutral pH, reflecting its stronger electron-donating properties.

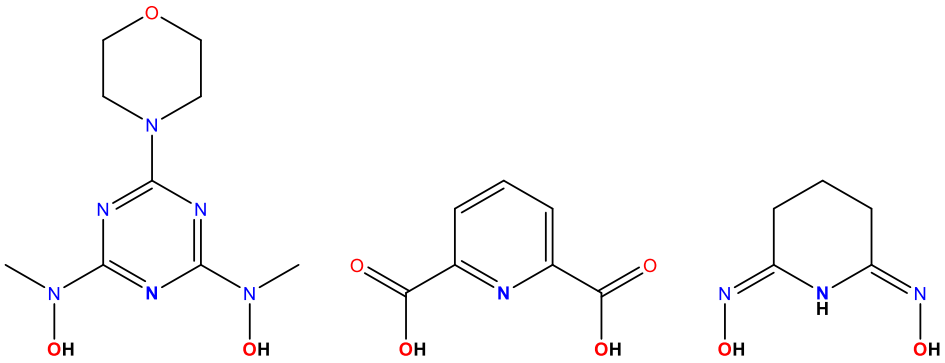

Figure 1. Structurally similar ligands investigated for selective uranyl binding

A limited of complexes of the 1,3,5-triazine ligands with other transition metals have also been reported, including with titanium[29] and molybdenum[30], largely in nonaqueous solvents. For the former, a 2:1 complex with distorted octahedral geometry, similar to the iron complex, was formed, and it was found to have high hydrolytic stability in the presence of neutral water. Molybdenum forms a dioxo species, like vanadium, however it is a neutral species due to the (VI) oxidation state, and is only stable at pH < 5.5 in water, with a similar monomer-dimer equilibrium but favouring the dimer.[30]

In order to study solution-state interactions of H_2bihyat with uranyl, similar techniques will be used as with vanadium as well as our previous studies of uranyl with seawater-relevant ligands.[31–34] Potentiometry is a key technique that allows us to determine quantitative binding constants (usually reported as formation constants, log β) as well as survey an entire system over a wide pH range. NMR spectroscopy also provides important solution-state binding information that can confirm the existence of complexes, and in some cases their symmetry or identity, and NMR has been extensively used in our previous work with vanadium. A solid-state structure has also been determined by X-ray crystallography, and while it does not directly inform about solution-state binding or selectivity, it provides further proof of metal-ligand interactions and support of speciation, and allows for the comparison of some bonding parameters which reflect the nature of metal-ligand interactions.

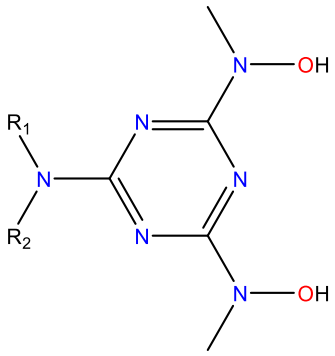

R_1, R_2 = H, OH, alkyl, aryl

R_1, R_2 = $-CH_2CH_2OCH_2CH_2-$ (H_2bihyat)
R_1 = OH, R_2 = CH_3 (H_3trihyat)

(a) General structure of 1,3,5-triazine hydroxylamine ligands.

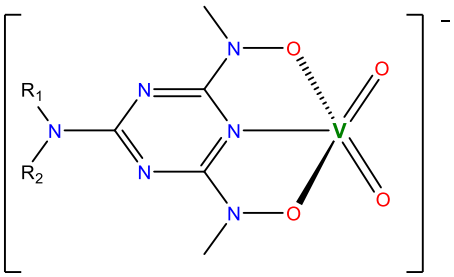

R_1, R_2 = $-CH_2CH_2OCH_2CH_2-$ (H_2bihyat)
R_1 = OH, R_2 = CH_3 (H_3trihyat)

(b) Vanadium complexes of H_2bihyat[19] and H_3trihyat[20] ligands.

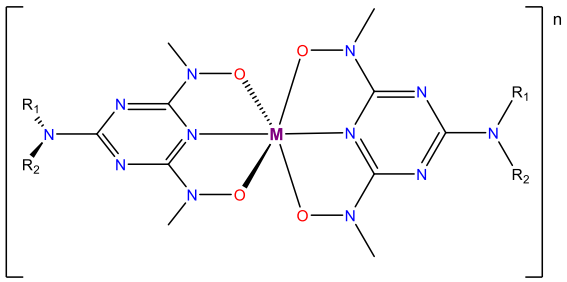

R_1, R_2 = $-CH_2CH_2OCH_2CH_2-$ (H_2bihyat)
R_1, R_2 = Cy
R_1, R_2 = $-CH_2COOEt$

For M = Fe, 8 more examples with other R_1, R_2
n = 0 for Ti, n= -1 for Fe (solution state)

(c) Titanium[29] and iron[18] complexes of triazine hydroxylamine ligands.

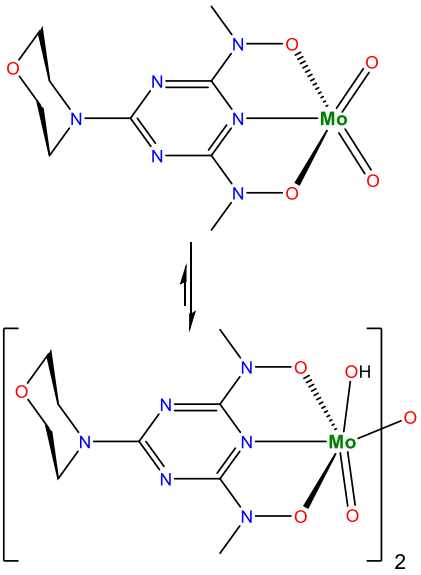

(d) Molybdenum(VI) complex of H_2bihyat showing monomer-dimer equilibrium in water.[30]

Figure 2. Related 1,3,5-triazine hydroxylamine ligands and previously reported transition metal complexes of these ligands.

Experimental

Chemicals

H_2bihyat was synthesized as described previously.[19] Uranyl stock solutions were prepared by dissolving UO_3 in perchloric acid or hydrochloric acid, followed by dilution with water. The concentration of uranium was determined by fluorimetry[35] or titration with Arsenazo III[36], and free acid concentration determined by Gran titration. Acid and base stock solutions were standardized before use.

Potentiometric titrations

Potentiometric titrations were performed using an autotitration unit consisting of a double jacket glass titration cell and a Metrohm dosimat (907 Titrando) connected to a pH electrode (Orion model 8102). The temperature of the titration cell was maintained at (25 ± 0.1) °C by circulating water from a constant temperature water bath. An inert atmosphere was maintained in the titration cell by passing Ar gas over the solution to exclude CO_2 during titrations. Prior to each titration, an acid/base titration with standardized HCl and NaOH was performed to obtain the electrode parameters E0, γH, and γOH. These parameters allowed the calculation of hydrogen ion concentrations from the measured EMF in subsequent titrations. In a typical titration, a solution (about 15 mL) containing appropriate amounts of UO_2^{2+} and ligand was titrated with a standardized solution of NaOH. Multiple titrations were conducted with solutions of different concentrations of metal ions. The potentiometric titration data were analyzed to obtain the stability constants of the metal/ligand complexes by the Hyperquad 2008 program.

UV-Visible absorbance spectroscopy

Absorption spectra were acquired on a Cary 50 Spectrophotometer. A 2 mm quartz cuvette was used, and the baseline corrected against a blank solution of water in the cuvette.

To prepare the solutions, H_2bihyat (3.2 mg, 0.0125 mmol) was suspended in water (15 mL, 0.8 mM), and an aqueous solution of uranyl chloride (0.00625 mmol in 0.1 mL) was added with stirring. The mixture immediately turned an amber color, and upon further stirring the ligand fully dissolved. After 30 minutes, the solution was measured to be pH 5-6. 1 mL aliquots were taken and adjusted to different pH values for absorption spectra. The remainder of the solution at pH 5-6 was allowed to stand for 3 weeks at room temperature, during which large very dark brown blocks suitable for X-ray diffraction formed.

X-ray crystallography

X-ray structural determination was performed on a Bruker APEX diffractometer with a Bruker fixed-Chi 3-Circle goniometer, a Bruker APEX I CCD detector, and a monochromatized fine-focus sealed Mo-kα X-ray source. A crystal was coated with paratone oil and mounted in a Kaptan loop, which was mounted on the goniometer with a nitrogen cryostream held at a temperature of 100 ± 0.5 K. Crystallography data was processed in the WinGX software package, solved using the SHELXTL software package and refined with the SHELXL software package, with semiempirical absorption correction with SADABS, included in SHELXTL.[37] All non-hydrogen atoms were refined anisotropically, and all hydrogen atoms were located in difference maps and refined isotropically.

NMR

^{1}H NMR spectra in H_2O or H_2O/D_2O mixtures were acquired on a Bruker AV-500 spectrometer (500 MHz) using a WATERGATE pulse sequence for solvent suppression, and referenced to an external standard of C_6D_6. ^{1}H NMR spectra in DMSO-*d*$_6$ and MeOD were acquired on a Bruker AV-500 spectrometer and referenced to the residual solvent peak. ^{13}C NMR spectra were acquired on a Bruker DRX-500 spectrometer (126 MHz), referenced to an external standard of C_6D_6.

Results and discussion

Potentiometric studies

The results of potentiometric titrations of the uranyl – H_2bihyat systems indicate that both 1:1 and 2:1 species can be formed, dependent on pH; the stability constants are summarized in Table 1 below. The modelled speciation at a 1:2 U/L ratio as a function of pH is shown in Figure 3 and a sample titration is provided in Figure 4. The ligand protonation constants (pKa) were determined in the 0.5 M NaCl ionic medium, and are very close to literature reported values.[19] H_2bihyat is more acidic than glutaroimide-dioxime, with the second protonation constant of 8.0 ± 0.3, so the protonation state in an oceanic environment of pH = 8 would mean that the ligand is half-deprotonated, further facilitating complexation.[38]

The same (*m*,*h*,*l*) stoichiometries and charges are observed for complexes of both glutaroimide-dioxime and H_2bihyat, such that comparison between species is straightforward. The stability constants are slightly higher for glutaroimide-dioxime overall, although the higher first pKa value means that they are generally comparable starting from the protonation states of the ligand that would be dominant at pH 7-9. For both systems, 2:1 complexes dominate at neutral to basic pH, while 1:1 complexes are favoured in acid, although 2:1 complexes are still present. The formation of $UO_2(HL)_2$, complex **6** for L=bihyat, shows the largest difference between the respective formation constants, although this is a relatively minor component of both systems and is not present in neutral to basic solution.

It should be noted that carbonate was not included in this system. Although this is not needed for comparison between glutaroimide-dioxime and H_2bihyat starting from the same uranyl carbonate species, comparisons between uranyl and vanadium are somewhat more qualitative in nature.[39] Nonetheless, the similar stability of the uranyl complexes and the much weaker nature of the vanadium complexes of H_2bihyat compared to glutaroimide-dioxime mean that U/V selectivity should be significantly improved with sorbents based on a triazine hydroxylamine structure.

Iron is another significant competitor for uranium extraction from seawater, although not to the same extent as vanadium.[28] To assess U/Fe selectivity, the formation constants for iron(III) can be compared between the H_2bihyat[18] and glutaroimide-dioxime[40] complexes in the same manner. The formation constant for $[Fe(bihyat)_2]^-$, the form isolated from water, is log $*\beta$ = -2.73 ± 0.3, which can be converted to a cumulative stability constant of 34.0 ± 0.4, compared to 36.02 ± 1.07 for glutaroimide-dioxime. This indicates that U/Fe selectivity may be slightly improved although not to the extent of U/V selectivity.

To avoid precipitation of uranium during titrations, all experiments were performed with an excess of ligand, with M/L ratios ranging from 1:2.1 to 1:3.3. Based on NMR evidence, we believe that an unobserved species **2** does form in solution with an approximate stability constant of log β = 7 ± 1. With a larger constant, we would expect to see **2** in the titrations performed. Further evidence and discussion of this complex is provided below.

Table 1. Summary of thermodynamic parameters for uranyl complexes with glutaroimide-dioxime and bis-(hydroxylamino)-1,3,5-triazine (H_2bihyat). Data for glutaroimide-dioxime and uranyl formation constants are from our past work.[31]

Reaction	Log β (25°C, 0.5 M NaCl)		
	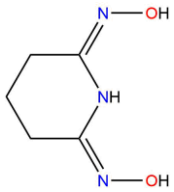	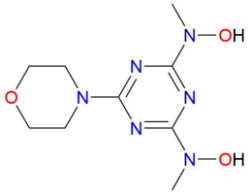	
$H^+ + L^{2-} = HL^-$	12.06 ± 0.23	10.40 ± 0.14	
$2H^+ + L^{2-} = H_2L$	22.76 ± 0.31	18.38 ± 0.23	
$3H^+ + L^{2-} = H_3L^+$	24.88 ± 0.35	23.71 ± 0.28	
$UO_2^{2+} + L^{2-} = UO_2(L)$	17.8 ± 1.1	17.47 ± 0.27	**1**
$UO_2^{2+} - H^+ + L^{2-} = UO_2(OH)(L)^-$		*7 ± 1 (estimated)*	**2**
$UO_2^{2+} + H^+ + L^{2-} = UO_2(HL)^+$	22.7 ± 1.3	19.9 ± 2.5	**3**
$UO_2^{2+} + 2L^{2-} = UO_2(L)_2^{2-}$	27.5 ± 2.3	26.7 ± 0.56	**4**
$UO_2^{2+} + H^+ + 2L^{2-} = UO_2(HL)(L)^-$	36.8 ± 2.1	33.4 ± 0.50	**5**
$UO_2^{2+} + 2H^+ + 2L^{2-} = UO_2(HL)_2$	43.0 ± 1.1	37.8 ± 2	**6**

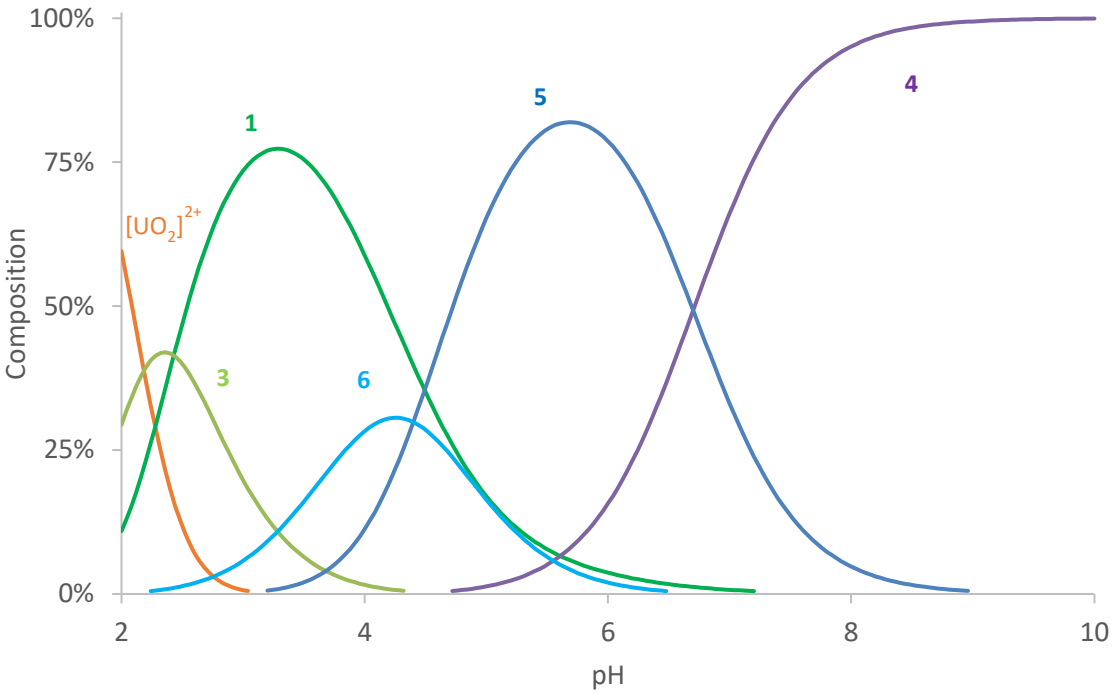

Figure 3. Calculated speciation as a function of pH. Species are as listed in Table 1. Conditions: $[UO_2]$ = 0.2 mM, [L] = 4 mM.

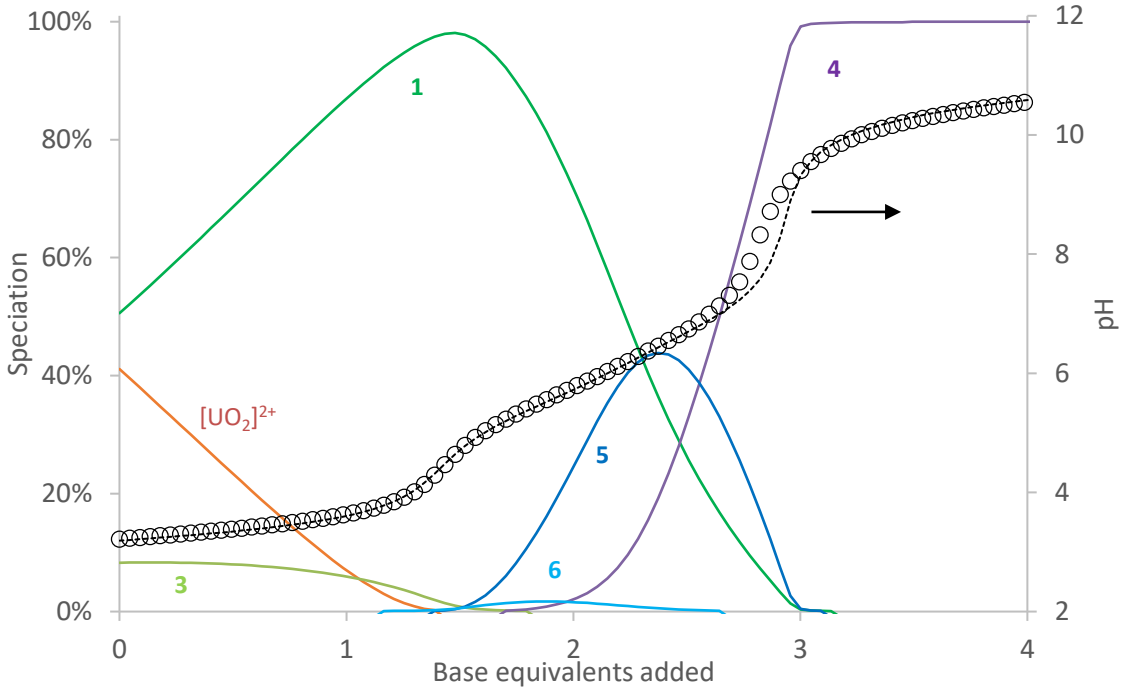

Figure 4. Sample titration of uranyl with H_2bihyat. Species are as listed in Table 1. Base equivalents are with respect to ligand. Black circles are measured pH, line is calculated pH. Conditions: $[UO_2]$ = 0.362 mM, $[UO_2]$:[L] = 2.17:1.

UV-Visible absorption

In order to corroborate changes in pH and investigate the electronic structure of the U(VI)-H_2bihyat complexes, we investigated their UV-Visible absorption spectra. During the titrations, a deep amber color was observed, and we sought to investigate if it varied at different acidities to use as another characterization of solution binding. Spectrophotometric titrations can be used in a similar manner as potentiometric titrations, by titrating acid into a mixture and fitting it to calculated or known absorption spectra of the individual components. Spectrophotometry is generally less accurate and reliable as potentiometric data when it is available, especially with uranyl, whose color tends to be weak and vary less than other actinide or transition metal species.[10,38,41]

The free ligand is colorless and has no visible absorption, but absorbs strongly in the ultraviolet region due to its conjugated aromatic core (Figure 5). Uranyl also has weak visible absorption, appearing pale yellow in solution. In contrast, when they are mixed, darker amber colors are observed. The dramatic change and increase in intensity of color is the result of new ligand-metal charge transfer transitions that can occur.[42] Interestingly, the UV absorption of the free ligand extends further towards the visible region than in complexes, with an absorption cutoff at about 320 nm, as opposed to 290-300 nm when uranyl is present. This indicates that the transitions observed in the triazine core are affected by the presence of uranyl, either through participation of the nitrogen atom in bonding or distortions in geometry upon binding which affects conjugation throughout the molecule.[20]

Although full spectrophotometric titrations were not performed, the spectra can nonetheless corroborate the different stoichiometries observed over a wide pH range. As the pH is raised from acidic to neutral, the major absorption band at 450 nm appears. The absorption does not change significantly with protonation state as the pH changes, however, the absorption decreases as the pH is increased further, and the band shifts to 425 nm in more basic solution, as the 2:1 complexes are formed. This absorption is slightly weaker, which is consistent with previously observed symmetric vs. asymmetric actinyl species.[10,41] Several absorption bands of lower intensity can be seen around 340 nm and 640 nm, the former of which contributes to the overall yellow-amber color observed.

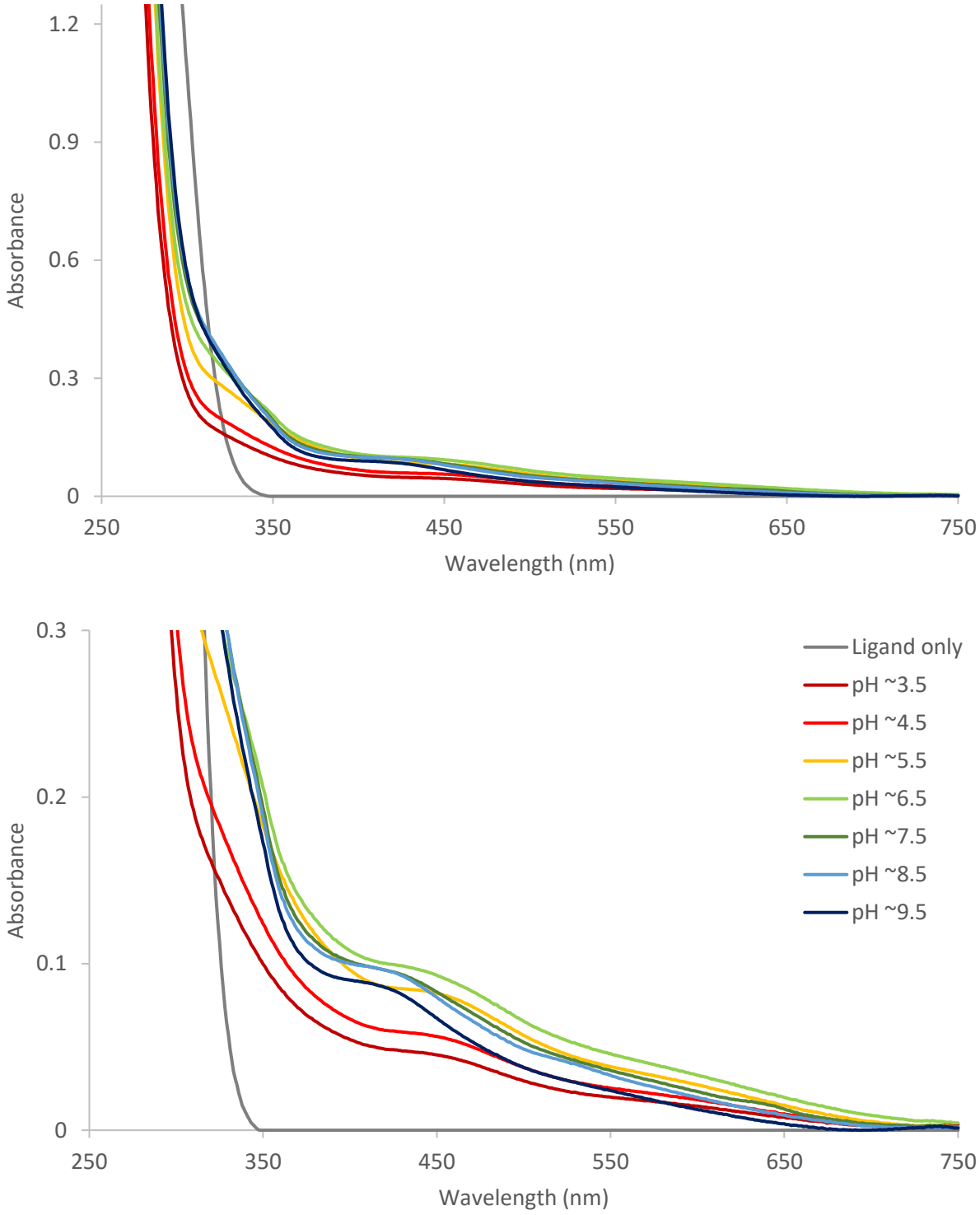

Figure 5. UV-Visible absorption spectra of uranyl – H_2bihyat solutions.
The lower spectrum is an inset of the upper spectrum.
Conditions: [L] = 0.8 mM, [UO_2] = 0.4 mM (except ligand only solution), 2 mm cuvette.

Solid-state binding

After the solutions were prepared and pH adjusted for the UV-Visible absorption spectroscopy studies, the solutions were allowed to stand at room temperature. Over the course of three weeks, dark brown-black blocks of **1·2H$_2$O** formed from the solution at pH 5.5 and the solution decolored. All of the other solutions remained colored but clear with no signs of precipitation or crystallization. At this pH, **1** is expected to be dominant uranium species in solution (Table 1 and Figure 3), although we are not able to explain why no solids were observed in the other containers where **1** was also dominant at pH 4.5 and 6.5. The long crystallization time and remaining color in the other containers also indicates that the uranium-H$_2$bihyat complexes are stable over long periods of time in the pH range observed here, which is necessary for prolonged immersion in the ocean and recycling if incorporated into polymer sorbents, with targets of 6 uses of 4-8 weeks each being targets for reuse.[28,43] Several attempts were made to isolate and crystallize a 2:1 complex; **4**, **5**, or **6**. However, all methods tested with either water or water and cosolvents containing these species never resulted in any isolable solid material, in contrast to the uranyl – glutaroimide-dioxime complex where the structure with 2:1 stoichiometry was obtained, not 1:1.

The crystal structure of **1·2H$_2$O** was obtained, and is shown in Figure 6. The complex crystallizes in the P2$_1$/c space group with no symmetry elements within the molecule. Selected bond lengths and angles are presented in Table 2 with comparisons to the U – glutaroimide-dioxime[31] and V – H$_2$bihyat complexes[19]. Crystal structure data is shown in Table 3 below.

In the structure, the uranyl ion remains close to linear, at 175.7° with typical U=O bond lengths of 1.787 and 1.779 Å. The U-ligand bonds of **1** are approximately 0.1Å shorter than the analogous bonds in the glutaroimide-dioxime complex. However, this could be a consequence of the ligand in 1 being of the form [bihyat]$^{2-}$, while glutaroimide-dioxime is in the [H-glutaroimide-dioxime]$^-$ protonation state. Despite having shorter bonds to uranyl, the O–M–O bite angle in **1** is slightly larger than glutaroimide-dioxime, at 126.6° compared to 121.1°. This would suggest that differences in bond lengths and angles may be due to ligand geometry rather than significantly different bond character, due to the rigidity of both ligands. The metal-ligand bond lengths for the vanadium complex [VO$_2$(bihyat)]$^-$ are significantly shorter than those in **1** as a consequence of the smaller ionic radius of V vs. U.

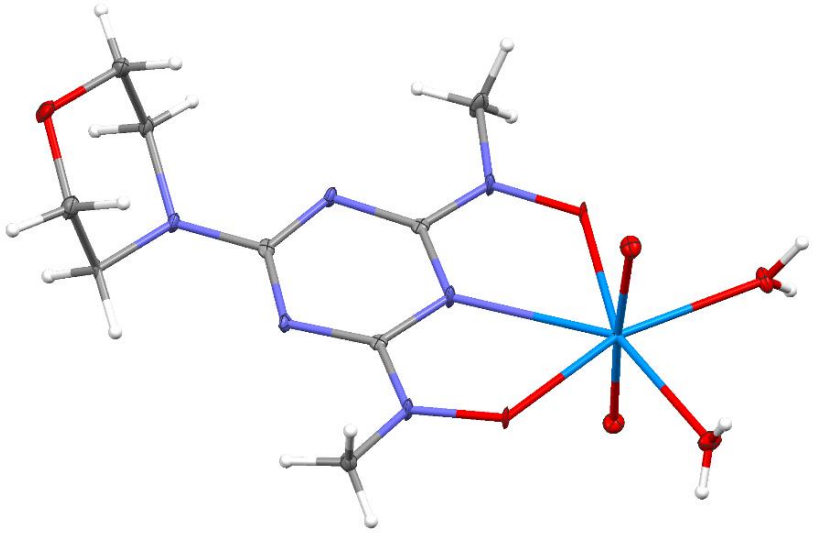

Figure 6. Crystal structure of the 1:1 U(VI)/H_2bihyat complex **1·2H_2O**. Thermal ellipsoids are at the 50% probability level. One water molecule is hidden for clarity.

Table 2. Selected Bond lengths and angles in the crystal structure of **1·2H_2O** and comparison to bis(glutaroimide-dioxime) uranyl[31] and V(V)/H_2bihyat.[19]

	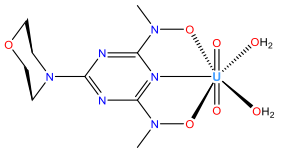	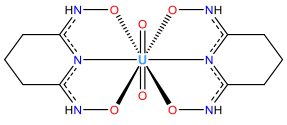	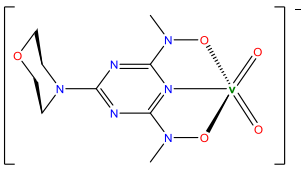
Bond length (Å) or angle (°)	**1·2H_2O**	**(UO_2)(glutaroimide-dioxime)$_2$**	**[VO_2(bihyat)]$^-$**
M–O (ligand)	2.362(2), 2.410(2)	2.535(3), 2.429(3)	1.974(3), 1.994(3)
M–N	2.439(2)	2.563(3)	1.993(3)
M=O (oxo)	1.787(2), 1.779(2)	1.785(3)	1.624(3), 1.637(3)
M–O (water)	2.368(2), 2.375(2)		
O–M–O (ligand)	126.61(7)	121.05(9)	145.52(12)
O=M=O (oxo)	175.70(9)	180.0	111.06(19)

Table 3. Crystal structure data for **1·2H_2O**.

	1·2H$_2$O
Formula	$C_9H_{20}N_6O_8U$
Formula weight (g·mol^{-1})	578.32
Space group	Monoclinic, $P2_1/c$
a (Å)	11.476(3)
b (Å)	13.364(3)
c (Å)	11.110(3)
α (°)	90
β (°)	106.465(4)
γ (°)	90
V (Å^3)	1634.1(7)
Z	4
ρ_{calc} (g·cm^{-3})	2.351
μ (mm^{-1})	9.986
F(000)	1088
Crystal size (mm × mm × mm)	0.100 × 0.060 × 0.060
Crystal color and form	Dark brown block
Theta range for data collection	1.850 to 25.371°
Index ranges	-13<=h<=13, -16<=k<=16, -13<=l<=13
Reflections collected	44023
Independent reflections	2983 [R(int) = 0.0386]
R1 ($I > 2\sigma(I)$)	0.0138
wR2 ($I > 2\sigma(I)$)	0.0345
R1 (all data)	0.0139
wR2 (all data)	0.0345
GoF	1.175
Largest difference peak/hole (e·Å^3)	0.619 / -0.891

NMR solution binding studies

NMR experiments were performed to determine solution speciation of the H_2bihyat/uranyl system to corroborate potentiometric titration experiments. In water, the 1:1 complex is observed in acidic to neutral solution (Figures 3 and 4). However, once crystallized from solution as $(L)(UO_2)\cdot 2H_2O$ (crystal structure), it is insoluble in neutral or acidic water, indicative of a neutral low-polarity species. All the spectra acquired have broad peaks, indicative of hydrogen bonding and/or dynamic equilibrium in solution.

Upon adding base to the 1:1 complex in water (3 equivalents, final pH = 12), it redissolves, likely due to exchange of water on uranyl with hydroxide. We propose that the complex is deprotonated in solution, forming the anionic complex $[(L)(UO_2)(OH)]^-$, **2**. This is not present in speciation models from the potentiometric titrations. However, experiments were only performed with a 2:1 or larger excess of ligand relative to uranyl. When a formation constant of log β = 7.0 for **2** (m,h,l = 1,-1,1) is added, it is never observed at 2:1 or higher U/L ratios but at a 1:1 ratio, it appears at pH = 9 and is the only species present at pH = 12. The addition of more ligand results in the solution becoming a slightly paler color, and the NMR spectra show that a new species is formed, which we assign to the 2:1 complex, with excess ligand and very small amounts of the 1:1 complex also present. The ^{13}C spectra are consistent with these species (Figure 9), and a 2D ^{1}H-^{13}C HSQC spectrum was acquired to confirm these assignments (Figure 10).

In addition to spectra in water, NMR spectra of the isolated 1:1 complex was also acquired in methanol and DMSO (Figure 8). In both cases, distinct peaks are observed for the 1:1 complex, showing coupling that is absent in water. Excess ligand was added to both solutions, where different behavior was seen between the different solvents. In DMSO, the ligand did not interact with the 1:1 complex even after standing for 12 hours. In this case, the 1:1 complex is preferred over the neutral 2:1 complex. In methanol, a complex mixture is formed, likely a mixture of 1:1 and 2:1 complexes, and possibly with methanol exchanging with coordinated water in the 1:1 complex. Peaks could not be assigned to specific species, although qualitatively several different complexes are present, likely all in dynamic equilibrium.

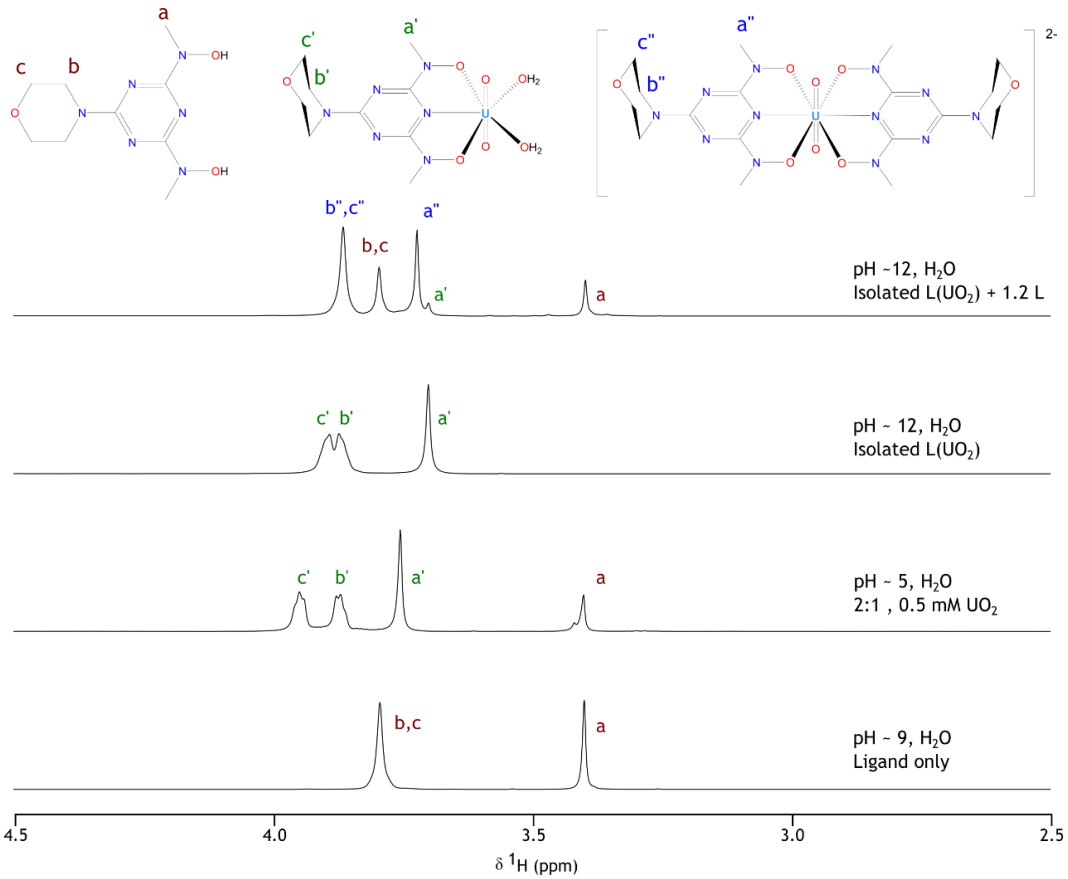

Figure 7. ^{1}H NMR spectra of H_2bihyat/UO_2^{2+} in water.

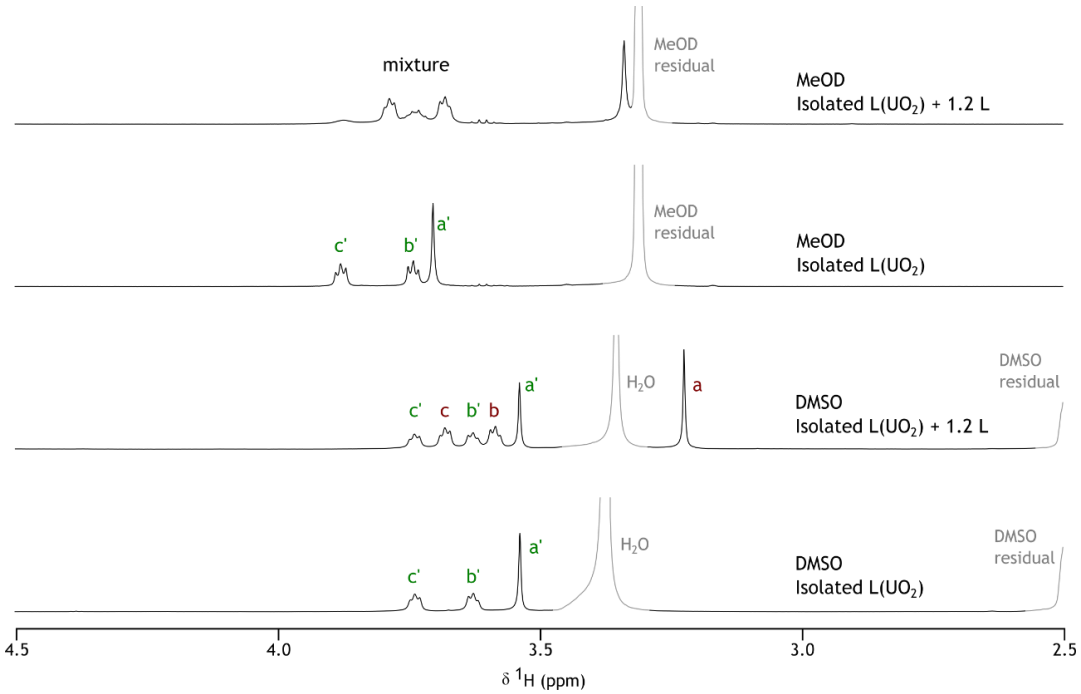

Figure 8. ^{1}H NMR spectra of H_2bihyat/UO_2^{2+} in Methanol and DMSO.

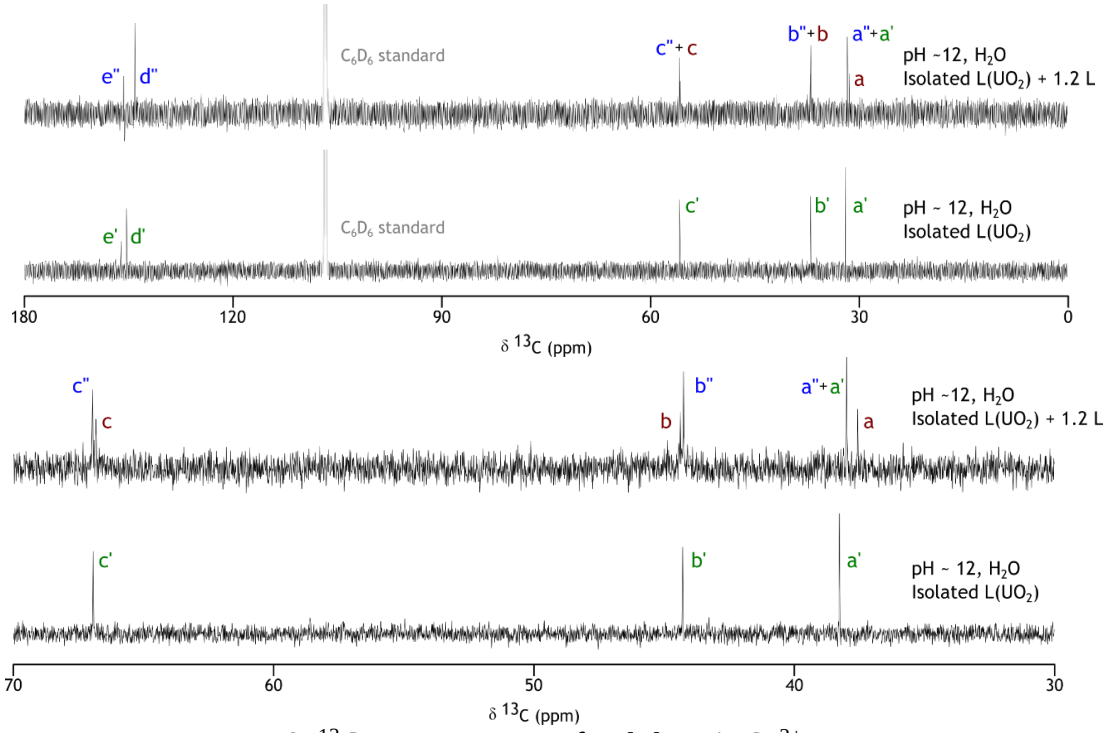

Figure 9. ^{13}C NMR spectra of H_2bihyat/UO_2^{2+} in water
(upper: full spectra; lower: aliphatic region only)

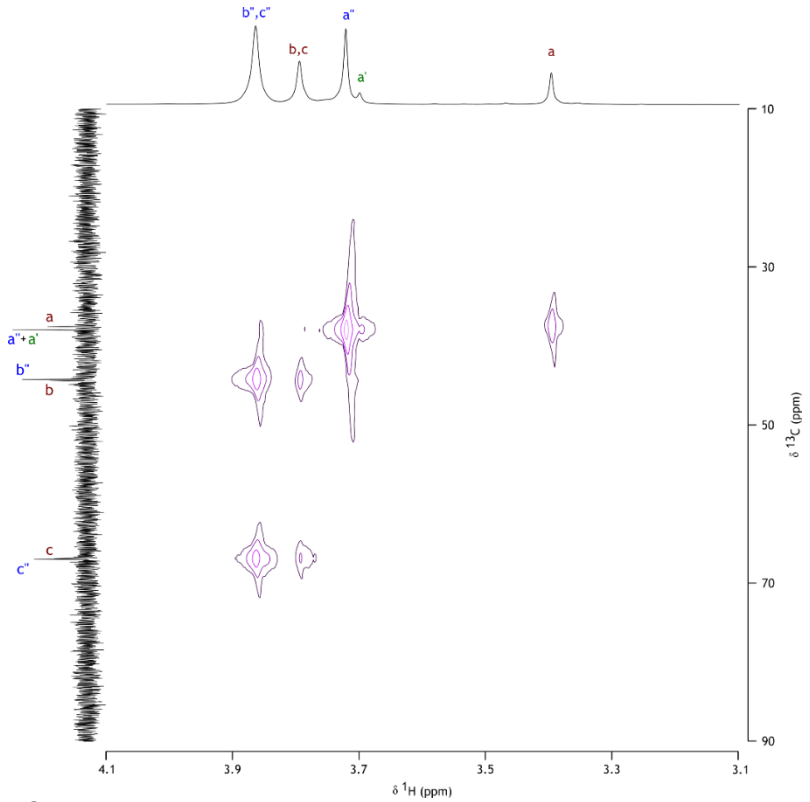

Figure 10. ^{1}H-^{13}C HSQC spectrum of the aliphatic region to confirm peak assignments

Summary and conclusions

In this study we have investigated the solution-state and solid-state interactions of uranyl with a 1,3,5-triazine hydroxylamine ligand, H_2bihyat. Solution and solid-state chemistry of this and closely-related triazine ligands have previously been studies with several metals, notably vanadium and iron, which are the major competitors for uranyl binding in polymer sorbents. The ligand has a rigid planar core and chelates to metals through (O,N,O) binding, in the same manner as glutaroimide-dioxime which is the ligand that has received the most attention for uranyl extraction.

Solution binding studies through potentiometry and NMR studies have shown that both 1:1 and 1:2 U/L complexes can form, with the former being favoured only at low pH. Formation constants for complexes are slightly lower than for the analogous glutaroimide-dioxime complexes, for instance, 43.0 vs. 37.8 for the respective neutral $UO_2(HL)_2$ species. This is somewhat offset by the ligand protonation state; at seawater pH glutaroimide-dioxime is in the neutral form while H_2bihyat is half deprotonated, so binding will occur more readily. NMR speciation is consistent with the stoichiometries observed by potentiometry, and the behaviour of the complex in other solvents gives insight into the binding mechanism. In the course of these studies, we isolated and crystallized the 1:1 U/H_2bihyat complex, obtaining the crystal structure through X-ray diffraction. The ligand binds in a tridentate fashion with bond lengths and angles typical of uranyl complexes, similar to the analogous glutaroimide-dioxime complex. It is unusual, however, that this complex with 1:1 stoichiometry was isolated, in contrast to glutaroimide-dioxime, where only the 2:1 complex was crystallized.

Although this ligand does not offer significantly improved binding affinity to uranyl when compared to glutaroimide-dioxime, it has much greater selectivity for uranium over vanadium. Consequently, overall uranium capacity should increase due to fewer binding sites being occupied by vanadium. Polymer reconditioning and reuse also benefits from weaker vanadium binding, since the strong acid needed to remove vanadium from glutaroimide-dioxime is not needed; base can be used instead. The incorporation of the triazine moiety into polymers may be a synthetic challenge, but research into this is currently underway. Additional solution state studies are planned for this system, including computational studies, solution and solid-state EXAFS studies, and investigating transuranic complexes of H_2bihyat.

References

(1) Sather, A. C.; Berryman, O. B.; Rebek, J. *J. Am. Chem. Soc.* **2010**, *132*, 13572–13574.
(2) Sather, A. C.; Berryman, O. B.; Moore, C. E.; Rebek, Jr., J.; Rebek, J. *Chem. Commun. (Camb).* **2013**, *49*, 6379–6381.
(3) Prudden, A. R.; Lien, N. R.; Telford, J. R. *Chem. Commun. (Camb).* **2004**, 172–173.
(4) Lashley, M. A.; Ivanov, A. S.; Bryantsev, V. S.; Dai, S.; Hancock, R. D. *Inorg. Chem.* **2016**.
(5) Parker, B. F.; Knight, A. S.; Vukovic, S.; Arnold, J.; Francis, M. B. *Ind. Eng. Chem. Res.* **2016**, *55*, 4187–4194.
(6) Zhou, L.; Bosscher, M.; Zhang, C.; Özçubukçu, S.; Zhang, L.; Zhang, W.; Li, C. J.; Liu, J.; Jensen, M. P.; Lai, L.; He, C. *Nat. Chem.* **2014**, *6*, 236–241.
(7) Mullen, L.; Gong, C.; Czerwinski, K. *J. Radioanal. Nucl. Chem.* **2007**, *273*, 683–688.
(8) Berry, R. E.; Smith, P. D.; Harben, S. M.; Helliwell, M.; Collison, D.; David Garner, C. *Chem. Commun.* **1998**, *2*, 591–592.
(9) Ghosh, S.; Biswas, S.; Bauzá, A.; Barceló-Oliver, M.; Frontera, A.; Ghosh, A. *Inorg. Chem.* **2013**, *52*, 7508–7523.
(10) Xu, C.; Tian, G.; Teat, S. J.; Rao, L. *Inorg. Chem.* **2013**, *52*, 2750–2756.
(11) Vukovic, S.; Hay, B. P. *Inorg. Chem.* **2013**, *0*, 7805–7810.
(12) Mehio, N.; Lashely, M. A.; Nugent, J. W.; Tucker, L.; Correia, B.; Do-Thanh, C.-L.; Dai, S.; Hancock, R. D.; Bryantsev, V. S. *J. Phys. Chem. B* **2015**, *119*, 3567–3576.
(13) Vukovic, S.; Watson, L. a; Kang, S. O.; Custelcean, R.; Hay, B. P. *Inorg. Chem.* **2012**, *51*, 3855–3859.
(14) Crans, D. C.; Mahroof-Tahir, M.; Johnson, M. D.; Wilkins, P. C.; Yang, L.; Robbins, K.; Johnson, A.; Alfano, J. A.; Godzala, M. E.; Austin, L. T.; Willsky, G. R. *Inorganica Chim. Acta* **2003**, *356*, 365–378.
(15) Hakimi, M.; Kukovec, B. M.; Rezvaninezhad, M.; Schuh, E.; Mohr, F. *Zeitschrift fur Anorg. und Allg. Chemie* **2011**, *637*, 2157–2162.
(16) Xu, C.; Tian, G.; Teat, S. J.; Liu, G.; Rao, L. *Chemistry* **2013**, *19*, 16690–16698.
(17) Allen, F. H. *Acta Crystallogr. Sect. B Struct. Sci.* **2002**, *58*, 380–388.
(18) Gun, J.; Ekeltchik, I.; Lev, O.; Shelkov, R.; Melman, A. *Chem. Commun. (Camb).* **2005**, 5319–5321.
(19) Nikolakis, V. A.; Tsalavoutis, J. T.; Stylianou, M.; Evgeniou, E.; Jakusch, T.; Melman, A.; Sigalas, M. P.; Kiss, T.; Keramidas, A. D.; Kabanos, T. A. *Inorg. Chem.* **2008**, *47*, 11698–11710.
(20) Nikolakis, V. a; Exarchou, V.; Jakusch, T.; Woolins, J. D.; Slawin, A. M. Z.; Kiss, T.; Kabanos, T. a. *Dalton Trans.* **2010**, *39*, 9032–9038.
(21) Hunks, W. J.; Jennings, M. C.; Puddephatt, R. J. *Inorg. Chem.* **1999**, *38*, 5930–5931.
(22) Maxim, C.; Matni, A.; Geoffroy, M.; Andruh, M.; Hearns, N. G. R.; Clérac, R.; Avarvari, N. *New J. Chem.* **2010**, *34*, 2319.
(23) Garner, M.; Reglinski, J.; Cassidy, I.; Spicer, M. D.; Kennedy, A. R. *Chem. Commun.* **1996**, *355*, 1975.
(24) Lewis, F. W.; Harwood, L. M.; Hudson, M. J.; Drew, M. G. B.; Desreux, J. F.; Vidick, G.; Bouslimani, N.; Modolo, G.; Wilden, A.; Sypula, M.; Vu, T. H.; Simonin, J. P. *J. Am. Chem. Soc.* **2011**, *133*, 13093–13102.

(25) Leggett, C. J.; Parker, B. F.; Teat, S. J.; Zhang, Z.; Dau, P. D.; Lukens, W. W.; Peterson, S. J. M.; Cardenas, A. J. P.; Warner, M. G.; Gibson, J. K.; Arnold, J.; Rao, L. *Chem. Sci.* **2016**, *7*, 2775–2786.
(26) Ivanov, A. S.; Leggett, C. J.; Parker, B. F.; Zhang, Z.; Arnold, J.; Dai, S.; Abney, C. W.; Bryantsev, V. S.; Rao, L. *Manuscript Submitted* **2017**.
(27) Oyola, Y.; Vukovic, S.; Dai, S. *Dalton Trans.* **2016**, 8532–8540.
(28) Kim, J.; Tsouris, C.; Oyola, Y.; Janke, C. J.; Mayes, R. T.; Dai, S.; Gill, G.; Kuo, L. J.; Wood, J.; Choe, K. Y.; Schneider, E.; Lindner, H. *Ind. Eng. Chem. Res.* **2014**, *53*, 6076–6083.
(29) Peri, D.; Alexander, J. S.; Tshuva, E. Y.; Melman, A. *Dalton Trans.* **2006**, 4169–4172.
(30) Vi, M.; Stylianou, M.; Nikolakis, V. A.; Chilas, G. I.; Jakusch, T.; Vaimakis, T.; Kiss, T.; Sigalas, M. P.; Keramidas, A. D.; Kabanos, T. A. *Inorg. Chem.* **2012**, *51*, 13138–13147.
(31) Tian, G.; Teat, S. J.; Zhang, Z.; Rao, L. *Dalton Trans.* **2012**, *41*, 11579–11586.
(32) Tian, G.; Teat, S. J.; Rao, L. *Dalton Trans.* **2013**, *42*, 5690–5696.
(33) Endrizzi, F.; Melchior, A.; Tolazzi, M.; Rao, L. *Dalton Trans.* **2015**, *44*, 13835–13844.
(34) Endrizzi, F.; Leggett, C. J.; Rao, L. *Ind. Eng. Chem. Res.* **2016**, *55*, 4249–4256.
(35) Smith, N. A.; Cerefice, G. S.; Czerwinski, K. R. *J. Radioanal. Nucl. Chem.* **2013**, *295*, 1553–1560.
(36) Savvin, S. *Talanta* **1961**, *8*, 673–685.
(37) Sheldrick, G. M. *Acta Crystallogr. Sect. A Found. Crystallogr.* **2015**, *71*, 3–8.
(38) Endrizzi, F.; Rao, L. *Chem. - A Eur. J.* **2014**, *20*, 14499–14506.
(39) Endrizzi, F.; Leggett, C. J.; Rao, L. *Ind. Eng. Chem. Res.* **2016**, *55*, 4249–4256.
(40) Sun, X.; Xu, C.; Tian, G.; Rao, L. *Dalton Trans.* **2013**, *42*, 14621–14627.
(41) Sun, X.; Tian, G.; Xu, C.; Rao, L.; Vukovic, S.; Kang, S. O.; Hay, B. P. *Dalton Trans.* **2014**, *43*, 551–557.
(42) Denning, R. G. *J. Phys. Chem. A* **2007**, *111*, 4125–4143.
(43) Gill, G. A.; Kuo, L.-J.; Janke, C. J.; Park, J.; Jeters, R. T.; Bonheyo, G. T.; Pan, H.-B.; Wai, C.; Khangaonkar, T.; Bianucci, L.; Wood, J. R.; Warner, M. G.; Peterson, S.; Abrecht, D. G.; Mayes, R. T.; Tsouris, C.; Oyola, Y.; Strivens, J. E.; Schlafer, N. J.; Addleman, R. S.; Chouyyok, W.; Das, S.; Kim, J.; Buesseler, K.; Breier, C.; D'Alessandro, E. *Ind. Eng. Chem. Res.* **2016**, *55*, 4264–4277.

Chapter 6

An alternative approach to selective U(VI) extraction from seawater using a combinatorial peptoid ligand system

Introduction

Much of the recent work on uranium recovery has focused on the amidoxime functional group that binds uranyl with a high affinity and with selectivity over many, but not all, other metal ions. The related glutaroimide-dioxime ligand (the cyclized product of two amidoxime groups) as well as monomeric amidoximes are also of interest as molecular analogues of the groups that are present on the amidoxime-functionalized polymer fibers.[1,2] These ligands are effective, but they have notable drawbacks, the most significant of which include: (1) a lack of selectivity for uranyl over vanadium and (2) degradation of the polymer under the harsh conditions that are needed to liberate the strongly bound uranium and other metal species from the adsorbent.[3,4]

Given the above limitations, there is significant interest in exploring new systems that can bind uranyl selectively over vanadium and other competing metal ions present at high concentrations. However, the process of designing and synthesizing large receptors to exploit the unique geometry of uranyl is inherently costly and time-consuming. Instead of relying solely on conventional, one-at-a-time ligand design, we are augmenting our efforts with combinatorial approach, using ligand libraries to identify robust and selective ligands through the use of large libraries of potential binding candidates.[5–7]

Combinatorial screening is a powerful technique that is commonly used for discovering new molecules for therapeutic applications and catalysis. Recently, an *in silico* screening approach has been used to explore uranyl-binding with engineered proteins, using a computational library to search for an appropriately-sized binding pocket.[8] This approach has been quite successful for the generation of an engineered protein that can bind with a very high affinity (at the femtomolar level). However, using engineered proteins is not feasible on the large scale that is proposed for polymer sorbents, as the cost would likely be prohibitively expensive.

The peptoid framework lends itself well to our goal, as it is a relatively inexpensive and versatile scaffold with the ability to create selective metal binding pockets.[7,9–12] In recent work, we have used a peptoid-based platform to identify selective ligands for toxic metals in complex environments: chromium in natural water sources and cadmium in blood.[13,14] Inspired by the successful removal of aqueous Cr(VI) from stream and seawater, the screening procedure was adapted to identify selective ligands for uranyl. These ligands were then resynthesized and verified for their uranyl binding ability. To provide insight into the binding interactions, a computational approach was implemented to model solution-state binding modes, which may be difficult to determine experimentally. Density functional theory (DFT) methods have been used previously to characterize the peptoid backbone;[15] here this approach has been extended to explore the binding modes and conformational flexibilities of peptoids when binding metals.

The contents of this chapter have been previously published in **"A Peptoid-Based Combinatorial and Computational Approach to Developing Ligands for Uranyl Sequestration from Seawater"**; Bernard F. Parker, Abigail S Knight, Sinisa Vukovic, John Arnold, Matthew B. Francis; *Industrial & Engineering Chemistry Research*; **2016**, 55 (15), p. 4187-4194.

In this report, we thus describe the full combination of combinatorial screening using a peptoid library and computational efforts implemented that are required to identify new, inexpensive ligand design leads that could be adapted for the sequestration of uranyl from seawater.

Methods

Peptoid synthesis

General techniques used for peptoid synthesis were according to procedures in our previous work.[13] Tentagel MB NH_2 resin (140-170 μm, 0.3 mmol/g) was purchased from Rapp-Polymere (Tuebingen, German). Butylamine, histamine, and piperonylamine were incorporated without protecting groups. *N*-boc-ethylenediamine was purchased and used as received. Cyesteamine was protectected with a trityl group as reported by Maltese.[16] β-alanine and glycine were purchased as hydrochloride salts of the respective *t*-butyl esters. To obtain the free bases, they were treated with 1 M NaOH solution saturated with NaCl and extracted with a mixture of 15:85 isopropanol:chloroform (v/v). The organic layers were dried over sodium sulfate and the solvent removed by evaporation to give the free bases. All other materials were purchased from commercial sources and used without further purification unless otherwise noted.

Tentagel MB NH_2 resin was swollen in dichloromethane (DCM) before peptoid synthesis. Fmoc solid-phase synthesis was used to incorporate the first four linker members using HCTU as a coupling agent. The resin was split evenly into seven fritted columns, then acylation and addition of the first amine were performed as developed by Zuckermann et. al.[17] For each acylation step, the resin beads were exposed to a solution of chloroacetic acid in dimethylformamide (DMF) (0.4 mM) as well as a solution of diisopropylcarbodiimide in DMF (2 M) with gentle agitation for 5 min on a nutator. The solutions were removed by filtration, and the resin rinsed with DMF. The resin beads were then exposed to a solution of amine in DMF (2 M) with gentle agitation for 2 h on a nutator. The solutions were removed by filtration, then all the resin was combined and mixed in DCM for 5 min. These steps were repeated three more times to add three more amines. After the resin was combined the last time, a solution of 4-methylpiperidine in DMF (20%) was added to the resin to remove any acyl groups from imidazoles. The resin was then filtered and rinsed with DMF. The protecting groups were removed by incubation with a cleavage solution of 95:2.5:2.5 trifluoroacetic acid:water:triisopropylsilane for 1.5 h, then rinsed with DCM, dried under vacuum, and refrigerated until use.

Screening and sequencing

Before incubating in the screening solution, a 40 mg portion of the resin was swelled in water overnight. The screening buffer (7 mL) was added, consisting of 2 mM $UO_2(OAc)_2$, 1 M NaCl, 1 M $MgSO_4$, 20 mM $NaHCO_3$, adjusted to pH 7, and incubated for 1 h. The library was then rinsed with water (3x1 mL) to remove ions not bound to the ligands, then with ethanol (1 mL) to remove excess water. The resin was then transferred to a Petri dish. No color changes were observed after incubation. The dye solution was prepared by diluting 50 μL of an aqueous 1 mM solution of arsenazo III sodium salt into 1 mL ethanol. This was then added to the beads and allowed to sit for 1 min before removal of the excess dye solution. Upon evaporation of the remaining solvent, the dye would be trapped in the resin, binding to the metal if present. The resin in the Petri dish was then examined using a Leica S6D Microscope (Leica, Germany). The 15 individual beads with the most intense blue-green color were selected for ligand identification.

To avoid radiological contamination and ensure proper sequencing, the metal ions were removed by placing the selected beads on the membrane of a centrifugal filter unit. Amberlite cation exchange resin (Na^+ form, 0.5 mg) was added to the filtrate collection tube of the filter unit, to which 1 M HCl (0.5 mL) was added. The tube was agitated gently on a nutator for 15 min, followed by centrifugation. The acid solution was then removed, and water was added (0.5 mL). The tube was again gently agitated on a nutator for 15 min, followed by centrifugation and removal of the water. The water rinse was repeated 3 times. The beads were then placed in a Petri dish with ethanol (0.5 mL), then individually selected and placed into individual Eppendorf tubes. Ethanol (5 μL) was added to each. The tubes were then placed in a computer controlled photoreactor with UVA bulbs for 8 h to cleave the peptoids from the resin beads.

After photocleavage, the ethanol was removed via evaporation and a solution (0.5 μL) consisting of 1:1 water:acetonitrile with tris(2-carboxyethyl)phosphine (0.5 mM). This solution was then mixed with matrix solution (0.5 μL) consisting of 1:1 water:acetonitrile with 0.1% trifluoroacetic acid, 0.6 M ammonium phosphate, and α-cyano-4-hydroxycinnamic acid (5 mg) and spotted on a stainless steel MALDI plate. MALDI-TOF MS (Voyager- DE instrument, Applied Biosystems) was used to identify the selected sequences by mass, and then and MALDI-TOF-TOF MS/MS (AB Sciex TF4800, Applied Biosystems) was used to sequence the peptoids by fragmentation.

Peptoid screening

Peptoid synthesis was performed according to the general procedures in our previous work on Tentagel MB NH_2 resin.[13] For incubation with uranyl, the resin was swelled in water overnight prior to the addition of the screening buffer, which consisted of 2 mM $UO_2(OAc)_2$, 1 M NaCl, 1 M $MgSO_4$, and 20 mM $NaHCO_3$, adjusted to pH 7. The resin was incubated for 1 h, then rinsed briefly with water (3x1 mL) to remove ions not bound to the ligands. No color changes were observed after incubation. Ethanol (1 mL) was then added to remove excess water. The resulting resin was transferred to a Petri dish. The dye solution was prepared by diluting 50 μL of an aqueous 1 mM solution of arsenazo III sodium salt into 1 mL of ethanol. This was then added to the beads for 1 min before removal of the excess dye solution. Upon evaporation of the remaining solvent, the dye was trapped in the resin, binding to the metal if present. The resin in the Petri dish was then examined using an optical microscope, and the 15 individual beads with the most intense blue-green colors were selected for ligand identification. Sequencing was then performed in the same fashion as in previous work.[13]

Fluorescence spectroscopy

Synthesis of peptoids for fluorescence experiments were also performed according to procedures in our previous work.[13] For preparative scale synthesis, the sequences were prepared analogously, using Fmoc-Rink Amide MBHA resin (Anaspec, Fremont, CA) instead of Tentagel MB NH_2 resin. The resin was treated with 20% 4-methylpiperidine in DMF to cleave the initial fluorenylmethyl (Fmoc) group, followed by a cleavage cocktail of 95:2.5:2.5 trifluoroacetic acid:water:triisopropylsilane to remove the peptoids from the resin and cleave the protecting groups from the submonomers. The trifluoroaceitc acid was removed by evaporation and the peptoids precipitated from diethyl ether, then suspended in water. They

were then purified by reverse-phase HPLC on a semi-preparatory HPLC column (Agilent). The fractions were then concentrated by speed vacuum and lyophilized.

A series of 2-20 μL portions of 10 mM or 80 mM solutions of $UO_2(NO_3)_2$ were added to each peptoid sample (100 μM, 1.00 mL) containing 20 mM HEPES buffer at pH 7. The fluorescence was then measured at each increment using a Photon Technology International Quanta Master 4 L-format scanning spectrofluorimeter with a LPS-220B 75W xenon lamp, using a 1 cm path length, 1.5 mL quartz cuvette. The excitation wavelength used was 200 nm, and emission was measured over 300-550 nm wavelengths, with the maximum emission at 321 nm, with 1 nm wavelength increments and 1 s integration times were used for all in. Concurrently, the uranyl fluorescence emission grew in at 369 nm, and at high uranyl concentrations (>1500 μM) it overlapped with the piperonyl emission. The emission was plotted against the concentration of uranyl and fit to a logistic binding curve (Equation 1). A1 and A2 are the asymptotes of the data, p is the slope of the curve, and x0 is the inflection point used to approximate the dissociation constant.

$$y = \frac{(A_1 - A_2)}{(1 + \frac{x}{x_0})^p} + A_2 \qquad (1)$$

DFT studies

Following prior calculations on uranyl amidoximate complexes (and references therein), electronic structure calculations were used to optimize geometries for uranyl complexes containing amidoximate and carbonate ligands.[18] These calculations were performed with the Gaussian 09 A2 package using density functional theory (DFT) at the B3LYP level of theory.[19–21] The Stuttgart Reactive small core 1997 effective core potential was used for uranium, replacing 60 core electrons to account for scalar relativistic effects.[22] The valence electrons in this basis set are represented by a contracted [8s/7p/6d/ 4f] basis; 6-31+G(d,p) basis sets were used for carbon, nitrogen, oxygen, and hydrogen atoms. Frequency calculations were performed to verify that geometries were minima. Solvation free energies have been calculated with the IEFPCM method, with corrections for standard concentrations.[23–26] Full coordinates for reported structures (optimized atomic coordinates, absolute energies, and images) are provided at the end of this chapter.

Results and Discussion

Library design

Given the success of the library screened for chromate ligands, an analogous library was synthesized with four variable positions (Figure 1). Each of these sites displayed a side chain chosen from the seven possible submonomers shown in the figure, providing 2401 possible structures.[13] The library was synthesized on poly(ethylene glycol) (PEG)-grafted polystyrene resin to allow for use in organic solvents during synthesis and in aqueous solutions during screening. A photocleavable residue was incorporated as the first residue to allow facile cleavage of the peptoid from the resin for ligand sequencing after the screening procedure. A previously established step-wise peptoid synthesis protocol using chloroacetic acid was used to incorporate the seven submonomers.[27] Binding moieties, including amines, carboxylic acids, and thiols, were included. In addition, two nonbinding groups were also incorporated to influence the secondary structures and steric interactions of the peptoids. The peptoid tetramers were attached to the resin via a linker to increase the distance between the ligands and the synthesis resin, and to include a bromine isotopic tag (^{79}Br/^{81}Br) to aid in the identification of the structures by MALDI-TOF-TOF MS/MS.

The library was evaluated for binding by incubation in a screening solution consisting of 1 M NaCl, 1 M $MgSO_4$, 20 mM $NaHCO_3$ (as a buffer, adjusted to pH 7), and 2 mM $UO_2(OAc)_2$. After one hour, the resin was rinsed with water to remove unbound or weakly bound uranyl (Figure 2; the resin shown is from preliminary tests in the absence of carbonate in the screening buffer to illustrate changes in color in the presence of uranyl). Due to the weak visible absorption of uranyl species, the screening solutions appeared colorless, and no color changes were observed in the library resin upon uranyl addition. To identify the uranyl binders, arsenazo III was used as a visualization agent.[28] It is an arsenic acid-based dye that has an intense purple color as the free acid or in the presence of alkali metal salts; however, upon binding to certain metals (such as uranyl) it changes to a blue or green color. After the incubation of the peptoid library with the screening solution, arsenazo III was added as a solution in ethanol to aid in the visualization of peptoids coordinated to uranyl. After the dye was added, less than 10% of the library beads showed any color change from purple. Of the beads that did change color, most were a lighter blue-purple shade, and only about 30 beads had a clear green color. A sample of library that was exposed to the buffer solution without uranyl followed by treatment with arsenazo III showed only purple beads, thus ruling out false positives due to peptoid interactions with the dye.

After the dye was applied and the resin was visualized under an optical microscope, fifteen individual beads were selected manually using a micropipette. In order to sequence the peptoids present on the beads, uranyl had to be removed to ensure proper fragmentation during MALDI-TOF-TOF MS/MS analysis for sequencing and to avoid radiological contamination of equipment and instruments. This was performed by transferring the selected beads to the top side of an ultrafiltration membrane, which was loaded with excess ion exchange resin (to chelate the uranyl) in the lower chamber. Aqueous HCl (1 M) was added to the top and bottom chambers, and the system was equilibrated for 1 h.

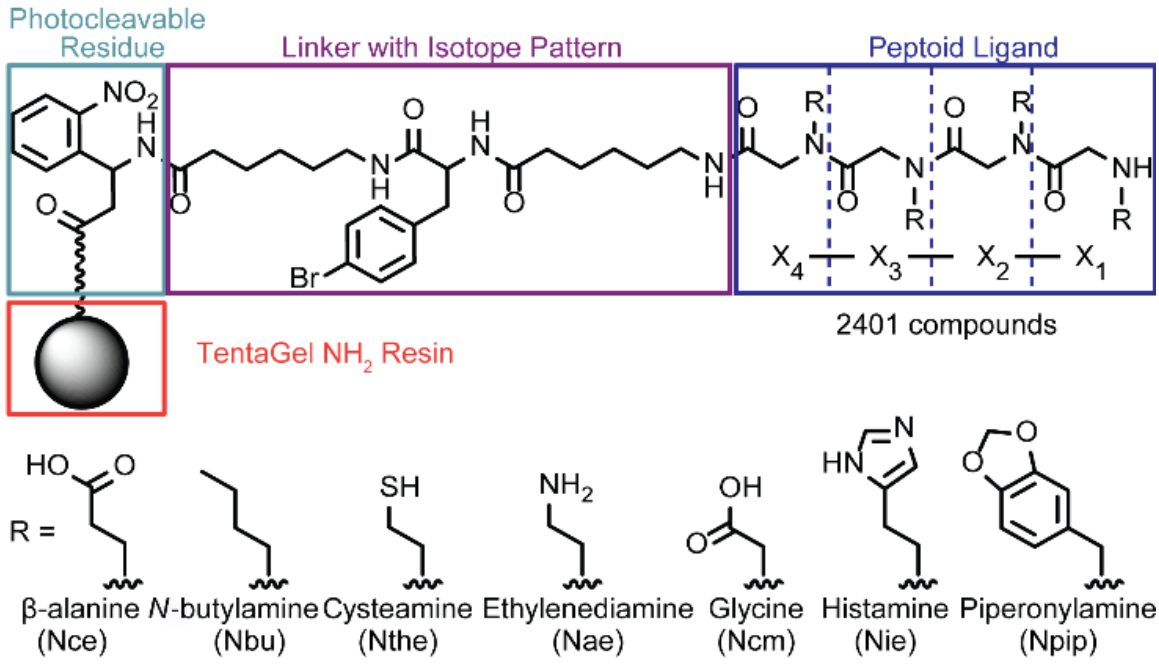

Figure 1. Peptoid structure and library schematic.

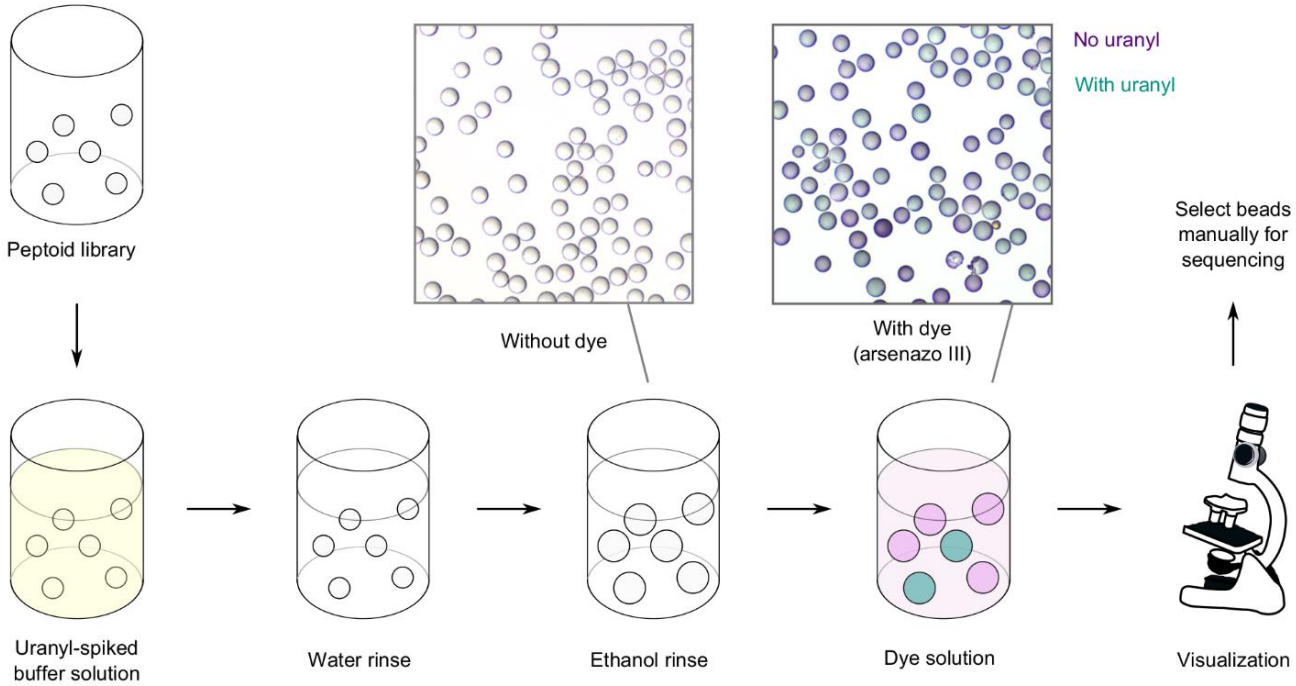

Figure 2. Screening methodology and application of the arsenazo III dye.

There are some drawbacks to using arsenazo III as a screening dye, the most significant of which is false positives caused by the interference of other ions. Ions that can interfere include the lanthanides, barium, lead, bismuth, thorium, a few transition metals, and, notably, calcium, which is present in high concentrations in natural seawater.[28] Interference from calcium was confirmed by testing ocean water, water with artificial aquarium salts, and calcium chloride solution, all with or without added uranyl (1-10 mM). In all assays, virtually all of the resin beads changed to a blue to blue-green color, indicative of calcium binding. Therefore, calcium was avoided in preparing the buffer solution used (see above). Additionally, quantitative arsenazo III assays have frequently been performed in strongly acidic solutions, which is not optimal to determine binding constants in ocean water conditions.[8,28,29]

Characterization of the uranyl ligands

Out of the fifteen beads selected, four were successfully sequenced using MALDI TOF-TOF MS-MS, and the three unique sequences were obtained. Notably, in these structures, the only groups that were present were carboxylic acids and non-binding side chains. This can be rationalized by differences in bonding preferences between uranyl and transition metal ions: the bonding between uranyl and ligands (including solvents) is generally quite ionic in character, with the short, strong U=O bonds being inert and *trans* to each other.[30] Ligands frequently bind in the equatorial plane around the linear dioxo groups, favoring higher coordination numbers with 5 or 6 equatorial donor atoms. Harder bases are generally preferred over softer groups such as thiols. Carboxylate groups often are bidentate ligands that can fill one or multiple coordination sites, unlike the other groups tested in the library.

In order to study binding of the peptoids to uranyl, sequence ***b*** was resynthesized on a larger scale on a different resin (Fmoc-Rink Amide MBHA resin instead of Tentagel MB NH_2 resin). The synthesis was performed in the same manner as the screening library. Before use, the peptoids were cleaved from the resin and purified by reverse-phase HPLC, lyophilized, then used as aqueous stock solutions.

Fluorescence spectroscopy was investigated as a technique to confirm binding and establish the affinities of the identified peptoids. The uranyl ion itself is fluorescent and indeed several bands can be observed directly under certain conditions. Its fluorescence spectrum and ability to quench other fluorophores varies widely with its chemical environment (pH, solvent, other ions present), and this feature can be used to study uranyl speciation by comparison with model uranyl compounds.[31,32] This technique does have drawbacks, however, as spectral measurements are often performed in the presence of phosphoric acid and time-resolved fluorescence spectroscopy is required.

Due to the difficulty in monitoring uranyl fluorescence, we sought to use a nearby fluorescent molecule that would be quenched by the proximity of uranyl. The piperonyl group in two of the peptoid sequences fluoresces weakly at 325 nm, and was therefore selected for monitoring. HEPES was chosen as a non-binding buffer and found not to interfere with uranyl fluorescence, unlike phosphate or carbonate-based buffers. The addition of sodium chloride also affected uranyl fluorescence, so measurements were performed in its absence. A titration of uranyl (0-5000 μM) into a solution of HEPES (20 mM) and peptoid (100 μM) (Figure 4), allowed the calculation of an approximate dissociation constant (700±200 μM) for sequence ***b***.

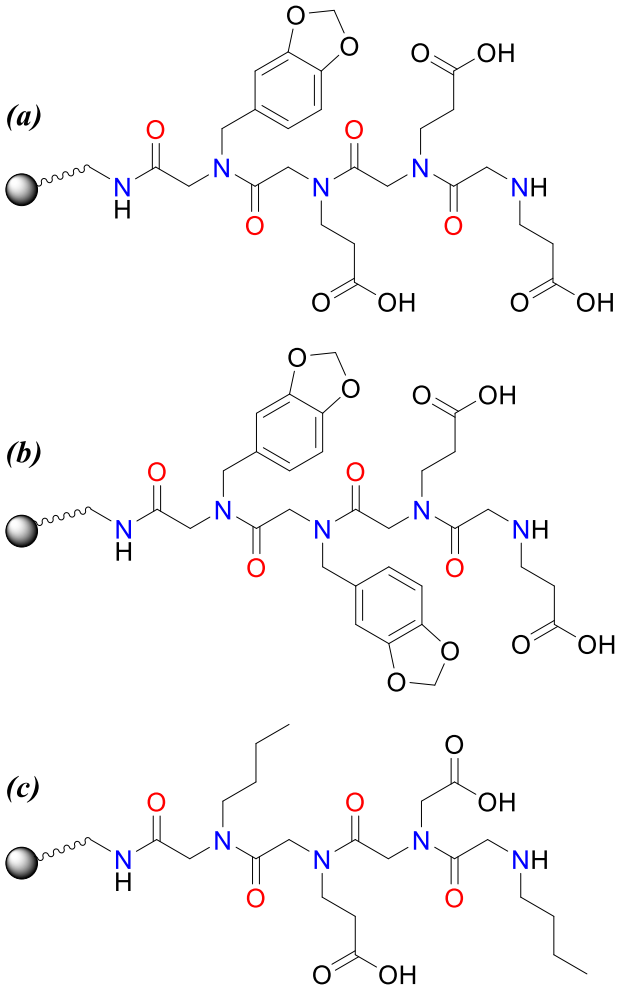

Figure 3. Uranyl-binding sequences obtained upon screening with a 2 mM uranyl solution.

Fluorescence of a uranyl-peptoid complex increased at 369 nm (one of several bands) during the titration, and an isosbestic point was present at about 353 nm, suggesting a 1:1 association at these concentrations.[33] At uranyl concentrations above 1500 μM this signal and a signal from free uranyl overlapped with the diminishing piperonyl fluorescence, resulting in an increase in fluorescence intensity at 325 nm from a shoulder of the uranyl peak. In a control experiment, no signal was observed for titrating uranyl at the concentrations used in these experiments (up to 5000 μM) into the same buffer solution in the absence of the peptoid, reflecting the different behavior of free uranyl depending on environment.

Fluorescence spectroscopy was attempted in the same manner with sequence ***a***, but the signal observed was much lower in intensity and did not change monotonically. This indicated that additional fluorescent species or other unusual behavior was involved in that case. The use of other dedicated fluorophores, rather than relying on the intrinsic fluorescence of the side chains, is an alternate approach that could be applied for future libraries. This is anticipated to increase the signal intensity, allow tuning of the fluorescence wavelength to reduce interference of uranyl fluorescence, and improve consistency between different sequences.

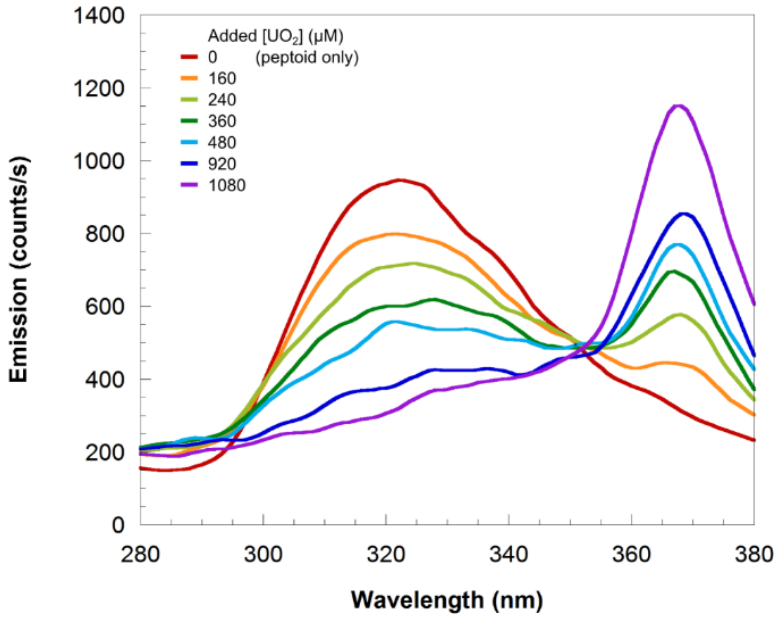

Figure 4. Peptoid sequence ***b*** fluorescence upon uranyl addition.

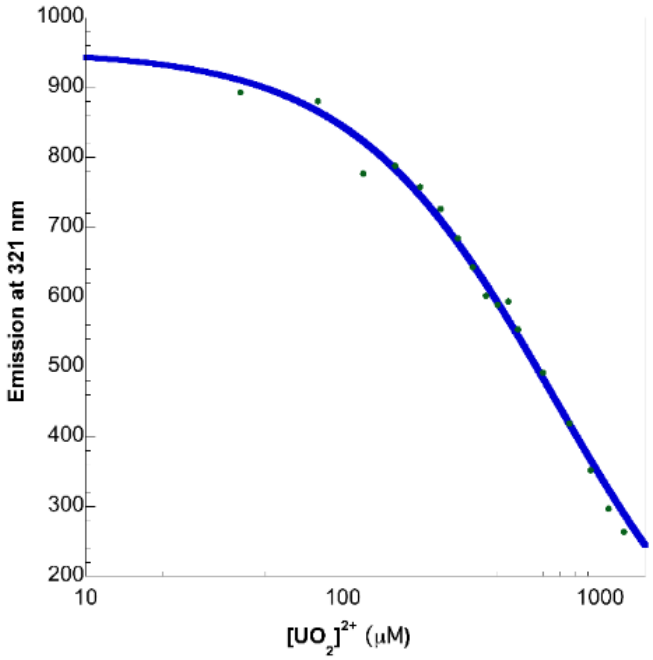

Figure 5. Peptoid sequence ***b*** binding curve constructued from data from Figure 4. K_d = 700±200 μM (the dissociation constant reflecting uranyl affinity for the peptoid) was calculated by approximating the inflection point of the binding curve.

Computational analysis

Computational methods are widely used to study proteins and metalloproteins, as well as small molecule organometallic complexes. Some computational work has been done on peptoid secondary structure in a similar fashion, but this is less well established and is hindered by the relative lack of structural data available. These previous studies also do not address metal binding.[15] Based on our extensive previous work on uranyl binding, Density Functional Theory (DFT) was chosen to model the binding of uranyl to the peptoid ligands in aqueous solution.[2,18,34]

The reactions of uranyl binding to a peptoid are shown in Equation 2

$$[\mathrm{UO_2(H_2O)_5}]^{2+} + \mathrm{Pep} \;\rightleftharpoons\; [\mathrm{UO_2Pep(H_2O)_{5-}}_n]^{2-x} + x\,\mathrm{H_3O^+} + (n-x)\,\mathrm{H_2O} \qquad (2)$$

where Pep is the peptoid, *x* is charge of the peptoid in the complex (since one proton is released upon binding of one carboxylate group to uranium) and *n* is the number of water molecules released from the equatorial plane of uranyl, $[UO_2(H_2O)^5]^{2+}$. In seawater conditions, uranyl is present as a triscarbonato complex, but this was not modeled here. For the purpose of identifying the most promising structural candidates as ligands the pentaaquo uranyl complex served as a model, providing dramatic savings in time-consuming calculations containing heavy atoms. For the same reason, the peptoids considered in the simulations were truncated versions of the original structures; linkers and non-binding residues were removed as including them would be inconsequential when modeling uranyl binding.[2] Such approximations also help in simplifying the conformational analysis of the free peptoids, which (even after shortening of the chain) still included thousands of conformers. Evaluation of the thermodynamic process for Equation 2 with only the most stable conformers was done by a standard expression shown in Equation 3.

$$\begin{aligned}\Delta G_{bind(aq)} \;=\; & G_{(aq)}\left([\mathrm{UO_2Pep(H_2O)_{5-}}_n]^{2-x}\right) + x \cdot G_{(aq)}(\mathrm{H_3O^+}) + (n-x)\cdot G_{(aq)}(\mathrm{H_2O}) \\ & - G_{(aq)}\left([\mathrm{UO_2(H_2O)_5}]^{2-x}\right) - G_{(aq)}(\mathrm{Pep}) \end{aligned} \qquad (3)$$

Calculations of free energies in solution were done by Density Functional Theory (DFT), the details of which are given in the Methods section. Full coordinates and images of the complexes presented and investigated are provided at the end of this chapter.

Out of three most promising peptoid sequences (Figure 3) only sequence ***a*** was studied in detail. Energetic differences between sequences ***a***, ***b***, and ***c*** are not known, and while the relative trends in binding for different conformers of one ligand can be accurately calculated, even the best computational approaches may be insufficient to predict the energies of binding for different ligands in solution reliably.[34] Our goal is not to determine this difference, but rather to use the computational results to understand what makes these three sequences successful, and use that knowledge to improve the peptoid library design in future generations of screening. Moreover, by studying sequence ***a*** we implicitly obtain results for sequence ***b*** and approximations for sequence ***c*** since special cases of ***a*** binding uranyl with only two carboxyl groups are almost identical to potential binding modes of the other sequences. Conformational

analysis was performed on this sequence (Figure 6) to determine the lowest energy conformer to use in binding calculations and assess the flexibility of the peptoid ligand.

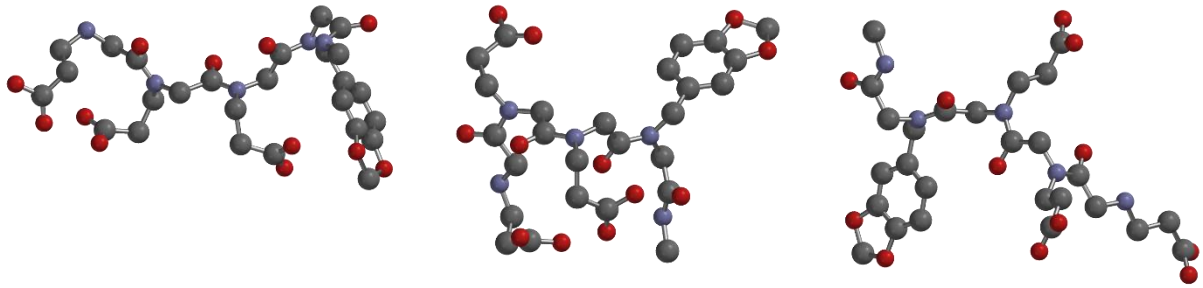

conf 1 conf 2 conf 3

Figure 6. Representative conformations for peptoid sequence ***a***. Conformation I was used for calculations of free energies of binding uranyl in solution in Equation 3.

Peptoid ***a*** can bind uranyl with three different motifs; with one, two or three carboxylate groups. Carboxylate groups bind in the equatorial plane of uranyl either as mono- or bidentate ligands, with a total of five or six atoms in the equatorial plane. Additionally, protons on the peptoid can establish hydrogen bonds to oxygen atoms of the uranyl ion. By systematic conformational search we optimized and obtained free energies in solution for all possible conformations of the complexes between peptoid ***a*** and uranyl. Relative energies for the most stable conformations for each of the binding motifs, with the most stable carboxylate binding modes and overall coordination number for that motif, are given in Table 2, with corrections for standard concentrations of solutes and water.[26]

Table 1. Relative energies for the most stable conformer for possible binding modes of peptoid sequence ***a*** to uranyl. Full calculations and data are available in Table 2.

Binding mode	Relative $\Delta G_{bind(aq)}$ [kcal/mol]	ΔS [cal/mol·K]
a1	4.86	68.4
a2	7.67	63.4
a3	6.06	68.6
a12	11.33	19.1
a23	3.90	22.3
a13	**0.0**	22.7
a123	8.69	-18.3
a123h	10.06	-20.5

Table 2. Energies for binding mode analysis of peptoid sequence ***a*** with uranyl. Corrections are made for standard concentrations of solutes (1 M) and water (55.34 M.)[26]

Gaussian09 B3LYP/6-31+G(d) SSD ECPsc60 IE

	Gaq [kcal/mol]	G [kcal/mol]	H [kcal/mol]	Eele [kcal/mol]	E [Hartree]	Eaq [Hartree]	Solvation [Hartree]	Gcorr [Hartree]	Hcorr [Hartree]	zpve [Hartree]	S [cal/molK]	E_corr [Hartree]
pep2												
conf I	**0.00**	0.00	0.00	0.00	-2188.441987	-2188.44993	-0.09417	-2187.8924	-2187.7666	0.632292	264.872	0.674464
conf II	**-4.23**	-5.16	-6.53	-5.84	-2188.451301	-2188.45907	-0.09269	-2187.9006	-2187.777	0.6312	260.26	0.67337
conf III	**-14.30**	-6.50	2.53	2.33	-2188.43828	-2188.45065	-0.10659	-2187.9028	-2187.7626	0.629981	295.156	0.674781

label	Gaq [kcal/mol]	G [kcal/mol]	H [kcal/mol]	Eele [kcal/mol]	E [Hartree]	Eaq [Hartree]	Solvation [Hartree]	Gcorr [Hartree]	Hcorr [Hartree]	zpve [Hartree]	S [cal/ mol K]	E_corr [Hartree]
H(+)					0		-0.4210295	-0.01	0.0023	0	26.14	0.001416
UO2_5W (++)					-1009.30892	-1009.53408	-0.2251646	-1009.2219	-1009.1636	0.128655	122.745	0.144403
pep (0)					-1313.47825	-1313.17098	0.3072755	-1313.1525	-1313.0569	0.392541	201.11	0.420374
H2O (0)					-76.42257	-76.43124	-0.0086644	-76.419793	-76.397698	0.021096	46.502	0.023931
relative stability												
pep1s_OU2_3W (+)	**0.00**	0.00	0.00	0.00	-2169.650627	-2169.76844	-0.1178153	-2169.2778	-2169.1481	0.460138	273.068	0.501582
pep2s_OU2_3W (+)	**2.81**	-0.92	-2.38	-2.38	-2169.654428	-2169.7663	-0.1118733	-2169.2793	-2169.1519	0.460365	268.163	0.501587
pep3s_OU2_3W (+)	**1.20**	-3.02	-2.95	-3.46	-2169.65614	-2169.76723	-0.1110951	-2169.2827	-2169.1528	0.461027	273.307	0.502394
pep13s_OU2_2W	**0.00**	0.00	0.00	0.00	-2092.871546	-2092.90824	-0.036697	-2092.514	-2092.4077	0.427506	223.775	0.4629
pep23s_OU2_2W	**3.90**	8.63	9.60	9.96	-2092.855673	-2092.89991	-0.044237	-2092.5003	-2092.3924	0.426751	227.034	0.46233
pep12s_OU2_2W	**11.33**	13.95	15.03	15.14	-2092.847411	-2092.88828	-0.040866	-2092.4918	-2092.3837	0.427325	227.414	0.46272
pep123s_UO2 (-)	**0.00**	0.00	0.00	0.00	-1939.479574	-1939.56872	-0.089146	-1939.1734	-1939.0848	0.365273	186.413	0.393809
pep123s_UO2_Hb (-)	**1.37**	1.56	0.90	0.50	-1939.478771	-1939.56822	-0.0894475	-1939.1709	-1939.0834	0.366078	184.19	0.394434

pep_s(0) + UO2_5W(2+) ---> pepN_s--UO2--nW(2-N) + N*H(+) + (5-n)W (N,n)=(1,2),(2,3),(3,5)

relative binding	Gaq	G	Gsolv	S	-TS		correction per molecule	correction per W	correction total (no H+)		**relative Gaq final**
pep1s_OU2_3W (+)	**-245.57**	154.96	-400.53	68.36	-20.37	(ref. **4**)	1	2	6.65	-238.92	**4.86**
pep2s_OU2_3W (+)	**-242.76**	154.05	-396.80	63.45	-18.91	correction per molecule	1	2	6.65	-236.11	**7.67**
pep3s_OU2_3W (+)	**-244.37**	151.94	-396.31	68.60	-20.44	1.89 kcal/mol	1	2	6.65	-237.72	**6.06**
pep13s_OU2_2W	**-254.69**	364.57	-619.26	19.06	-5.68	correction per W	2	3	10.92	-243.77	**0.00**
pep23s_OU2_2W	**-250.79**	373.20	-624.00	22.32	-6.65	2.38 kcal/mol	2	3	10.92	-239.87	**3.90**
pep12s_OU2_2W	**-243.36**	378.52	-621.88	22.70	-6.77		2	3	10.92	-232.44	**11.33**
pep123s_UO2 (-)	**-254.54**	672.71	-927.25	-18.30	5.45		4	5	19.46	-235.08	**8.69**
pep123s_UO2_Hb (-)	**-253.17**	674.27	-927.44	-20.52	6.12		4	5	19.46	-233.71	**10.06**

Two opposing effects of binding multiple carboxylate groups can be observed in the relative binding energies of the different coordination modes. Binding multiple carboxylate groups increases the enthalpy of binding, while there is a corresponding decrease in the entropy of the system due to the chelation of the peptoid around the metal. This trend can be observed in Table 2, where ***a1***, ***a2*** and ***a3*** (binding through carboxylate group 1, 2, or 3, respectively) are less stable than ***a13*** due to the enthalpy of binding, while ***a123*** (binding through all three carboxylates) is less stable than ***a13*** due to the loss of entropy. This trend is the same if uranyl is not explicitly solvated with five water molecules. The situation with two groups binding uranyl is quite different; the changes in the strain of the peptoid backbone favor certain binding modes. Peptoid ***a12*** is one of the least preferred binding modes, while ***a13*** represents one of the best. Although ***a13*** is the most stable complex, we are not categorically declaring any conformation to be the single preferred motif of binding between peptoid ***a*** and uranyl because the energies are quite close and margins of error from our methods do not give us confidence to definitively favor one over the other Images of the three dimensional complexes of this binding mode as well as ***a123*** and ***a123h*** are shown in Figure 7.

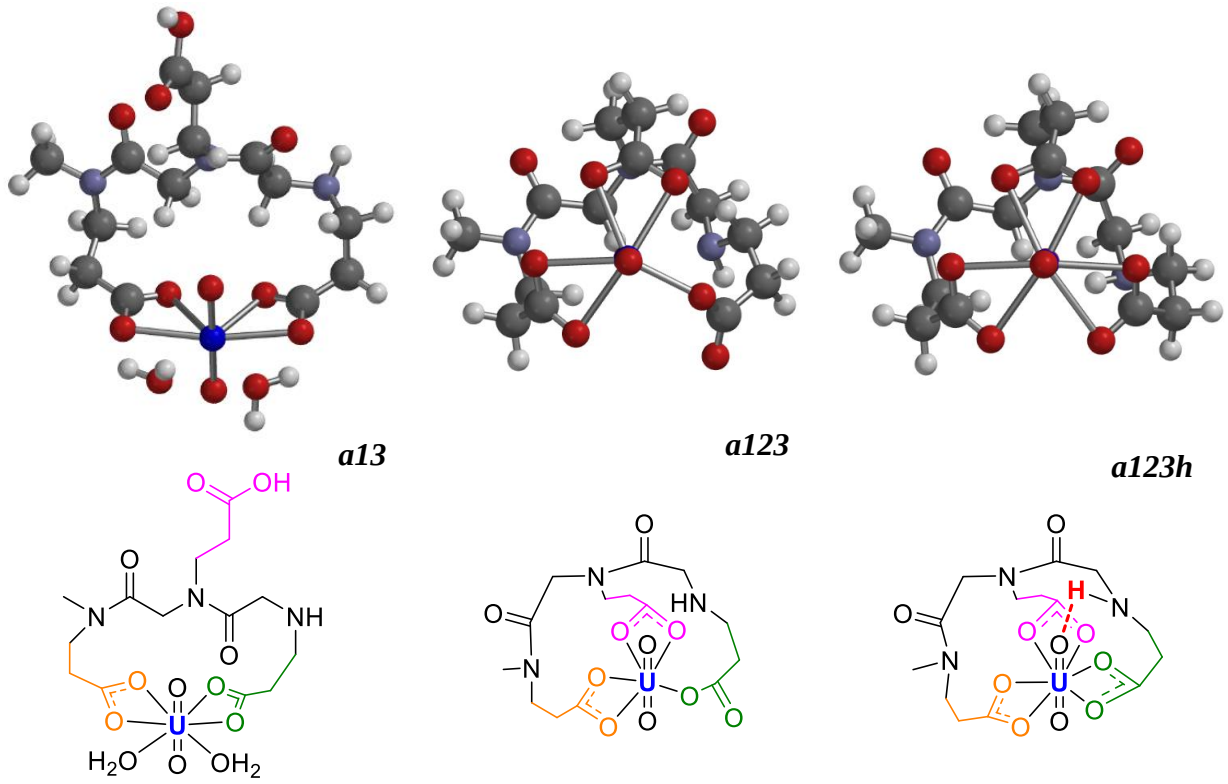

Figure 7. Selected optimized structures and schematics of peptoid sequence ***a*** with uranyl. Colors are used to distinguish the different carboxylate residues (orange: carboxylate 1, pink: carboxylate 2, green: carboxylate 3). Relative energies are reported in Tables 1 and 2 and full coordinates can be found at the end of this chapter.

Another aspect of the uranyl ion's unique geometry is the possible Lewis basicity of the uranyl oxo groups, which has been explored for possible selective recognition through hydrogen bonds in molecular ligands;[35–37] these generally involve tethering a hydrogen bond donor to the functional groups that bind uranyl in its equatorial plane, with the goal being that complexes formed with uranyl are stabilized relative to other metals due to this interaction as well as other possible geometrical constraints of the ligand. For this reason, the binding mode where all three carboxylate residues coordinate to uranyl has been explored with a hydrogen bonding interaction with the terminal N-H atom of the peptoid interacting with one of the uranyl oxo groups (Figure 7, ***a123h***). This does not take into account the strength of the hydrogen bond, but rather geometric constraints that may favor or disfavor it. In situations where the terminal N-H proton is distant from the oxo group, both groups are expected to form hydrogen bonds with water molecules (which were not modeled explicitly). Based on the small difference in energy between structures ***a123*** and ***a123h*** (Figure 7), this hydrogen bond may form but is not expected to be a driving factor in binding and is unlikely to contribute towards selectivity over other metals. This small difference in energy also demonstrates the multiple potential binding modes of the carboxylate residues, either monodentate or bidentate. The peptoid backbone conformation and sterics influences the favored carboxylate binding mode as well as overall uranyl coordination number, analogous to effects seen in polymer adsorbents.[38] Since this hydrogen bond is not anticipated to be significant for binding and selectivity, future libraries may incorporate other moieties at this position, such as an additional residue or a fluorophore, to improve binding or assist with spectroscopy, respectively.

Summary and conclusions

In this work, techniques were adapted and established for the screening of combinatorial peptoid libraries to discover new ligands for uranyl binding for purposes of extraction from seawater. A dye-based screening process with arsenazo III was used to visualize resin beads that displayed uranyl-binding peptoid sequences, from which three unique sequences were identified. Fluorescence spectroscopy was used to estimate the affinity of one of the sequences, which was found to be approximately 700 ± 200 μM, indicating relatively weak binding that will be improved upon in future library generations. DFT was used to model peptoid binding to help elucidate the solution-state configuration of the peptoid. This information that the large size of uranyl favors multidentate ligands such as carboxylates and that the peptoid backbone folding may constrain binding is being used to guide future library design.

The combinatorial and modular nature of the peptoid synthesis and screening lends itself well to straightforward testing of future libraries, using the same screening techniques but with new library designs designs and members. The shortfalls of the initial library may be addressed with a new selection of submonomers, including groups that are expected to have a higher affinity for uranyl such as phosphonates and amidoximes.[39] Other submonomers and linkers in the peptoid backbone can also be considered to tune the secondary structure. Some other improvements are also possible for binding; since the terminal N-H group is not likely to be important to binding, this is a suitable attachment point for a fluorophore to quantify binding. For computations, molecular modeling techniques are being explored in addition to DFT, due to the greater processing speed to allow for rapid modeling of peptoids and uranyl binding.

References

(1) Tian, G.; Teat, S. J.; Zhang, Z.; Rao, L. *Dalton Trans.* **2012**, *41*, 11579–11586.
(2) Vukovic, S.; Hay, B. P. *Inorg. Chem.* **2013**, *0*, 7805–7810.
(3) Kim, J.; Tsouris, C.; Mayes, R. T.; Oyola, Y.; Saito, T.; Janke, C. J.; Dai, S.; Schneider, E.; Sachde, D. *Sep. Sci. Technol.* **2013**, *48*, 367–387.
(4) Kang, S. O.; Vukovic, S.; Custelcean, R.; Hay, B. P. *Ind. Eng. Chem. Res.* **2012**, *51*, 6619–6624.
(5) Francis, M. B.; Finney, N. S.; Jacobsen, E. N. *J. Am. Chem. Soc.* **1996**, *118*, 8983–8984.
(6) Nitz, M.; Franz, K. J.; Maglathlin, R. L.; Imperiali, B. *ChemBioChem* **2003**, *4*, 272–276.
(7) Nalband, D. M.; Warner, B. P.; Zahler, N. H.; Kirshenbaum, K. *Biopolymers* **2014**, *102*, 407–415.
(8) Zhou, L.; Bosscher, M.; Zhang, C.; Ozçubukçu, S.; Zhang, L.; Zhang, W.; Li, C. J.; Liu, J.; Jensen, M. P.; Lai, L.; He, C. *Nat. Chem.* **2014**, *6*, 236–241.
(9) Simon, R. J.; Kania, R. S.; Zuckermann, R. N.; Huebner, V. D.; Jewell, D. a; Banville, S.; Ng, S.; Wang, L.; Rosenberg, S.; Marlowe, C. K. *Proc. Natl. Acad. Sci.* **1992**, *89*, 9367–9371.
(10) Maayan, G.; Ward, M. D.; Kirshenbaum, K. *Chem. Commun.* **2009**, 56–58.
(11) Knight, A. S.; Zhou, E. Y.; Francis, M. B.; Zuckermann, R. N. *Adv. Mater.* **2015**, n/a-n/a.
(12) Izzo, I.; Ianniello, G.; De Cola, C.; Nardone, B.; Erra, L.; Vaughan, G.; Tedesco, C.; De Riccardis, F. *Org. Lett.* **2013**, *15*, 598–601.
(13) Knight, A. S.; Zhou, E. Y.; Pelton, J. G.; Francis, M. B. *J. Am. Chem. Soc.* **2013**, *135*, 17488–17493.
(14) Knight, A. S.; Zhou, E. Y.; Francis, M. B. *Chem. Sci.* **2015**, 4042–4048.
(15) Butterfoss, G. L.; Renfrew, P. D.; Kuhlman, B.; Kirshenbaum, K.; Bonneau, R. *J. Am. Chem. Soc.* **2009**, *131*, 16798–16807.
(16) Maltese, M. *J. Org. Chem.* **2001**, *66*, 7615–7625.
(17) Zuckermann, R. N.; Kerr, J. M.; Kent, S. B. H.; Moos, W. H. *J. Am. Chem. Soc.* **1992**, *114*, 10646–10647.
(18) Vukovic, S.; Watson, L. a; Kang, S. O.; Custelcean, R.; Hay, B. P. *Inorg. Chem.* **2012**, *51*, 3855–3859.
(19) Frisch, M. J. et. al. Gaussian 09, revision A.2; Gaussian, Inc.: Wallingford, CT, 1997.
(20) Becke, A. D. *J. Chem. Phys.* **1993**, *98*, 5648.
(21) Lee, C.; Yang, W.; Parr, R. G. *Phys. Rev. B* **1988**, *37*, 785–789.
(22) Dolg, M.; Stoll, H.; Preuss, H.; Pitzer, R. M. *J. Phys. Chem.* **1993**, *97*, 5852–5859.
(23) Miertuš, S.; Scrocco, E.; Tomasi, J. *Chem. Phys.* **1981**, *55*, 117–129.
(24) Cancès, E.; Mennucci, B.; Tomasi, J. *J. Chem. Phys.* **1997**, *107*, 3032.
(25) Mennucci, B.; Cancès, E.; Tomasi, J. *J. Phys. Chem. B* **1997**, *101*, 10506–10517.
(26) Kremleva, A.; Krüger, S.; Rösch, N. *Inorganica Chim. Acta* **2009**, *362*, 2542–2550.
(27) Burkoth, T. S.; Fafarman, A. T.; Charych, D. H.; Connolly, M. D.; Zuckermann, R. N. *J. Am. Chem. Soc.* **2003**, *125*, 8841–8845.

(28) Savvin, S. *Talanta* **1961**, *8*, 673–685.
(29) Alimarin, I. P.; Sawin, S. B. *Pure Appl. Chem.* **1966**, *13*.
(30) Denning, R. G. *J. Phys. Chem. A* **2007**, *111*, 4125–4143.
(31) Bernhard, G.; Geipel, G.; Brendler, V.; Nitsche, H. *J. Alloys Compd.* **1998**, *271–273*, 201–205.
(32) Matsushima, R.; Sakuraba, S. *J. Am. Chem. Soc.* **1971**, *93*, 7143–7145.
(33) Thordarson, P. *Chem. Soc. Rev.* **2011**, *40*, 1305–1323.
(34) Vukovic, S.; Hay, B. P.; Bryantsev, V. S. *Inorg. Chem.* **2015**, *54*, 3995–4001.
(35) Sather, A. C.; Berryman, O. B.; Rebek, J. *J. Am. Chem. Soc.* **2010**, *132*, 13572–13574.
(36) Franczyk, T. S.; Czerwinski, K. R.; Raymond, K. N. *J. Am. Chem. Soc.* **1992**, *114*, 8138–8146.
(37) Watson, L. a; Hay, B. P. *Inorg. Chem.* **2011**, *50*, 2599–2605.
(38) Abney, C. W.; Mayes, R. T.; Piechowicz, M.; Lin, Z.; Bryantsev, V. S.; Veith, G. M.; Dai, S.; Lin, W. *Energy Environ. Sci.* **2016**, *9*, 448–453.
(39) Culf, A. S.; Ouellette, R. J. *Molecules* **2010**, *15*, 5282–5335.

Coordinates and 3D images for all optimized structures

a1

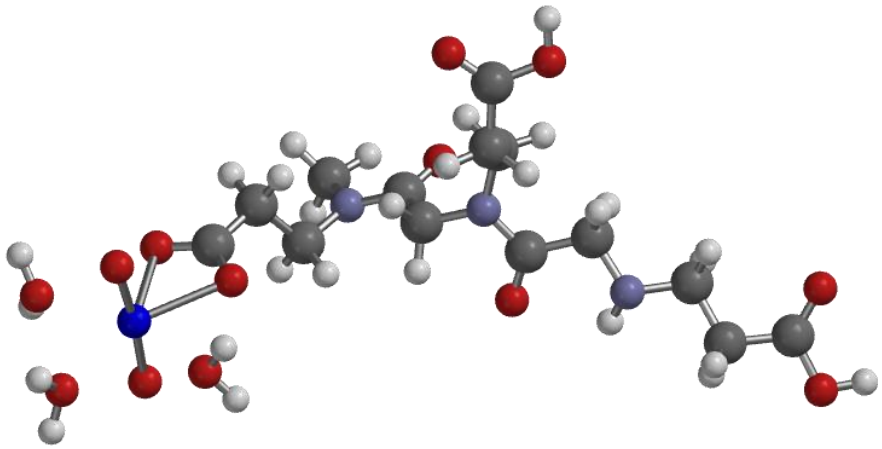

C	-1.18823	-1.61654	-1.76942	H	4.126476	-2.89717	-2.07748
O	-1.03178	-1.42389	-2.96799	C	5.509544	-1.83621	-3.19858
N	-2.33392	-2.19556	-1.261	H	5.848351	-0.79497	-3.24585
C	-0.09726	-1.20103	-0.75587	H	5.155828	-2.09468	-4.21347
H	0.215932	-2.06289	-0.16209	C	6.687497	-2.73194	-2.81791
H	-0.49303	-0.43726	-0.07354	H	7.033875	-2.48694	-1.80508
C	-2.57288	-2.42157	0.151991	H	6.395462	-3.7898	-2.78892
H	-3.07293	-3.39181	0.263007	C	7.859376	-2.58701	-3.7626
C	-3.39607	-2.59531	-2.18591	O	8.812517	-3.52216	-3.5216
H	-3.03146	-2.47026	-3.20471	O	7.976325	-1.74573	-4.62919
H	-4.29419	-1.97842	-2.05486	C	-3.45876	-1.31466	0.800335
H	-3.6588	-3.64661	-2.0187	H	-4.44078	-1.26987	0.323615
C	2.107472	-1.57286	-1.65604	H	-2.96379	-0.34424	0.677044
O	2.052634	-2.73662	-1.25772	C	-3.64245	-1.55761	2.268148
N	1.082716	-0.68605	-1.41975	O	-4.78411	-1.84405	2.775413
C	3.314754	-1.08296	-2.45508	O	-2.64454	-1.51017	3.07573
H	3.009167	-1.07787	-3.52265	O	-3.66128	-3.76469	4.837367
H	3.574818	-0.04851	-2.20131	U	-3.94479	-2.0278	4.990917
C	1.025336	0.680582	-1.93652	O	-4.25658	-0.3283	5.356377
H	-0.00527	0.875394	-2.24708	O	-1.57246	-1.74055	5.78765
H	1.632863	0.766082	-2.8382	H	-1.15078	-0.86375	5.749472
C	1.473172	1.720461	-0.87958	O	-4.23491	-2.45054	7.470581
H	0.938941	1.5537	0.059686	H	-4.16844	-3.31025	7.921201
H	2.5476	1.619741	-0.69351	H	-4.4361	-1.78244	8.148642
C	1.156415	3.129155	-1.33149	O	-6.42337	-2.46294	5.100126
O	0.212453	3.789529	-0.9495	H	-7.04298	-1.73818	4.902605
O	2.036968	3.569959	-2.26116	H	-6.79131	-3.25902	4.677156
H	-1.62842	-2.48619	0.692569	H	-0.88996	-2.38431	5.527205
N	4.455111	-1.93957	-2.19408	H	1.762201	4.466733	-2.53445

2

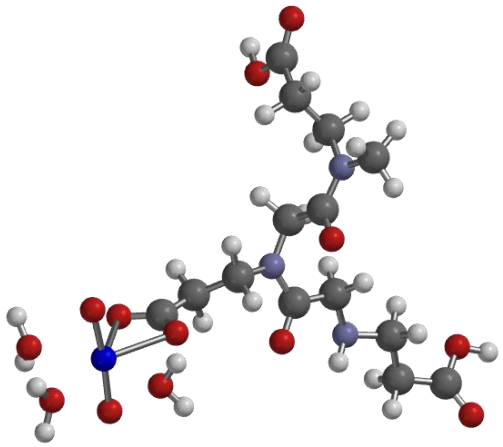

C	-0.92333	-3.16668	-4.60865	H	2.771304	-6.4019	-7.12199
O	-0.92479	-2.72634	-5.75648	H	3.310886	-6.90929	-5.51442
N	-1.99067	-3.83499	-4.07729	C	4.925191	-6.64237	-6.92709
C	0.333888	-2.98483	-3.71815	H	5.21607	-5.96922	-7.73903
H	0.701683	-3.95515	-3.37747	H	5.675317	-6.55998	-6.13087
H	0.079809	-2.42183	-2.81246	C	4.958043	-8.04837	-7.48398
C	-2.09112	-4.25173	-2.68055	O	4.593918	-8.97303	-6.55537
H	-2.5579	-5.24345	-2.65629	O	5.271593	-8.35495	-8.61424
C	-3.17988	-3.99906	-4.92014	C	-2.92304	-3.2702	-1.82008
H	-2.87019	-4.15203	-5.95461	H	-3.94491	-3.19407	-2.19839
H	-3.82948	-3.11559	-4.88415	H	-2.46209	-2.27555	-1.85695
H	-3.74197	-4.8698	-4.57183	C	-3.00092	-3.71958	-0.37578
C	2.303991	-2.90425	-5.24154	O	-3.99882	-4.09465	0.196302
O	3.053906	-2.23946	-5.95731	O	-1.78057	-3.67176	0.225187
N	1.394324	-2.27981	-4.41656	O	1.208118	4.553465	-4.51251
C	2.358951	-4.43102	-5.26036	U	2.750193	4.01644	-5.1896
H	2.292304	-4.84187	-4.24413	O	4.321026	3.701621	-5.93365
H	1.454236	-4.77606	-5.80252	O	3.94231	5.001897	-3.19869
C	1.246162	-0.83339	-4.6066	H	4.839518	4.685245	-2.99126
H	0.295598	-0.52819	-4.16124	O	3.033907	6.399348	-6.00312
H	1.197978	-0.61721	-5.67572	H	2.404355	7.131116	-5.88294
C	2.413576	-0.05567	-3.969	H	3.778439	6.739733	-6.52874
H	2.421248	-0.12113	-2.87615	O	1.704719	3.842023	-7.47935
H	3.353384	-0.49717	-4.3303	H	2.135248	3.242472	-8.11529
C	2.463738	1.386834	-4.36375	H	0.750812	3.656845	-7.54258
O	3.015108	2.272584	-3.61314	H	3.473203	5.06642	-2.34805
O	2.002771	1.80182	-5.48827	H	-1.89297	-3.98404	1.143995
H	-1.09524	-4.36228	-2.25086	H	4.652199	-9.84898	-6.98294
N	3.597785	-4.87407	-5.86869				
C	3.554787	-6.24942	-6.35473				

a3

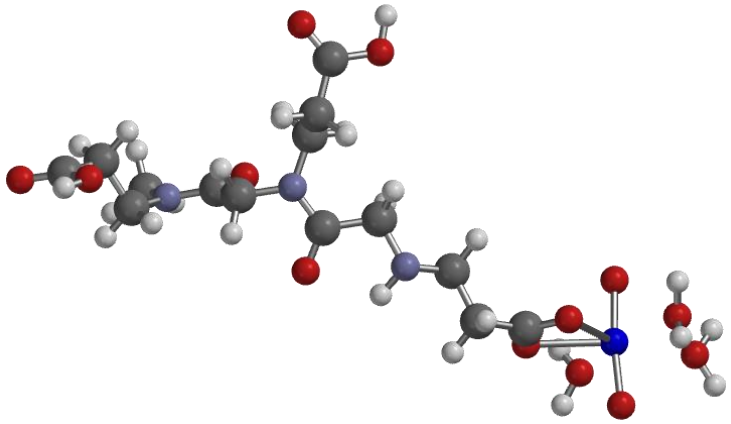

C	4.951096	4.896685	-7.82328	C	10.76444	5.81189	-10.9275
O	5.515047	3.861822	-8.17501	H	10.63715	5.619975	-12.0007
N	4.171252	4.958586	-6.70181	H	10.9251	4.832764	-10.437
C	5.115542	6.192622	-8.65374	C	12.01277	6.704976	-10.7181
H	5.53065	6.990699	-8.03477	H	11.88752	7.638041	-11.2729
H	4.14531	6.528739	-9.03692	H	12.11536	6.932027	-9.65038
C	3.384531	6.123441	-6.30892	C	13.26211	6.018927	-11.1693
H	3.459545	6.232528	-5.22053	O	13.80186	6.263947	-12.3093
C	3.993713	3.728888	-5.92493	O	13.84236	5.128964	-10.4447
H	4.919589	3.152772	-5.94669	C	1.892293	6.00592	-6.70995
H	3.190463	3.102057	-6.33246	H	1.437324	5.134801	-6.23259
H	3.749658	3.995141	-4.89268	H	1.812944	5.895849	-7.79715
C	7.348007	6.201232	-9.56023	C	1.118132	7.229279	-6.2693
O	7.774991	6.670721	-8.5037	O	0.38974	7.295245	-5.30386
N	6.01705	5.978885	-9.77387	O	1.365605	8.294329	-7.07781
C	8.334623	5.828509	-10.6757	O	14.68375	3.408054	-12.7948
H	8.439479	4.726193	-10.6505	U	15.56421	4.720261	-12.0034
H	7.946105	6.092016	-11.6662	O	16.63737	5.926298	-11.2847
C	5.473771	5.307393	-10.9542	O	15.90915	5.814027	-14.2501
H	4.697191	4.614935	-10.6168	H	16.12264	6.763757	-14.2754
H	6.24326	4.692537	-11.4234	O	17.676	3.540184	-12.759
C	4.887663	6.310197	-11.9775	H	17.7234	2.709423	-13.2629
H	4.126459	6.932712	-11.5002	H	18.58908	3.83158	-12.5924
H	5.684336	6.95835	-12.3571	O	15.97546	3.217486	-10.0192
C	4.227408	5.579298	-13.1257	H	16.19372	3.629114	-9.16412
O	3.04049	5.361413	-13.2327	H	15.32854	2.51636	-9.82391
O	5.138402	5.139477	-14.0348	H	15.24603	5.667287	-14.9479
H	3.813266	7.025311	-6.74696	H	0.855749	9.051523	-6.73027
N	9.595675	6.51671	-10.4374				
H	9.656202	6.707208	-9.43585				

a12

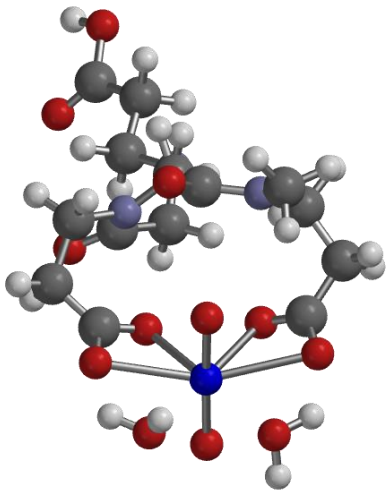

C	-0.75142	3.480891	0.733919	N	-3.44121	0.347134	-1.91093
O	-1.8516	3.929161	1.043097	H	-4.29817	0.85788	-1.71141
N	0.280138	4.2941	0.325887	C	-3.75062	-1.09183	-1.83808
C	-0.46431	1.962624	0.80974	H	-3.96946	-1.42919	-0.81728
H	0.384547	1.788043	1.478552	H	-4.66051	-1.22301	-2.43402
H	-0.14063	1.589584	-0.1637	C	-2.6608	-1.9933	-2.44874
C	1.56232	3.800128	-0.17101	H	-2.20301	-1.53007	-3.33083
H	2.344084	4.49546	0.152231	H	-3.12071	-2.92985	-2.79618
C	0.018688	5.732918	0.23666	C	-1.5687	-2.39776	-1.48422
H	0.950638	6.276451	0.41785	O	-0.44219	-2.85639	-1.87994
H	-0.72176	6.005361	0.989616	O	-1.74751	-2.26083	-0.23267
H	-0.37628	6.015144	-0.74747	C	1.643055	3.614631	-1.70556
C	-2.64133	0.826945	0.457065	H	2.577237	3.080652	-1.92678
O	-3.72287	0.447973	0.892111	H	0.813224	3.00496	-2.07159
N	-1.59335	1.191501	1.287953	O	0.432656	-4.07082	1.043821
C	-2.38192	0.880425	-1.06745	U	0.532372	-2.405	0.434225
H	-2.23305	1.928539	-1.35962	O	0.797626	-0.78858	-0.25353
H	-1.44499	0.360677	-1.29533	C	1.660535	4.89478	-2.51283
C	-1.77659	1.059609	2.737137	O	0.909799	5.170459	-3.42346
H	-2.66861	0.448212	2.869478	O	2.660799	5.729706	-2.11786
H	-1.97117	2.041637	3.188497	H	2.623963	6.516222	-2.69497
C	-0.57277	0.40248	3.457164	H	2.834144	-1.92	2.073413
H	0.267645	1.089435	3.59946	O	2.981959	-2.54619	1.334638
H	-0.90856	0.108078	4.460752	H	3.204945	-3.39653	1.746457
C	-0.06464	-0.83193	2.738807	H	2.454297	-4.22251	-1.33682
O	-0.89717	-1.62946	2.207552	O	2.103383	-3.32215	-1.42244
O	1.183795	-1.03927	2.567583	H	1.437165	-3.34891	-2.13905
H	1.785534	2.838735	0.29425				

a13

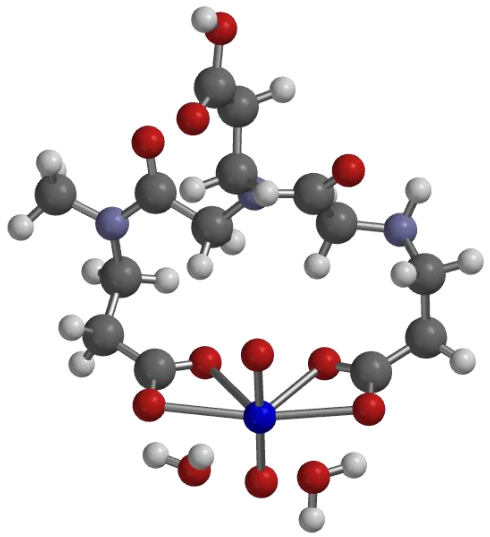

C	-1.51273	-3.30237	0.987562	H	5.158556	-0.14503	0.848964
O	-1.38655	-4.47625	0.646917	H	3.678406	-0.23213	-0.09537
N	-2.68645	-2.83427	1.536302	C	3.719323	1.324154	1.449726
C	-0.40946	-2.25937	0.726664	H	4.443131	2.035895	1.040224
H	-0.1137	-1.79788	1.667703	H	3.795403	1.321647	2.542001
H	-0.83952	-1.45592	0.114775	C	2.345765	1.796344	1.047148
C	-2.83797	-1.5863	2.293687	O	1.303826	1.37991	1.648711
H	-3.46493	-1.82462	3.15963	O	2.179557	2.58148	0.047807
C	-3.80447	-3.77312	1.639763	C	-3.47351	-0.40817	1.513794
H	-3.81314	-4.27905	2.615491	H	-4.07013	-0.75702	0.665056
H	-3.71734	-4.52884	0.859615	H	-4.15898	0.142402	2.173294
H	-4.74541	-3.22619	1.517548	C	-2.46046	0.610657	1.024846
C	2.049751	-2.47417	0.417835	O	-1.35416	0.735962	1.636829
O	3.007634	-2.82731	-0.27521	O	-2.69317	1.348346	0.012124
N	0.764876	-2.79953	0.057021	O	-0.666	3.649536	0.92899
C	2.308727	-1.67499	1.718052	U	-0.28428	2.183953	0.008456
H	1.636613	-0.82068	1.809336	O	0.069611	0.774565	-1.01128
H	2.101695	-2.33381	2.573672	C	0.666793	-5.42646	-2.7358
C	0.582617	-3.36925	-1.2923	O	0.089662	-4.86548	-3.64764
H	1.187146	-2.78871	-1.99613	O	1.113874	-6.70536	-2.85247
H	-0.46565	-3.24579	-1.5681	H	0.870006	-7.00932	-3.74737
C	0.967401	-4.84869	-1.37702	H	0.474845	4.688854	-1.72035
H	2.032854	-4.98193	-1.16461	O	0.743128	3.759551	-1.80881
H	0.407751	-5.42174	-0.62977	H	1.68025	3.709228	-1.53539
H	-1.87468	-1.26398	2.692566	H	-1.57764	2.696181	-2.79165
N	3.678489	-1.19089	1.832667	O	-1.86854	2.971161	-1.90665
H	4.303319	-1.97389	1.654541	H	-2.6687	2.453516	-1.69384
C	4.067564	-0.10163	0.926765				

a23

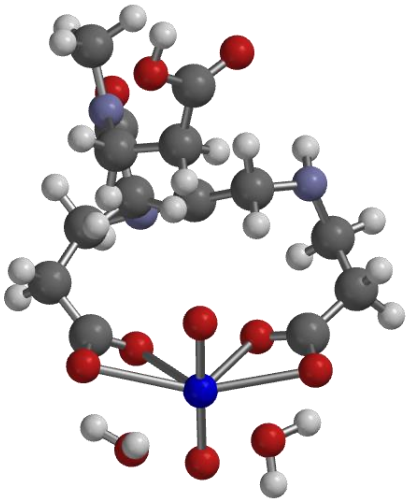

C	2.3208	-0.47976	-0.86774	N	0.187582	-4.44695	0.990428
O	2.449178	0.008713	-1.99195	H	1.107497	-4.3958	0.554813
N	2.993045	0.052055	0.208852	C	-0.55266	-5.59568	0.454211
C	1.574946	-1.82522	-0.72739	H	-1.53018	-5.62633	0.945431
H	1.615362	-2.19938	0.289648	H	-0.75192	-5.52696	-0.62662
H	2.185489	-2.50875	-1.34092	C	0.22014	-6.87899	0.763721
C	2.82595	-0.28586	1.626559	H	0.43359	-6.93286	1.840247
H	2.004537	-0.99082	1.736259	H	1.196298	-6.89448	0.261532
C	3.967678	1.108067	-0.08678	C	2.532192	0.932238	2.534806
H	3.516401	2.104361	-0.02635	H	2.415441	0.556607	3.560523
H	4.345576	0.969386	-1.1	H	3.356996	1.649378	2.548273
H	4.794034	1.036402	0.628914	C	1.254216	1.645708	2.136618
C	-0.76549	-2.6463	-0.53502	O	1.164623	2.915524	2.123607
O	-1.82949	-2.9325	-1.09053	O	0.283467	0.944182	1.717156
N	0.180371	-1.88269	-1.1821	O	-2.08888	2.883058	1.14419
C	-0.50556	-3.15645	0.893032	U	-0.59358	2.650435	0.218778
H	0.026924	-2.41761	1.500414	O	0.909726	2.602211	-0.71709
H	-1.49713	-3.27708	1.337356	C	-0.53044	-8.1337	0.380493
C	-0.16965	-1.4054	-2.53397	O	-1.71259	-8.21305	0.12169
H	-0.38983	-2.27211	-3.1701	O	0.285354	-9.22269	0.377813
H	0.706463	-0.8912	-2.92588	H	-0.27034	-9.99411	0.155442
C	-1.40799	-0.46829	-2.61663	H	-0.6975	5.531255	1.427388
H	-1.47879	-0.07942	-3.63715	O	0.030939	5.064468	0.986073
H	-2.30509	-1.06075	-2.4069	H	0.670918	4.817392	1.683094
C	-1.40465	0.684704	-1.6484	H	-0.61017	5.027505	-1.78852
O	-1.177	0.45331	-0.41512	O	-1.34423	4.489431	-1.44978
O	-1.59615	1.898197	-1.99957	H	-1.62293	3.901726	-2.18042
H	3.744053	-0.76884	1.99275				

a123

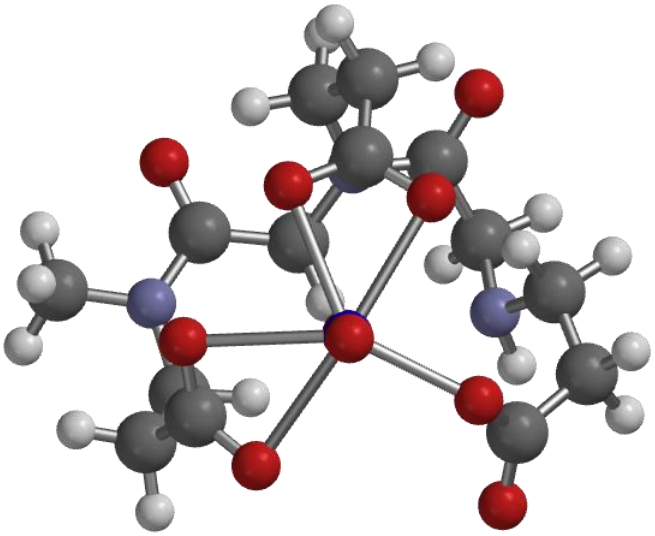

C	-1.68159	-1.61463	-1.92928	C	0.98725	1.58471	-0.79159
O	-1.7446	-1.43689	-3.15198	O	1.69945	1.56606	0.26768
N	-2.80852	-1.51371	-1.14517	O	-0.23899	1.91174	-0.71712
C	-0.34869	-2.06246	-1.31317	H	-1.99153	-2.04773	0.72121
H	-0.26312	-3.10866	-1.64223	N	1.98821	-2.48645	0.87475
H	-0.34389	-2.0452	-0.22873	H	1.97902	-3.27513	1.51859
C	-2.96675	-1.8889	0.26677	C	2.91728	-1.45174	1.35095
H	-3.51092	-2.84686	0.29656	H	2.68462	-0.5119	0.84322
C	-4.05682	-1.1911	-1.83737	H	3.96392	-1.70662	1.09196
H	-3.9233	-1.35537	-2.906	C	2.85776	-1.2463	2.8741
H	-4.33045	-0.14282	-1.67044	H	3.15551	-2.16993	3.38659
H	-4.86157	-1.83571	-1.46138	H	3.59532	-0.47168	3.12076
C	2.09686	-1.85935	-1.54598	C	1.50278	-0.8202	3.46019
O	3.10402	-1.44427	-2.13211	O	0.86317	-1.59497	4.16627
N	0.85526	-1.33173	-1.79014	O	1.13158	0.41779	3.19423
C	2.26563	-2.96218	-0.48033	C	-3.77128	-0.88553	1.14545
H	1.59751	-3.80841	-0.68511	H	-4.06458	-1.42027	2.05442
H	3.30397	-3.31078	-0.61701	H	-4.67961	-0.56468	0.62594
C	0.81288	-0.1359	-2.66165	C	-2.9417	0.32654	1.54127
H	-0.22688	0.1203	-2.83231	O	-2.40043	0.36179	2.69642
H	1.25907	-0.39526	-3.62868	O	-2.66517	1.20395	0.67156
C	1.55913	1.10296	-2.10942	O	-0.28862	-0.39016	1.02701
H	2.62522	0.90335	-1.99892	U	-0.31503	1.25946	1.67928
H	1.424	1.89855	-2.85489	O	-0.3623	2.90789	2.35961

a123h

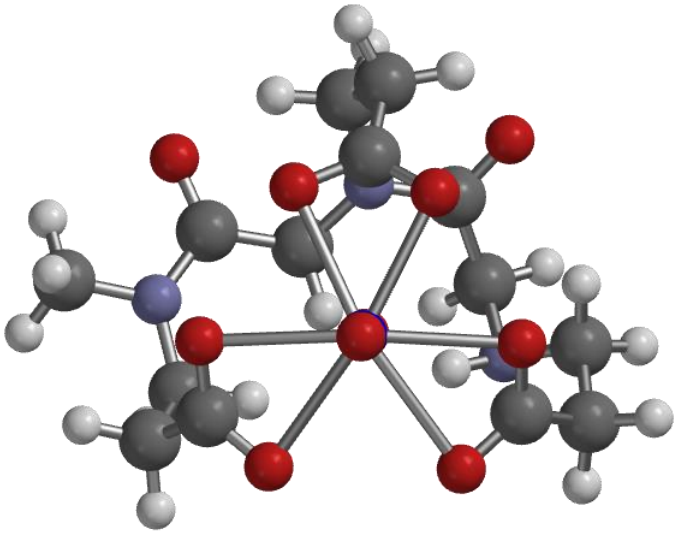

C	-1.74091	-1.49408	-1.99762	C	0.7442	1.66292	-0.93957
O	-1.86046	-1.1747	-3.18647	O	1.48675	1.88232	0.07254
N	-2.83147	-1.48466	-1.15905	O	-0.51641	1.73121	-0.81168
C	-0.39332	-2.04937	-1.50622	H	-1.94455	-2.22376	0.60258
H	-0.32345	-3.02356	-2.01631	N	1.99546	-2.54639	1.07782
H	-0.41295	-2.2311	-0.43825	H	1.12888	-2.03221	1.22387
C	-2.93589	-2.01424	0.20629	C	3.10648	-1.76636	1.64871
H	-3.48287	-2.96992	0.15473	H	3.35539	-0.87101	1.06106
C	-4.10146	-1.05849	-1.74921	H	3.99511	-2.41339	1.65828
H	-4.02115	-1.10322	-2.83456	C	2.79042	-1.32486	3.09697
H	-4.33627	-0.02999	-1.45198	H	2.43011	-2.17168	3.68999
H	-4.9041	-1.72534	-1.40958	H	3.71832	-0.94576	3.5442
C	2.04935	-1.72456	-1.36933	C	1.76051	-0.19775	3.12281
O	3.1032	-1.22289	-1.77773	O	0.61319	-0.34485	3.63325
N	0.82723	-1.25763	-1.80462	O	2.03995	0.87265	2.48305
C	2.12528	-2.88708	-0.34458	C	-3.68683	-1.10874	1.22224
H	1.38499	-3.66336	-0.57218	H	-3.91556	-1.72594	2.09711
H	3.11569	-3.32723	-0.49996	H	-4.62906	-0.75044	0.79607
C	0.85107	-0.13795	-2.77394	C	-2.82773	0.06605	1.66095
H	-0.15936	-0.01019	-3.14508	O	-2.19535	0.00471	2.76052
H	1.48993	-0.43098	-3.6171	O	-2.62611	1.01893	0.84814
C	1.38793	1.20999	-2.23828	O	-0.07667	-0.45858	0.91447
H	2.46705	1.16492	-2.08742	U	-0.24372	1.16027	1.65555
H	1.17231	1.95789	-3.01483	O	-0.46697	2.74976	2.42236